DOCKET NO: 49530/252687 (22100-0100)

IN THE UNITED STATES PATENT AND TRADEMARK OFFICE

In re Application of:	**Carl G. Hellerqvist**		
Application No.:	**09/776,865**	Art Unit:	**1642**
Filed:	**February 2, 2001**	Examiner:	**Stephen L. Rawlings**
For:	**Methods for Preventing or Attenuating Pathoangiogenic Conditions**		

SECOND DECLARATION OF DR. CARL G. HELLERQVIST UNDER 37 C.F.R. §1.132

I, Carl G. Hellerqvist, Ph.D., do hereby declare:

1. I am an expert in the field of the invention. My qualifications are of record on the U.S. Patent Application Serial Number 09/776,865, filed February 2, 2001, (hereinafter referred to as "the present application").

2. I am a sole named inventor on the present application. I am familiar with the Office Actions mailed by the United States Patent and Trademark Office in the present application on July 16, 2003 and July 26, 2004, the Final Office Action mailed by the United States Patent and Trademark Office on February 24, 2005, and the Non-Final Office Action mailed September 6, 2005.

3. As one of ordinary skill in the art in the field of the invention, I declare that, in the field of tumor angiogenesis studies, observations in appropriately selected mouse models reasonably correlate with the observations in other mammals, such as humans. Mouse animal models used in the examples of the present application are selected so that they are reasonably correlating with human pathological angiogenesis for the purpose of

demonstration of the ability of Group B ß-hemolytic *Streptococci* ("GBS") toxin receptors or immunogenic fragments thereof to attenuate pathological angiogenesis, in particular, the pathological angiogenesis associated with cancer in a mammal, including a human. This is because the methods disclosed and claimed in the present application affect homologous targets in pathological vasculature, common to the animals and the humans.

4. I discovered that Group B Streptococcal toxin, GBS toxin/CM101 is an agent that induced respiratory distress in human neonates by binding to neonatal vasculature. I did so by using a sheep model because GBS is a sheep pathogen. The damage induced by GBS to sheep lung vasculature correlated with damage to human neonatal lung vasculature. See, for example, the present application, p. 5, lines 5-26; Fu *et al., Clin. Cancer Research*, v. 7, pp. 4182-4194 (2001; of record in the present application) and references cited therein on p. 4182, second column. Similarly to human neonates, mice neonates are susceptible to GBS infections. Madoff L.C., *et al., J. Clin. Invest.*, v. 94, pp. 286-292. (1994; Exhibit A). Accordingly, GBS-induced damage in neonatal mouse lung vasculature is expected to correlate with the damage in neonatal humans. While not wishing to be bound by the following hypothesis, I suggest that tumors originate from cells reverting back towards an embryonic stage. Therefore, tumor-recruited vasculature in humans and mice may also have neonatal characteristics, such as GBS binding. Applicants generated antibodies to GBS toxin/CM101 and showed by immunohistochemistry that CM101 bound to human and mouse tumor vasculature but not to normal vasculature in humans, mice. See, for example, Yan *et al., Angiogenesis*, 2: 219-233 (1998;Exhibit B); Wamil *et al., J. Can. Res. Clin. Oncol.*, v. 123, pp. 173-179 (1997; Exhibit C). Thus, mouse and human tumor vasculature possess similar GBS toxin-binding markers.

5. I used a nude mouse model implanted with a human carcinoma of the breast in order to conduct preclinical studies of the cancer-attenuating properties of CM101. Infusing CM101 every other day for twenty-one days lead to a 60% decrease in tumor volume. See, for example, US Patent No. 5,010,062 (Example 2; Exhibit D). I demonstrated that CM101

induced a Complement C3 activated cytokine driven inflammatory response targeting the tumor vasculature. See, for example, Yan *et al.* (1998 Exhibit B).

The above results from the mouse models correlated with the results of clinical testing in human patients. Patients responded to catalytic amounts of GBS toxin/CM101 with a complement activated cytokine driven inflammatory response that targeted the tumor vasculature and induced pain at the sites of tumors. See, for example, Wamil *et al.* (1997 Exhibit C); DeVore *et al.*, *J. Clin. Can. Res.* v. 3, pp. 365-372 (1997; Exhibit E). The observations of induced inflammation, breakdown of immunoprivilege in the tumor, and tumor cell apoptosis in human patients were confirmed in a mouse model. See Yakes *et al.*, *Cancer Research* v. 60, pp. 5740-5746 (2000; Exhibit F). Thus, I demonstrated the correlation of the effects of GBS toxin administration in mouse cancer models and human cancer patients.

6. By cloning and identifying HP59, the target protein for GBS toxin/CM101, in humans and sheep, and by immunohistochemical studies in mice, I showed the existence of a conserved molecular marker for neonatal and pathologic vasculature in mammals. See Fu *et al.* (2001). I also showed that HP59 is present in the tumor vasculature independently of site and type. See Table 1 in Fu *et al.* To my knowledge, all antibodies generated to the human and sheep HP59 analogue cross-react with pathologic vasculature in mice rats and pigs. Thus, HP59 is a target in pathologic vasculature which is common to humans, mice rats and pigs.

7. I showed in Fu *et al.* (2001) and in the present application that immunization with HP59 and Sp55 peptides attenuated tumor growth in a mouse animal model by inhibiting pathoangiogenesis and vasculogenesis. The HP59 derived vaccines are able to inhibit pathologic angiogenesis and to generate a cellular immune response. I further demonstrated that the immunized mice that survived repeated intravenous melanoma injections developed a cellular immune response to the vascular target. This immune response led to attenuation of the pathologic angiogenesis. White blood cells (WBC) were

isolated from the tumor resistant mice or control mice and infused in naïve mice carrying Lewis lung tumor or melanoma in a cutaneous window model. WBC from control mice had no effect on the naïve mice, whereas administration of WBC from the tumor-challenged immunized mice to model animals attenuated pathological vasculature in the model animals. See Figure 1 - Exhibit G. HP59 target is unique to pathologic vasculature and common to the pathologic vasculature of at least humans, sheep and mice. Thus, I identified HP59 as a target for attenuating cancer-associated pathologic angiogenesis in various mammals.

8. I declare that the publications cited by the Examiner in the last Office Action predominantly deal with the limitations of mouse models for predicting clinical outcomes during development of **drugs targeting various tumor-specific targets, and not treatments directed at pathological vasculature-specific targets.** For example, Wang *et al.* (2001) deals with anti-cancer vaccines against tumor-specific antigens. Accordingly, the cited publications are not relevant to the methods and compositions of the present application.

Genetic and phenotypical diversity of the tumor tissues makes it difficult to target tumor-specific targets. This genetic and phenotypical diversity of the tumor tissues negatively influences the correlation between mouse models and humans when tumor targets are affected. See, for example, Axelson *et al.*, *Semin. Cell. Dev. Biol.* v. 16, 554-63 (2005; Exhibit G):

> "Histopathological examination of solid tumors frequently reveals pronounced tumor cell heterogeneity with regards to cell organization, cell morphology, cell size, nuclei morphology, etc. Analyses of gene expression patterns by immunohistochemistry or in situ hybridization techniques further strengthen the actual presence of phenotypic heterogeneity, often demonstrating substantial diversity within a given tumor. The molecular mechanisms underlying the phenotypic heterogeneity are very complex with genetic, epigenetic and environmental components."

Maternal Immunization of Mice with Group B Streptococcal Type III Polysaccharide-Beta C Protein Conjugate Elicits Protective Antibody to Multiple Serotypes

Lawrence C. Madoff,*‡ Lawrence C. Paoletti,* Joseph Y. Tai,§ and Dennis L. Kasper*‡
*Channing Laboratory, Brigham and Women's Hospital, and ‡Division of Infectious Diseases, Beth Israel Hospital, Harvard Medical School, Boston, Massachusetts 02115; and §North American Vaccine, Inc., Beltsville, Maryland 20705

Abstract

Group B streptococcal infection is a major cause of neonatal mortality. Antibody to the capsular polysaccharide protects against invasive neonatal disease, but immunization with capsular polysaccharides fails to elicit protective antibody in many recipients. Conjugation of the polysaccharide to tetanus toxoid has been shown to increase immune response to the polysaccharide. In animal models, C proteins of group B streptococci are also protective determinants. We examined the ability of the beta C protein to serve in the dual role of carrier for the polysaccharide and protective immunogen. Type III polysaccharide was covalently coupled to beta C protein by reductive amination. Immunization of rabbits with the polysaccharide–protein conjugate elicited high titers of antibody to both components, and the serum induced opsonophagocytic killing of type III, Ia/C, and Ib/C strains of group B streptococci. Female mice were immunized with the conjugate vaccine and then bred; 93% of neonatal pups born to these dams vaccinated with conjugate survived type III group B streptococcal challenge and 76% survived type Ia/C challenge, compared with 3% and 8% survival, respectively, in controls ($P < 0.001$). The beta C protein acted as an effective carrier for the type III polysaccharide while simultaneously inducing protective immunity against beta C protein–containing strains of group B streptococci. (*J. Clin. Invest.* 1994. 94:286–292.) Key words: *Streptococcus agalactiae* • vaccines, synthetic • antigens, bacterial • immunity, maternally acquired • streptococcal infections • carrier proteins

Introduction

Recent epidemiologic data confirm that group B streptococci (GBS)[1] remain the leading cause of serious neonatal infection (1). The rates of mortality and severe neurologic sequelae that result from this pathogen are unacceptably high, despite continued sensitivity to antibiotics and improved recognition and therapy. Each year in the U.S., several thousand infants become seriously infected with this pathogen, and it is estimated that 15% succumb. In addition, the importance of GBS infections in adults has increasingly been recognized; cases in adults now account for fully half of invasive GBS disease. Immunization has been proposed as a strategy for the prevention of GBS infection (2). The capsular polysaccharides of the most prevalent serotypes causing disease have been the most widely explored antigens for this purpose (3, 4). While the polysaccharides alone are not sufficiently immunogenic to elicit protective antibodies in some recipients, glycoconjugate vaccines with the type-specific polysaccharides covalently linked to tetanus toxoid (TT) have shown high rates of protective immunization in experimental animals (5–10). Human trials of vaccines based on capsular polysaccharide-TT conjugates are now under way. Four capsular polysaccharides (serotypes Ia, Ib, II, and III) currently predominate among GBS strains causing invasive disease. Therefore, to be highly-effective, this type of GBS vaccine will need to be multivalent, containing each of the prevalent capsular serotypes. The widespread use of TT as both a vaccine and a carrier protein in conjugate vaccines may have drawbacks, including uncomfortable local reactions to immunization and suppression of responses to the hapten (11, 12). Thus, we wish to explore the use of alternative carrier proteins, which themselves may elicit protective immunity to GBS.

C proteins are surface-expressed antigens of GBS that also elicit protective immunity in experimental animals (13, 14). Although the alpha and beta C proteins are rarely found in type III strains of GBS, one or both of these antigens are expressed in most strains of other serotypes (15, 16). We and others have shown that both alpha and beta C proteins are protective antigens for GBS in experimental animals (17–19). In addition to its capacity to elicit protective antibody, the beta C protein is known to bind human IgA to the surface of GBS (20, 21). Active immunization with the beta C protein in female mice protects their offspring from lethal infection with strains that express this antigen (22). A glycoconjugate vaccine composed of the type III polysaccharide and C proteins could, in theory, protect against infection with the vast majority of GBS strains. If the C protein could act as both protective immunogen and carrier for the polysaccharide, it would obviate the need for TT as a carrier. However, little is known about the ability of the carrier protein in a glycoconjugate vaccine to elicit protective antibody responses. In this paper we describe the synthesis of a glycoconjugate vaccine composed of the beta C protein and the type III capsular polysaccharide. We demonstrate the ability of the vaccine to stimulate immune responses to both components and, via maternal immunization, to protect neonatal mice from lethal challenge with more than one serotype of GBS.

Methods

Bacterial strains. Strains were from the collection of the Channing Laboratory or were clinical isolates from hospitals associated with the

Address correspondence to L. C. Madoff, Channing Laboratory, 180 Longwood Ave., Boston, MA 02115.

Received for publication 21 December 1993 and in revised form 24 February 1994.

1. *Abbreviations used in this paper:* GBS, group B streptococci; GC-MS, gas chromatography-mass spectrometry; TT, tetanus toxoid.

J. Clin. Invest.

0021-9738/94/07/0286/07 $2.00
Volume 94, July 1994, 286–292

Table I. Group B Streptococcal Serotype, Strain, and C Protein Phenotype

Capsular polysaccharide serotype	Strain	C protein		Reference
		Alpha	Beta	
Ia	515	+	−	(19)
	A909	+	+	(13)
Ib	H36B	+	+	(13)
	S40	+	+	(16)
	S42	−	+	(16, this paper)
	7357b	−	+	(22)
II	18RS21	−	−	(13)
III	M781	−	−	(25)
	S23	−	−	(16)

Baylor College of Medicine (generously provided by Dr. Carol J. Baker, Baylor College of Medicine, Houston, TX) and have been previously described (16). The serotypes of these strains are shown in Table I.

Beta C protein. The beta C protein was generously provided by Dr. Milan Blake (Rockefeller University, New York) and was produced by extraction into SDS from serotype Ib/C GBS strain H36B5, purified by gel filtration chromatography as described previously (20). Purity was assessed by observation of a single 130-kD band on silver-stained SDS–polyacrylamide gel.

Oxidation of GBS type III polysaccharide. Type III GBS capsular polysaccharide (< 200,000 M_r) was purified from GBS strain M781 as previously described (5). Aldehydes were formed on GBS type III polysaccharide by the conversion of a portion of the side chain sialic acid residues by limited oxidation with use of sodium periodate as described previously (5, 23). Briefly, 8.1 mg of purified GBS type III polysaccharide, possessing ~ 8 μmoles of sialic acid, was combined with 2 μmoles of freshly prepared sodium m-periodate (Sigma Chemical Co., St. Louis, MO) in a total volume of 0.5 ml of water. The mixture was incubated at room temperature for 90 min in the dark. After incubation, excess periodate was consumed by the addition of ethylene glycol. Confirmation of the extent of oxidation was obtained by gas chromatography-mass spectrometry (GC-MS) of trimethylsilyl derivatives (5). The mixture was placed in dialysis tubing (Spectropor #1; Spectrum Medical Industries, Inc., Los Angeles, CA) and dialyzed at 4°C against a total of 8 liters of water. The dialyzed sample was filtered (0.45 μm) and dried by lyophilization.

Conjugation of GBS type III polysaccharide to GBS beta C protein. oxidized type III polysaccharide (5.5 mg) was combined with 5 mg of beta C protein in a total volume of 0.5 ml of phosphate buffered saline, pH 9.0–9.5. Sodium cyanoborohydride (33 mg) was added and the mixture incubated at room temperature in the dark. To insure complete coupling an additional 12 mg of sodium cyanoborohydride was added to the mixture after 6 d of incubation. The pH of the reaction was monitored by spotting a 2-μl aliquot onto pH paper and maintained at 9.0–9.5 by the addition of 0.1 N NaOH. Conjugation failed to occur when the pH was not maintained above 8.0. The progress of the conjugation was monitored by gel filtration chromatography of samples as described previously (9). The conjugation was determined to be complete when the magnitude of the protein peak occurring at the void volume (indicative of a high-M_r complex) of a Superose 6 column (Pharmacia Fine Chemicals, Piscataway, NJ) remained constant. After 7 d of incubation, the conjugate vaccine was separated from uncoupled components with use of an S-300 HR (Pharmacia Fine Chemicals) gel filtration column (2.6 × 91.5 cm). Fractions that eluted in the void volume were collected, and uncoupled aldehyde groups on the polysaccharide were reduced by the addition of ~ 2 mg of sodium borohydride. The reduction reaction was allowed to proceed for 1 h at room temperature. The GBS type III polysaccharide-beta C protein conjugate (III-β) was dialyzed at 4°C against a total of 16 liters of water and dried by lyophilization.

Biochemical analysis of III-β vaccine. The carbohydrate and protein content of the III-β vaccine were determined as previously described (8, 10).

Immunoblotting. Analysis of the vaccine was performed by western blotting, as previously described, with monoclonal antibody 3E7 specific for the beta C protein (16), rabbit antiserum raised to type III polysaccharide conjugated to TT (5), or human myeloma IgA_1 (graciously provided by Dr. Andrew Wright, Tufts University, Boston) (16).

Immunogenicity of III-β vaccine in rabbits. The immune response to the III-β vaccine was evaluated in rabbits. Two New Zealand White female rabbits (Millbrook Farms, Amherst, MA) each weighing 2–3 kg were immunized subcutaneously with 50 μg of III-β vaccine emulsified with complete Freund's adjuvant in a total volume of 1.0 ml. Booster doses of vaccine mixed with incomplete Freund's adjuvant were administered by the same route 21 and 41 d after the primary dose. A second set of three rabbits were immunized with uncoupled beta C protein with use of the same route, adjuvant and schedule as with the conjugate vaccine. Serum was collected on days 0, 21, 41, 55, and 72. Animals received food and water ad libitum.

ELISA. Antibodies to the type III GBS polysaccharide and to the beta C protein were measured by ELISA as described previously (5, 22). The titers were determined by serial twofold dilution (from a starting dilution of 1:3,200) as the greatest dilution with $A_{405} \geq 0.2$ after 30 min of development.

ELISA inhibition. Relative binding affinities of antibodies to beta C protein in sera prepared to purified beta C protein, either alone or as part of the conjugate vaccine, were assessed by inhibition of ELISA reactivity. Purified beta C protein at concentrations ranging from 5 to 5,000 ng/ml was used to inhibit the binding of the antisera (anti–beta C protein diluted 1:400,000 and anti–III-β diluted 1:200,000 to achieve similar ELISA reactivity) to plates coated with purified beta antigen. The absorbance values were plotted against $\log_{10}$ of beta C protein concentration to generate inhibition curves.

Similarity of epitope expression of purified protein either alone or as part of a conjugate vaccine was assessed by determining their relative abilities to compete with the beta C protein expressed on intact GBS for binding to antiserum raised to the beta C protein. ELISA plates were coated with type Ib/C GBS strain 7357b as previously described (22). ELISA was performed with antiserum to the purified protein (diluted 1:100,000) incubated with either the III-β conjugate or the beta C protein ranging in protein concentration from 0.05 to 5 μg/ml.

Relative binding affinities of the beta C protein and the III-β conjugate for human IgA_1 was measured by inhibition of binding of IgA_1 to ELISA plates coated with beta C protein as follows: III-β conjugate and unconjugated beta C protein were serially diluted twofold from a starting protein concentration of 2.0 μg/ml and preincubated with an equal volume of human myeloma IgA_1 (1.0 μg in 50 μl) for 2 h at room temperature. The mixture (100 μl) was transferred to ELISA plates coated with beta C protein (200 ng/well) and incubated at room temperature for 1 h. After washing, goat anti–human IgA conjugated to alkaline phosphatase (Tago, Inc., Burlingame, CA), diluted 1:1000, was added to the ELISA wells and incubated at 37°C for 1 h.

The plates were washed and developed with commercial substrate (Sigma Chemical Co.). Percentage inhibition was calculated as [(A_{405} without inhibitor-A_{405} with inhibitor)/A_{405} without inhibitor] × 100. The point of 50% inhibition was determined graphically.

Opsonophagocytic assay. The functional capacity of antibodies to C proteins of GBS was assessed by an opsonophagocytic assay (24) measuring in vitro killing of GBS. In brief, a 300-μl volume of human polymorphonuclear leukocytes (~ 3×10^6 cells) was mixed with the test GBS strain (~ 1.5×10^6 CFU), 50 μl of human serum (prepared for use as a complement source by absorption on ice for 30 min with GBS of homologous serotype), and 100 μl of antibody diluted 1:100. Pooled rabbit antisera to GBS type-specific polysaccharides conjugated to TT were used as the reference sera (5, 8, 10). ELISA titers of these antisera to the homologous polysaccharides were as follows: Ia:

200,000; Ib: 100,000; II: 100,000, III: 64,000. Viable GBS cells were enumerated as 10-fold dilutions on blood agar plates immediately and after a 60-min incubation at 37°C, and the difference was calculated as killing. The assay was repeated in the absence of antibody. The result is reported as the "log kill," which is the difference between killing with and without antibody for at least two determinations per strain.

Neonatal mouse protection. A neonatal mouse model of GBS infection was used to assess the protective efficacy of active immunization with the type III polysaccharide-beta C protein conjugate (III-β) vaccine (25). Female CD-1 mice 8 wk of age (Charles River Laboratories, Wilmington, MA) were vaccinated intraperitoneally with two 20-μg doses of III-β with and without alum (Alhydrogel, final concentration 1.5%) as adjuvant at 21-d intervals. Control dams received 10 μg of beta C protein alone or 2 μg type III polysaccharide-tetanus toxoid conjugate (III-TT) with alum by the same route and schedule. Mice were bred immediately after immunization and neonatal mouse pups (born ~ 4 wk later) were challenged with a beta C protein-positive strain of GBS (A909, Ia/C alpha+, beta+) or with a type III strain (M781 type III C protein-negative). Pups were challenged with an inoculum of each strain lethal for 80–90% of nonimmune pups of the same age (5×10^4 CFU of GBS strain A909 and 5×10^6 CFU of strain M781) within 48 h of birth. The challenge dose was administered intraperitoneally with a tuberculin syringe via a 27-gauge needle in a total of 0.05 ml of Todd-Hewitt broth. The number of pups that survived GBS infection was assessed 48 h after challenge and survival data compared using Fisher's exact test.

Results

Conjugation of GBS type III polysaccharide with GBS beta C protein. 47% of sialic acid residues on the type III polysaccharide were oxidized to C8 derivatives (5-acetamido-3,5-dideoxy-D-galactosyloctulosonic acid) by treatment with sodium periodate as determined by GC-MS analysis of trimethylsilyl derivatives of the periodate-treated polysaccharide. The recovery of oxidized type III polysaccharide was 6.6 mg or 81%. Conjugation of type III polysaccharide with beta C protein resulted in the formation of a high-M_r ($> 1 \times 10^5$) polymer. The recovery of type III-beta C protein conjugate (III-β) vaccine was 3.9 mg or 37%. The III-β vaccine was composed by weight of 44% protein and 56% carbohydrate. Further confirmation of conjugation was demonstrated by immunoblot with antiserum to type III polysaccharide and monoclonal antibody 3E7 to beta C protein (not shown). By immunoblot reactivity, the M_r of the conjugate vaccine was > 200,000 and uncoupled protein was not detected.

Immunogenicity of III-β vaccine in rabbits. Rabbits immunized with III-β conjugate developed ELISA antibody titers of > 100,000 against the type III polysaccharide and > 400,000 against the beta C protein (Table II). Rabbits immunized with unconjugated beta C protein had beta-specific ELISA titers exceeding 600,000. As expected the beta C protein did not elicit antibodies to the type III polysaccharide.

Epitope expression on beta C protein in conjugate vaccine. ELISA inhibition experiments were performed to assess the expression of epitopes on the beta C protein within the conjugate vaccine. ELISA plates were coated with purified beta C protein and tested against antisera raised to either the beta C protein or the III-β conjugate. Inhibition of antibody binding was achieved with increasing concentration of beta C protein preincubated with diluted antisera. These inhibition curves were used to estimate the relative overall binding affinity to uncoupled beta C protein of antibodies in these two sera. The concentrations of beta C protein required to inhibit 50% of binding were similar: 220 μg/ml for anti–beta C protein (uncoupled) and 175 μg/ml for anti-III-β.

To compare the antigenicity of the beta C protein alone and coupled to the type III polysaccharide with that of the antigen as presented on intact bacteria, an ELISA inhibition experiment was performed with ELISA plates coated with intact beta-C-protein–positive GBS. The competitive binding curves for the two antigens were essentially identical (not shown). Normalized for beta C protein content, the concentration required to inhibit 50% of binding was 1.15 μg/ml for the beta C protein and 0.92 μg/ml for the III-β conjugate, thus demonstrating that conjugation with polysaccharide did not alter important beta antigenic epitopes in the conjugate.

IgA binding. IgA binding to the conjugate appears markedly diminished compared with the native protein on the immunoblot, even when five times the amount of conjugate was applied to the gel (Fig. 1). The protein–polysaccharide conjugate had a higher M_r than the unconjugated protein, barely entering the running gel. In the ELISA inhibition experiments (Fig. 2), 50% inhibition of IgA_1 binding occurred at a concentration of 3 μg/ml of uncoupled beta C protein and > 90% inhibition occurred at 25 μg/ml, whereas less than 60% inhibition of IgA binding could be achieved by the conjugate at 200 μg/ml (=100 μg/ml beta C protein), the highest concentration tested.

Opsonophagocytosis of GBS strains by serum raised to the III-β vaccine. Antiserum raised to the III-β conjugate vaccine induced killing by human polymorphonuclear leukocytes (PMNs) in the opsonophagocytic assay against strains expressing either the beta C protein or the type III capsular polysaccharide (Table III). The log reduction in CFU (minus the log reduction in CFU in the absence of antiserum) was comparable to that induced by antiserum raised to the III-TT vaccine. Strains that expressed neither the type III capsular polysaccharide nor the beta C protein (i.e., 515 serotype Ia/C alpha+ beta–, and 18RS21 serotype II) were not rendered susceptible to phagocytic killing by the III-β conjugate vaccine-induced antiserum. One strain, S42 was previously reported to be beta C protein negative (16) but exhibited a high level of opsonophagocytic killing with the anti-III-β serum. On reexamination of the strain S42 with monoclonal antibody to beta (3E7) by western blot, this strain was found, in fact, to express low levels of the beta C protein.

Neonatal mouse protection by immunization with III-β vaccine. Active immunization with III-β vaccine greatly enhanced survival of mice challenged either with type Ia/C (alpha+, beta+) strain A909 or with type III strain M781 (Table IV): 93% of neonatal pups whose mothers were immunized with the III-β vaccine survived intraperitoneal challenge with type III GBS compared with 4% of those whose mothers were immunized with the beta C protein alone ($P < 0.001$) and 83% of those whose mothers were immunized with III-TT (NS); 76% of neonatal mice whose mothers were immunized with the III-β vaccine survived challenge with the Ia/C strain of GBS compared with 3% of those whose mothers were immunized with III-TT ($P < 0.001$) and 62% of those whose mothers were immunized with beta C protein alone (NS). While there was improved survival among the neonates of dams who received alum as an adjuvant with the vaccine, it was not statistically significant. Survival rates between litters within a test group were similar and each litter within a test group showed statistically significant increase in survival compared with the heterologous control ($P < 0.02$).

Table II. Antibody Response in Rabbits Elicited by Immunization with III-β Conjugate Vaccine or with beta C Protein Alone

Immunogen	n	Coating antigen	Geometric mean ELISA titer				
			day 0	21	42	55	72
III-β vaccine	2	III PS	3200	3200	12800	102400	144815
		β C protein	3200	3200	51200	144815	409600
Beta C protein	3	III PS	3200	3200	3200	3200	3200
		β C protein	3200	25600	204800	409600	650200

ELISA titers were determined for each rabbit at each time point. The geometric mean ELISA titer is shown. Rabbits immunized with either the III-β or the beta C protein developed high-titered antibody to beta. Those immunized with the beta C protein alone demonstrated high antibody titers to the beta C protein but not to type III polysaccharide.

Discussion

The optimal design of conjugate vaccines remains an important goal. Protein–polysaccharide conjugate vaccines have been formulated to use a carrier protein to augment the immunogenicity of the polysaccharide antigen. In theory, the immune response to the polysaccharide is rendered T cell dependent and thus immune responsiveness increases with repeated immunization (26). The IgG response is enhanced, and the duration of immunity is prolonged. Previous vaccine formulations have generally used a carrier protein irrelevant to the primary disease for which the vaccine is designed. The currently available vaccines for Haemophilus influenzae type b (Hib), for example, use TT, diphtheria toxoid, or outer membrane protein of *Neisseria meningitidis* as carrier proteins (27).

The use of a limited number of carrier proteins for a growing number of conjugate vaccines has potential disadvantages. For example, the history of immunization to the carrier protein may affect the response to the polysaccharide antigen after immunization with a conjugate vaccine (11, 28, 29). Recent immunization with TT appears to diminish the immune response to the Hib polysaccharide in a Hib-TT conjugate (12). Repeated immunization with the same carrier protein may result in uncomfortable local reactions, thereby diminishing the palatability and perhaps the acceptance of these vaccines.

In the case of GBS, at least four capsular polysaccharides (serotypes Ia, Ib, II, and III) currently predominate among GBS strains causing invasive disease, therefore, a polysaccharide based GBS vaccine will need to be multivalent containing each of the prevalent capsular serotypes. In such a multivalent vaccine, the quantity of TT required as a carrier may exceed the allowable amount for routine immunizations. Also, the widespread use of TT as both a vaccine and a carrier protein in this and other polysaccharide–protein conjugate vaccines may have drawbacks, including uncomfortable local reactions to immunization and suppression of responses to the hapten (11, 12).

In contrast, the use of a protective antigen from the target organism may enhance the effectiveness of a conjugate vaccine by eliciting antibodies that are themselves protective. The pro-

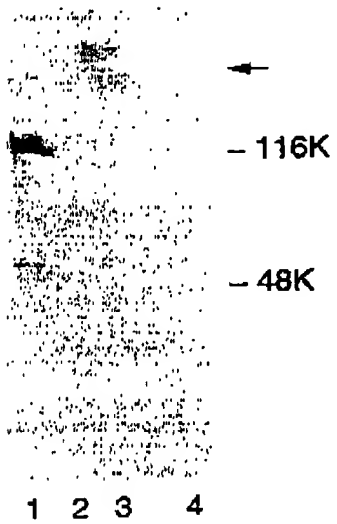

Figure 1. Immunoblot of beta C protein and group B streptococcal type III polysaccharide–beta C protein conjugate probed with human IgA_1 at 10 μg/ml. Goat antiserum to human IgA labeled with alkaline phosphatase diluted 1:1,000 is used as the secondary antibody. Lane *1* contains the unconjugated beta C protein (1 μg); Lane *2* contains 2 μg; and lane *3* contains 10 μg of the glycoconjugate. Lane *4* contains 10 μg type III polysaccharide–tetanus toxoid conjugate (5) as a control. The immunoblot demonstrates reduction in binding to IgA after conjugation and increase in M_r after conjugation.

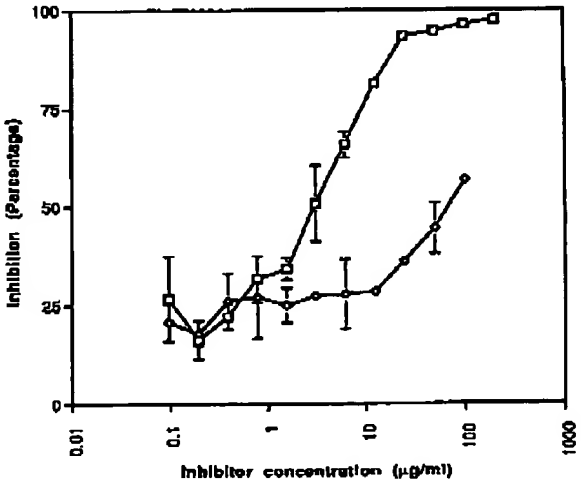

Figure 2. ELISA inhibition of human IgA_1 binding to plates coated with beta C protein by beta C protein (□) or by III-beta conjugate (○) (normalized for the beta C protein content of each). Points are mean of two determinations and standard deviation of the mean is plotted. The curves demonstrate a loss of IgA binding capacity by the conjugate compared with the native protein.

Table III. In Vitro Opsonophagocytic Killing of GBS by Human Peripheral Blood Leukocytes

GBS strain	Beta C protein	Reduction in GBS CFU ($\log_{10}$): Homologous reference sera	Reduction in GBS CFU ($\log_{10}$): anti-III-β
Type Ia			
A909	+	1.80	1.16
515	−	1.57	0.08
Type Ib			
H36B	+	0.80	1.78
S40	+	0.50	1.18
S42	+	0.82	1.16
Type II			
18RS21	−	0.92	−0.13
Type III			
M781	−	0.69	1.06
S23	−	0.84	0.93

Group B streptococci were grown to mid-log phase and incubated with rabbit antiserum (1% final concentration), human serum as a source of complement, and human polymorphonuclear leukocytes. Organisms were enumerated by dilution on blood agar plates immediately and after 60 min. The result (mean of duplicate determinations) is expressed as the $\log_{10}$ reduction in CFU. Rabbit antisera to group B streptococcal type-specific polysaccharides covalently conjugated to tetanus toxoid were used as the reference sera (5, 8, 10). The experiment demonstrates that strains which express either the type III polysaccharide or the beta C protein are rendered susceptible to killing by anti-III-β serum.

tective level of antibody elicited by the vaccine may increase if both antigens are present on the same pathogen. In addition, the carrier protein may expand the coverage of the vaccine to include organisms that possess a different capsular polysaccharide.

Most vaccines currently under study for the prevention of GBS infection are based on the capsular polysaccharide antigens (5, 7, 8, 10, 30). The most prevalent type-specific polysaccharides are well characterized and have been shown to be critical targets for specific immunity in preventing neonatal GBS infection (3, 4, 31). These antigens have been safely used to immunize pregnant women, and type-specific antibody has been shown to cross the placenta at levels protective to newborns (4). Although the polysaccharides are themselves not adequately immunogenic in some recipients, conjugate vaccines composed of type-specific polysaccharide conjugated to tetanus toxoid have been shown to elicit protective antibodies in animals and are currently in human trials (5, 8).

In addition to the capsular polysaccharides, GBS possess protective surface protein antigens including the C proteins alpha and beta present mainly in non-type III strains (15, 16), the Rib protein present mainly in strains of capsular serotypes II and III (32), and the R proteins found in several capsular types (33, 34). We have chosen to study one of these surface proteins for its use as both carrier and immunogen in a conjugate vaccine. The beta C protein elicits maternal antibodies that protect neonatal mice from lethal challenge with GBS which express the beta C protein (22). We now demonstrate that the beta C protein can be covalently coupled to the type III GBS polysaccharide through limited oxidation of polysaccharide sialic acid residues followed by reductive amination. Conjugation by this method which is thought to occur mainly at lysine residues of the protein component (35), may have been facilitated by the extremely lysine-rich nature of the beta C protein, which has 156 lysine residues out of 1,134 amino acids (36, 37). Conjugation of these two molecules required careful titration of pH because of the highly acidic nature of both the beta C protein and the type III polysaccharide (36, 37).

Immunization of rabbits with the III-β conjugate vaccine elicited high antibody titers against the type III polysaccharide, whereas the type III polysaccharide alone has been shown to be nonimmunogenic in rabbits (5). Thus, the beta C protein functions as an effective carrier protein in this vaccine presumably by allowing the development of T cell–dependent immunity to the polysaccharide. The conjugate vaccine also elicited antibodies to beta C protein at titers comparable with those elicited by the beta C protein alone (22). Conjugate vaccine-induced beta C protein antibodies reacted with the beta C protein

Table IV. Neonatal Mouse Survival after Maternal Immunization with III-β Conjugate Vaccine and Challenge with GBS

Dams immunized with	Adjuvant	Challenge strain (serotype)	No. dams	No. pups	No. (%) surviving	P compared with heterologous control
β C-protein alone	None	M781 (III)	2	26	1 (4)	—
β C-protein alone	None	A909 (Ia/C)	2	29	18 (62)	< 0.001
III-β vaccine	None	M781 (III)	2	24	17 (70)	< 0.001
III-β vaccine	None	A909 (Ia/C)	2	23	15 (65)	< 0.001
III-β vaccine	Alum	M781 (III)	2	27	25 (93)	< 0.001
III-β vaccine	Alum	A909 (Ia/C)	2	25	19 (76)	< 0.001
III-TT	Alum	M781 (III)	3	29	24 (83)	< 0.001
III-TT	Alum	A909 (Ia/C)	3	37	1 (3)	—

Female mice were immunized with the agent shown. Mice were bred after immunization and their newborn pups (born ~ 4 wk later) were challenged with 90% lethal doses of either group B streptococcal strain A909 (type Ia/C, beta positive) or M781 (type III, beta negative). Survival at 48 h was compared with heterologous controls (i.e., pups of dams immunized with beta C protein alone challenged with type III strain or pups of dams immunized with III-TT challenged with Ia/C beta positive strain). Maternal immunization with the III-β conjugate vaccine conferred significant protection against neonatal challenge with both group B streptococcal serotypes.

with similar relative binding affinities (as measured by ELISA inhibition) to that elicited by the beta C protein alone. In addition, whether uncoupled or coupled to the polysaccharide, the beta C protein competed with beta C protein antigen on whole bacteria for binding to beta C protein–specific sera, thus demonstrating that conjugation to the polysaccharide did not alter important antigenic epitopes on the protein. The biological significance of the preserved antigenicity of the beta C protein after coupling is confirmed by the fact that the antiserum to the conjugate is highly opsonic for strains expressing the beta C protein. It appears as if protective antigenic epitopes remained available to the immune system despite covalent linkage of the protein to the polysaccharide.

Antibodies to both components of the III-β conjugate vaccine were shown to be functionally active in an opsonophagocytic assay, i.e., capable of mediating complement-dependent killing of GBS by PMNs. Moreover, the rabbit antibodies induced killing of both type III strains and strains of different capsular serotypes that expressed the beta C protein. Thus this is an example of a carrier protein extending the spectrum of coverage of a conjugate vaccine.

In the neonatal mouse model of protection, active immunization of female mice with the III-β vaccine protected the offspring of the mice against challenge with either a type III GBS strain or a Ia/C GBS strain. This result implies the generation of protective type-specific antibodies to both components and the transplacental passage of these antibodies to the pups. Levels of protection were comparable to those elicited by the beta C protein alone for the Ia/C strain and those elicited by the III-TT conjugate vaccine. Whereas a III-TT vaccine construct provides protection against GBS type III serotypes, the III-β vaccine has expanded the coverage to include not only type III GBS strains but other non-type III GBS serotypes as well. The use of alum as an adjuvant did not alter the survival of pups significantly, although there was a trend toward greater survival among pups whose mothers received vaccine with adjuvant. Flores et al. (38) showed that some parturient women colonized with GBS possess naturally occurring antibody to the beta C protein and that there was concordance between ELISA titers of antibody in these women and their neonates suggesting transplacental passage of beta-specific antibody in humans.

The beta C protein binds specifically to human IgA via a nonimmune mechanism (20). One theoretical drawback to the use of the beta C protein in a conjugate vaccine is the ability of the vaccine to bind to human IgA. The consequences of this binding are not clear, and there are no unusual immune phenomena associated with infection with GBS strains that express these proteins (or other bacteria that express immunoglobulin binding proteins). Conjugation to the polysaccharide appeared to diminish greatly the affinity of the protein for IgA binding. However, the immunoblot of the conjugate to human IgA demonstrated some detectable binding, even after conjugation. The diminution of binding may occur via steric interference with the IgA binding site, through partial denaturation of the protein, or by binding to lysine residues in or adjacent to the active site. It may be possible to eliminate this theoretical concern associated with use of the beta C protein by fully eliminating IgA binding through alteration of the nature of the conjugation, for example, by increasing the percentage of sialic acid residues that are oxidized and thus increasing the degree of cross-linking in the glycoconjugate. Alternatively, the beta C protein could be modified, for example, by mutagenesis, to eliminate IgA binding. Finally non–IgA binding variants of the beta C protein have been described that, if fully immunogenic and protective, may represent alternative carrier proteins (39). Despite this alteration in functional activity, conjugation did not appear to alter antigenic or immunogenic properties of the protein.

The beta C protein is found in ~ 40% of non-type III GBS clinical isolates (15). The alpha C protein, which is also a protective determinant, is present in approximately half of all clinical isolates and in more than 90% of non-type III isolates (15). Thus, a type III polysaccharide–alpha C protein conjugate vaccine would theoretically offer nearly universal coverage of GBS isolates with a single vaccine construct. We are currently exploring the use of this protein for such purposes.

The conjugation of the type III GBS capsular polysaccharide to the beta C protein from the same species of organism demonstrated that specific, protective immunity can be elicited to both components of the conjugate vaccine and that the protein component can act as both carrier and immunogen. This work lays the foundation for further studies of this novel type of vaccine and for further optimization of glycoconjugate vaccines.

Acknowledgments

GC-MS analysis was performed by R. Pon and H. Jennings, National Research Council, Ottawa. The superb technical assistance of Elizabeth W. Gong and Kenneth Johnson is acknowledged. The contents of this publication do not necessarily reflect the views or policies of the Department of Health and Human Services, nor does mention of trade names, commercial products, or organizations imply endorsement by the U.S. government.

This research was supported in part by Public Health Service Contract NO1 AI25152 "Prevention of group B streptococcal infection in neonatal and infant populations" and National Institutes of Health grants AI00981, AI08222, and AI23339.

References

1. Farley, M. M., R. C. Harvey, T. Stull, J. D. Smith, A. Schuchat, J. D. Wenger, and D. S. Stephens. 1993. A population-based assessment of invasive disease due to group B Streptococcus in nonpregnant adults. *N. Engl. J. Med.* 328:1807–1811.

2. Baker, C. J., and D. L. Kasper. 1985. Vaccination as a measure for prevention of neonatal GBS infection. *Antibiot. Chemother.* 35:281–290.

3. Baker, C. J., D. L. Kasper, M. S. Edwards, and G. Schiffman. 1980. Influence of preimmunization antibody levels on the specificity of the immune response to related polysaccharide antigens. *N. Engl. J. Med.* 303:173–178.

4. Baker, C. J., M. A. Rench, M. S. Edwards, R. J. Carpenter, B. M. Hays, and D. L. Kasper. 1988. Immunization of pregnant women with a polysaccharide vaccine of group B *Streptococcus*. *N. Engl. J. Med.* 319:1180–1220.

5. Wessels, M. R., L. C. Paoletti, D. L. Kasper, J. L. DiFabio, F. Michon, K. Holme, and H. J. Jennings. 1990. Immunogenicity in animals of a polysaccharide-protein conjugate vaccine against type III group B Streptococcus. *J. Clin. Invest.* 86:1428–1433.

6. Baker, C. J., M. A. Rench, and D. L. Kasper. 1990. Response to type III polysaccharide in women whose infants have had invasive group B streptococcal infection. *N. Engl. J. Med.* 322:1857–1860.

7. Lagergard, T., J. Shilonch, J. B. Robbins, and R. Schneerson. 1990. Synthesis and immunological properties of conjugates composed of group B streptococcus type III capsular polysaccharide covalently bound to tetanus toxoid. *Infect. Immun.* 58:687–694.

8. Paoletti, L. C., M. R. Wessels, F. Michon, J. DiFabio, H. J. Jennings, and D. L. Kasper. 1992. Group B *Streptococcus* type II polysaccharide-tetanus toxoid conjugate vaccine. *Infect. Immun.* 60:4009–4014.

9. Paoletti, L. C., M. R. Wessels, F. Michon, H. J. Jennings, and D. L. Kasper. 1992. Group B *Streptococcus* type III glycoconjugate vaccines. *Trends Glycosci. Glycotechnol.* 4:269–278.

10. Wessels, M. R., L. C. Paoletti, A. K. Rodewald, F. Michon, J. DiFabio, H. J. Jennings, and D. L. Kasper. 1993. Stimulation of protective antibodies

against type Ia and Ib group B streptococci by a type Ia polysaccharide-tetanus toxoid conjugate vaccine. *Infect. Immun.* 61:4760–4766.

11. Herzenberg, L. A., and T. Tokuhisa. 1982. Epitope-specific regulation. I. Carrier-specific induction of suppression for IgG anti-hapten antibody responses. *J. Exp. Med.* 155:1730–1740.

12. Barington, T., M. Skettrup, L. Juul, and C. Heilmann. 1993. Non-epitope-specific suppression of the antibody response to Haemophilus influenzae type b conjugate vaccines by preimmunization with vaccine components. *Infect. Immun.* 61:432–438.

13. Lancefield, R. C., M. McCarty, and W. N. Everly. 1975. Multiple mouse-protective antibodies directed against group B streptococci. Special reference to antibodies effective against protein antigens. *J. Exp. Med.* 142:165–179.

14. Wilkinson, H. W., and R. G. Eagon. 1971. Type-specific antigens of group B streptococcus. *Infect. Immun.* 4:596–604.

15. Johnson, D. R., and P. Ferrieri. 1984. Group B streptococcal Ibc protein antigen: distribution of two determinants in wild-type strains of common serotypes. *J. Clin. Microbiol.* 19:506–510.

16. Madoff, L. C., S. Hori, J. L. Michel, C. J. Baker, and D. L. Kasper. 1991. Phenotypic diversity in the alpha C protein of group B streptococcus. *Infect. Immun.* 59:2638–2644.

17. Madoff, L. C., J. L. Michel, and D. L. Kasper. 1991. A monoclonal antibody identifies a protective C-protein alpha-antigen epitope in group B streptococci. *Infect. Immun.* 59:204–210.

18. Bevanger, L., and A. I. Naess. 1985. Mouse-protective antibodies against the Ibc proteins of group B streptococci. *Acta. Pathol. Microbiol. Immunol. Scand, Sect. B Microbiol.* 93:121–124.

19. Michel, J. L., L. C. Madoff, D. E. Kling, D. L. Kasper, and F. M. Ausubel. 1991. Cloned alpha and beta C-protein antigens of group B streptococci elicit protective immunity. *Infect. Immun.* 59:2023–2028.

20. Russell-Jones, G. J., E. C. Gotschlich, and M. S. Blake. 1984. A surface receptor specific for human IgA on group B streptococci possessing the Ibc protein antigen. *J. Exp. Med.* 160:1467–1475.

21. Anthony, B. F., N. F. Concepcion, S. M. Pucutes, and N. R. Payne. 1990. Nonimmune binding of human immunoglobulin A to type II group B streptococci. *Infect. Immun.* 58:1789–1795.

22. Madoff, L. C., J. L. Michel, E. W. Gong, A. K. Rodewald, and D. L. Kasper. 1992. Protection of neonatal mice from group B streptococcal infection by maternal immunization with beta C protein. *Infect. Immun.* 60:4989–4994.

23. Jennings, H. J., and C. Lugowski. 1981. Immunochemistry of groups A, B, and C meningococcal polysaccharide-tetanus toxoid conjugates. *J. Immunol.* 127:1011–1018.

24. Baltimore, R. S., D. L. Kasper, C. J. Baker, and D. K. Goroff. 1977. Antigenic specificity of opsonophagocytic antibodies in rabbit anti-sera to group B streptococci. *J. Immunol.* 118:673–678.

25. Rodewald, A. K., A. B. Onderdonk, H. B. Warren, and D. L. Kasper. 1992. Neonatal mouse model of group B streptococcal infection. *J. Infect. Dis.* 166:635–639.

26. Avery, O. T., and W. F. Goebel. 1931. Chemo-Immunological studies on conjugated carbohydrate-proteins. V. The immunological specificity of an antigen prepared by combining the capsular polysaccharide of type III pneumococcus with foreign protein. *J. Exp. Med.* 54:437–447.

27. Decker, M. D., K. M. Edwards, R. Bradley, and P. Palmer. 1993. Responses of children to booster immunization with their primary conjugate Haemophilus influenzae type B vaccine or with polyribosylribitol phosphate conjugated with diphtheria toxoid. *J. Pediatr.* 122:410–413.

28. Schutze, M.-P., C. Leclerc, M. Jolivet, F. Audibert, and L. Chedid. 1985. Carrier-induced epitopic suppression, a major issue for future synthetic vaccines. *J. Immunol.* 135:2319–2322.

29. Schutze, M. P., C. Leclerc, P. R. Vogel, and L. Chedid. 1987. Epitopic suppression in synthetic vaccine models: analysis of the effector mechanisms. *Cell. Immunol.* 104:79–90.

30. Paoletti, L. C., D. L. Kasper, F. Michon, J. DiFabio, K. Holme, H. J. Jennings, and M. R. Wessels. 1990. An oligosaccharide-tetanus toxoid conjugate vaccine against type III group B Streptococcus. *J. Biol. Chem.* 265:18278–18283.

31. Kasper, D. L., D. K. Goroff, and C. J. Baker. 1978. Immunochemical characterization of native polysaccharides from group B streptococcus: the relationship of the type III and group B determinants. *J. Immunol.* 121:1096–1105.

32. Stalhammar, C. M., L. Stenberg, and G. Lindahl. 1993. Protein rib: a novel group B streptococcal cell surface protein that confers protective immunity and is expressed by most strains causing invasive infections. *J. Exp. Med.* 177:1593–1603.

33. Linden, V., K. K. Christensen, and P. Christensen. 1983. Correlation between low levels of maternal IgG antibodies to R protein and neonatal septicemia with group B streptococci carrying R protein. *Int. Arch. Allergy Appl. Immunol.* 71:168–172.

34. Flores, A. E., and P. Ferrieri. 1989. Molecular species of R-protein antigens produced by clinical isolates of group B streptococci. *J. Clin. Microbiol.* 27:1050–1054.

35. Schwartz, B. A., and G. R. Gray. 1977. Proteins containing reductively aminated disaccharides. Synthesis and chemical characterization. *Arch. Biochem. Biophys.* 181:542–549.

36. Lindahl, G., B. Akerstrom, J. P. Vaerman, and L. Stenberg. 1990. Characterization of an IgA receptor from group B streptococci: specificity for serum IgA. *Eur. J. Immunol.* 20:2241–2247.

37. Heden, L. O., E. Prithz, and G. Lindahl. 1991. Molecular characterization of an IgA receptor from group B streptococci: sequence of the gene, identification of a proline-rich region with unique structure and isolation of N-terminal fragments with IgA-binding capacity. *Eur. J. Immunol.* 21:1481–1490.

38. Flores, A. E., J. A. Nelson, X. Y. Wu, and P. Ferrieri. 1993. Antibody profiles to the group B streptococcal beta antigen in maternal and infant paired sera. *APMIS (Acta Pathol. Microbiol. Immunol. Scand.).* 101:41–49.

39. Brady, L. J. and M. D. Boyle. 1989. Identification of non-immunoglobulin A-Fc-binding forms and low-molecular-weight secreted forms of the group B streptococcal beta antigen. *Infect. Immun.* 57:1573–1581.

Angiogenesis 1998; 2: 219–233

ORIGINAL ARTICLE

Functional studies on the anti-pathoangiogenic properties of CM101

He-Ping Yan, Clint E. Carter, En-ze Wang,[1] David L. Page,[2] Kay Washington,[2] Barbara D. Wamil,[1] F. Michael Yakes,[1] Gary B. Thurman[1] and Carl G. Hellerqvist[1]

Department of Biology, Vanderbilt University, and Departments of [1]Biochemistry and [2]Pathology, Vanderbilt University School of Medicine, Nashville, TN 37232, USA

Group B streptococcus (GBS) isolated from human neonates diagnosed with sepsis and respiratory distress produces a polysaccharide exotoxin (CM101) which has been previously described as GBS toxin. CM101 infused i.v. into tumor-bearing mice causes rapid tumor neovascularitis, infiltration of inflammatory cells, inhibition of tumor growth and tumor apoptosis. CM101 has successfully completed phase I studies in refractory cancer patients with very encouraging results. We have now demonstrated a mechanism of action for CM101. Using a normal mouse tumor model, we have examined tumor and normal tissues which were harvested at 0, 5, 15, 30 and 60 min post-infusion of either CM101 or dextran. We present evidence that CM101 is rapidly (within the first 5 min) bound to the tumor neovasculature. Complement is activated by the alternative pathway (C3) and leukocytes start to infiltrate the tumor within the first 5 min. Through RT-PCR and immunohistochemical techniques, we demonstrate that proinflammatory cytokines, Interleukin-6 and tumor necrosis factor (TNF)-α, are up-regulated in infiltrating leukocytes and TNF receptor 2 is up-regulated in the targeted tumor neovasculature. Combined, these events constitute possible explanations for the observed pathophysiology of tumor ablation.

Key words: Anti-tumor action, complement, cytokines, endothelial cells, immunohistochemistry, polysaccharide, RT-PCR.

(Received 3 February 1998; accepted in revised form 21 May 1998)

Correspondence to C. G. Hellerqvist, Vanderbilt University, 23rd@Pierce, 634 MRB I, Nashville, TN 37232-0146, USA. Tel: (+1) 615 322-4339; Fax: (+1) 615 322-6354.

Financial support received from CarboMed, Inc., in which H.-P. Y., C. E. C., D. L. P., B. D. W., F. M. Y., G. B. T. and C. G. H. have a commercial interest.

Introduction

Group B streptococcus (GBS) infection in human newborn infants causes pneumonia and presents with signs of sepsis, granulocytopenia and respiratory distress. It is characterized by pulmonary hypertension and pulmonary edema. The disease is marked by a strong inflammatory response in the lung with pulmonary sequestration of granulocytes and extensive pulmonary vascular damage, and is associated with high morbidity and mortality.[1,2]

We have previously reported that the pathophysiology associated with neonatal GBS pneumonia could be readily duplicated using a sheep model when a polysaccharide called GBS toxin was infused in picomolar quantities.[1,3] GBS toxin induced a pulmonary inflammatory response leading to vascular damage which was evidenced by changes in hemodynamics.[4,5] GBS toxin has been further subfractionated[5,6] and the resulting pathophysiologically more active component of GBS toxin is now called CM101.

By ELISA, we have recently demonstrated the presence of CM101 in the serum, spinal fluid and urine from infants diagnosed with GBS pneumonia or meningitis. CM101 was common to all serotypes (Iab/c, II III and V) present in different patients.[6]

Hellerqvist *et al.*[1] postulated that CM101 (GBS toxin) binds embryonic receptors in neonatal lung neovasculature and induces an inflammatory response which can lead to respiratory failure. Hellerqvist[5] speculated that similar receptors would be present in developing

tumor neovasculature making the tumor susceptible as a target for inflammation. Humans and mice as neonates are susceptible to GBS infections. CM101 was demonstrated efficacious against tumor progression in our mouse models with evidence of inflammation[7] and tumor ablation[8] with no toxicity to other organs.[7] We have also demonstrated elevated systemic tumor necrosis factor (TNF)-α, interleukin (IL)-1 and IL-6[9] in tumor-bearing mice, rapid infiltration of the tumor by leukocytes, neovascularitis, and tumor cell apoptosis following infusion of CM101[10] in two different tumor models in two different strains of mice[10] (Jain *et al.*, 1996 pers. commun.).

CM101 entered clinical trials as an anti-cancer agent in 1993. Data obtained from the patients studied support the hypothesis that CM101 induces a tumor neovasculature-targeted inflammatory response, evidenced by a time- and dose-dependent systemic cytokine cascade and infiltration of the tumor by activated leukocytes.[11,12]

In this study, we expand on our understanding of the mechanism by which CM101 targets pathologic angiogenesis and neovasculature. We demonstrate that CM101 activates complement in both mouse and human. We present evidence that CM101 *in vivo* rapidly binds tumor endothelial cells of newly formed blood vessels in Madison lung tumor-bearing mice and co-localizes with either endogenous mouse C3 or exogenous human C3. This sequence of events effectively opsonizes tumor endothelium for destruction by the infiltrating leukocytes.[13] We used RT-PCR techniques to examine the mRNA expression levels of several proinflammatory cytokines. We report herein the results with IL-6 and TNF-α and their respective receptors in liver and tumor tissue from animals treated with either CM101, dextran or phosphate-buffered saline (PBS). These same tissues were used in immunohistochemical studies to localize the cytokines and corresponding receptors. The results support the suggested mode of action observed in cancer patients where the responses and biopsies were indicative of a complement-induced cytokine-driven inflammatory response.[11,12,14]

Materials and methods

CM101 preparation

Briefly, clinical grade CM101 was produced by culturing Group B β-hemolytic Streptococcus (GBS) in Todd Hewitt Broth (Becton Dickinson, Princeton, NJ) to late log phase. The culture was autoclaved, and bacteria removed by centrifugation and filtration. The supernatant was concentrated by recovering the retentate from a 10 K nominal molecular weight limit (NMWL) polysulfone cassette filter (Millipore, Bedford, MA). CM101 was recovered from an alcohol precipitate by phenol–water extraction, and DEAE–Sephadex and Sepharose column chromatography. Final purification was achieved by lentil lectin chromatography.[5] The resultant polysaccharide solution was filter sterilized, aliquoted into sterile vials at a concentration of 150 μg/ml and then lyophilized by a FDA-approved contractor for clinical use. Samples of CM101 from this lot were provided for use in this study. CM101 was suspended in PBS to establish appropriate doses for i.v. injections into tumor-bearing mice. CM101 has an average molecular weight of 300 kDa by gel filtration and is composed of GalNAc, GlcNAc, Gal, Glc and Man in an approximate ratio of 1:1:3:1:1.

Biotinylation of CM101

Twenty-five micrograms of lyophilized CM101 was dissolved in 250 μl labeling buffer at 100 mM sodium acetate, 0.02% sodium azide. Aqueous meta-periodate (125 μl of 30 mM) was added and the oxidation was allowed to proceed in the dark for 30 min at room temperature. The reaction was terminated by adding 80 mM Na_2SO_3 to the solution. The resultant aldehydes were reacted with 125 μl of 5 mM NHS-LC-Biotin (mol. wt 556.58) (Pierce, Rockford, IL) for a 1 h incubation at room temperature to form biotinylated CM101. Excess biotin was removed by dialysis against four changes of 1 L PBS at 4°C. The product was purified by gel filtration on an Ultrahydrogel 1000 (Waters, Millford, MA) HPLC,[7] lyophilized and stored at −70°C until use.

Murine lung tumor model

A murine lung tumor cell line (G-50073, Madison Lung Tumor) was obtained from the Tumor Repository of the National Cancer Institute at the Frederick Cancer Research Facility. This tumor originated in BALB/c mice and has been employed in our previous studies.[7,8,10]

A frozen vial of stock G-50073 tumor cells was thawed in a 37°C water bath. The cells were dispersed into a single cell suspension and washed twice with RPMI 1640 medium by centrifugation. The cells were then suspended in a 0.6% solution of agarose at a concentration of 4×10^5/0.1 ml. The suspension was loaded into a tuberculin syringe and allowed to gel for 30 min at 4°C. Eight-week-old normal male BALB/c mice were injected s.c. with 2×10^5 cells in the ventral area with a 21 gauge needle. Mice, in three separate studies, were randomized into two groups (experimental and control) and monitored for tumor development. Fourteen days after injecting cells, the mice in the experimental group were injected i.v. with CM101 and in the control groups with dextran 200 000 in PBS at a concentrations of 240 μg/kg per mouse or with PBS alone. At 0 (non-treated), 5, 15, 30 and 60 min after infusion, mice from both experimental and control groups were sacrificed. Tumor and liver tissues were removed, split in half and each half was processed for either RT-PCR or immunohistochemistry. For immunohistochemistry, the tissues were immediately fixed in 10% neutral formalin. The tissues were then dehydrated, paraffin embedded and 10–20 × 8 micron sections were cut for each antibody used for immunohistochemical staining.

Monoclonal antibody

BALB/c mice were initially injected with 250 μg of CM101 mixed with 50 μg concanavalin A (Con A) as an adjuvant in Hunter's Titer Max™ Adjuvant. Four weeks after the initial injection, the mice were boosted with 50 μg of CM101 mixed with 15 μg Con A. The boost was repeated twice at 1 week intervals. Antibody titer was then determined by ELISA. Three days prior to cell fusion, 50 μg of CM101 was injected i.v. into the mice as a final boost. On the day of cell fusion, spleen cells from mice immunized with CM101 were fused with X63-Ag-8.653 murine myeloma cells as described by Fu and Carter.[13] Fused cells were plated into 96-well culture plates (Costar, Cambridge, MA) and subsequently screened for IgG recognizing highly purified CM101. Positive cultures were then expanded and subcloned.

Anti-CM101 monoclonal antibody IgG (2A2B4) was purified from ascites fluid by Protein G (Sigma, St Louis, MO) affinity chromatography. Ascites fluid was prepared by Charles River Laboratories (lot no. WA 93142) by i.p. injection of 2A2B4 hybridoma cells into primed BALB/c mice.

The purified monoclonal antibody 2A2B4 was then dialyzed against two changes of PBS at 4°C overnight. Antibody concentration was determined by the Bradford protein assay and by ELISA using purified mouse IgG (Sigma) as a standard. Antibody was aliquoted and stored at −80°C until use.

ELISA for detection of complement bound to CM101

Concentrations of 30 μg/ml of either sheep anti-human or sheep anti-mouse complement C3 or C5 IgG (The Binding Site, San Diego, CA) in 0.1 M carbonate buffer, pH 9.6 was coated onto 96-well ELISA plates (Immulon IV; Dynatech, Chantilly, VA) by incubation at 37°C for 1 h, then overnight at 4°C. The plates were washed with PBS and then blocked with 4% non-fat milk in PBS for 1 h at 37°C. Biotinylated CM101 was incubated with either normal human or mouse serum at room temperature for 15 min and then overnight at 4°C. This was accomplished by mixing 50 μl of a 10 μg/ml solution of biotinylated CM101 plus 50 μl of serum diluted in PBS for final dilutions of 1:2, 1:10, 1:20, 1:40, 1:80, 1:160 and 1:320. For controls, biotinylated CM101 was incubated with heat-inactivated serum (human or mouse) at the same dilutions as described above. After washing the plates, the serum–CM101 samples were added to either the anti-C3- or anti-C5-coated ELISA plates and incubated for 2 h at 37°C.

The plates were then washed and streptavidin–β-galactosidase (Gibco/BRL Life Technologies, Gaithersburg, MD) was added to each well. The plates were incubated for 1 h at 37°C and washed with PBS. Substrate (pNPG; Gibco/BRL Life

Technologies) was then added and incubated for 1 h at 37°C. The reaction was stopped by addition of 50 µl of 0.2 M Na_2CO_3. The plates were read at 405 nm using a model MKII computerized Titertek® Multiskan Plus ELISA reader.

Immunohistochemical assay

Between 10 and 20 × 8 micron sections of tumor or liver tissue from three separate experiments were prepared for immunohistochemical analysis.

Preparation steps. Sections were deparaffinized by immersing slides in xylene at room temperature twice for 5 min each. The slides were then transferred to fresh absolute alcohol at room temperature and rehydrated through a graded alcohol series to PBS over a 40 min period. The prepared sections were treated with 2% hydrogen peroxide prepared in 30% aqueous methanol for 20 min at room temperature to quench endogenous peroxidase activity.

Blocking. The slides were then washed with PBS and blocked with 2% BSA in PBS, washed again and the tissue stained as described below.

Method I: probing with monoclonal antibody against CM101. Monoclonal antibody 2A2B4 (75 µl; 10 µg/ml) was placed on the sections and incubated for 1 h in a humid chamber. This was followed by washing the slides with PBS and incubating the sections with sheep anti-mouse IgG–peroxidase (The Binding Site) for 1 h at room temperature in a humid chamber.

Processing steps. The slides were washed with PBS and color was developed by adding DAB (Sigma) as substrate. Reactions were terminated by immersion of slides in distilled water for 5 min. The sections were then counter-stained with 0.5% methyl green for 10 min at room temperature. The slides were washed again with distilled water, dehydrated by washing with 1-butanol followed by two consecutive immersions for 5 min in xylene and mounted on cover slips.[16] Controls included staining with secondary sheep anti-mouse IgG, peroxidase alone and monoclonal antibody alone for each time point examined.

Method II: probing with sheep anti-mouse complement C3. Tumor tissue sections were washed with PBS followed by incubation with sheep anti-mouse C3 IgG–peroxidase conjugate (The Binding Site) for 1 h in a humid chamber. Subsequent processing steps were the same as described in Method I. Controls included tumors from untreated mice and tumors from treated mice tissue incubated with an irrelevant sheep anti-human IgG.

Method III: probing with sheep Anti-human complement C3 IgG. Diluted human serum (75 µl) was added to appropriate tumor tissue sections and incubated for 1 h at room temperature in a humid chamber. Sections were then washed with PBS followed by incubation with sheep anti-human C3 IgG–peroxidase conjugate (The Binding Site) for 1 h at room temperature in a humid chamber. Processing of the slides followed the procedure outlined above for Method I. Controls included no exogenous human C3 but sheep anti-human C3 IgG peroxidase, and with exogenous human C3 but no sheep anti-human C3 peroxidase conjugate added, for each time point examined.

Method IV: staining for cytokines and their receptors. Eight micron sections of either tumor or liver were prepared for immunohistochemical staining using the processing steps described above. The slides were then washed with PBS and blocked with PBS containing 2% BSA plus 1% normal goat serum for 15–20 min at room temperature. After washing with PBS, excess liquid was removed, the sections circled with a PAP pen (The Binding Site) to conserve reagents and then stained with the antibodies described below.

The different antibodies (75 µl) were used at different dilutions in PBS. The rat anti-mouse IL-6 receptor polyclonal antibody (Genzyme, Cambridge, MA), the rabbit anti-mouse IL-6 polyclonal antibody (Genzyme) and the rabbit anti-mouse TNF-α receptor polyclonal antibody (Accurate Chemical and Scientific, West Bury, NY) were used at a 1:100 dilution, and the rabbit anti-mouse TNF-α polyclonal antibody (Genzyme) was used at a 1:40 dilution. Diluted antibodies were incubated with appropriate tissue sections for 1 h at room temperature in a humidified slide box. The slides were then washed three times with PBS, incubated with either a goat anti-rat IgG–Fc-specific antibody conjugated to horseradish peroxidase (Jackson Immuno Research, West Grove, PA), or goat anti-

rabbit IgG–Fc-specific antibody conjugated to horseradish peroxidase (Cappel, West Chaster, PA) diluted 1:500 in PBS for 1 h at room temperature using a humid slide box. The slides were again washed with PBS and the sections were developed by adding DAB (Sigma) substrate for 3–5 min. The reaction was terminated by immersion of slides in distilled water for 5 min. The sections were counter-stained with 0.5% methyl green for 10 min at room temperature. The slides were again washed with distilled water and subsequently dehydrated with 100% 1-butanol followed by immersion in xylene twice for 5 min each. Coverslips were then mounted. The first control included the above steps minus the primary antibody, but included the secondary peroxidase conjugated antibody. A second control included primary antibody minus secondary peroxidase conjugate.

mRNA isolation

Isolation of mRNA from all tissues was performed using the QuickPrep Micro mRNA Purification Kit (Pharmacia Biotech, Piscataway, NJ) as described by the manufacturer. Briefly, tissues were excised and immediately homogenized in extraction buffer, diluted with 2 volumes of elution buffer and then applied to an oligo dT–cellulose column (supplied with the kit). The column was washed with 5 × 1 ml of low salt buffer and mRNA was eluted with 2 × 0.2 ml of elution buffer at 65°C.

Primer and probe sequence

The primers (sense and antisense) and probe sequences are listed in Table 1.

cDNA synthesis, PCR, probe labeling and hybridization

cDNA synthesis was performed using the First Strand cDNA Synthesis kit (Pharmacia Biotech) as described by the manufacturer. One microgram of purified mRNA was reverse transcribed at 37°C with the respective 3′ cytokine primer. An aliquot of this reaction was then subjected to PCR at 94, 56 and 72°C for 20–40 cycles. The components of the PCR reactions were as follows: 1 × Perkin Elmer Buffer II, 200 μM dNTPs (Perkin-Elmer, Norwalk, CT), 1.1 mM Mg^{2+}, 10 pmol each primer and 1 unit of Taq DNA Polymerase (Perkin-Elmer). For each gene product, the optimum number of cycles was determined for linear amplification. As a control for RNA levels, β-actin was also reverse transcribed and subjected to PCR as described above. An equal aliquot of each PCR reaction was analyzed on a 1.5% agarose gel and stained with ethidium bromide (1 mg/ml) for

Table 1. RT-PCR primer and probe sequences used in this study

	Oligonucleotide	Sequence
β-actin	(5′) primer	5′-GTG GGC CGC TCT AGG CAC CAA-3′
	(3′) primer	5′-CTC TTT GAT GTC ACG CAC GAT TTC-3′
(X03765)[a]	(5′) probe	5′-TTC AAC ACC CCA GCC ATG TAC GTA GCC ATC-3′
Mouse IL-6	(5′) primer	5′-ATG AAG TTC CTC TCT GCA AGA GAC T-3′
	(3′) primer	5′-CAC TAG GTT TGC CGA GTA GAT CTC-3′
(M20572)[a]	(5′) probe	6′-CAA AGA AAT GAT GGA TGC TAC CAA-3′
Mouse IL-6Rα	(5′) primer	5′-AAT GCG TCA TCC ATG ATG CCT TGC GAG G-3′
	(3′) primer	5′-GTG GTT TAC GGT ATT GTC AGA CCC AGA GC-3′
(X51975)[a]	(5′) probe	5′-TGG AGT GAA TGG TCC CCA GAG GTC A-3′
Mouse TNF-α	(5′) primer	5′-TTC TGT CTA CTG AAC TTC GGG GTG ATC GGT CC-3′
	(3′) primer	5′-GTA TGA GAT AGC AAA TCG GCT GAC GGT GTG GG-3′
(Y00467)[a]	(5′) probe	5′-CTC CTG GCC AAC GGC ATG GAT CTC-3′
Mouse TNFR-2	(5′) primer	5′-GCC CGA AGT CTA CTC CAT CAT TTG TAG GG-3′
	(3′) primer	5′-CAT CCA CCA CAG CAT ACA GAA TCG CAA GG-3′
(X57796)[a]	(5′) probe	5′-TCT TCG GTC CTA GTA ACT GGC AGT T-3′

a: Accession number

visualization. The DNA was denatured by soaking the gel in 1.5 M NaCl, 0.5 M NaOH for 45 min. The gel was then rinsed for 5 min in double-distilled water and neutralized by washing twice in 0.5 M NaCl, 0.5 M Tris (pH 7.4), first for 30 min and then again for 15 min. The DNA was then transferred to a nylon transfer membrane (Micron Separations, West Borough, MA) by vacuum blotting. The membrane was UV cross-linked, baked at 80°C for 2 h, followed by a 2 h prehybridization at 42°C. The prehybridization and hybridization solutions (0.2 ml/cm^2) contained 1 × SSPE (150 mM NaCl, 10 mM sodium diphosphate, 1 mM EDTA), 2 × Denhardt's solution (1 × Denhardt's solution = 0.02 polyvinylpyrrolidone, 0.02% ficoll and 0.02% bovine serum albumin), 10% dextran sulfate, 2% SDS and 200 µg/ml salmon sperm DNA.

Probe labeling was performed as described by Manniatis.[17] Briefly, a 50 µl labeling reaction containing 100 ng of oligonucleotide probe, 70 mM Tris–HCl, pH 7.6, 10 mM $MgCl_2$, 50 mM DTT, 1-µCi of [^{32}P]-ATP (NEN, Boston, MA) and 20 units of T_4 was incubated at 37°C for 5 min and radiolabeled probe was purified using a G-25 Sephadex Quick Spin column. The purified labeled probe was added to the hybridization solution and hybridization was carried out at 37°C for 18 h. After the hybridization, the membranes were briefly washed at 25°C with 1 × SSPE/0.5% SDS/0.1% non-fat dry milk followed by a 30 min wash with the same solution. The membranes were then washed twice for 30 min at 45°C with 0.1 × SSPE/0.5% SDS, followed by a final wash with 0.1 × SSPE/0.5% SDS also for 30 min. The membranes were air dried and scanned using the Ambis Radioanalytic Imaging System.

Results

Complement binding *in vitro*

An *in vitro* ELISA assay for complement binding to CM101 was developed to further our understanding of the role of complement in the *in vivo* inflammatory response to CM101. In this assay, sheep anti-C3 or -C5 was used to capture C3 or C5 preincubated with biotinylated CM101 *in vitro*, respectively. Detection was accomplished via streptavidin-β-galactosidase. A typical anti-human C3 binding profile is presented in Figure 1(A). A series of normal human serum dilutions was used to preconjugate C3 or C5 with a constant amount of biotinylated CM101. Minimal binding of CM101 is observed at high concentrations of human serum where complement is far in excess. CM101 detection peaks at a serum dilution of 1:20 and then subsides with increased dilutions. Substituting anti-mouse C3 IgG for the human IgG as the capture antibody yields a similar dilution profile (Figure 1B). The observed decrease in CM101 binding at serum dilutions from 1:40 should reflect insufficient amounts of C3 to bind the available CM101 present in the preincubation step. No CM101 is detected when the same assay is performed using heat-inactivated human serum. When the ELISA capture antibody is an anti-human C5 antibody, a CM101 binding profile similar to that for C3 can be seen, although the amount of CM101 detected at each serum dilution is considerably reduced (Figure 1C). Based on normal C3 concentration in serum (1 mg/ml), we can estimate that 3–5 mol of C3 binds per mole of CM101.

Immunohistochemical analysis

CM101 Binding in vivo. Immunohistochemical analysis of tumor tissue sections from the different time points demonstrate that CM101 binds tumor endothelium within 5 min post-CM101 infusion (Figure 2). The reaction product is strong and widely spread throughout the endothelial cells of the tumor (Figure 2A). The amount of CM101 detected at successive time points decreased progressively (Figure 2B). By 60 min post-infusion, the signal was weak and scattered in the tumor endothelium (Figure 2C). No signal was observed in tumor tissue from untreated mice (Figure 2D).

Complement binding

Additional mouse tumor tissue sections, from the same time points as described above, were tested for complement activation by measuring endogenous mouse C3 binding to tumor endothelium in CM101-treated animals and controls. The ob-

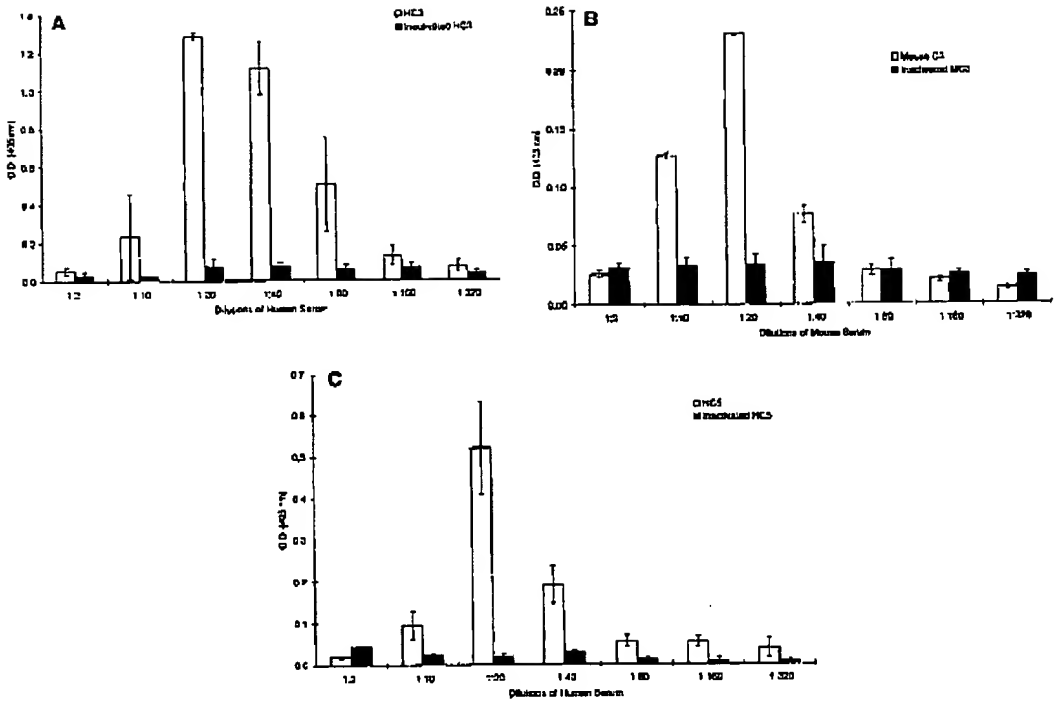

Figure 1. (A) Detection of CM101 bound to human complement C3. A constant concentration of biotinylated CM101 was conjugated to human C3 using various dilutions of either normal human serum or heat-inactivated human serum as the C3 source and detected by sandwich ELISA. Three different sera were used in these assays. Detection of CM101 peaks at a 1:20 serum dilution with a mean OD_{405} of 1.28. Biotinylated CM101 could not be detected at any serum dilution when heat-inactivated serum was used. (B) Detection of CM101 bound to murine complement C3. A constant amount of biotinylated CM101 was conjugated to murine C3 using various dilutions of either normal mouse serum or heat-inactivated mouse serum as a C3 source and detected by ELISA. The assay procedure was described in detail in Materials and methods. Three different sera were used in these assays. Peak OD_{405} (0.231) occurs at a 1:20 serum dilution. Heat-inactivated control serum remained at background absorbance levels at all dilutions tested. (C) Detection of CM101 bound to human complement C5. A constant amount of biotinylated CM101 was conjugated to human C5 using various dilutions of either normal human serum or heat-inactivated human serum as the C5 source and detected by ELISA. Three donor sera were tested in these assays. Detection of CM101 was maximal at a 1:20 serum dilution with a mean OD_{405} of 0.517. Controls using heat-inactivated serum were consistently at background levels.

served binding of an anti-mouse C3 antibody again correlated well with the binding of our anti-CM101 monoclonal antibody (Figure 3). That is, binding is intense at 5 min and diminishes with time. In addition, at 5 min, complement activation is obvious throughout the tumor tissue. In contrast, control tissues were negative in this assay. Tissue sections were also incubated with human serum to allow binding of human C3 to CM101. Figure 4(A–C) shows localization patterns for anti-human C3 antibody that are essentially identical to the pattern observed with our monoclonal anti-CM101 antibody. Control tumor tissues (from animals without infusion of CM101) incubated with human serum shows essentially no background reaction product (Figure 4D).

Activation of inflammatory cytokines

Immunohistochemistry was employed to establish the presence of cytokines and cytokine receptors at the cellular level in liver and tumor tissue pre- and post-CM101 infusion.

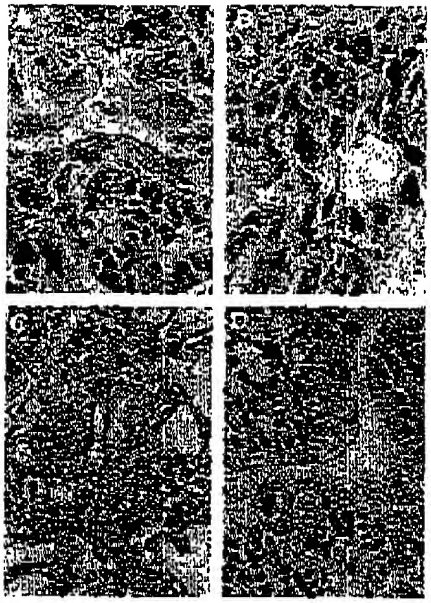

Figure 2. Endothelial localization of CM101 in transplanted mouse Madison lung tumors from mice treated with CM101 *in vivo*. The sections were incubated with anti-CM101 mouse monoclonal antibody. Control tumor sections were not exposed to CM101 *in vivo* but the sections were treated with mouse anti-CM101 monoclonal antibody. Localization of anti-CM101 IgG was demonstrated with goat anti-mouse IgG conjugated to horseradish peroxidase. (A–C) High power views (× 400) of tumor tissue at either 5, 15, and 60 min post-infusion of CM101 indicating the presence of CM101 located in association with endothelial cells of newly formed blood vessels. Note that with time the distribution and intensity of the anti-CM101 signal decreased and became scattered. (D) High power view (× 400) of a control tumor section where no reaction product could be detected.

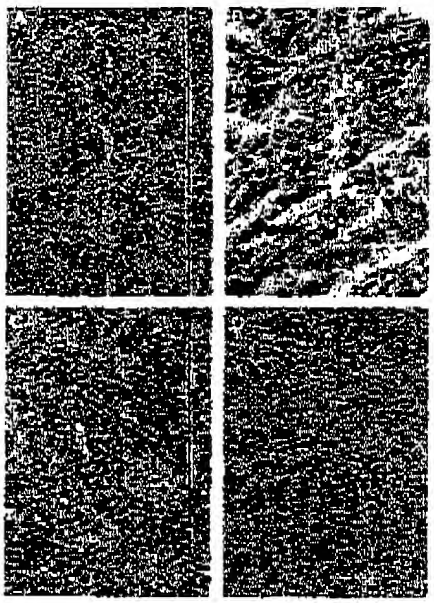

Figure 4. Endothelial localization of exogenous complement (C3) in tumor allografts in mice treated with CM101. Tumors were extracted from mice treated by I.v. injection of CM101. Tumor tissue sections were incubated with exogenous human serum followed by goat anti-human C3 IgG conjugated to horseradish peroxidase. (A–C) High power views (× 400) of tumor tissue sections at either 5, 15 or 60 min post-infusion with CM101, indicating reaction product with human complement C3. (D) Control tissue section from tumors not exposed to CM101 *in vivo*. Note lack of reaction product in the absence of CM101 treatment.

Liver tissue

IL-6. Using antibodies to IL-6, a weak staining of scattered sinusoidal lining cells was present at 5 min (Figure 5A) and did not increase with time. No staining of large vessels or hepatocytes above control levels was observed at any time point.

IL-6R. In livers from mice exposed to CM101, staining for IL-6R was observed in the endothelium of large vessels, primarily the central veins

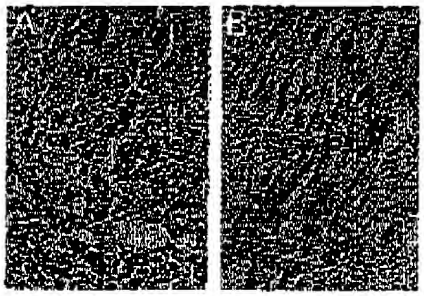

Figure 3. Evidence of endogenous complement (C3) activation in tumor tissue from mice treated with CM101. Tumors were exposed *in vivo* by I.v. injection of CM101. Tumor tissue was taken at 5 min post-infusion of CM101 and tissue sections were incubated with sheep anti-mouse complement C3 IgG horseradish peroxidase conjugate. (A) High power view (× 400) of tumor tissue indicating the presence of endogenous mouse C3 reaction product localized on the tumor vessel endothelium. (B) Control tissue from mice not treated with CM101.

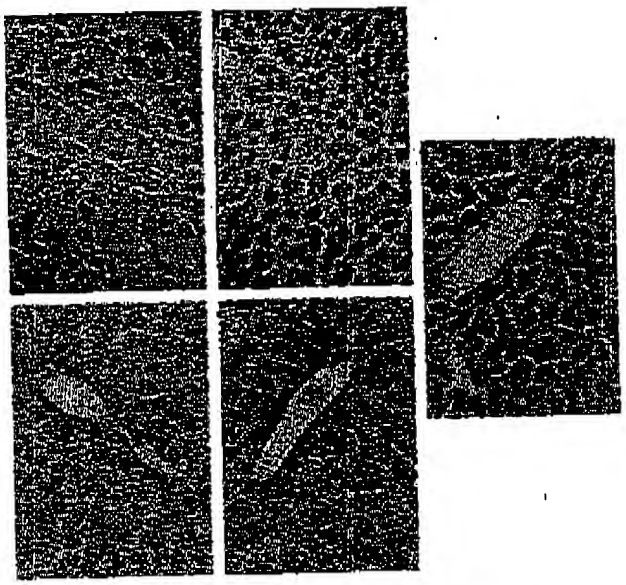

Figure 5. Detection of IL-6 and IL-6R in the livers of tumor-bearing mice treated with CM101. Liver tissue sections were incubated with rabbit anti-mouse IL-6 (A and B). (A) High power view (× 400) of liver tissue taken at 5 min post-infusion with CM101 indicates lightly stained sinusoidal lining cells. (B) Control tissue at 5 min. Localization of IL-6R (D and E). At 15 min post-infusion with CM101 (C), reaction product is largely localized to the endothelium of the major vessels. By 60 min (D), hepatocytes throughout the section display a diffuse reaction product. (E) Controls for the different time points.

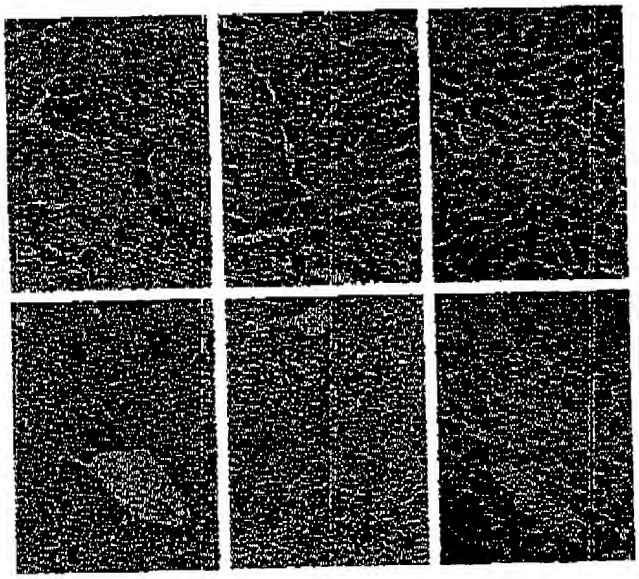

Figure 6. Localization of TNF-α and TNFR2 in sections of liver tissue from tumor-bearing mice treated with CM101. Tissue sections were reacted with rabbit anti-mouse TNF-α. (A) At 15 min post-infusion, a weak reaction product is localized to the endothelial lining of large vessels and hepatocytes stain diffusely positive. (B) At 60 min, a mild increase in reaction product is observed in the large vessel endothelium and hepatocytes were diffusely positive demonstrating a cytoplasmic staining pattern. (C) Control tissue at 5 min from untreated mice. (D) At 15 min post-infusion, reaction with anti-TNFR2 was localized in large vessel endothelial cells and hepatocytes. (E) By 30 min post-infusion, staining of the hepatocytes was faded. (F) Representative control for all time points.

and branches of the portal vein by 15 min (Figure 5C). Less conspicuous staining was also observed in branches of the hepatic artery. A few centrilobular hepatocytes stained positively with a granular cytoplasmic staining pattern. Occasional centrilobular hepatocytes were strongly positive. The endothelial lining of the large centrilobular sinusoids were weakly positive in some areas. At 30 min, granular hepatocyte staining was stronger and distributed more diffusely throughout the section. The same staining pattern was observed at 60 min (Figure 5D) post-infusion although the intensity was increased.

TNG-α. At 15 min post-infusion, a weak positive staining for TNF-α of the lining in large vessels was observed in some areas but diffusely stained hepatocytes with a cytoplasmic pattern dominate (Figure 6A). The intensity of staining of the hepatocytes decreased and an increased staining of the large vessel endothelium is apparent at 60 min (Figure 6B). Figure 6(C) is a representative control for all time points.

TNFR2. The lining of the large vessels was positive for TNFR2 at 15 min (Figure 6D) post-infusion and the intensity of vascular staining increased with time, with the highest intensity at 60 min (not shown). Hepatocytes were positive at 15 min but faded by 30 min (Figure 6E) and were virtually negative by 60 min (not shown). The sinusoidal lining cells were positive at 15 and 30 min with weaker staining by 60 min (Figure 6E).

Tumor tissue

Infiltration of the tumor by leukocytes is striking at the 5 min time point and continues over the studied 60 min time period.

IL-6. Tumor-infiltrating macrophages stained positively for IL-6 at 30 min (Figure 7A). By 30 min post-infusion, we observed weak nuclear and cytoplasmic staining within the tumor cells, and this staining increased with time (not shown). Small blood vessels were strongly positive by 30 min (Figure 7A). The strongest vascular staining was observed at 30 min (Figure 7A) and was slightly decreased by 60 min (not shown).

IL-6R. Tumor-infiltrating macrophages and occasional tumor cells were positive at 5 min with a cytoplasmic staining pattern and nuclear staining was observed in some tumor cells by 30 min (Figure 7C) with a slight increase by 60 min (Figure 7D).

TNF-α. The strongest staining intensity for TNF-α was seen in tumor-infiltrating macrophages (Figure 8A and B). This staining increased with time and was maximal at 60 min (Figure 8B). We observed a weak TNF-α cytoplasmic staining in tumor cells at 15 min, and the intensity increased with time and was strongest by 60 min. Staining of tumor blood vessels above control levels was not observed.

TNFR2. Staining for TNFR2 was confined to vessels and was negative in tumor cells (Figure 8D and E). Staining in tumor endothelium was distinct at 15 min (Figure 8D), increased with time and was slightly stronger at 60 min (Figure 8E).

RT-PCR

RT-PCR was used to establish a semi-quantitative profile for the mRNA expression of IL-6, IL-6R, TNF-α and TNFR2 after treatment of tumor-bearing mice with CM101. Samples of either tumor or liver tissues were taken at time intervals of 15, 30 and 60 min after treatment of CM101 and from untreated controls.

Liver tissue

IL-6 mRNA expression increased several fold within 15 min after treatment with CM101 (Figure 9A). IL-6 mRNA levels continued to be elevated at the 60 min time point where a 7-fold increase in expression was observed.

TNF-α. TNF-α expression was increased 4-fold at 15 min post-infusion of CM101 (Figure 9A). Levels of expression at 30 and 60 min were only slightly (1.5-fold) above the expression levels observed in untreated control tissue at any time point.

IL-6R. mRNA expression of IL-6R from liver tissues was elevated several fold within 15 min after CM101 treatment compared to controls (Figure 9B). By 30 min, however, IL-6R mRNA expression returned essentially to background levels.

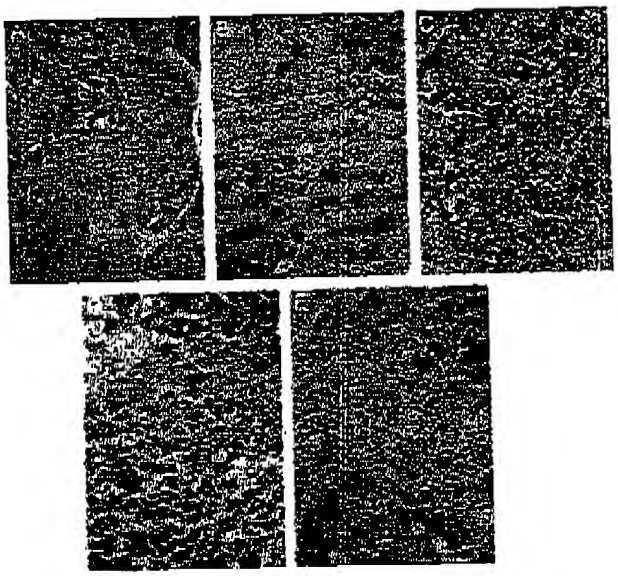

Figure 7. Localization of IL-6 and IL-6R in tumor tissue from mice treated with CM101. (A) Anti-IL-6 reaction product at 30 min post-infusion; one clearly sees immunostained endothelium and infiltrating macrophages (arrows). (B) Representative control from untreated mice at different times. Tumor cells and macrophages stained with anti-IL-6R 30 (C) and 60 (D) min post-infusion with CM101. (E) Representative control tissue from mouse not treated with CM101.

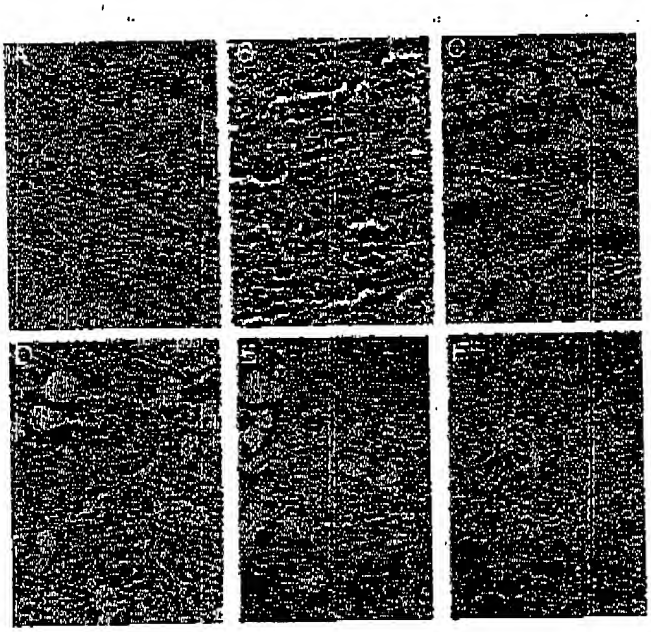

Figure 8. Immunolocalization of TNF-α and TNFR2 in tumor from mice post-infusion with CM101. The tissue was reacted with either anti-mouse TNF-α or anti-mouse TNFR2. (A) By 30 min post-infusion with CM101, TNF-α was observed primarily with monocytes and lymphocytes located within the tumor. (B) By 60 min, a larger number of macrophages stain with higher intensity. (C) Representative control. (D) By 15 min post-infusion with CM101, anti-TNFR2 was localized to tumor vasculature. (E) At 60 min, the same localization pattern was observed with slightly increased intensity of staining. (F) Representative control section for TNFR2.

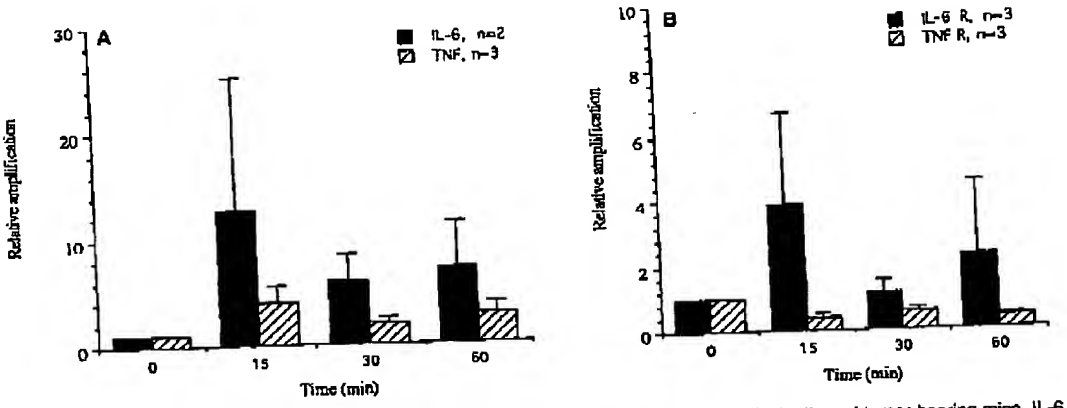

Figure 9. Effects of CM101 treatment on IL-6, IL-6R, TNF-α, and TNFR2 mRNA expression in the liver of tumor-bearing mice. IL-6 mRNA expression levels in liver tissue increased with time, peaking at 15 min post-infusion of CM101. TNF-α expression level also peaked at 15 min and then decreased somewhat with time (A). IL-6 receptor mRNA expression level in the liver was elevated 4-fold within 15 min but decreased by 60 min (B). Levels of TNFR2 mRNA were essentially unchanged at the time intervals measured (B).

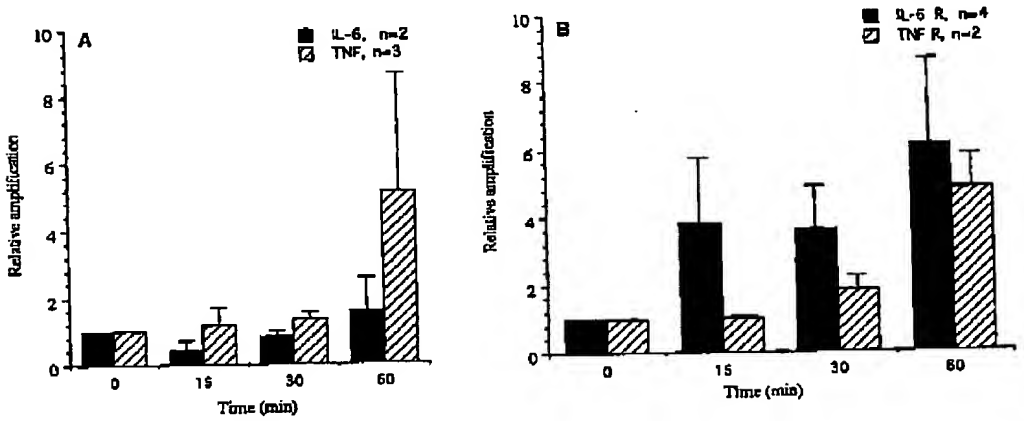

Figure 10. Effects of CM101 treatment on mRNA expression levels of IL-6, IL-6R, TNF-α, and TNFR2 of the tumor in tumor-bearing mice. In tumor tissues, receptor mRNA expression patterns paralleled the respective cytokine mRNA. IL-6 and TNF-α mRNA expression levels in tumor tissue increased with time, peaking at 60 min post-infusion of CM101 (A). Levels of TNFR2 mRNA were elevated 5-fold by the 60 min time point (B).

TNFR2. TNFR2 mRNA levels were essentially unchanged during the time intervals observed (Figure 9B).

Tumor tissue

IL-6. mRNA levels for IL-6 increased only slightly by 60 min compared to control (Figure 10A).

TNF-α. A significant increase of TNF-α mRNA was observed by 60 min (Figure 10A) correlated with the increased number of infiltrating TNF-α positive macrophages.

IL-6R. Message for IL-6R increased 4-fold by 15 min and was further elevated by 60 min (Figure 10B), consistent with the immunohistochemical data.

TNFR2. Immunohistochemically, the increase in TNFR2 is cofined to the tumor endothelium and the message for TNFR2 in the tumor tissue increases 5-fold by 60 min (Figure 10B).

Discussion

CM101 has been administered to cancer patients with encouraging results. The collected data supported a mechanism of action whereby CM101 acted by inducing a tumor-targeted inflammatory response which was evidenced by a systemic dose- and time-dependent cytokine cascade, tumor pain, and a biopsy demonstrating infiltration of inflammatory cells[11] and tumor apoptosis.[23] Engagement of tumor endothelium in the inflammatory process was corroborated by elevated systemic sE-Selectin in response to CM101.[12] It is well understood that the products of the complement cascade mediate a wide range of proinflammatory activities including altered vascular permeability and tone, leukocyte chemotaxis,[18] increased cytokine and adhesion molecule expression,[19,20] and activation and lysis of a variety of cell types, all of which are applicable to the action of CM101.

Humans and mice are susceptible as newborns to GBS infection. This unique feature allows us to study the molecular mechanism of CM101 in mice,[11,12] and make extrapolations toward human cancer patients.[7,11] Infusion of picomole levels of CM101 into tumor-bearing mice induced systemic cytokines, tumor neovascularitis and infiltration of inflammatory cells with subsequent inhibition of tumor growth, and tumor ablation.[7–9] Mice without a tumor do not exhibit a systemic cytokine response to CM101.[9] We have recently reported on the effect of CM101 on tumors in the ear skin of mice.[10] Infusion i.v. of CM101 resulted in neovascularitis with proinflammatory activation of tumor endothelial cells, infiltration of leukocytes into the tumor interstitium and subsequent tumor cell apoptosis.[10]

The results from our mouse model presented here offer detailed immunohistochemical data in support of the suggested mechanism of action for CM101. We postulate that this mechanism applies also to the cancer patients. Clearly, CM101 binds specifically to tumor neovasculature within minutes of i.v. infusion. Complement activation by the alternative pathway is evidenced by immunolocalization of endogenous C3 within the tumor. Our observation that human C3 also binds to CM101 within mouse tumor neovasculature strongly suggests that the anti-tumor activity of CM101 is similar in tumor-bearing mice and human cancer patients.

The inflammatory response is evidenced in the patients by systemic cytokines,[11,12] and is further substantiated in this mouse model by elevation of cytokines systemically[9] and intracellularly as shown by increased message for the corresponding cytokine or its receptor and a rapid early infiltration of the tumor by activated leukocytes.

A short burst of TNF-α and TNFR2 expression was observed immunohistochemically early in the liver post-CM101 treatment corresponding to an early brief increase in mRNA expression although this did not translate into hepatotoxicity.[7] However, TNFR2 is present in the tumor endothelium and message is continually up-regulated over the 60 min examination time. The corresponding TNF-α stain is seen early only in infiltrating macrophages. The massive infiltration of TNF-α-producing macrophages results in an increase of TNF-α in the cytoplasm of tumor cells.

TNF-α has been successfully used to destroy tumor vasculature by intralesional infusion in clinical trials.[21] The anti-angiogenic effect of CM101 is postulated to occur via its ability to target a complement (C3)-mediated leukocyte killing[13] to the tumor neovasculature. The observations described herein support that vascular damage to more mature tumor vasculature occurs through TNF-α/TNFR2-mediated apoptosis,[22] with TNF-α being delivered by tumor infiltrating macrophages and TNFR2 being up-regulated in the tumor endothelial cells as a consequence of the CM101-induced cytokine cascade.[9,11]

The apoptotic tumor cells seen at 60 min in the ear model[10] explains the mechanism of tumor ablation seen in mice[8] and, in two instances, in the early clinical development of CM101.[11,23]

Toxicology studies on nude mice following repeat infusions of CM101 showed no toxicity to any organ.[7] A weak binding of CM101 to Kupffer cells in liver tissue can, however, be seen within 5 min post-CM101 infusion (data not shown). There is neither complement activation nor infiltration of inflammatory cells following binding to presumably the lectin receptors. The binding of CM101 to Kupffer cells could be blocked by co-

16. Oncor. *In Situ Apoptosis Detection* 1994.
17. Sambrook J, Fritsch EF, Maniatis T. *Molecular Cloning – A Laboratory Manual*, 2nd edn. Cold Spring Harbor, NY: Cold Spring Harbor Laboratory Press 1989: 10.51–10.69.
18. Liszewki KM, Atkinson JP. The complement system. In: Paul WE, ed. *Fundamental Immunology*, New York: Raven Press, 1993: 917–939.
19. Ochs HD, Nonoyama S, Zhu Q, *et al.* Regulation of antibody responses: the role of complement and adhesion molecules. *Clin Immunol Immunopathol* 1993; 67, 33–40.
20. Ward PA. Role of complement, chemokines and regulatory cytokines in acute lung injury (Review). *Ann NY Acad Sci* 1996; 796, 104–112.
21. Parkinson DR. Present status of biological response modifiers in cancer. *Am J Med* 1995; 99, 545.
22. Donato NJ and Perez M. Tumor necrosis factor-induced apoptosis stimulates p53 accumulation and -21 WAF1 proteolysis in ME-180 cells. *J Biol Chem* 1998; 273, 5067–5072.
23. Hellerqvist CG, Wang E, Wamil BD, *et al.* Evidence of induced apoptosis in cancer patients treated with CM101. *Proc Am Soc Clin Oncol* 1997; 16, 546a.
24. Hellerqvist CG, Yan HP, Carter CE, *et al.* Identification of GBS toxin in neonatal fluids from group B streptococcus (GBS) infected neonates. *Proc Am Soc Microbiol* 1996; B-348, 215.
25. Hellerqvist CG, Yan HP, Carter CE, *et al.* CM101 induces a complement-activated inflammatory response targeting tumor neovasculature. *Proc Am Ass Cancer Res* 1996; 73, 487 (abstr 3328).

J Cancer Res Clin Oncol (1997) 123:173–179

ORIGINAL PAPER

Barbara D. Wamil · Gary B. Thurman
Hakan W. Sundell · Russell F. DeVore
Gail Wakefield · David H. Johnson · Yue-Fen Wang
Carl G. Hellerqvist

Soluble E-selectin in cancer patients as a marker of the therapeutic efficacy of CM101, a tumor-inhibiting anti-neovascularization agent, evaluated in phase I clinical trial

Received: 12 May 1995/Accepted: 6 September 1996

Abstract A polysaccharide toxin, GBS toxin, is produced by group B *Streptococcus* (GBS) isolates from neonates who died of "early-onset disease". GBS toxin, named CM101 in the clinic, was hypothesized, on the basis of our previous in vivo studies, to induce inflammation in pulmonary neovasculature in neonates by cross-linking of embryonic receptors still expressed after birth and in tumor neovasculature in adults. Immunohistochemical in vitro analysis of human biopsies showed that tumor neovasculature is indeed a binding site for CM101. In vivo studies in mice have demonstrated that CM101 induced inflammatory responses in neoplastic tumor neovasculature causing inhibition of tumor growth and tumor cell necrosis. These experimental observations warranted a phase I clinical trial for CM101 as an anti-neovascularization agent in human cancer therapy. Cancer patients received one cycle of therapy consisting of three treatments during 1 week. CM101 was administered over 15 min by i.v. infusion. Dosages of 7.5 μg/kg (1 U/kg), $n = 3$; 15 μg/kg (2 U/kg), $n = 6$; 24.75 μg/kg (3.3 U/kg), $n = 3$; and 37.5 μg/kg (5 U/kg), $n = 3$ were used. Enzyme-linked immunosorbent sandwich assays (ELISA) of the patients' sera showed a marked elevation of soluble E-selectin with a peak concentration observed at 8–12 h after each CM101 infusion. The average baseline value for soluble E-selectin prior to the first treatment was 97.3 ± 23.4 ng/ml (mean ± SEM, $n = 15$) and the average peak level at 8 h was 441.6 ± 62.4 (mean ± SEM, $n = 15$; $P < 0.001$). Subsequent treatments gave average maximum soluble E-selectin levels again at 8 h of 466.9 ± 87.6 and 412.0 ± 67.8 ng/ml, for treatments 2 and 3 respectively. Baseline values for treatments 2 and 3 were 192.3 ± 26.4 and 226.4 ± 26.1 ng/ml respectively ($p < 0.01$ versus treatment 1). Out of 15 patients, 5 showed tumor reduction or stabilization and were given additional cycles of therapy. CM101 induced an increase in soluble E-selectin levels, which remained elevated over baseline at the start of the following treatment cycles. The baseline remained elevated for several weeks after the final treatment, i.e., $P < 0.01$ for levels before treatment 1 compared to those at week 4 after treatment. Elevated soluble E-selectin is considered proof of endothelial engagement in an inflammatory process. Our data support the contention that the inflammatory response observed in these cancer patients is targeting the tumor neovasculature and that measurement of soluble E-selectin levels in patients treated with CM101 can provide important information on the magnitude of CM101-mediated neovascular endothelial activation and tumor cell damage in cancer of endothelial origin, or cancer with a major neo-angiogenic component.

Key words CM101 · GBS toxin · Cancer · Inflammation · Neovascularization · Angiogenesis

Abbreviations *GBS* group B *Streptococcus* · *CM101* polysaccharide *GBS* bacterial exotoxin · *TNFα* tumor necrosis factor · *IL* interleukin

This work was supported by CarboMed, Inc., 5115 Maryland Way, Brentwood, Tennessee 37027, USA, and National Institute of Health, General Clinical Research Center grant M01 RR00095

B.D. Wamil · G.B. Thurman · Y.-F. Wang · C.G. Hellerqvist (✉)
Department of Biochemistry, Vanderbilt University, Nashville, Tennessee 37232-0146, USA.
Fax: 615 322 6354

H.W. Sundell
Department of Pediatrics, Vanderbilt University, Nashville, Tennessee 37232-2370, USA

R.F. DeVore · G. Wakefield · D.H. Johnson
Department of Medicine, Vanderbilt University, Nashville, Tennessee 37232-5536, USA

Introduction

Group B *Streptococcus* of different serotypes, isolated from neonates who had died from respiratory distress,

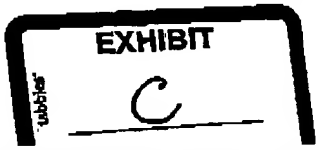

infusion of biotinylated CM101 with equal molar concentrations of mannan and asialofetuin, whereas binding to tumor neovasculature was not (data not shown).

The data presented herein lend support to a mechanism of action where CM101 binds tumor neovasculature and complement C3 is activated resulting in C3b bound to CM101 and C3a being released as a chemoattractant for leukocytes.[24,25] C3a is evidenced systemically in cancer patients 30 min post-infusion with CM101.[23] C3b bound to CM101, a polysaccharide, fulfills the requirement described by Ross[13] for the two components, C3b and a polysaccharide, necessary for phagocytosis by leukocytes. The subsequent cytokine cascade[9,11] leads to further infiltration of activated leukocytes and up-regulation of TNFR2 in tumor endothelium, which combined with intra-tumor TNF produced by infiltrating leukocytes, contributes further to the tumor ablative effect of CM101.

Conclusion

We have demonstrated that CM101 binds specifically to tumor endothelium within minutes and activates complement by the alternative pathway. The opsonization leads to a cytokine cascade infiltration of activated leukocytes which mediate the observed tumor ablation. Immunohistochemical and RT-PCR analysis allow us to conclude that IL-6 and TNF-α are produced in the tumor by infiltrating leukocytes, and that tumor endothelium is sensitized for destruction through induced up-regulation of TNFR2.

References

1. Hellerqvist CG, Rojas J, Green RS, *et al.* Studies on group B β-hemolytic streptococcus. I. Isolation and partial characterization of an extracellular toxin. *Pediatr Res* 1981; 15, 892–898.
2. Rojas J, Green RS, Hellerqvist CG, *et al.* Studies on group B β-hemolytic streptococcus. II. Effects on pulmonary hemo-dynamics and vascular permeability in unanesthetized sheep. *Pediatr Res* 1981; 15, 899–904.
3. Sandberg K, Edberg KE, Fish W, *et al.* Thromboxane receptor blockage (SQ 29548) in group B streptococcal (GBS) toxin challenge in young lambs. *Pediatr Res* 1994; 35, 571–579.
4. Rojas J, Larrson LE, Hellerqvist CG, *et al.* Pulmonary hemodynamic and ultrastructural changes associated with group B β-hemolytic streptococcal toxemia in adult sheep and newborn lambs. *Pediatr Res* 1983; 17, 1002–1008.
5. Hellerqvist CG. Therapeutic agent and method of inhibiting vascularization of tumors. *US Patent 5,010,062*, April 23, 1991.
6. Sundell HW, Yan H-P, Wu K, *et al.* Isolation and identification of group B beta-hemolytic streptococcal (GBS) toxin from septic newborn infants. *Pediatr Res* 1997; 39, 302A.
7. Hellerqvist CG, Thurman GB, Page DL, *et al.* Anti-tumor effects of GBS toxin: a polysaccharide exotoxin from group B β-hemolytic streptococcus. *J Cancer Res Clin Oncol* 1993; 120, 63–70.
8. Thurman GB, Russell BA, York GE, *et al.* Effects of GBS toxin on long-term survival of mice bearing transplanted Madison lung tumors. *J Cancer Res Clin Oncol* 1994; 120, 479–484.
9. Hellerqvist CG, Thurman GB, Russell BA, *et al.* Anti-tumor effects of GBS toxin are caused by induction of a targeted inflammatory reaction. In: Maragoudakis ME, Gullino PM, Lelkes PI, eds. *NATO/ASI Series – Angiogenesis: Molecular Biology, Clinical Aspects, Series A: Life Sciences*. New York: Plenum 1993; 263, 265–269.
10. Thurman GB, Page DL, Wamil BD, *et al.* Acute inflammatory changes in subcutaneous microtumors in mice ears induced by intravenous CM101 (GBS toxin). *J Cancer Res Clin Oncol* 1996; 122, 549–553.
11. DeVore RF, Hellerqvist CG, Wakefield GB, *et al.* A phase I study of the antineovascularization drug CM101. *J Clin Cancer Res* 1997; 3, 365–372.
12. Wamil BD, Thurman GB, DeVore RF, *et al.* Soluble e-Selectin in cancer patients as a marker of the therapeutic efficacy of CM101, a tumor inhibiting agent, evaluated in phase I clinical trial. *J Cancer Res Clin Oncol* 1997; 123, 173–179.
13. Vervicka V, Thornton BP, Ross GD. Soluble beta-glucan polysaccharide binding to the lectin site of neutrophil or natural killer cell complement receptor type 3 (CD11b/CD18) generates a primed state of the receptor capable of mediating cytotoxicity of iC3b-opsonized target cells. *J Clin Invest* 1996; 98, 50–61.
14. Hellerqvist CG, Lloyd S, Wang B, *et al.* Modulation of interleukin-12 mRNA expression in leukocytes of cancer patients treated with CM101. *Ann NY Acad Sci* 1995; 795, 346–348.
15. Fu C, Career CE. Detection of circulating antigen in human schistosomiasis japonica using monoclonal antibody. *Am J Trop Med Hyg* 1990; 42, 347–351.

produces a polysaccharide exotoxin, which was isolated from the culture medium and named GBS toxin (Hellerqvist et al. 1981; Rojas et al. 1981). GBS toxin, when infused into sheep, was found to induce a lung pathophysiology similar to that seen in diseased human neonates diagnosed with the early-onset disease (Rojas et al. 1983; Sundell et al. 1990). Susceptibility in human neonates to GBS pneumonia, "early-onset disease" is limited to 4 days after birth. Hellerqvist proposed that GBS toxin bound to embryonic receptors in developing lung vasculature and could bind also to pathological neovasculature in human tumors but not to mature vasculature in vital human organs (Hellerqvist 1991). Subsequently, GBS toxin was shown to bind to capillary endothelium of human tumor tissue (Hellerqvist et al. 1993).

Mice, like humans, are susceptible to GBS at birth but not shortly thereafter, and, in mouse tumor models, GBS toxin was found to be effective against neoplastic disease, bringing about inhibition of tumor growth (Hellerqvist et al. 1993). Extended treatment with GBS toxin was also shown to prolong survival time significantly (Thurman et al. 1994a). Previous and ongoing studies revealed a potential mechanism of action of GBS toxin, suggesting a complement-activated, cytokine-driven (Sundell et al. 1996; Hellerqvist et al. 1995a; 1996; Wamil et al. 1996) inflammatory response targeting the tumor neovasculature. This response resulted in vasodilatation, infiltration with granulocytes, lymphocytes and monocytes, endothelial and tumor cell necrosis, and capillary thrombosis (Hellerqvist et al. 1993; Thurman et al. 1996). On the basis of these neonatal, developmental and experimental observations, we are developing GBS toxin, now called CM101, as an anticancer agent targeting the tumor neovasculature.

An inflammatory event includes adhesion of subsets of activated leukocytes to activated endothelium (Gearing and Newman 1993) via E-selectin. Transcription of the gene for soluble E-selectin is subsequently induced by the inflammatory cytokines interleukin-1β (IL-1β) (Whitley et al. 1994) and tumor necrosis factor α (TNFα) (Meekins et al. 1994). The migration of leukocytes to the extravascular tissue, initiated by infection, injury, ischemia, etc., is essential for normal host-defense mechanisms and is an example of the complex role of adhesion molecules (Mackay and Imhof 1993). Elevated systemic soluble E-selectin is considered proof of the engagement of endothelium in the inflammatory processes (Bevilacqua and Nelson 1993) in numerous diseases and disorders including septic shock (Newman et al. 1993). Elevated soluble E-selectin is also seen in cancer patients (Banks et al. 1993; Sawada et al. 1994; Hakomori 1994).

The overall objective of the phase I clinical study of CM101 was to establish the maximum tolerated dosage, toxicity profiles and possible tumor responses. Those results are being published elsewhere (DeVore et al. 1996). In this study, we report on the serum levels of soluble E-selectin in 15 cancer patients from 15 min before to 12 h during CM101 treatment. The data reported here to demonstrate that i.v. infusion of picomole quantities of CM101 into cancer patients leads to an inflammatory response presumed to target the tumor neovasculature. Preliminary and partial results of this work have been presented recently (Hellerqvist et al. 1995b; DeVore et al. 1995).

Materials and methods

Patient selection

This study was carried out at the Clinical Research Center at Vanderbilt University Medical Center. Patients with refractory malignancies or resistance to standard therapy were qualified for the study. Patients with an Eastern Clinical Oncology Group (ECOG) performance status no higher than 2, older than 18 years and with a life expectancy of 12 weeks were eligible. In addition, the following criteria had to be met: a bone marrow-white blood cell count of at least 3000/μl and a platelet count of at least 100 000/μl; a renal serum creatine no greater than twice the upper limit of normal; and hepatic factors no more than twice the upper limit of normal. Patients had not to have received antineoplastic therapy in the 4 weeks prior to treatment. The maximum tolerated dose was reached with the last three patients. One patient with hypothyroidism of the 15 was withdrawn from the study after the first infusion because of severe flu-like symptoms. The 15 patients [9 male, 6 female; mean age = 53.8 years, median = 52.5 years; range 37–63] years received three treatments (1 week); 5 patients experienced disease stabilization or tumor shrinkage warranting additional treatment cycles (every Monday, Wednesday, and Friday). Patients selected for this study had been diagnosed with the following types of neoplasms (all with metastases): colorectal tumors (4 patients), biliary tract carcinoma (1), duodenal adenocarcinoma (1), esophageal cancer (1), hepatocellular carcinoma (1), Kaposi sarcoma (1), leiomyosarcoma (2), ovarian tumor (2), prostate gland tumor (1), renal cell cancer (2). Thirteen patients had undergone chemotherapy; 13 of the 15 received surgical treatment and 7 out of the 15 received radiation therapy.

Drug administration

CM101 in saline was administered intravenously by infusion pump over 15 min every Monday, Wednesday, and Friday at 7.5 μg/kg (1 U/kg), 15 μg/kg (2 U/kg), 24.75 μg/kg (3.3 U/kg), and 37.5 μg/kg (5 U/kg). 1 U/kg is defined as the amount of CM101 that induces an elevation of pulmonary artery pressure in a sheep model by 100%–150% and reduces the white blood cell count by 40%–60% (Hellerqvist et al. 1981; Rojas et al. 1983). Cohorts of 3 patients were treated at each CM101 dose level. Drug doses were escalated on a modified Fibonacci schedule only if no more than 1/3 patients at a given dose level experienced grade III or higher toxicities. If more than 1 patient experienced grade III or higher toxicities, 3 additional patients were treated at the same dose level. If no additional grade III toxicities were encountered, the dose was subsequently increased one level (DeVore et al. 1996).

Specimen collection

Venous blood samples for determination of the serum concentration of soluble E-selectin were obtained 15 min before infusion, and 2, 4,

8, and 12 h after infusion. Blood was drawn into serum vacutainer tubes. Samples were allowed to clot for 2–4 h at room temperature and the serum was collected after centrifugation and stored frozen at −80 °C until assayed.

Soluble E-selectin measurements

Concentration of serum soluble E-selectin was measured using a commercially available ELISA kit (catalog no. BBE 2B, R&D Systems, Minneapolis, Minn). The average soluble E-selectin serum level for normal humans is 46.25 ng/ml with a range from 29.14 to 63.36 ng/ml ± 1 SD (R&D Systems) in the assays we have used. The ELISA were performed according to the manufacturer's instructions. Data examination was performed using Lotus 1-2-3 software.

Statistical analysis

Statistical analysis and significance of differences in parametric data were tested with the paired *t*-test (mean ± 1 SEM). For non-parametric data, i.e., percentages of controls, the significance of differences was determined using the Clopper-Pearson test for dichotomous outcomes ($\alpha = 0.05$; Hollander and Wolfe 1973).

Results

Effect of CM101 on soluble E-selectin levels

A gradual increase in soluble E-selectin levels was determined in sera of cancer patients who were treated with CM101. All 15 patients receiving 1–5 U/kg of CM101 had markedly and consistently elevated serum levels of soluble E-selectin, the peak concentration being reached between 4 h and 8 h following infusion (Fig. 1).

The average baseline soluble E-selectin serum concentration prior to the first treatment (treatment 1) with CM101 was 97.3 ± 23.4 ng/ml (± SEM, $n = 15$). This is insignificantly higher than the normal range of 29.1–63.4 given by the manufacturer of the soluble E-selectin kit. The peak average level at 441.6 ± 62.4 ng/ml was achieved at about 8 h after infusion (treatment 1; $n = 15$; $P < 0.001$). This CM101-induced increase in systemic soluble E-selectin concentration began to decrease at 12 h but did not reach baseline levels before the following treatment 48 h later. Baseline values at the time of treatments 2 and 3 were significantly elevated: 192.3 ± 26.4 ng/ml compared to treatment 1 ($P < 0.01$) and 226.4 ± 26.1 ng/ml compared to treatment 1 ($P < 0.01$) respectively (black circles in Fig. 1). Soluble E-selectin levels peaked during treatments 2 and 3 after about 8 h at 466.9 ± 87.6 ng/ml and 412.0 ± 67.8 ng/ml respectively, $n = 15$ ($P < 0.001$). Soluble E-selectin levels remained elevated above baseline for several weeks after infusion (Fig. 1).

Dose-dependent effects of CM101 on soluble E-selectin levels

Administration of four doses of CM101 (1 U/kg, 2 U/kg, 3.3 U/kg and 5 U/kg) in the Monday/Wednesday/Friday protocol, revealed a dose-dependent increase in serum soluble E-selectin (Fig. 2A–D).

Average soluble E-selectin levels in 3 patients receiving 1 U/kg increased during the first treatment from 78.9 ± 12.1 ng/ml to 147.8 ± 10.9 ng/ml ($P < 0.01$). By the third infusion, soluble E-selectin levels reached 176.4 ± 18.6 ng/ml ($P < 0.01$ versus treatment 1). At 4 weeks after the third CM101 infusion, soluble E-selectin levels were 110.1 ± 37.5 ng/ml; $P < 0.05$, still 40% higher than the original baseline control.

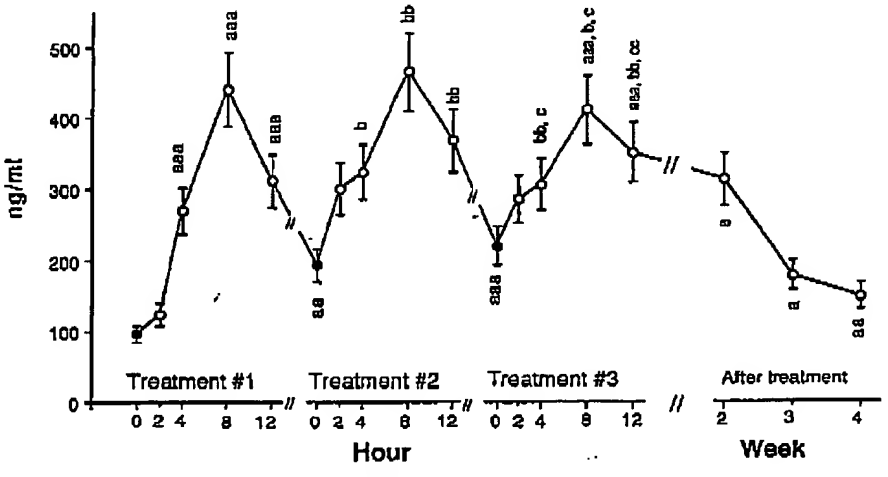

Fig. 1 Soluble E-selectin levels in response to CM101 average soluble E-selectin levels in serum from 15 patients following three infusions (blackened circles) of CM101: 1 U/kg ($n = 3$), 2 U/kg ($n = 6$), 3.3 U/kg ($n = 3$) and 5 U/kg ($n = 3$), including follow-up during weeks 2, 3 and 4 after infusion. Statistical significance is marked by (*a*) curve analysis compared to the soluble E-selectin levels of treatment 1, (*b*) curve analysis versus treatment 2, and (*c*) curve analysis versus treatment 3

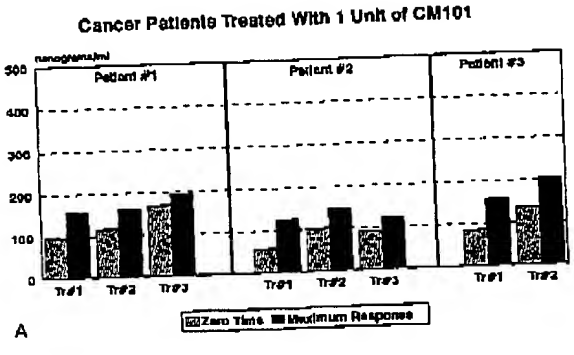

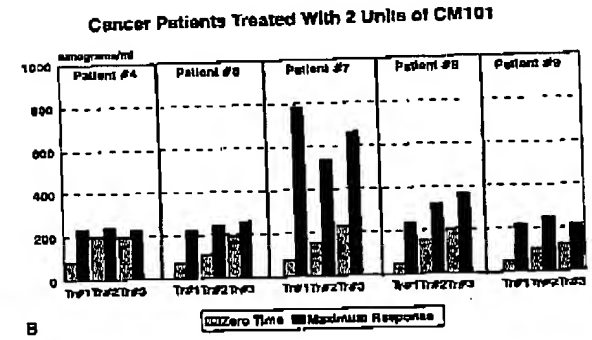

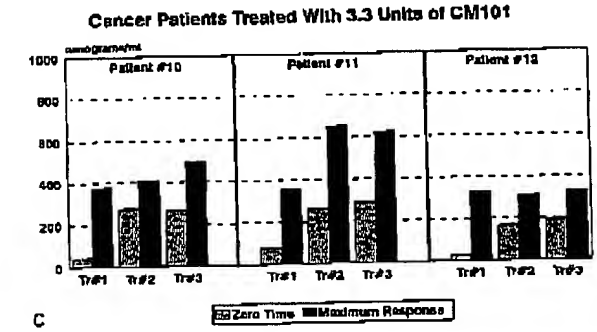

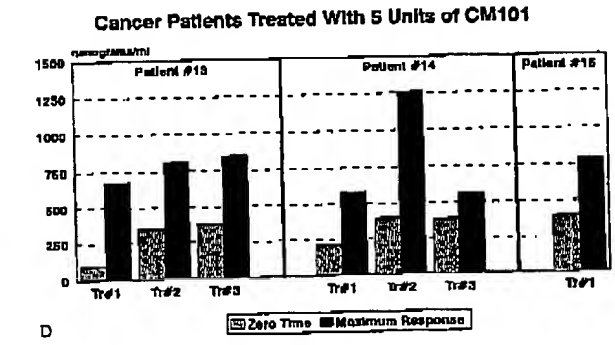

Of the 6 patients treated with 2 U/kg CM101, 5 received three infusions (Fig. 2B). Peak levels of soluble E-selectin were 328.1 ± 90.9 ng/ml over the baseline 66.9 ± 5.8 ng/ml at treatment 1, $P < 0.01$, and 376.2 ± 112.6 ng/ml at treatment 3, $P < 0.001$). Measurement of soluble E-selectin levels 2 weeks after the last treatment still showed a substantial elevation, 348.9 ± 105.4 ng/ml, $P < 0.05$ versus control, $n = 5$. The soluble E-selectin concentration 3 weeks after treatment cessation was 243.7 ± 64.3 ng/ml, $P < 0.01$, a four-fold elevation over the control for this group.

Patients receiving 3 U/kg of CM101 at treatment 1 reached soluble E-selectin concentrations of 353.0 ± 13.7 ng/ml, $P < 0.001$ versus control: 60.3 ± 17.9 ng/ml, $n = 3$ (Fig. 2C). The baseline for treatment 3 was 248.0 ± 28.3 ng/ml, and the peak treatment 3 was 449.3 ± 88.3 ng/ml ($P < 0.001$ versus control prior to treatment 1). The soluble E-selectin level did not reach baseline within 4 weeks (the end of the study protocol).

In 3 patients treated with the highest dose of CM101, 5 U/kg, soluble E-selectin baseline concentration was 226.7 ± 89.4 ng/ml (Fig. 2D). It doubled within 4 hours (529.1 ± 106.1 ng/ml) and reached the maximum increase at 12 h (617.6 ± 65.1 ng/ml).

The baseline measurement prior to treatment 2 (367.5 ± 24.1 ng/ml, $P < 0.005$) was increased compared to the treatment 1 control. A peak of soluble E-selectin level during treatment 2 was reached at 12 h (992.4 ± 267.1 ng/ml). The baseline for treatment 3 was 383 ± 1.2 ng/ml and there was a peak at 12 h of 665.9 ± 104.1 ng/ml. Two weeks after treatment 3, levels of soluble E-selectin were still elevated and the average concentration was 429.3 ± 83.9 ng/ml.

Change in soluble E-selectin level in response to prolonged therapy with CM101

No significant change in response amplitudes was measured after up to 11–12 treatments had been performed in 2 patients receiving an extended treatment protocol (patient 8, Fig. 3A; patient 11, Fig. 3B). Patient 7, suffering from Mediterranean classic Kaposi sarcoma, experienced a very significant improvement in his disease status. From having had 20–30 new lesions every month, the patient had only 1 new lesion over the next five cycles. Soluble E-Selectin levels in this patient showed a continuous decrease both in amplitude and in difference in values before and after treatment over the period of investigation (Fig. 3C).

Fig. 2A–D CM101 dose-dependent soluble E-selectin response. Serum levels of soluble E-selectin in patients receiving CM101 every Monday, Wednesday and Friday (treatments 1, 2 and 3) at 1 U/kg (A), 2 U/kg (B), 3.3 U/kg (C), and 5 U/kg (D)

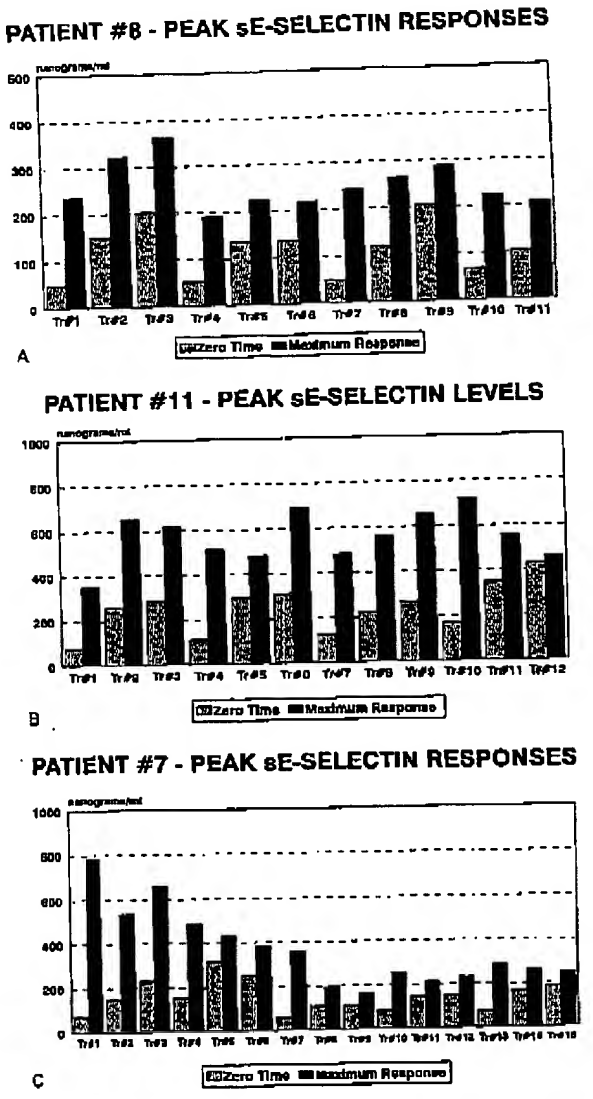

Fig. 3A–C Prolonged treatment with CM101. Soluble E-selectin levels in response to CM101 in patient 8 (A), patient 11 (B), and patient 7 (C)

Discussion

CM101, formerly known as GBS toxin, is a high-molecular-mass polysaccharide (Hellerqvist et al. 1981). CM101 produces a strong inflammatory response in sheep lung, with pulmonary sequestration of granulocytes and extensive capillary endothelial damage (Rojas et al. 1983; Hellerqvist et al. 1993). The pathophysiology associated with CM101 or GBS toxin in the sheep model mimicks the often-tragic respiratory distress associated with neonatal GBS pneumonia. The loss of susceptibility to GBS toxin in neonates 4 days after birth led to the hypothesis that CM101 would bind only to developing neovasculature in the neonate and that a similar susceptibility to binding would recur in humans only in pathological neovasculature (Hellerqvist 1991). We demonstrated, in a series of experiments in normal and tumor-bearing mice which, like humans, are susceptible to GBS infection only as newborns, that CM101 causes tumor shrinkage and ablation (Thurman et al. 1994a). Histopathological studies showed that CM101 was causing vasodilatation and hemorrhage, endothelium damage, capillary thrombosis and coagulation, and infiltration of tumors with leukocytes, lymphocytes and monocytes (Hellerqvist et al. 1993). These observations underlie the rationale for introducing CM101 as an anticancer agent targeting the tumor neovasculature. Anti-angiogenic activity, as defined by Nguyen et al. (1994), is indicated with CM101 in 1 patient with ovarian cancer where treatment with 1 U/kg CM101 resulted in a decrease from 84 pg/ml to 0 in serum basic fibroblast growth factor levels after three infusions.

In sera of normal individuals, soluble E-selectin was found in the range 29.14–63.36 ng/ml, suggesting that, even in the absence of inflammatory processes, it is synthesized and released into the bloodstream. In our patients, pre-infusion soluble E-selectin average serum levels were exceeding 60 ng/ml. This may suggest that progressive neoplastic diseases in our patients were primarily responsible for the increase in soluble E-selectin (Banks et al. 1993; Sawada et al. 1994; Hakomori 1994). A dose-dependent increase was seen only from 1 U/kg to 2 U/kg, after which serum levels reached a plateau as the dosage was escalated to 3.3 U/kg and 5 U/kg respectively, suggesting saturation of the neovasculature with CM101. Serum levels of soluble E-selectin persisted significantly, elevated throughout the treatment period (weeks). We could, therefore, consider each administration of CM101 as a hostile stimulation of endothelium. Additional pharmacokinetic studies showed a cascade release of macrophage inflammatory protein 1α, TNFα, IL-6, IL-8 and IL-10 (Thurman et al. 1994b; DeVore et al. 1996) which may also stimulate endothelium (Warren 1993).

The inflammatory response induced by CM101 infusion is further manifested by leukopenia after 1 h, followed by an increase in circulating granulocytes (DeVore et al. 1995). The peak of granulocytosis occurs within 6–8 h after infusion and corresponds with the peak of serum soluble E-selectin levels in all treatment groups. Increased granulocyte adhesion and extravasation leads to an up-regulation of soluble E-selectin, which may moderate the rate of adhesion of granulocytes to endothelial membranous E-selectin as a defense against excessive extravasation and

migration and subsequent inflammation (Gearing and Newman 1993).

A patient with a non-HIV Kaposi sarcoma (endothelial hyperplasia) demonstrated the most significant reduction of tumor lesions (Hellerqvist et al. 1994; DeVore et al. unpublished result). The patient's serum levels of soluble E-selectin increased after the first dose and declined during prolonged treatment as he responded to treatment. Elevated soluble E-selectin serum levels in non-HIV Kaposi sarcoma patients have not been previously observed (Sciacca et al. 1994).

On the basis of our combined clinical and preclinical experiences, we propose that monitoring changes in soluble E-selectin levels can provide valuable information on the degree of CM101-mediated neovascular tumor endothelial activation and subsequent inflammation. We also suggest that, after extended therapy, reduction in neoplastic endothelium by CM101-induced inflammation leads to a decline in the soluble E-selectin level as seen in the Kaposi sarcoma patient following treatment.

Acknowledgements We are indebted to Minghua Zhang and Gerry York for their dedication to the production of CM101. We thank Ms. Pam Chunn for her skillful assistance in preparing the manuscript and Billy Gilbert for assisting in sample management. Some of the authors of this manuscript (B.D.W., G.B.T. H.W.S., Y.F.W., C.G.H.) have financial involvement with CarboMed Inc., the source of funding for this study.

References

Banks RE, Gearing AJH, Hemingway IK, Norfolk DR, Perren TJ, Selby PJ (1993) Circulating intercellular adhesion molecule-1 (ICAM-1), E-Selectin and vascular cell adhesion molecule-1 (VCAM-1) in human malignancies. Br J Cancer 68:122–124

Bevilacqua MP, Nelson RM (1993) Selectins. J Clin Invest 91:379–387

DeVore R, Johnson DR, Hellerqvist C, Wakefield G, Browning P, Page D, Sundell H, Johnson DH (1995) A phase I study of the anti-neovascularization drug CM101. Proc Am Soc Clin Oncol Annu Meet 14:487

Gearing AJH, Newman W (1993) Circulating adhesion molecules in disease. Immunol Today 14:506–512

Hakomori S (1994) Novel endothelial cell activation factor(s) released from activated platelets which induce E-selectin expression and tumor cell adhesion to endothelial cells: a preliminary note. Biochem Biophys Res Commun 203:1605–1613

Hellerqvist CG (1991) Therapeutic agent and method of inhibiting vascularization of tumors. US Patent 5010062, 23 April 1991. Patents have been issued in Europe, Canada, Australia and Japan

Hellerqvist CG, Rojas J, Green RS, Sell S, Sundell H, Stahlman MT (1981) Studies on group B β-hemolytic streptococcus. I. Isolation and partial characterization of an extra-cellular toxin. Pediatr Res 15:892–898

Hellerqvist CG, Thurman GB, Page DL, Wang Y-F, Russell BA, Montgomery CA, Sundell HW (1993) Anti-tumor effects of GBS toxin: a polysaccharide exotoxin from group B β-hemolytic streptococcus. J Cancer Res Clin Oncol 120:63–70

Hellerqvist CG, DeVore RF, Sundell HW, Thurman GB, Wamil BD, Wakefield GB, Johnson DH (1994) Preliminary results of a phase I trial of CM101 in cancer patients. J Leukoc Biol [Suppl] 112:35

Hellerqvist C, DeVore R, Thurman G, Wamil B, Zhang M, Wakefield G, Sundell H, Carter C, Yan H, Johnson D (1995a) Cytokine production in cancer patients receiving the anti-neovascularization drug CM101. Proc Am Soc Clin Oncol Annu Meet 14:488

Hellerqvist CG, DeVore RF, Sundell HW, Thurman GB, Wamil BD, Page DL, Wakefield, GB, Johnson DH (1995b) Early results of a phase I trial of CM101 in cancer patients. Proc Am Assoc Cancer Res Ann Meet 36:224

Hellerqvist CG, Yan H-P, Carter CE, Liu L, Wamil BD, Page DL, Thurman GB, Sundell HW (1996) CM101 induces a complement-activated inflammatory response targeting tumor neovasculature. Proc Am Assoc Cancer Res Ann Meet 37:487

Hollander M, Wolfe DA (1973) The dichotomous data problem. In: RA Bradley, JS Hunter, DG Kendall and GS Watson (Eds) Nonparametric statistical Methods. John Wiley and Sons, New York, 15–25

Mackay CR, Imhof BA (1993) Cell adhesion in the immune system. Immunol Today 14:99–102

Meekins JW, McLaughlin PJ, West DC, McFadyen IR, Johnson PM (1994) Endothelial cell activation by tumour necrosis factor-alpha (TNF-alpha) and the development of pre-eclampsia. Clin Exp Immunol 98:110–114

Newman W, Beall LD, Carson CW, Hunder GG, Graben N, Randhawa ZI, Gopal TV, Wiener-Kronish J, Matthay MA (1993) Soluble E-selectin is found in supernatant of activated endothelial cells and is elevated in the serum of patients with septic shock. J Immunol 150:644–654

Nguyen M, Watanabe H, Budson AE, Richie JP, Hayes DF, Folkman J (1994) Elevated levels of an angiogenic peptide, basic fibroblast growth factor, in the urine of patients with a wide spectrum of cancer. J Natl Cancer Inst 86:356–361

Rojas J, Green RS, Hellerqvist CG, Olegard R, Brigham KL, Stahlman MT (1981) Studies on group B β-hemolytic streptococcus. II. Effects on pulmonary hemodynamics and vascular permeability in unanesthetized sheep. Pediatr Res 15:899–904

Rojas J, Larson LE, Hellerqvist CG, Brigham KL, Gray ME, Stahlman MT (1983) Pulmonary hemodynamic and ultra-structural changes associated with group B streptococcal toxemia in adult sheep and newborn lambs. Pediatr Res 17:1002–1008

Sawada R, Tsuboi S, Fukuda M (1994) Differential E-selectin-dependent adhesion efficiency in sublines of a human colon cancer exhibiting distinct metastatic potentials. J Biol Chem 269:1425–1431

Sciacca FL, Stürzl M, Bussolino F, Sironi M, Brandstetter H, Zietz C, Zhou D, Matteucci C, Peri G, Sozzani S, Benelli R, Arese M, Albini A, Colotta F, Mantovani A (1994) Expression of adhesion molecules, platelet-activating factor, and chemokines by Kaposi's sarcoma cells. J Immunol 153:4816

Sundell HW, Fish WG, Sandberg KL, Edberg KE, Pappas RS, Hellerqvist CG (1990) Lung injury by streptococcal toxins. In: Brigham L, Stahlman MT (eds) Respiratory distress syndromes. Vanderbilt University Press, Nashville, Tenn, pp 58–70

Sundell HW, Yan H-P, Wu K, Wamil BD, Guddipati R, Carter CE, Stahlman MT, Hellerqvist CG (1996) Isolation and identification of group B β-hemolytic streptococcal (GBS) toxin from septic newborn infants. Pediatr Res 39:302A

Thurman GB, Russell BA, York GE, Wang Y-F, Page DL, Sundell HW, Hellerqvist CG (1994a) Effects of GBS toxin on long-term survival of mice bearing transplanted Madison lung Tumors. J Cancer Res Clin Oncol 120:479–484

Thurman GB, Wamil BD, Yan H, Zhang M, Johnson DH, DeVore RF, Wakefield GB, Hellerqvist CG (1994b) Cytokine production in cancer patients in response to CM101, a polysaccharide exotoxin from group B streptococcus (GBS). J Leukoc Biol [Suppl] 113:36

Thurman GB, Page DL, Wamil BD, Wilkinson LE, Kasami M, Hellerqvist CG (1996) Acute inflammatory changes in subcutaneous microtumors in the ears of mice induced by intravenous CM101 (GBS toxin). J Cancer Res Clin Oncol 122:549–553

Wamil BD, Price JO, Minton PA, Sundell HW, Thurman GB, Yan H-P, Carter CE, Hellerqvist CG (1996) Leukocyte activation in response to CM101 treatment of cancer patients. Proc Am Assoc Cancer Res Annu Meet 37:487

Warren JS (1993) Cellular processes such as leukocyte activation, chemotaxis, intercellular adhesion and secretion of proinflammatory soluble mediators are regulated by a complex set of cell surface, matrix-associated and soluble mediators. Drug News Perspect 6:450–459

Whitley MZ, Thanos D, Read MA, Maniatis T, Collins T (1994) A striking similarity in the organization of the E-selectin and beta interferon gene promoters. Mol Cell Biol 14:6464–6475

Vol. 3, 365–372, March 1997

Phase I Study of the Antineovascularization Drug CM101[1]

Russell F. DeVore,[2] Carl G. Hellerqvist, Gail B. Wakefield, Barbara D. Wamil, Gary B. Thurman, Patricia A. Minton, Håkan W. Sundell, He-Ping Yan, Clint E. Carter, Yue-Fen Wang, Gerald E. York, Ming-Hua Zhang, and David H. Johnson

Departments of Medicine [R. F. D., G. B. W., D. H. J.], Biochemistry [C. G. H., B. D. W., G. B. T., Y-F. W., G. E. Y., M-H. Z.], Pediatrics [P. A. M., H. W. S.], and Biology [H-P. Y., C. E. C.], Vanderbilt University, Nashville, Tennessee 37232

ABSTRACT

CM101 is a bacterial polysaccharide that induces neovascular inflammation in malignant tumors. Fifteen patients with refractory malignancies received CM101 i.v. by a 15-min infusion every other day, three times in 1 week, at doses ranging from 1 unit (7.5 μg)/kg to 5 units/kg. Serum was analyzed for anti-CM101 IgG and IgM weekly. Plasma levels of inflammatory cytokines, including tumor necrosis factor α, interleukin 8, interleukin 10, MIP-1α, and soluble E-selectin, were analyzed from −15 min to 12 h during each treatment.

Dose-limiting toxicities, including grade IV dyspnea and arrhythmia, were encountered at the 5-unit/kg level. Toxicities occurred primarily within the first 12 h after therapy and included mild-to-moderate fever and chills, nausea, cough, headache, facial flushing, dyspnea, myalgias, and acute tumor-related pain. No patient developed detectable antibodies to CM101. All patients experienced marked time- and dose-dependent elevations in all cytokines studied. Three patients experienced tumor shrinkage.

The results show that CM101 can be safely administered at doses that produce evidence for severe, and possibly tumor-specific, inflammation. Further study is necessary to better characterize the mechanism of action and determine the optimal dose and schedule of this new agent.

INTRODUCTION

Angiogenesis is a process by which new blood vessels are formed. Although highly regulated during embryogenesis (1), neovascularization becomes excessive in pathological states such as arthritis, diabetic retinopathy, atherosclerosis, and cancer (2). Malignant tumors require angiogenesis for growth beyond the size of a few millimeters (3) and for the dissemination of metastases (4). As our understanding of the angiogenic process increases, so do the opportunities for identifying various molecules and processes involved in pathological neovascularization that might be potential therapeutic targets (5).

CM101 is a complex polysaccharide exotoxin isolated from culture supernatants of GBS[3] recovered from infants who died of early onset septicemia (6). Referred to previously as GBS toxin, CM101 is thought to be instrumental in the development of neonatal GBS early onset disease (7, 8) characterized by septic shock and pneumonia with respiratory failure (9). This disease is most pronounced in premature infants, and humans are usually susceptible only during the first few days after birth.

Young and mature sheep develop a pulmonary response similar to human neonates when exposed to CM101 or when experiencing GBS bacteremia. Accordingly, sheep have been used as a model for studying the pathophysiology of GBS septicemia (7, 8). Histological sections of sheep lungs after i.v. exposure to purified CM101 demonstrate extensive capillary endothelial damage, dense inflammatory infiltrates, and hemorrhage. These findings are similar, if not identical, to those observed in human neonates with early onset disease (8). After i.v. administration to sheep, immunological and histochemical analysis of posttreatment lung tissue demonstrates binding of CM101 to capillaries and arterioles (10). These and other studies support the hypothesis that CM101 binds to developing human neovasculature via endothelial cell surface receptors and induces a severe local inflammatory response. Hellerqvist *et al.* (11, 12) hypothesized that the pathological neovasculature of human malignancies would also express receptors for CM101 and thus provide a selective target for cancer therapy.[4]

Several preclinical studies provide evidence for a possible use of CM101 as an anticancer agent. For example, using immunohistochemistry, Hellerqvist *et al.* (11) demonstrated that CM101 binds to the neovasculature of human carcinomas. In addition, i.v. administration of picomolar quantities of CM101 into nude mice implanted with human large-cell adenocarcinomas induces tumor necrosis and hemorrhagic lesions and inhibits tumor progression. In immunocompetent BALB/c mice with established Madison lung carcinoma, CM101 induces a severe inflammatory response targeting the tumor, as evidenced by vasodilation, endothelial and tumor cell necrosis, invasion by inflammatory cells, and capillary thrombosis. Short-term treatment with CM101 improves the median survival of treated mice.

Received 4/24/96; revised 10/16/96; accepted 12/3/96.

The costs of publication of this article were defrayed in part by the payment of page charges. This article must therefore be hereby marked *advertisement* in accordance with 18 U.S.C. Section 1734 solely to indicate this fact.

[1] This work was supported by a grant from CarboMed, Inc., in which C. G. H., B. D. W., G. B. T., Y-P. W., H. W. S., P. A. M., and H-P. Y. have a financial interest, and NIH General Clinical Research Center Grant M01 RR00095.

[2] To whom requests for reprints should be addressed, at Division of Medical Oncology, 1956 The Vanderbilt Clinic, Nashville, TN 37232-5536.

[3] The abbreviations used are: GBS, group B β-hemolytic *Streptococcus*; MTD, maximally tolerated dose; sE-selectin, soluble E-selectin; TNF, tumor necrosis factor; IL, interleukin.

[4] C. G. Hellerqvist. Therapeutic agent and method of inhibiting vascularization of tumors. United States Patent 5,010,062. 1991.

and protracted therapy renders some animals disease-free (12). In these animal models, no organ toxicity or evidence of toxicity to nontumor vasculature is observed.

On the basis of these preclinical data, a Phase I feasibility trial of CM101 was undertaken in patients with refractory malignancies. Because preclinical studies indicate that a protracted treatment schedule is necessary for significant antitumor activity, it was desirable to administer CM101 by a protracted schedule in humans (12). However, due to safety concerns relating to the potential for delayed toxicities, it was determined that a feasibility trial testing a three times weekly schedule for 1 week was first required to establish safety before proceeding with the study of a protracted schedule. In the current report, we present the results of a feasibility study describing the first 15 patients treated with CM101. The purpose of this study was to determine the safety profile of a three times weekly (×1 week) schedule of CM101. Patients were also observed for evidence of antitumor activity, development of anti-CM101 antibodies, and development of a systemic inflammatory cytokine response.

MATERIALS AND METHODS

Patient Selection. Patients with malignancies considered refractory or resistant to standard therapy were eligible. Previously untreated patients for which there was no accepted "standard" therapy (*e.g.*, metastatic renal cell cancer or pancreatic cancer) were also eligible. Pretreatment assessment consisted of a history and physical examination, complete blood count, differential and platelet count, urinalysis, chest radiography, electrocardiogram, pulmonary function testing, and tumor measurements (if applicable). Eligibility required an Eastern Cooperative Oncology Group performance status of ≤2, age ≥18 years, estimated life expectancy of ≥12 weeks, and adequate renal (serum creatinine less than or equal to 2× the upper limit of normal), hepatic (bilirubin less than or equal to 2× the upper limit of normal), and bone marrow function (WBC count ≥3,000/μl and platelet count ≥100,000/μl). Previous antineoplastic therapy must have been completed at least 4 weeks (except palliative radiotherapy) before therapy with CM101. Patients with central nervous system disease, hematological malignancies, previous allergic reactions to *Streptococcus*, or restrictive lung disease with carbon monoxide diffusion capacity <60% of predicted value (unless related to lung involvement with tumor) were ineligible.

Drug Administration. The initial dose in this trial was 1 unit/kg (7.5 μg/kg) CM101 given each treatment day. One unit of CM101 is defined as the amount of drug, when administered i.v. to sheep, required to induce an elevation in the pulmonary artery blood pressure by 100–150% and to reduce the circulating WBC count by 40–60% of baseline (13). In normal mice, up to 40 mg/kg CM101 have been administered without causing lethal toxicity, and the LD_{10} for lead-sensitized mice was between 4 and 16 mg/kg (6).

All patients were treated in the outpatient center of the Vanderbilt University General Clinical Research Center. Lyophilized CM101 was initially reconstituted in normal saline and diluted to a total of 30 cc immediately before administration. CM101 was administered i.v. by infusion pump over 15 min on a Monday, Wednesday, and Friday of the same week. No premedications were given. Blood pressure, pulse, and respiratory rate were monitored beginning 15 min before treatment, every 15 min for the first hour after treatment, again at 90 min, and at 2, 3, 4, 6, 8, 10, and 12 h. Patients who experienced tumor regression or stabilization, and who did not experience dose-limiting toxicities, were retreated every 3–4 weeks.

Table 1 Dose escalations

Dose units/kg[a]	Patient no.[b]	No. of cycles
1	3	3
2	6 (3)	14
3.3	3 (1)	6
5	3 (1)	4
Total	15	27

[a] units/kg body weight.
[b] Numbers in parentheses refer to the number of patients with stable or responding tumors after cycle 1.

Cohorts of three patients were treated at each CM101 dose level. Drug doses were escalated on a modified Fibonacci schedule only if less than or equal to one-third of the patients at a given dose level experienced grade III or greater toxicities (see Table 1). If more than one patient experienced grade III or greater toxicities, three additional patients were treated at the same dose level. If no additional grade III toxicities were encountered, the dose was subsequently increased one level. Dose-limiting toxicity was defined as any grade III or IV toxicity. Although it was not the primary intention of the study to define a MTD using the current schedule, an estimate of the MTD was desired to help direct future studies using a protracted schedule of CM101. Therefore, the MTD was defined as the highest dose for which the incidence of DLT was <33%.

Toxicity Monitoring. Patients were evaluated weekly, with a history, physical examination, and complete blood counts. Serum chemistries, blood counts, differentials, platelet counts, urinalyses, chest radiographs, and tumor measurements were obtained monthly and at the end of the study.

Specimen Collection for Biological Correlative Studies. With each CM101 infusion, heparinized blood samples were collected for biological correlative studies at the following time points: −15, 0, 15, 30, and 45 min, and at 1, 1.5, 2, 3, 4, 6, 8, 10, and 12 h. Three hundred units of preservative-free heparin (Sigma H3149, St. Louis, MO) were added per milliliter of blood. One-half ml of this mixture was dispensed to a 2-ml polypropylene microcentrifuge tube (Sigma T3531) for blood count and differential analysis. The syringe containing the remaining blood was placed nose-up in a rack to allow gravity sediment for 1–2 h at room temperature. The leukocyte-rich plasma was then expressed out of the syringe into a 1.5-ml polypropylene microcentrifuge tube (United Scientific Products MCT-175, San Leandro, CA). Tubes were centrifuged in a microcentrifuge (Costar, Cambridge, MA) for 3 min at 500 × *g*. The plasma was recovered and clarified by another centrifugation at 5600 × *g* for 10 min at 4°C. The cell pellets from the first spin (red cells and leukocytes separately) were resuspended in PBS (Sigma D8662), split into two aliquots each, and frozen at −85°C for subsequent studies.

Determination of WBC Counts. WBC counts were obtained using a Coulter Counter (model Zbi). Three cell counts

were averaged for each time point. Differentials were obtained by microscopically scoring 100 cells on Wright-stained blood smears on glass slides for each time point.

Cytokine Measurements. Appropriate plasma samples were removed once from the freezer and thawed at room temperature for testing cytokine levels using commercially available sandwich ELISA kits. TNF-α, IL-6, and IL-10 kits were obtained from Biosource International (Camarillo, CA). MIP-1α, sE-selectin, and IL-8 kits were obtained from R&D Systems (Minneapolis, MN). The manufacturers' protocols and reagents were used exclusively. When samples were off scale, retesting was done at appropriate dilutions.

Substrate in the ELISA plates was read at the appropriate wavelength in a Tuerek Multiskan Plus MKII Reader (ICN Biomedical, Costa Mesa, CA), and the data were electronically filed as a .PRN file using a GWBASIC program developed for that purpose. The data were retrieved into a LOTUS 123 worksheet, and the cytokine standard curve was analyzed by regression analysis as numbers and as logarithms for the best fit of linear regression. Using the regression equation of best fit, patient cytokine values were determined from the sample's absorbance in the ELISA assay. Single values for each sample were determined. In those rare cases in which single values did not fit well on the pharmacokinetic curve, samples were reevaluated in a subsequent assay. Samples were thawed only once and were immediately analyzed.

Testing for CM101 Antibody Formation. Patient serum was analyzed for anti-CM101 IgG and IgM before beginning therapy, weekly after treatment, and 1 month after cessation of therapy. Goat antimurine antibody was added to an ELISA plate in coating buffer. After incubation, the plate was washed extensively and blocked with extraneous protein. Murine monoclonal IgG anti-CM101, generated with protein-CM101 conjugates,[3] was added to the plate and captured by the goat antimurine antibody with the antigen combining site exposed. After incubation, the plate was washed. CM101 was added to the test wells and bound to the murine monoclonal IgG, leaving free antigenic sites available for subsequent interaction. An equal concentration of dextran was added to control wells. After incubation, the plates were washed.

Analysis for the presence of anti-CM101 antibodies was performed by adding patient serum to 12 wells (six dextran controls and six with CM101) at various dilutions, including and between 1:16 to 1:1024. After incubation, the plates were washed. Biotinylated goat antihuman IgM was added to three dextran control wells and three CM101 wells. Biotinylated goat antihuman IgG was added to the remaining six wells (three dextran control wells and three CM101 wells). After incubation, the plates were washed. Streptavidin-β-galactosidase conjugate was then added to each well, and after incubation, the plates were washed. Substrate (*p*-nitrophenyl-β-D-galactoside) was added to each well, and after 1–2 h of incubation at room temperature, the reaction was terminated with alkali, and the plates were read in an ELISA Plate Reader at 405 nm. If the readings for either human IgM or IgG at three consecutive serum dilutions were significantly higher (greater than 2-fold; $P \leq 0.05$ by Student's *t* test) in the CM101 wells than that of dextran controls, the test was considered positive for anti-GBS toxin antibodies.

Table 2 Patient characteristics

No. of patients	15
Male	9
Female	6
Median age, years (range)	51 (37–73)
ECOG performance status	
0	8
1	5
2	2
Previous therapy	
None	0
Chemotherapy	13
Radiotherapy	4
Immunotherapy	2
Hormonal therapy	4
Primary tumor type	
Colon/rectum	3
Kidney	2
Soft tissue sarcoma	2
Lung	1
Ovary	1
Biliary	1
Esophagus	1
Classical Kaposi's sarcoma	1
Small bowel adenocarcinoma	1
Hepatocellular carcinoma	1
Prostate	1

CM101 Skin Testing. Before each retreatment cycle, skin testing for CM101 was performed by subcutaneously administrating 1.5 μg of CM101 in 50 μl of normal saline. A reaction to CM101 was considered positive if after 48–72 h a 1–2-mm raised area of induration was detected.

RESULTS

Patient Characteristics. Patient characteristics are shown in Table 2. All 15 patients had refractory malignancies for which no effective standard treatment alternative existed.

Dose Escalations. A total of 27 full or partial cycles of therapy were administered. Five patients had at least stable disease after cycle 1 of therapy and received subsequent treatment cycle(s).

Three patients were treated at the first dose level (1 unit/kg), of which two received all three CM101 injections (Table 1). Two of these patients experienced tumor progression within 3 weeks of receiving CM101, and a third patient received two of three infusions and was removed due to grade III toxicity. Six patients were treated at the second dose level (2 units/kg), two of whom had tumor shrinkage. A third patient with stable disease after the first cycle was taken off treatment due to toxicity occurring during the second cycle of therapy. Two patients were removed after the first cycle due to tumor progression, and one refused further therapy after being hospitalized for nausea and vomiting, which occurred after the first infusion of CM101.

Three patients were treated at level 3 (3.3 units/kg). One patient experienced tumor reduction and received multiple treat-

[3] C. G. Hellerqvist, unpublished observations.

Table 3 Common toxicities

CM101 dose (units/kg)	#	Fever/Chills Grade 1/2	3	4	Nausea/ Vomiting Grade 1/2	3	4	Cough Grade 1/2	3	4	Dyspnea Grade 1/2	3	4	Headache Grade 1/2	3	4	Myalgia Grade 1/2	3	4	Flushing Grade 1/2	3	4	Pain Grade 1/2	3	4
1	3	3			1							1		1											
2	6	6			4			3			2	1		4			4			5			1		
3.3	3	3			2			1			1			2			1			3				3	
5.5	3	3			2			1			2		1	2	1		1						3		

ment cycles. A second patient had stable disease after cycle 1, but was removed from the study during cycle 2 due to toxicity. The third patient was removed after cycle 1 due to tumor progression. At the 5-unit/kg dose level, two of three patients experienced grade IV toxicity, and therefore, further dose escalation was discontinued.

Toxicities. Toxicities are outlined in Table 3. Grade I/II fever and chills lasting 1–2 h were universal and accompanied by mild tachypnea, tachycardia, and an asymptomatic decline in blood pressure in most patients (Fig. 1*A*). Two patients experienced grade II or greater hypotension: one at dose level 2 and one at dose level 4. The patient at dose level 4 (5 units/kg) had a history of supraventricular tachycardia and developed the same arrhythmia and resultant grade III hypotension, requiring brief hospitalization. Both patients required i.v. fluids. One patient treated at dose level 2 developed a flu-like syndrome with associated weakness, myalgias, headache, diarrhea, fever, chills, and nausea lasting approximately 1 week after a single dose of CM101. All toxicities were reversible and occurred primarily during the first 1–12 h after CM101 administration.

Dose-limiting toxicity occurred in two of three patients treated with 5 units/kg CM101. In addition to the patient who developed supraventricular tachycardia (grade IV arrhythmia) and grade III hypotension, a second patient experienced severe (grade IV) dyspnea. Although both incidents of grade IV toxicity occurred at the 5-unit/kg dose level, the association between dose and toxicity was inconsistent. Grade III dyspnea occurred in two patients: one each at dose levels 1 and 2. All three patients experiencing grade III or IV dyspnea had lung metastases and a carbon monoxide diffusion capacity ≤76% of the predicted value. No patient with a carbon monoxide diffusion capacity >76% of predicted experienced grade III or IV dyspnea. The most severe cases of dyspnea were associated with expiratory wheezing; however, bronchospasm was not always present in dyspneic patients. Dyspnea was generally maximal 1–3 h after therapy when patients were also experiencing fever, chills, and tachycardia. Dyspnea was not improved with bronchodilators.

Because there was concern that the grade IV dyspnea and arrhythmia were precipitated by cardiovascular effects evidenced by significant decreases in blood pressure encountered at the higher dose levels, no further dose escalations were attempted. The median decreases in systolic blood pressures from baseline for each dose level were as follows: 35, 42, 7, and 16 mmHg at dose levels 5, 3.3, 2, and 1 unit(s)/kg, respectively. Therefore, it was felt that the MTD was established and that further escalation was prohibitive due to the risk of further acute cardiovascular toxicities.

Other than acute dyspnea, no additional pulmonary toxicity was evident. Likewise, other than transient supraventricular tachycardia, dyspnea, and hypotension, no specific cardiac toxicity was encountered. There were no renal or neurological toxicities. Other than transient leukopenia occurring during the first few hours after therapy, no patient experienced clinically significant leukopenia, thrombocytopenia, or anemia during the study, although a single patient experienced a drop in hematocrit from 38 to 33% within 2 weeks of therapy. Three patients experienced a rise in serum liver enzymes (lactate dehydrogenase, aspartate aminotransferase, and alkaline phosphatase) while receiving CM101. However, all three had liver metastases and documented disease progression.

After CM101 infusion, pain at the site of the tumor was observed in seven patients. Three patients experienced grade III pain, all at the 3.3-unit/kg dose level; one of them experienced an objective tumor regression and one stabilized disease. The third patient experienced progressive disease after the first cycle of therapy.

Leukocyte Responses to CM101. A time course for changes in leukocyte counts in response to CM101 is shown in Fig. 1*B*. Initially, granulocyte levels declined precipitously, followed by a rebound above baseline at approximately 3–4 h. This rebound was associated with the appearance of a large number of immature granulocytes in the peripheral blood at all dose levels. Circulatory lymphocytes decreased to a nadir at 2–4 h after treatment with 2, 3.3, and 5 units/kg and were nearly baseline by 12 h. Circulating monocyte levels decreased most significantly at the two highest dose levels and remained suppressed for 8–12 h.

Cytokine Responses to CM101. All patients experienced a time- and dose-dependent elevation of systemic cytokines after CM101 (Table 4). TNF-α, MIP-1α, IL-8, IL-6, and IL-10 peaked at 60–90, 60–90, 120, 180, and 240 min, respectively, suggesting an interdependent cascade of inflammatory events. Cytokine levels generally returned to baseline within 4–8 h of CM101 administration. In most cases, peak levels were detected on day 1 of each treatment cycle, and peaks were significantly less pronounced after treatment on days 2 and 3 (Wednesday and Friday). In patients who received more than one cycle of CM101, peak cytokine levels and response patterns were similar to those achieved during the initial dose of CM101. The amplitude of the systemic cytokine response increased exponentially with increasing CM101 doses and peaked at 3.3 units/kg (Table 4).

Systemic sE-selectin, a putative marker of endothelial inflammation (14), was elevated approximately 2-fold over "normal" in all patients at baseline and increased further in response

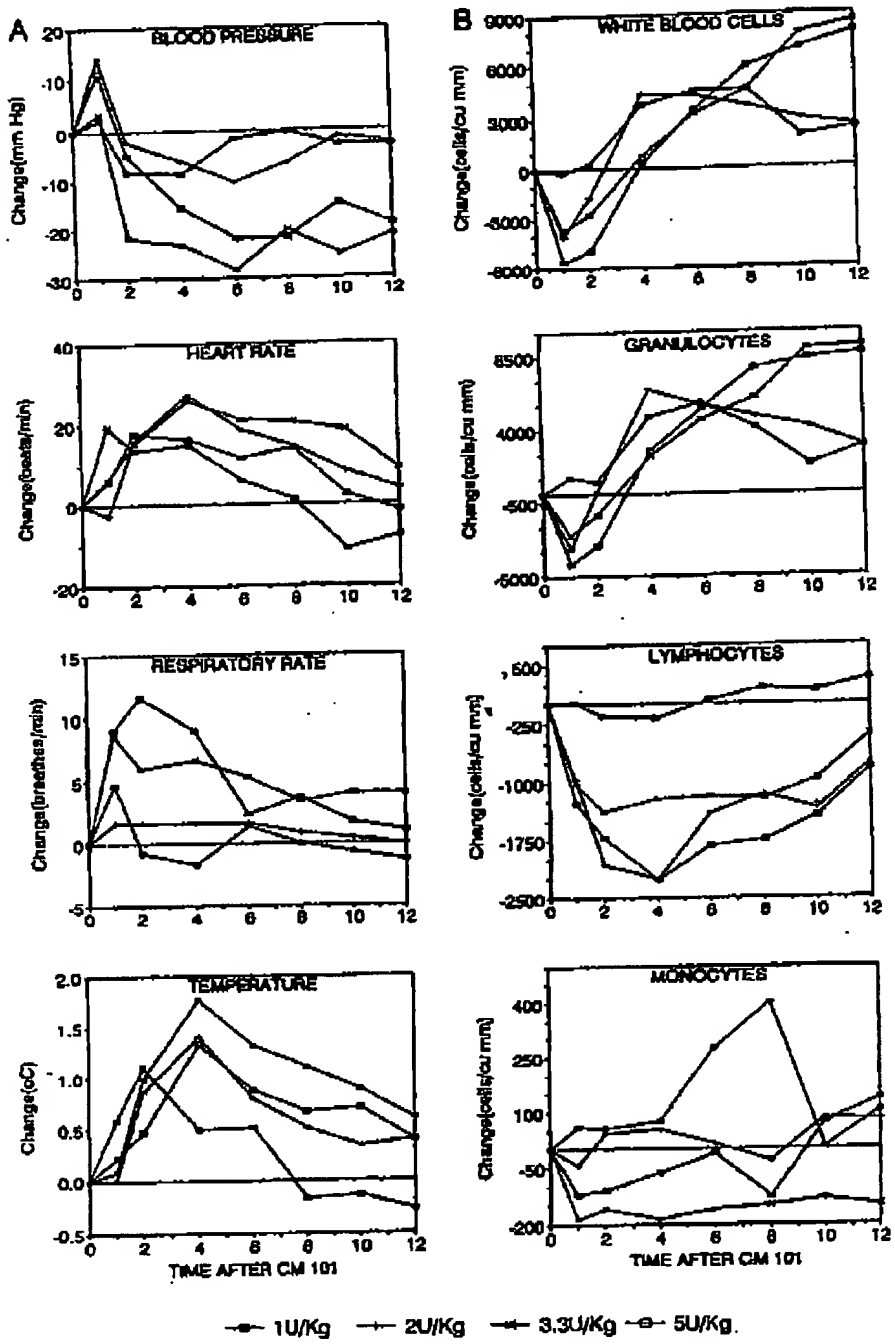

Fig. 1 A, mean change from baseline values in blood pressure, heart rate, respiratory rate, and temperature after treatment with CM101 at four different doses. *B*, mean change from baseline values in total WBCs, granulocytes, lymphocytes, and monocytes after treatment with CM101 at four different doses. Time is expressed as hours after CM101 administration.

Table 4 Peak cytokine responses of cancer patients treated with CM101

Patient no.	Peak plasma cytokine levels (pg/ml)					
	TNF-α	MIP-1α	IL-6	IL-8	IL-10	sE-selectin (ng/ml)
CM101 (1 unit/kg)						
1	143	710	283	1,582	80	195.8
2	192	535	420	2,729	136	148.7
3	425	703	10,150	5,413	171	205.0
CM101 (2 units/kg)						
4	462	2,168	1,155	3,232	435	237.0
5	4,598	4,114	3,100	16,155	1,329	218.0
6	208	961	481	3,335	994	258.6
7	319	1,115	376	2,053	297	778.5
8	871	1,696	1,952	3,622	611	364.2
9	1,375	1,838	1,130	5,918	346	244.0
CM101 (3.3 units/kg)						
10	4,922	6,178	9,542	8,818	476	788.7
11	4,888	8,174	9,419	9,334	468	651.0
12	2,771	1,274	2,204	10,190	422	329.5
CM101 (5 units/kg)						
13	1,847	3,173	1,526	10,948	1,333	848.7
14	249	1,263	212	1,690	1,463	1,259.4
15	1,174	2,009	2,303	7,601	1,969	788.7

to CM101. Both baseline and peak values usually rose during subsequent infusions in the first cycle and reached peak values from 200 to 800 ng/ml by the end of the first cycle. After discontinuation of therapy, sE-selectin levels slowly trended downward, approaching baseline at 4 weeks after the last treatment. In patients receiving more than one cycle of CM101, baseline and peak sE-selectin levels were similar to those observed during the initial cycle of therapy. However, in the patient with Kaposi's sarcoma who experienced a gradual and substantial regression of his malignancy, baseline and peak levels trended downward throughout his five cycles of therapy, possibly reflecting a gradual decline in the amount of malignant neovasculature.

CM101 Antibody and Skin Testing. Two patients refused to have antibody testing performed. Of the remaining 13 patients, 5 of whom received multiple courses of CM101, none developed antibodies to CM101. None of the five patients given multiple courses of CM101 developed reactivity to skin testing.

Efficacy. Three patients exhibited tumor shrinkage after CM101. A 63-year-old male with classical Kaposi's sarcoma and multiple lower extremity lesions previously treated with external beam radiotherapy, multiple surgical excisions, and i.v. vinblastine was developing multiple new lesions on the left lower extremity each month. One week after receiving his first dose of CM101 (2 units/kg), the largest marker lesion (a lesion raised approximately 1 cm from the skin surface and 1 cm in diameter) became obviously flattened. It was no longer detectable at 3 weeks. Three additional marker lesions each measuring approximately 5 mm in diameter were unchanged in size. However, several smaller lesions became pale, decreased in size, and desquamated by 3 weeks after cycle 1 of therapy. The disease-related discoloration and severe edema of the extremity dramatically improved and almost completely resolved during therapy. He received a total of five cycles of therapy until a new lesion appeared, and he was discontinued from study.

A 43-year-old female with metastatic adenocarcinoma of the small bowel involving a supraclavicular lymph node had previously failed treatment with 5-fluorouracil and was treated with 2 units/kg CM101. There was an obvious reduction in the size of the lymph node within 2 weeks of receiving the first dose of CM101. There was an approximately 90% reduction in the size of the lymph node after four monthly cycles of CM101. However, after the second course of CM101 a new supraclavicular lymph node appeared and enlarged after the subsequent treatment cycle. Both lymph nodes were excised approximately 5 h after treatment with day 1, cycle 4 of CM101. Pathological examination revealed adenocarcinoma in both lymph nodes with leukocytic infiltration of the tumor. The patient was taken off study at that point and eventually developed recurrent disease in the supraclavicular area 7 months after completing CM101 therapy.

A 45-year-old male treated with 3.3 units/kg CM101 had hepatocellular carcinoma previously treated with etoposide and cisplatin and three hepatic lesions, one measuring 13 cm in greatest diameter. After two monthly treatment cycles, there was a measurable decrease in the size of all three lesions, but this was most remarkable in the smaller lesions. Overall, the reduction in tumor size was 25%. Approximately 1 h after CM101 treatments, he experienced acute onset of severe pain in areas of previous tumor-related pain, necessitating premedication with i.v. narcotics in subsequent treatments. He developed progressive disease after five monthly cycles of CM101, and study treatment was withdrawn.

DISCUSSION

In selected animal tumors, CM101 has been shown to bind to malignant neovascular endothelium and induce a rapid and severe local inflammatory response characterized by leukocyte chemotaxis and tumor infiltration, small blood vessel coagulation and destruction, and tumor necrosis and hemorrhage (11).

The results of this Phase I study suggest that CM101 may generate a similar effect in patients with refractory malignancies. (*a*) Treatment with CM101 led to high levels of systemic cytokines known to be associated with an inflammatory response. (*b*) Levels of sE-selectin were markedly elevated in response to CM101. (*c*) A rapid and substantial decline in circulating leukocytes occurred. As shown previously, leukopenia and pulmonary sequestration of leukocytes occurs in neonatal GBS early onset disease and in the sheep model (8). Also, CM101 induces leukocyte infiltration of malignant tumors in mouse models (11). Evidence of this was seen in a patient biopsy obtained after CM101 administration. (*d*) The toxicity profile observed with CM101 was consistent with an inflammatory response. (*e*) The development of acute tumor-related pain in 7 of 15 treated patients is suggestive of acute tumor-specific inflammation. (*f*) Antitumor activity was demonstrated by tumor regression in three patients.

The time- and dose-dependent cytokine cascade observed in all patients in response to CM101 strongly supports our supposition that CM101 is inducing inflammation. The early presence of MIP-1α suggests that "activated" granulocytes may release this potent chemoattractant for monocytes (15) and lymphocytes (16). In turn, these cells are a reported source for TNF-α (17). Activated granulocytes also produce IL-8, which recruits additional granulocytes to inflammatory sites (18). The observed systemic IL-6 produced by monocytes (19) is a potent stimulator of the acute-phase response. The elevation of IL-10 is yet another indication of a regulated inflammatory response terminating in IL-10-induced down-regulation of TNF-α (20).

E-selectin is a cell surface adhesion molecule present in endothelial cells (14). A truncated form, sE-selectin, is thought to be produced exclusively by cytokine-activated endothelium, and the release of soluble E-selectin into the systemic circulation is considered direct evidence for endothelial activation (15). This elevation has been observed in pathophysiological states such as sepsis, vasculitis, and cancer. Thus, the rapid elevation of sE-selectin levels in patients treated with CM101 is strong evidence that the drug is inducing endothelial inflammation (21). The absence of vascular leakage and hepatic and renal toxicities suggests that the endothelial engagement may be limited to the tumor (11).

CM101 was relatively well tolerated in most patients because toxicities were short-lived. Dose-limiting toxicities were cardiovascular and pulmonary. The actual pathophysiology for dyspnea was not apparent and did not appear to be directly related to bronchospasm. We propose that dyspnea is related to multifactorial cardiovascular compromise induced by the drug and therefore is dependent on the patient's pretreatment pulmonary reserve and resulting tolerance to generalized cardiovascular compromise. This impression is supported by the varied clinical presentations of dyspneic patients, the propensity for dyspnea to occur only in patients with underlying pulmonary pathophysiology, and the common occurrence of hypotension. Although there appeared to be a dose-response effect for cytokine activation, hypotension and acute tumor-related pain were the only toxicities that appeared to be dose-related. Both of these toxicities may directly reflect the inflammatory mechanism of action of CM101 and be related to the extensive release of inflammatory cytokines. Given the degree of hypotension occurring at the two highest dose levels and the associated cardiac and pulmonary events occurring at the highest dose level, a dose-response relationship to toxicity was considered established, and further dose escalation was considered unsafe.

In a mouse model, CM101 was curative only when the drug was administered on a protracted schedule (3 times weekly for 11 weeks; Ref. 12). In the current trial, treatment was interrupted after just 1 week of therapy due to the concern that delayed toxicities might occur. Therefore, more protracted treatment scheduling should be studied. The optimal dose of CM101 also requires further study. In animal studies, there appeared to be a bell-shaped curve for the CM101 dose/efficacy relationship (12). Therefore, there are theoretical reasons to believe that a MTD may not be therapeutically ideal for this compound. Clearly, dosing and scheduling issues require further investigation in future studies.

Currently, we are continuing the Phase I study of CM101 using a once weekly schedule for 10 consecutive weeks. The initial CM101 dose in that study is 3.3 units/kg. We believe that the inflammatory cytokine levels may directly or indirectly reflect the antineovascular activity of CM101 and have therefore hypothesized that a 1-week treatment interval may allow for maximal induction of inflammation.

In conclusion, CM101 can be safely administered at doses that produce evidence for severe, and possibly tumor-specific, inflammation. Studies to further characterize the mechanism of action of CM101 in patients and to determine the optimal dose and schedule of this new agent are under way.

ACKNOWLEDGMENTS

We thank Pam Chinn and Diane Ray for administrative coordination, data management, and typing of the manuscript, and William Gilbert for assistance in patient sample management.

REFERENCES

1. Plate, K. H., Breier, G., and Risau, W. Molecular mechanisms of developmental and tumor angiogenesis. Brain Pathol., *4:* 207–218, 1994.

2. Maragoudakis, M. E., Gullino, P. M., and Lelkes, P. I. (eds.). Angiogenesis: molecular biology, clinical aspects, Vol. 263, pp. 1–372. New York: Plenum Press, 1994.

3. Folkman, J. Tumor angiogenesis: therapeutic implications. N. Engl. J. Med., *285:* 1182–1186, 1971.

4. Fidler, I. J. Critical factors in the biology of human cancer metastasis. Cancer Res., *50:* 6130–6138, 1990.

5. Fidler, I. J., and Ellis, L. M. The implications of angiogenesis for the biology and therapy of cancer metastasis. Cell, *79:* 185–188, 1994.

6. Hellerqvist, C. G., Rojas, J., Green, R. S., Sell, S., Sundell, H., and Stahlman, M. T. Studies on group B β-hemolytic *Streptococcus*. I. Isolation and partial characterization of an extracellular toxin. Pediatr. Res., *15:* 892–898, 1981.

7. Rojas, J., Green, R. S., Hellerqvist, C. G., Olegard, R., Brigham, K. L., and Stahlman, M. T. Studies on group B β-hemolytic *Streptococcus*. II. Effects on pulmonary hemo-dynamics and vascular permeability in unanesthetized sheep. Pediatr. Res., *15:* 899–904, 1981.

8. Rojas, J., Larsson, L. E., Hellerqvist, C. G., Brigham, K. L., Gray, M. E., and Stahlman, M. T. Pulmonary hemodynamic and ultrastructural changes associated with group B streptococcal toxemia in adult sheep and newborn lambs. Pediatr. Res., *17:* 1002–1008, 1983.

9. Weisman, L. E., Stoll, B. J., Cruess, D. F., Hall, R. T., Merenstein, G. B., Hemming, V. G., and Fischer, G. W. Early-onset group B

streptococcal sepsis: a current assessment. J. Pediatr., *121:* 428–433, 1992.

10. Russell, B. A., Pappas, R. S., Brandt, J. M., Sundell, H. W., and Hellerqvist, C. G. Immunological and histochemical studies on the pathophysiology of group B streptococcal toxin manifested in early-onset disease. Glycoconj. J., *6:* 399, 1988.

11. Hellerqvist, C. G., Thurman, G. B., Page, D. L., Wang, Y-F., Russell, B. A., Montgomery, C. A., and Sundell, H. W. Anti-tumor effects of GBS toxin: a polysaccharide exotoxin from group B β-hemolytic *Streptococcus*. Cancer Res. Clin. Oncol., *120:* 63–70, 1993.

12. Thurman, G. B., Russell, B. A., York, G. E., Wang, Y-F., Page, D. L., Sundell, H. W., and Hellerqvist, C. G. Effects of GBS toxin on long-term survival of mice bearing transplanted Madison lung tumors. Cancer Res. Clin. Oncol., *120:* 479–484, 1994.

13. Sandberg, K., Edberg, K. E., Fish, W., Parker, R. A., Hellerqvist, C. G., and Sundell, H. Thromboxane receptor blockage (SQ 29548) in group B streptococcal (GBS) toxin challenge in young lambs. Pediatr. Res., *35:* 571–579, 1994.

14. Gearing, A. J. H., and Newman, W. Circulating adhesion molecules in disease. Immunol. Today, *14:* 506–512, 1993.

15. Kasama, T., Strieter, R. M., Standiford, T. J., Burdick, M. D., and Kunkel, S. L. Expression and regulation of human neutrophil-derived macrophage inflammatory protein 1 alpha. J. Exp. Med., *178:* 63–72, 1993.

16. Taub, D. D., Conlon, K., Lloyd, A. R., Oppenheim, J. J., and Kelvin, D. J. Preferential migration of activated CD4+ and CD8+ T cells in response to MIP-1α and MIP-1β. Science (Washington DC), *260:* 355–358, 1993.

17. Beutler, B., and Cerami, A. Cachectin/tumor necrosis factor: an endogenous mediator of shock and inflammation. Immunol. Res., *5:* 281, 1986.

18. Cassatella, M. A. The production of cytokines by polymorphonuclear neutrophils. Immunol. Today, *16:* 21–26, 1995.

19. Baumann, H., and Gauldie, J. The acute phase response. Immunol. Today, *15:* 74–80, 1994.

20. Gomez, J. J., Martin, M. C., Sanri, R., Segura, R. M., Esteban, F., Ruiz, J. C., Nuvials, X., Boveda, J. L., Peracaula, R., and Salgado, A. Interleukin-10 and monocyte/macrophage-induced inflammatory response in septic shock. J. Infect. Dis., *171:* 472–475, 1995.

21. Warnil, B. D., Thurman, G. B., Sundell, H., DeVore, R. F., Wakefield, G., Johnson, D. H., Wang, Y-F., and Hellerqvist, C. G. Soluble E-selectin in cancer patients as a marker of the therapeutic efficacy of CM101, a tumor inhibiting anti-neovascularization agent, evaluated in phase I clinical trial. J. Cancer Res. Clin. Oncol., in press, 1997.

tumor and normal endothelium are distinct at the molecular level, a finding that may have significant implications for the development of anti-angiogenic therapies."

l demonstrate that HP59 homologous protein, are expressed in cutaneous wounds also in pigs and that CM101 treatment accelerates wound healing by blocking pathologic angiogenesis See Nanney LB, et al Angiogenesis. 2001-4(1)61-70 Exhibit J)

"The immunolocalization HP59 in the microvessels of the cutaneous wound bed in control but not in CM101 wounds of untreated pigs suggests that CM101 inhibits the pathologic inflammatory angiogenesis accompanying the normal granulation processes. The net biological effect of inhibited inflammatory pathoangiogenesis is a diminished, suggested and purely physiologic, microvascular bed which translates into an enhanced rate of epithelial resurfacing and therefore an overall accelerated rate of wound repair."

11. An example of the successful application of targeting pathologic vasculature are anti-cancer therapies targeting vascular endothelial growth factor (VEGF). The mouse models used with anti-VEGF antibodies correlated reasonably in colon and breast cancer. See Ferrara *et al.*, *Biochem. Biophys. Res. Commun.* v. 333, pp. 289-91 (2005; Exhibit K):

"VEGF plays an essential role in developmental angiogenesis and is important also for reproductive and bone angiogenesis. Substantial evidence also implicates VEGF as a mediator of pathological angiogenesis. Anti-VEGF monoclonal antibodies and other VEGF inhibitors block the growth of several tumor cell lines in nude mice. Clinical trials with VEGF inhibitors in a variety of malignancies are ongoing. Recently, a humanized anti-VEGF monoclonal antibody (bevacizumab; Avastin) has been approved by the FDA as a first-line treatment for metastatic colorectal cancer in combination with chemotherapy. Furthermore, VEGF is implicated in intraocular neovascularization associated with diabetic retinopathy and age-related macular degeneration."

12. In the present application, my methods and compositions target a protein common to pathologic vasculature of various types of tumors and shared by at least humans,

mice, rats and pigs. I elucidated the mechanism of action of GBS toxin during angiogenesis, and, in particular how CM101 binds to HP59 and induces an inflammatory cascade, which leads to infiltration of granulocytes, lymphocytes and lymphocytes and destruction through apoptosis of the pathologic conditions. See Yakes *et al.*, *Cancer Research* v. 60, pp. 5740-5746 (2000; Exhibit F). The attenuation of cancer-associated angiogenesis in the mouse models used in the working examples of the present application is reasonably correlating with the human pathologic angiogenesis associated with conditions such as cancer, due to the presence of common CM101 target proteins in mice and humans and common mechanism of action of my claimed methods.

13. I declare further that all statements made herein are of my own knowledge and are true, and that all statements made on information and belief are believed to be true; and further that these statements were made with the knowledge that wilful false statements and the like so made are punishable by fine, or imprisonment, or both, under Section 1001 of Title 18 of the United States Code and that such wilful false statements may jeopardize the validity of any patent issuing on this application.

Signature

Carl G. Hellerqvist, Ph.D.
Name

2/7/2006
Date

[CANCER RESEARCH 60, 5740–5746, October 15, 2000]

CM101 Treatment Overrides Tumor-induced Immunoprivilege Leading to Apoptosis[1]

F. Michael Yakes, Barbara D. Wamil, Fenglei Sun, He-Ping Yan, Clint E. Carter, and Carl G. Hellerqvist[2]

Departments of Biochemistry [F. M. Y., B. D. W., F. S., C. G. H.] and Biology [H-P. Y., C. E. C.], Vanderbilt University, Nashville, Tennessee 37232

ABSTRACT

CM101, a bacterial polysaccharide exotoxin produced by group B *Streptococcus* (GBS), also referred to as GBS toxin, has been shown to target pathological neovasculature and activate complement (C3), thereby inducing neovascularitis, infiltration of inflammatory cells, inhibition of tumor growth, and apoptosis in murine tumor models. Data from refractory cancer patients in a Phase I clinical trial with CM101 indicated a similar mechanism of tumor-targeted inflammation. To further our understanding of the mechanism of action of CM101 as an antitumor agent, we examined the role of the inflammatory response in inducing tumor apoptosis in a normal mouse and tumor-bearing mouse model. The i.v. infusion of CM101 into B16BL-6 melanoma tumor-bearing mice elevated *p53* mRNA in circulating leukocytes as measured by reverse transcription-PCR, and immunohistochemistry demonstrated infiltration and sequestration of leukocytes. Whole tumor lysates from excised tumors exhibited an increase in binding to the murine $p21^{Waf1/Cip1}$-derived p53 DNA binding sequence compared with control whole tumor lysates, in which minimal or no DNA binding was observed. CM101 infusion led to elevated levels of Fas protein within the tumors as well as a decrease in the expression of fas ligand (fasL). Furthermore, tumors were apoptotic as determined by terminal deoxynucleotidyl transferase-mediated nick end labeling and DNA fragmentation assays. Collectively, these data suggest that CM101 up-regulates p53 in tumor-infiltrating leukocytes, initiating a loss of tumor immunoprivilege and consequently rendering the tumor sensitive to Fas/fasL-mediated apoptosis. CM101 induced loss of tumor immunoprivilege through changes in the expression of leukocyte p53, tumor Fas and fasL coupled with neovascularitis and leukocyte infiltration, constitutes a plausible molecular pathway for tumor reduction observed in cancer patients.

INTRODUCTION

Infection of newborn infants with GBS[3] is associated with a lung-specific inflammatory response, pulmonary hypertension, significant endothelial cell damage, and capillary thrombosis. The causative agent associated with these symptoms has been identified as a polysaccharide exotoxin, which, when injected into sheep, reproduces the lung pathophysiology observed in infected neonates (1–4). This observation led to the hypothesis that the binding of GBS toxin to embryonic receptors of the newborn lung neovasculature induced an inflammatory response that ultimately caused the respiratory distress syndrome known as "early onset disease" (1). It was further hypothesized that these receptors would be present in tumor neovasculature but not in mature vasculature, thereby rendering tumors susceptible to GBS toxin-induced inflammation. One active component of GBS toxin now referred to as CM101 has been further purified (5, 6) and shown to bind to human tumor neovasculature (7). The above-mentioned hypothesis has been substantiated in murine tumor models, in which CM101 has been demonstrated to inhibit tumor growth (7), promote long-term survival (8), and induce acute inflammation targeting the tumor neovasculature (9). Recently, we have demonstrated that CM101 *in vivo* binds to the tumor neovasculature within 5 min and activates complement C3 (10, 11). This results in the release of C3a, which effectively functions as a chemoattractant for leukocytes. C3-dependent infiltration of TNF-α-expressing macrophages of the tumor was shown to be coincident with up-regulation of TNFR II in mature endothelium, leading to apoptosis of this vasculature (11).

CM101 does not bind to leukocytes, tumor cells, or normal cells (with the exception of some primary endothelial cells *in vitro*) and has no apparent biological effect on any of these cell types.[4] The p53 tumor suppressor gene has been identified as a transcriptional regulator of downstream effector genes associated with cellular proliferation and apoptosis (Ref. 12 and the references therein). In response to cellular stress including DNA damage and hypoxia, transcription of p53-dependent genes such as *GADD45* (13), $p21^{Waf1/Cip1}$ (14, 15), *KILLER/DR5* (16, 17), and *Fas* (18–20) is up-regulated. Expression of these gene products and others commits the cell to either cell cycle arrest, allowing for efficient DNA repair, or, alternatively, apoptosis, eliminating heavily damaged cells. Cellular proliferation in the absence of repair may lead to mutations that promote the growth of tumors. It is known that some human tumors harbor mutant or inactive p53 (21). In these tumors, p53 has lost the ability to bind to its DNA-binding consensus sequence and is therefore unable to activate transcription (22). Loss of p53-dependent transcription could negatively effect cellular homeostasis and could promote the proliferation of aberrant cells that might otherwise be eliminated. Although p53-independent mechanisms of apoptosis have been described previously (23, 24), studies investigating p53 as an important component of tumor suppression remain critical in the development of cancer therapies.

The significance of mutant p53 in tumors becomes important within the context of immune surveillance and tumor immunoprivilege. Fas (APO-1/CD95) is a member of the tumor necrosis family of type I membrane proteins capable of eliciting an apoptotic response on specific ligand interaction. The binding of fasL or agonistic antibodies to the Fas receptor protein initiates a molecular signaling cascade resulting in apoptotic cell death (25, 26). Fas protein is constitutively expressed in many tissues such as the liver, thymus, heart, and ovary (27). In contrast, fasL protein has been shown to be primarily limited to activated cell lineages of the immune system such as T cells (28, 29), B lymphocytes (30), natural killer cells (31), monocytes/macrophages (32), and immunoprivileged tissues (27, 28, 33, 34). Recently, blockade of the Fas/fasL signal transduction pathway has been suggested to participate in the establishment of tumor immunoprivilege in a variety of nonlymphoid human tumors (35–38). In the tumors examined, fasL was markedly elevated throughout the tumor when compared with Fas protein. In this manner, the expression of tumor fasL would result in the induction of apoptosis of the Fas-presenting immune effector cells and contribute to the establishment of tumor immunoprivilege (reviewed in Refs. 33, 34, and 39). In a striking example, fasL-positive hepatocellular carcinoma cells increased lymphocyte cell death when Jurkat T cells were plated on hepatocellular

Received 12/28/99; accepted 8/15/00.

The costs of publication of this article were defrayed in part by the payment of page charges. This article must therefore be hereby marked *advertisement* in accordance with 18 U.S.C. Section 1734 solely to indicate this fact.

[1] Supported by a grant from CarboMed Inc. in which all of the authors have a financial interest.

[2] To whom requests for reprints should be addressed, at Vanderbilt University School of Medicine, 21st & Pierce, 634 MRB I, Nashville, TN 37232-0146. Phone: (615) 322-4339; Fax: (615) 322-6354; E-mail: carl.g.hellerqvist@vanderbilt.edu.

[3] The abbreviations used are: GBS, group B *Streptococcus*; TNF, tumor necrosis factor; TNFR, TNF receptor; IL, interleukin; RT-PCR, reverse transcription-PCR; fasL, fas ligand; TdT, terminal deoxynucleotidyltransferase; TUNEL, TdT-mediated nick end labeling; DAB, 3,3'-diaminobenzidine; HRP, horseradish peroxidase.

[4] F. Shi, S. Bordhan, G. D. Thurman, and C. G. Hellerqvist, unpublished observations.

EXHIBIT F

carcinoma cryostat sections (40). Recently, human vascular endothelial cells have been shown both *in vivo* and *in vitro* to express fasL (41, 42) that is down-regulated after local administration of the inflammatory cytokine TNF-α. The down-regulation of fasL correlated with adherence and extravasation of leukocytes within the endothelial milieu, suggesting an important relationship between inflammatory signaling and activation of the endothelium. Our previous studies establishing the up-regulation of TNFR II on the tumor endothelium concomitant with leukocyte adhesion[5] and infiltration (11) suggest that CM101 may be a potent mediator of a tumor-targeted inflammatory response.

It is evident that several molecular pathways are likely to be involved in the establishment of tumor immunoprivilege. Several hypotheses have been suggested that involve the inability of mutant p53 or, alternatively, the absence of wild-type p53 to up-regulate Fas expression within the tumor (18–20). Although it is not clear how p53 would modulate such activity *in vivo*, the role of p53 in effective therapeutic strategies targeting tumor vascular disruption has become an area of great interest (21).

In this report, we present evidence that the CM101-induced inflammatory response elevated *p53* mRNA in tumor-infiltrating leukocytes *in vivo*. Examination of whole tumor lysates demonstrated that CM101 treatment resulted in an increase in p53 sequence-specific DNA binding compared with control whole tumor lysates. This increase in DNA binding correlated with a concomitant increase of total p53 in whole tumor lysates. In addition, immunohistochemical data indicated that prior to CM101 treatment, tumors were immunoprivileged with high expression of fasL and little or no expression of Fas. However, treatment with CM101 down-regulated fasL and up-regulated Fas within the tumor cells. The data presented herein suggest that CM101 treatment reduces tumor immunoprivilege through down-regulation of tumor fasL, up-regulation of tumor Fas, and up-regulation of p53 mRNA in tumor-infiltrating leukocytes. Observations of tumor reduction in human cancer patients, coupled with both inflammatory cytokine and Fas/fasL data from pre- and post-CM101 treatment biopsies, suggests a similar mechanism of induced tumor apoptosis (43).

MATERIALS AND METHODS

Mice, Tumor Cells, and Treatment Protocol

C57BL/6 mice (body weight, 22–25 grams) were obtained from Taconic (Germantown, NY) and maintained at the Vanderbilt Animal Care facility according to established protocols. The B16BL-6 murine melanoma cell line used in this study was obtained from the Tumor Repository of the National Cancer Institute (Frederick, MD). B16BL-6 cells were expanded and briefly maintained in Eagles MEM (Life Technologies, Inc.) supplemented with 10% FCS (Hyclone), 1 mM nonessential amino acids, 1 mM MEM vitamins, 2 mM glutamine, 1 mM sodium pyruvate, and 0.2% $NaHCO_3$ (all from Life Technologies, Inc.). Animals were injected s.c. with 1×10^5 B16BL-6 cells, and the tumors were allowed to grow for 5–7 days until palpable. Tumor-bearing mice were randomly segregated into control and experimental groups and injected i.v. via the tail vein every Monday, Wednesday, and Friday with either PBS or 60 μg/kg CM101, respectively. Clinical grade CM101 was produced as described previously (7).

Leukocyte Isolation and RT-PCR

Isolation of peripheral blood leukocytes was performed by gradient density centrifugation according to the manufacturer's protocol (Sigma Diagnostics). Samples were kept on ice during the entire isolation period. Total cellular RNA was isolated from purified leukocytes with the RNeasy MiniKit (Qiagen, Valencia, CA) and quantitated, and cDNA was synthesized using the First Strand cDNA Synthesis Kit (Pharmacia Biotech). Total RNA (2–5 μg) was reverse transcribed at 42°C with antisense gene-specific primers for *p53* and *β-actin*. An equal aliquot of the reverse transcription reaction was subjected to PCR (11). The primer pairs were as follows: (*a*) *p53* (GenBank accession number X01237). 5′-GGGACAGCCAAGTCTGTTATGTGC-3′ (sense primer) and 5′-CTGTCTTCCAGATACTCGGGATAC-3′ (antisense primer); and (*b*) *β-actin* (GenBank accession number X03765), 5′-AGCAAGAGAGGCATCCTGAC-3′ (sense primer) and 5′-CAGCTCATAGCTCTTCTCCA-3′ (antisense primer). Primer pairs spanning intron/exon junctions were selected to ensure that the desired PCR product was derived from RNA. For each gene product, the optimum number of PCR cycles was determined for linear amplification. All PCR products were verified by hybridization with a probe internal to the PCR primers.

Electrophoretic Gel Mobility Shift Assay of Whole Tumor Lysates

Tumor sections were homogenized with a Teflon Potter-Elvehjem style grinder in ice-cold lysis buffer [20 mM Tris (pH 7.5), 20% glycerol, 100 mM NaCl, 1% NP40, 1.5 mM $MgCl_2$, 1 mM DTT, 0.1 mM EDTA, 1 mM phenylmethylsulfonyl fluoride, and 10 μg/ml aprotinin (44)] and maintained on ice for 30 min. The samples were then expressed through an 18-gauge needle and centrifuged at 12,000 rpm for 10 min, and the protein concentration was determined by using the standard Bio-Rad assay. The double-stranded oligonucleotide probe containing the p53 DNA-binding sequence in the murine $p21^{Waf1/Cip1}$ gene promoter (45) was synthesized and end-labeled with [γ-^{32}P]ATP by T4 kinase (Promega Corp.) DNA binding reactions contained 50 μg of whole tumor lysate in 1× binding buffer [20 mM Tris (pH 7.5), 50 mM KCl, 5 mM $MgCl_2$, 1 mM DTT, 0.5 mM EDTA, and 30% glycerol] and 500

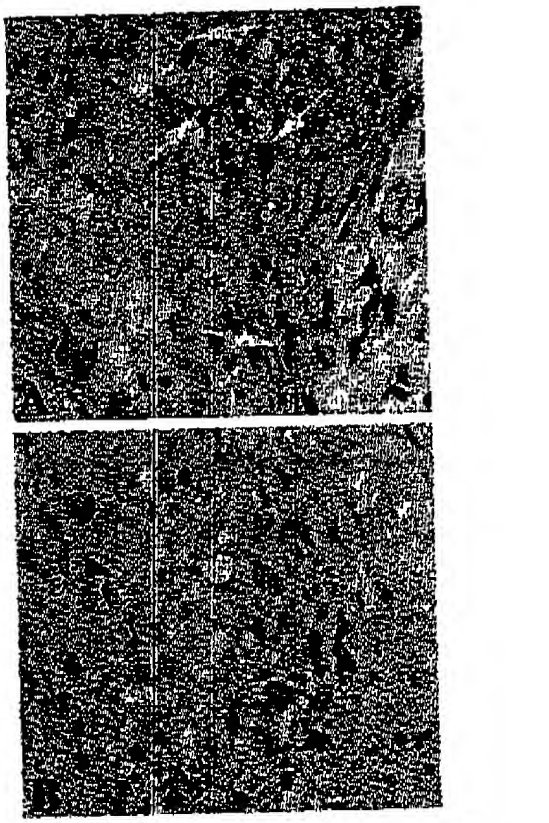

Fig. 1. Immunolocalization of CD45-positive cells in B16BL-6 melanoma tumors. Sections (7 μm) of tumors excised from CM101-treated animals were probed with either goat antimouse CD45 (*A*) or normal goat serum (*B*) followed by visualization with antigoat IgG HRP. In a representative tumor excised from a CM101-treated mouse, CD45-positive staining is observed within the tumor interstitium. *Bar*, 30 μm; magnification, ×400.

[5] R. J. Melder, R. K. Jain, and C. G. Hellerqvist, unpublished observations.

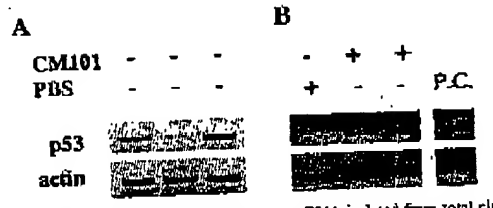

Fig. 2. *A*, RT-PCR analysis of *p53* and *β-actin* mRNA isolated from total circulating leukocytes from non-tumor-bearing C57BL/6 mice ($n = 3$). Amplification of a *p53*-specific PCR product derived from exons 4–6 generated an expected product of 280 bp; *β-actin* amplification served as a control for RNA quality, generating an expected product of 500 bp. *B*, RT-PCR analysis of *p53* and *β-actin* mRNA isolated from circulating leukocytes of B16BL-6 tumor-bearing mice treated with either PBS or 60 μg/kg CM101. Note the complete absence of *p53* mRNA in the PBS-treated sample. The data are representative of two experiments. *P.C.*, positive control.

ng of sheared, single-stranded DNA. A human phorbol ester-treated cell lysate (C32; Santa Cruz Biotechnology) was used as a positive control for binding, and unlabeled double-stranded probe in excess was used as a specific competitor. The DNA binding reactions were visualized by autoradiography after resolution on a 6%/0.25× Tris-borate EDTA polyacrylamide gel.

Immunoblot Analysis of p53, Fas, and Actin from Whole Tumor Lysates

Whole tumor lysates were prepared as described above. Equal amounts of total protein were loaded on each lane of a minigel and separated on a 4–15% SDS-PAGE gel (Bio-Rad). The proteins were electroblotted onto a polyvinylidene difluoride membrane and blocked with 5% nonfat dry milk in PBS [for p53 and actin, 150 mM NaCl, 10 mM Tris (pH 7.5); for Fas, 250 mM NaCl, 10 mM Tris (pH 7.5)] containing 0.1% Tween 20 for 1 h at room temperature. The membrane was then incubated for 1 h at room temperature with either rabbit anti-p53 polyclonal antibody FI-393, goat anti-actin polyclonal antibody I-19, or rabbit anti-Fas polyclonal antibody N-20 (all from Santa Cruz Biotechnology) diluted 1:400 in the respective PBS buffers described above. Incubation with antirabbit HRP-conjugated IgG (for p53 and Fas) or antigoat HRP-conjugated IgG (actin) diluted 1:6000 was performed for 1 h at room temperature. Immunoreactive bands were visualized by enhanced chemiluminescence (Amersham Life Sciences). The membrane was stripped with 0.2 N NaOH for 5 min and washed with PBS between individual antibody incubations.

Immunohistochemistry of Tumor Tissue

Fas/fasL. Immunohistochemical analysis was performed with the automated Ventana Immunohistochemical Stainer according to the manufacturer's suggested protocols (Ventana, Tuscon, AZ). Tumor sections (7 μm) were deparaffinized for 2 h at 75°C, followed by three changes of xylene for 5 min each, three changes of 100% ethanol for 5 min, 5 min in 95% ethanol, 3 min in tap water, and, finally, 3 min in Ventana's APK buffer. The samples were blocked for 20 min at 37°C with 5% BSA, washed, and then incubated for 32 min at 37°C with the appropriate diluted (1:100) antibody [rabbit anti-Fas or rabbit anti-fasL (both from Santa Cruz Biotechnology)]. Normal rabbit IgG was used as a control. For DAB detection, the slides were incubated in 1% H_2O_2 for 15 min before blocking with BSA. An avidin/biotin blocker (Ventana) was applied to the samples for 8 min at 37°C, followed by incubation with the appropriate biotin-conjugated secondary antibody. For Fast Red visualization, the samples were incubated for 12 min with avidin-conjugated alkaline phosphatase, washed, and incubated with Ventana Enhancer for 4 min, followed by incubation in Fast Red A/naphthol (Ventana) for 8 min. Fast Red B was then immediately added for an additional 8 min. The samples were washed, counterstained with hematoxylin, dehydrated, and mounted in toluene-free mounting medium. For DAB visualization, the sections were incubated with avidin-HRP for 12 min at 37°C, washed, and then incubated with DAB/H_2O_2 for an additional 8 min. The sections were finally incubated with a copper enhancer (Ventana) for 4 min, washed, counterstained with hematoxylin, and mounted. Photographic documentation was performed with an Olympus microscope outfitted with an Olympus 3.0 digital camera and software.

CD45. Tumor sections were deparaffinized in xylene, rehydrated with a graded ethanol series, and rinsed with PBS. The slides were then blocked with 1% H_2O_2 in 30% methanol/PBS for 40 min at room temperature to eliminate endogenous peroxidase activity. The slides were rinsed in PBS, blocked with 5% normal donkey serum/5% BSA in PBS for 40 min, and then incubated with 5 μg/ml goat antimouse CD45 (Santa Cruz Biotechnology) for 1.5 h at room temperature. The slides were rinsed in PBS, incubated with donkey antigoat IgG (biotin-conjugate) (Santa Cruz Biotechnology) for 30 min at room temperature and then rinsed again with PBS. Visualization was performed by incubation with streptavidin-HRP followed by incubation with DAB/H_2O_2. The sections were counterstained with 0.5% methyl green, dehydrated, and mounted.

Apoptotic Indices

Apoptosis was detected in tumor sections by labeling the 3′ OH ends of DNA with biotin-14-dCTP (46). Briefly, paraffin-embedded material was deparaffinized, rehydrated, and then subjected to proteinase K [20 μg/ml in 10 mM Tris (pH 7.5), 10 mM NaCl, and 2 mM $CaCl_2$] digestion for 20 min at room temperature. The labeling reaction was prepared on ice containing 1× TdT reaction buffer, 50 μM biotin-14-dCTP, and 0.22 unit/μl recombinant TdT (all from Life Technologies, Inc.). A sufficient volume of the labeling reaction was added to each slide and incubated at room temperature for 15 min. A reaction mixture without TdT was used as a negative control. Streptavidin-alkaline phosphatase (Life Technologies, Inc.) was diluted 1:1000 in 1× PBS (containing 0.1% NP40 and 3% BSA) and applied to each slide for 15 min at room temperature. Visualization of apoptotic nuclei was performed with 1-Step™ NBT/BCIP (Pierce) until sufficient color development occurred. High molecular weight DNA was isolated from mouse tumor tissue by lysis in a buffer containing 100 mM NaCl, 10 mM Tris (pH 8.0), 25 mM EDTA, 0.5% SDS, and 100 μg/ml proteinase K. The lysates were incubated for 4 h at 50°C, precipitated with ethanol, resuspended in 10 mM Tris (pH 8.0)-1 mM EDTA, and quantitated and analyzed on a 1.5% agarose gel.

RESULTS

Infiltration of CD45-positive Cells into B16BL-6 Melanoma Tumors after CM101 Treatment. Consistent with our previously reported data in other tumor models (6), CD45-positive cells were found to infiltrate the B16BL-6 tumor after treatment with CM101 (Fig. 1*A*). However, in tumors isolated from mice treated with PBS, leukocytes were evident within the lumen of blood vessels, but no margination of the vessel wall or infiltration of the tumor was observed (data not shown).

Up-Regulation of Leukocyte *p53* mRNA. In peripheral blood leukocytes isolated from non-tumor-bearing C57BL/6 mice, measurable levels of *p53* mRNA were detected by RT-PCR in all animals tested (Fig.

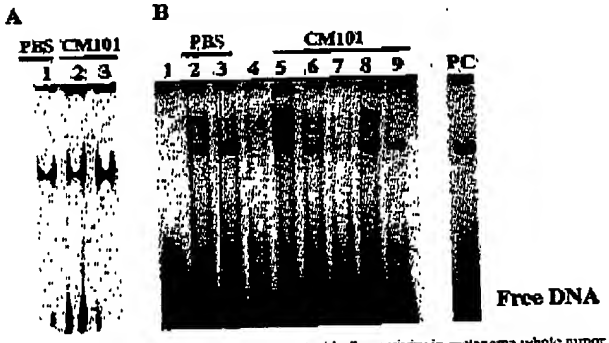

Fig. 3. Effect of CM101 on p53-specific DNA binding activity in melanoma whole tumor lysates. *A*, representative melanoma whole tumor lysate derived from a PBS-treated animal demonstrating low sequence-specific binding to the $p53^{wt/wt/wt}$-derived p53 DNA binding sequence (*Lane 1*). CM101 treatment of two tumor-bearing animals resulted in an increase in specific DNA binding in both whole tumor lysates (*Lanes 2* and *3*). *B*, in a separate experiment, low DNA binding was again observed in whole tumor lysates derived from PBS-treated animals (*Lanes 2* and *3*), whereas whole tumor lysates from CM101-treated animals demonstrated increased p53-specific DNA binding (*Lanes 5–9*). A liver extract from a CM101-treated animal showed no DNA binding (*Lane 4*). A human C32 phorbol ester-treated lysate served as a positive control for p53 DNA binding activity (*Lane PC*).

2A, *Lanes 1–3*). Similar analysis of peripheral blood leukocytes isolated 1 h after PBS treatment of a representative B16BL-6 tumor-bearing mouse demonstrated that PBS treatment did not stimulate an elevation in *p53* mRNA (Fig. 2B, *Lane 1*). No measurable *p53* mRNA could be detected in any PBS-treated tumor-bearing animal. However, within 1 h of i.v. infusion of CM101, a significant elevation of *p53* mRNA could be measured in circulating leukocytes (Fig. 2B, *Lanes 2* and *3*). *β-Actin* mRNA was measured in each sample as a control for RT-PCR efficiency (Fig. 2, *A* and *B*, *bottom panel*).

CM101-induced p53 Sequence-specific DNA Binding in Whole Tumor Lysates. B16BL-6 melanoma cells *in vitro* express low levels of p53 by Western blot analysis (47) and RT-PCR (data not shown). However, these particular techniques do not indicate whether or not the identified p53 species is transcriptionally active. Whole cell lysates from B16BL-6 melanoma cells were tested for the ability to bind to the murine $p21^{Waf1/Cip1}$-derived p53 DNA-binding consensus sequence. No DNA binding was observed when compared with an equal concentration of a control lysate prepared from human C32 phorbol ester-induced cells (data not shown). The absence of sequence-specific p53 DNA binding suggests that the p53 expressed in these cells is a mutant phenotype and is therefore unable to participate in p53-dependent signaling pathways. However, low expression of wild-type p53 cannot be ruled out. This is consistent with the results of several studies exploring the role of p53 transcriptional activity in tumor growth suppression (22).

Whole tumor lysates were prepared from animals treated every Monday, Wednesday, and Friday with PBS or 60 μg/kg CM101 and subjected to the electrophoretic mobility shift analysis assay with the murine $p21^{Waf1/Cip1}$-derived p53 DNA-binding sequence. In two independent experiments, whole tumor lysates from PBS-treated animals demonstrated a low background binding (Fig. 3A, *Lane 1* and Fig. 3B, *Lanes 2* and *3*). However, whole tumor lysates from CM101-treated animals exhibited at least a 2-fold increase in p53-specific DNA binding (Fig. 3A, *Lanes 2* and *3*). p53 DNA binding in experiment 2 was more varied among the five tumor extracts analyzed (Fig. 3B, *Lanes 5–9*). The resulting shifts could be specifically competed with excess unlabeled, specific competitor DNA. No binding was detected in a liver lysate from a CM101-treated animal (Fig. 3B, *Lane 4*).

Increased p53 and Fas Proteins in Whole Tumor Lysates. To account for the variability of p53 DNA binding observed in experiment 2, Western blot analysis of total p53, Fas, and actin in whole tumor lysates was performed. No significant differences in the amount of tumor actin protein were observed among the tumor lysates examined (Fig. 4A, *bottom panel*). Animals treated with PBS demonstrated an even distribution of tumor p53 protein, although three of five tumor lysates from CM101-treated animals exhibited an increase in p53 protein (Fig. 4A, *top panel*). In the context of uniform actin detection, the differences in p53 protein levels are most likely the result of *in vivo* responses to CM101 and are not associated with protein quantitation or transfer to the polyvinylidene difluoride membrane. Whole tumor lysates that exhibited elevated total p53 protein levels correlated with those lysates that demonstrated an increase in p53 DNA-binding activity. Increased levels of Fas protein were also detected in the same tumor lysates of CM101-treated animals when compared with tumor lysates from PBS-treated animals (Fig. 4A, *middle panel*).

Immunolocalization of Fas and fasL. The increase of Fas protein within whole tumor lysates suggested that a mechanism of action of CM101 might be the reduction of immunoprivilege established by the tumor. RT-PCR analysis of B16BL-6 tumor cells maintained *in vitro* indicated these cells express fasL (data not shown). Before CM101 treatment of tumor-bearing mice, expression of fasL is distributed throughout the tumor (Fig. 5A), and the pattern of cytoplasmic staining is localized exclusively to the tumor cells. In contrast, the expression of Fas protein was not detected (Fig. 5B). These results are consistent with the RT-PCR analysis. After CM101 treatment, a significant decrease in tumor cell fasL was observed (Fig. 5C). Some tumor cells were still positive for fasL; however, the number of cells expressing fasL was greatly diminished when compared with the number of cells expressing fasL in the PBS-treated tumor. In contrast, tumor cell Fas expression was significantly elevated in the CM101-treated tumor (Fig. 5D) and evenly distributed throughout the tumor. Normal rabbit IgG did not result in any positive staining (Fig. 5E).

Apoptosis Indications. Increased expression of Fas protein within the tumor cells after CM101 treatment suggested that the tumor might have become sensitized to apoptosis. TUNEL-positive nuclei were absent in the PBS-treated tumor examined (Fig. 6A). DNase I digestion of a serial section of the same tumor before TUNEL labeling served as a positive control (Fig. 6C). In the CM101-treated tumor, a significant number of TUNEL-positive nuclei with a distinctive pattern of labeling were evident (Fig. 6B). Isolation of high molecular weight tumor DNA from PBS-treated animals indicated no DNA fragmentation (Fig. 7, *Lane 1*). However, tumor DNA isolated from a CM101-treated animal exhibited significant smearing of high molecular weight DNA and the generation of the classical DNA ladder (Fig. 7, *Lane 2*).

DISCUSSION

Our previous experiments in murine tumor models demonstrated that repeated i.v. infusion of CM101 resulted in a significant reduction in tumor volume of human tumor xenografts (7) and promoted the long-term survival of BALB/c mice bearing Madison lung tumors (8). In response to CM101, significant capillary

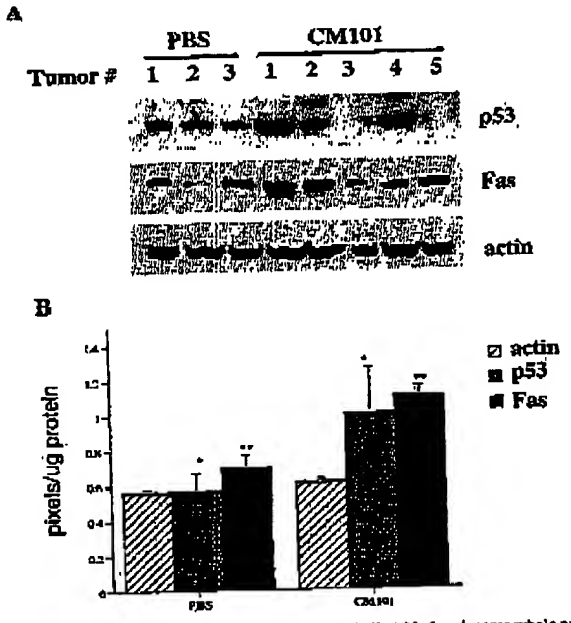

Fig. 4. Analysis of p53 and Fas protein expression in B16BL-6 melanoma whole tumor lysates. *A*, immunoblot analysis. Whole tumor lysates prepared from either PBS- or CM101-treated mice were separated with 4–15% SDS-PAGE followed by immunoblotting with anti-p53, anti-Fas, or anti-actin antibodies. The same membrane was stripped and reprobed for each antibody examined. *B*, semiquantitative analysis of p53 and Fas proteins normalized to actin. Columns and respective error bars represent the mean ± SD from one experiment (for the PBS samples, $n = 3$ for p53, Fas, and actin; for CM101 samples, $n = 5$ for p53, Fas, and actin). Statistical analysis was determined at the 95% confidence interval using the Mann-Whitney test by Statmost (DataMost Corp., Salt Lake City, UT). *, $P = 0.05$ relative to PBS; **, $P = 0.03$ relative to PBS. The figure is representative of two independent experiments.

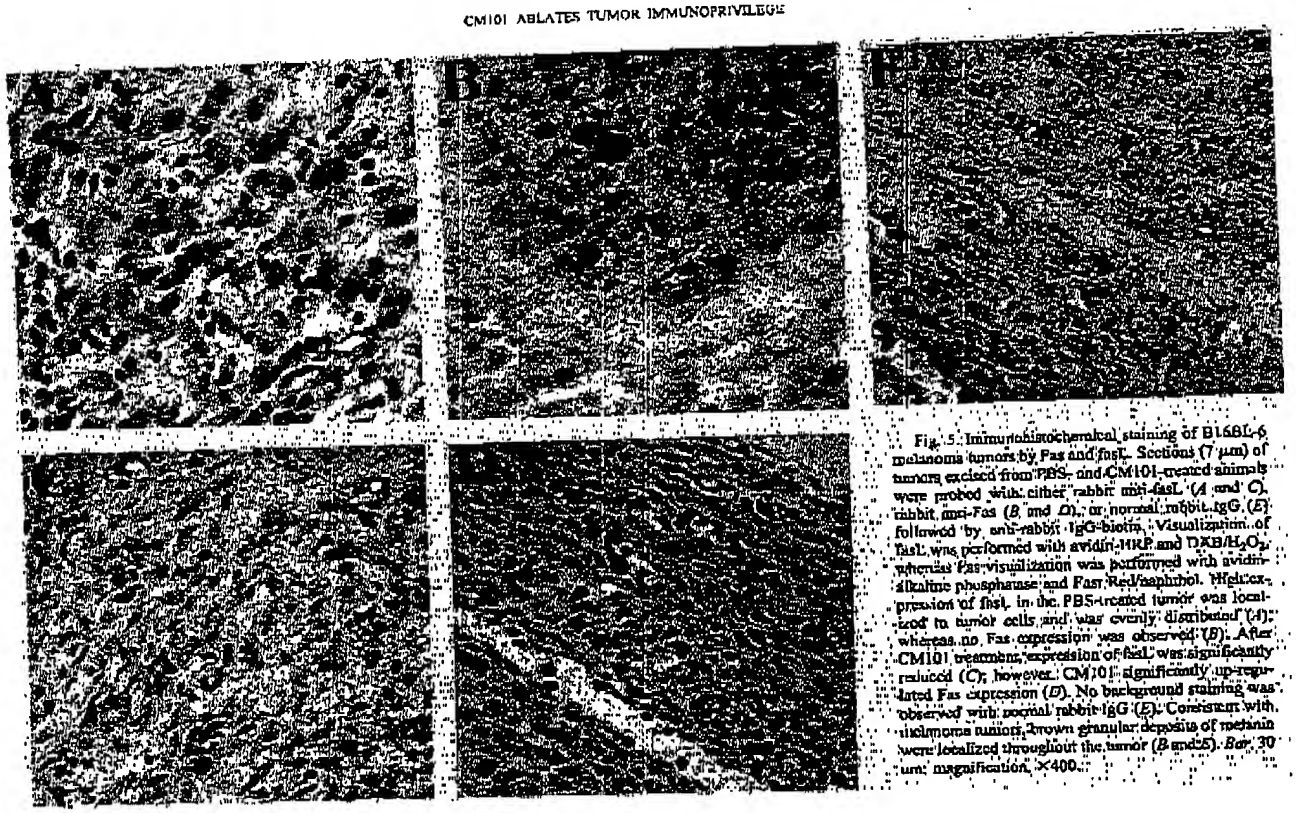

Fig. 5. Immunohistochemical staining of B16BL-6 melanoma tumors by Fas and fasL. Sections (7 μm) of tumors excised from PBS- and CM101-treated animals were probed with either rabbit anti-fasL (*A* and *C*), rabbit anti-Fas (*B* and *D*), or normal rabbit IgG (*E*) followed by anti-rabbit IgG-biotin. Visualization of fasL was performed with avidin-HRP and DAB/H_2O_2, whereas Fas visualization was performed with avidin-alkaline phosphatase and Fast Red/naphthol. High expression of fasL in the PBS-treated tumor was localized to tumor cells and was evenly distributed (*A*); whereas no Fas expression was observed (*B*). After CM101 treatment, expression of fasL was significantly reduced (*C*); however, CM101 significantly up-regulated Fas expression (*D*). No background staining was observed with normal rabbit IgG (*E*). Consistent with melanoma tumors, brown granular deposits of melanin were localized throughout the tumor (*B* and *E*). *Bar*, 30 μm; magnification, ×400.

thrombosis, hemorrhage, and endothelial cell damage were observed within the tumor vasculature, with no evidence of toxicity to the vasculature of other organs. Furthermore, CM101 also induced an inflammatory response with increased numbers of leukocytes within both the tumor vasculature and the tumor itself (9). CM101 has no effect on normal physiological neovasculature such as that occurring during pregnancy (48), or wound healing (49). Recently, we have demonstrated that CM101 binds within 5 min to the endothelium of newly established tumor vasculature (11). CM101 activates complement C3, allowing activated leukocytes to adhere and extravasate into the tumor. This ability of CM101 to promote leukocyte adhesion on otherwise leukocyte-adhesion protected tumor vasculature (50) initiates the breakdown of tumor immunoprivilege (11). Therefore, these observations strongly suggest that CM101 selectively targets and inhibits pathological and not physiological angiogenesis through the engagement of the tumor endothelium. Up-regulation of TNFR II on the mature tumor endothelium, concomitant with infiltration of TNF-α-expressing activated inflammatory cells (11), provides supporting evidence for CM101-induced tumor apoptosis mediated through targeting of the vasculature. Indeed, a time- and dose-dependent systemic elevation of the inflammatory cytokines MIP-1α, TNF-α, IL-6, IL-8, and IL-10 has been demonstrated in human cancer patients in a successful Phase I study with CM101 (51), indicative of an activated tumor-targeted inflammatory response. Elevation of plasma levels of soluble-E-selectin provided further proof for engagement of the tumor endothelium in the inflammatory process (52). The fact that CM101 Phase I cancer patients experienced tumor-localized pain and that tumor biopsies acquired from these same patients before and after treatment showed tumor infiltration of inflammatory cells after CM101 treatment (43) corroborates a mechanism of tumor-targeted inflammation. The similarity of the apparent tumor response in human cancer patients and tumor-bearing mice to CM101 treatment prompted a closer examination of the role of CM101-induced inflammation in the breakdown of the immunoprivilege imposed by the tumor.

Circulating peripheral blood leukocytes obtained from tumor-bearing mice do not express *p53* mRNA, in contrast to non-tumor-bearing mice, which do express *p53* mRNA (Fig. 2). However, within 60 min of CM101 administration, elevated leukocyte *p53* mRNA was detected that coincided with leukocyte (CD45-positive) infiltration of the tumor (Figs. 1 and 2). PBS treatment of tumor-bearing animals did not elevate peripheral blood leukocyte *p53* mRNA, nor did it cause leukocyte infiltration of the tumor. These observations suggest that transcription of *p53* in immune effector cells is suppressed in tumor-bearing mice, and the consequences of this suppression contribute to the tumor immunoprivilege.

B16-F10 melanoma cells in culture express low but detectable levels of p53 protein and little or no Fas protein (47). RT-PCR analysis of cultured B16BL-6 melanoma cells revealed a positive signal for both *p53* and *fasL* mRNA; however, no *Fas* mRNA could be detected (data not shown). Additionally, p53 protein in these cells is unable to bind DNA as determined by a specific DNA binding assay. p53 binds to DNA in a sequence-specific manner in response to a variety of extracellular signals initiating the transcription of genes associated with cellular proliferation and/or apoptosis (13–20). In the DNA binding studies described here, we used oligonucleotides representing the consensus p53-binding site in the murine $p21^{Waf1/Cip1}$ gene promoter known to be induced by p53 (14). Detection of a p53 sequence-specific DNA complex would serve as an indicator of active p53 within the tumor. After CM101 administration, whole melanoma tumor lysates exhibited

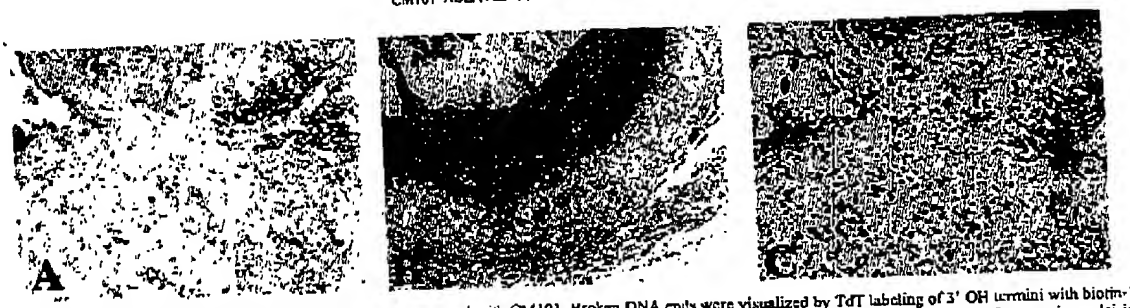

Fig. 6. *In situ* detection of apoptosis in B16BL-6 melanoma tumors treated with CM101. Broken DNA ends were visualized by TdT labeling of 3' OH termini with biotin-14-dCTP and subsequent detection with streptavidin-alkaline phosphatase. *A*, no labeling was observed in the tumors treated with PBS. *B*, extensive labeling of apoptotic nuclei is evident throughout the tumor derived from a CM101-treated animal. *C*, a DNase I-positive control of the tumor derived from the PBS-treated animal.

an increase in p53-specific DNA binding activity when compared with whole tumor lysates from PBS-treated animals (Fig. 3). Those extracts that demonstrated an increase in DNA binding activity also had an increase in the amount of total p53 protein. Because the tumor-infiltrating leukocytes demonstrated an up-regulation of *p53* mRNA, they could constitute the source for increased p53 protein activity within the whole tumor lysates.

Within the context of the experiments described in this report, it is not entirely clear how the up-regulation of *p53* mRNA in the infiltrating leukocytes contributes to CM101-induced apoptosis of the tumor cells. It is possible that the suppression of a host wild-type *p53* allele in the tumor cells is overridden by the sequence of events associated with the tumor-targeted inflammatory response induced by CM101. Therefore, immunosuppression induced on the host by the tumor may be overcome through the activation of a suppressed wild-type *p53* allele in the melanoma tumor cell that is not seen *in vitro*.

Studies by others of human colon and esophageal tumors have demonstrated that immune evasion through alteration of Fas/fasL expression is a possible mechanism of tumor growth and survival (35–37). Human esophageal carcinoma tumors displayed evidence of apoptotic CD45-positive tumor-infiltrating lymphocytes in regions of the tumors with elevated fasL expression. In contrast, fasL-negative regions of the tumors were positive for infiltrating CD45-positive cells, with no evidence of apoptosis. It has been suggested (40, 43, 53) that fasL-mediated depletion of tumor-infiltrating immune cells might contribute to tumor immunoprivilege. The data presented herein support and expand on these studies. Immunolocalization studies clearly show that after CM101 treatment, Fas protein is distributed throughout the tumor, which was previously negative for Fas protein expression. The elevated fasL protein seen in the tumors before CM101 treatment is down-regulated after CM101 treatment as the tumor becomes apoptotic, presumably via Fas-fasL interactions. The targeted inflammatory response induced by CM101 overrides the immunoprivilege and may be a plausible explanation for its antitumor effect.

Increased p53 activity has been correlated with Fas expression (18–20). Our data also show that leukocytes targeting the tumor vasculature after administration of CM101 have elevated *p53* mRNA. These leukocytes may have the potential to deliver known or otherwise unknown p53-dependent effectors associated with apoptosis to the Fas-positive tumors cells.

Indeed, the development of therapeutic strategies reintroducing wild-type p53 into p53-deficient tumors is an area of great interest. Recently, adenoviral delivery of p53 into human colon cancer cells has been reported to inhibit tumor-induced angiogenesis (54). However, CM101 is unique in that it stimulates the immune system and targets and delivers leukocytes with elevated *p53* mRNA to the tumor via the tumor neovasculature. This specific antipathoangiogenic mechanism of action leads to an apoptotic response in the tumor cells and in the endothelium (11).

The p53 DNA binding experiments with whole tumor lysates and the immunohistochemistry of tumor sections after CM101 treatment show that p53 activity is elevated within the tumors, fasL expression is reduced, and apoptotic tumor cells are present. The mechanism of up-regulation of transcription of *p53* in the leukocytes of tumor-bearing mice and the issue of whether the same mechanism would apply to the onset of apoptosis in human tumors as observed previously (43) remain to be elucidated. Attempts to address this issue are in progress in p53 knockout mice.

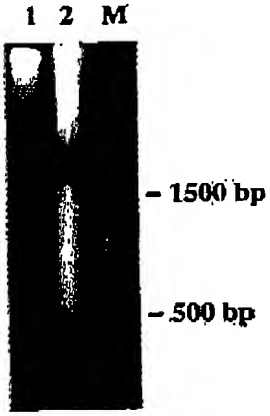

Fig. 7. Fragmentation of high molecular weight B16BL-6 melanoma tumor DNA. High molecular weight DNA was isolated, and equal amounts of DNA based on $A_{260\ nm}$ were subjected to agarose gel electrophoresis (5 μg/lane). No DNA fragmentation was observed in tumor DNA isolated from a PBS-treated animal (*Lane 1*). However, tumor DNA from a CM101-treated animal displayed a significant amount of fragmentation as indicated by the loss of high molecular weight DNA and the appearance of the classical DNA ladder (*Lane 2* versus *Lane 1*).

ACKNOWLEDGMENTS

We thank Dr. R. Stephen Lloyd and Dr. James V. Sturos for helpful discussions throughout this work, Dr. Jennifer Pietenpol and Dr. David Carbone for critical and valuable comments regarding the manuscript, and Pamela T. Chunn for preparation of the manuscript.

REFERENCES

1. Hellerqvist, C. G., Rojas, J., Green, R. S., Sell, S., Sundell, H., and Stahlman, M. T. Studies on group B β-hemolytic *Streptococci*. Isolation and partial characterization of an extra-cellular toxin. Pediatr. Res., *15*: 892–898, 1981.
2. Rojas, J., Larson, L. E., Hellerqvist, C. G., Brigham, K. L., and Stahlman, M. T. Pulmonary hemodynamic and ultra-structural changes associated with Group B

streptococcal toxemia in adult sheep and newborn lambs. Pediatr. Res., *17:* 1002–1008, 1983.
5. Sundell, H. W., Fish, W. G., Sandberg, K. L., Edberg, K. E., Pappas, R. S., and Hellerqvist, C. G. Lung injury by streptococcal toxins. *In:* L. Brigham and M. T. Stahlman (eds), Respiratory Distress Syndromes, pp. 58–70. Nashville, TN: Vanderbilt University Press, 1990.
4. Sundell, H. W., Yan, H-P., Wu, K., Wamil, B. D., Gaddipati, R., Carter, C. E., Stahlman, M. T., and Hellerqvist, C. G. Isolation and identification of group B β-hemolytic streptococcal (GBS) toxin from septic newborn infants. Pediatr. Res., *39:* 302A, 1997.
5. Hellerqvist, C. G. Therapeutic Agent and Method of Inhibiting Vascularization of Tumors. United States Patent 5,010,062. 1991.
6. Hellerqvist, C. G. CM101: an anti-pathoangiogenic agent, pre-clinical and clinical experiences. *In:* M. E. Maragoudakis (ed.). Angiogenesis: Models, Modulators, and Clinical Applications, pp. 449–457. New York: Plenum Press, 1998.
7. Hellerqvist, C. G., Thurman, G. B., Page, D. L., Wang, Y-F., Russell, B. A., Montgomery, C. A., and Sundell, H. W. Antitumor effects of GBS toxin: a polysaccharide exotoxin from group B β-hemolytic *Streptococcus*. J. Cancer Res. Clin. Oncol., *120:* 63–70, 1993.
8. Thurman, G. B., Russell, B. A., York, G. E., Wang, Y-F., Page, D. L., Sundell, H. W., and Wamil, B. D. Effects of group B *Streptococcus* toxin on long-term survival of mice bearing transplanted Madison lung tumors. J. Cancer Res. Clin. Oncol., *120:* 479–484, 1994.
9. Thurman, G. B., Page, D. L., Wamil, B. D., Wilkinson, L. E., Kasumi, M., and Hellerqvist, C. G. Acute inflammatory changes in subcutaneous microtumors in the ears of mice induced by intravenous CM101 (GBS toxin). J. Cancer Res. Clin. Oncol., *122:* 549–553, 1996.
10. Hellerqvist, C. G., Thurman, G. B., Russell, B. A., Page, D. L., York, G. E., Wang, Y-F., Castillo, C., and Sundell, H. W. Anti-tumor effects of GBS toxin are caused by induction of a targeted inflammatory reaction. *In:* M. E. Maragoudakis (ed.). Angiogenesis: Molecular Biology, Clinical Aspects, 1994.
11. Yan, H.-P., Carter, C. E., Wang, E., Page, D. L., Washington, K., Wamil, B. D., Yakes, F. M., Thurman, G. B., and Hellerqvist, C. G. Functional studies on the anti-pathoangiogenic properties of CM101. Angiogenesis, *3:* 219–233, 1998.
12. Brown, J. M., and Wouters, B. G. Apoptosis, p53, and tumor cell sensitivity to anticancer agents. Cancer Res., *59:* 1391–1399, 1999.
13. Kastan, M. B., Zhan, Q., El-Deiry, W. S., Carrier, F., Jacks, T., Walsh, W. V., Plunkett, B. S., Vogelstein, B., and Fornace, A. J. A mammalian cell cycle checkpoint pathway utilizing p53 and GADD45 is defective in ataxia-telangiectasia. Cell, *71:* 587–597, 1992.
14. El-Deiry, W. S., Tokino, T., Velculescu, V. E., Levy, D. B., Parsons, R., Trent, J. M., Lin, D., Mercer, W. E., Kinzler, K. W., and Vogelstein, B. WAF1, a potential mediator of p53 tumor suppression. Cell, *75:* 817–825, 1993.
15. El-Deiry, W. S., Harper, J. W., O'Connor, P. M., Velculescu, V. E., Canman, C. E., Jackman, J., Pietenpol, J. A., Burrel, M., Hill, D. E., Wang, Y., and Vogelstein, B. WAF1/CIP1 is induced in p53-mediated G_1 arrest and apoptosis. Cancer Res., *54:* 1169–1174, 1994.
16. Wu, G. S., Burns, T. B., McDonald, E. R., Jiang, W., Meng, R., Krantz, I. D., Kao, G., Gan, D. D., Zhou, J. Y., Muschel, R., Hamilton, S. R., Spinner, N. B., Markowitz, S., Wu, G., and El-Deiry, W. S. KILLER/DR5 is a DNA damage-inducible p53 regulated death receptor gene. Nat. Genet., *17:* 141–143, 1997.
17. Sheikh, M. S., Burns, T. F., Huang, G., Wu, G. S., Amundson, S., Brooks, K. S., Fornace, A. J., Jr., and El-Deiry, W. S. p53-dependent and independent regulation of the death receptor KILLER/DR5 gene expression in response to genotoxic stress and tumor necrosis factor-α. Cancer Res., *58:* 1593–1598, 1998.
18. Owen-Schaub, L. B., Zhang, W., Cusack, J. C., Angelo, L. S., Santee, S. M., Fujiwara, T., Roth, J. A., Deisseroth, A. B., Zhang, W. W., and Kruzel, E. Wild-type human p53 and a temperature-sensitive mutant induce Fas/APO-1 expression. Mol. Cell. Biol., *15:* 3032–3040, 1995.
19. Bennett, M., Macdonald, K., Chan, S-W., Luzio, J. P., Simari, R., and Weissberg, P. Cell surface trafficking of Fas: a rapid mechanism of p53-mediated apoptosis. Science (Washington DC), *282:* 290–293, 1998.
20. Muller, M., Wilder, S., Bannasch, D., Israeli, D., Lehlbach, K., Li-Weber, M., Friedman, S. L., Galle, P. R., Stremmel, W., Oren, M., and Krammer, P. H. P53 activates the CD95 (APO-1/Fas) gene in response to DNA damage by anticancer drugs. J. Exp. Med., *188:* 2033–2045, 1998.
21. Harris, C. C. Structure and function of the p53 tumor suppressor gene: clues for rational cancer therapeutic strategies. J. Natl. Cancer Inst., *88:* 1442–1455, 1996.
22. Pietenpol, J. A., Tokino, T., Thiagalingam, S., El-Deiry, W. S., Kinzler, K. W., and Vogelstein, B. Sequence-specific transcriptional activation is essential for growth suppression by p53. Proc. Natl. Acad. Sci. USA, *91:* 1998–2002, 1994.
23. Gonfredi, V., Perschiaroli, A., Fimia, G. M., and Maione, R. p53-independent apoptosis induced by muscle differentiation stimuli in polyomavirus large T-expressing myoblasts. J. Cell Sci., *112:* 2397–2407, 1999.
24. Wang, C. H., Chen, Y. L., Tsao, Y. P., and Chen, S. L. Simian virus 40 T antigen induces p53-independent apoptosis but does not suppress erbB2/neu gene expression in immortalized human epithelial cells. Cancer Lett., *137:* 107–115, 1999.
25. Itoh, N., Yonehara, S., Ishii, A., Yonehara, M., Mizushima, S., Sameshima, M., Hase, A., Seto, Y., and Nagata, S. The polypeptide encoded by the cDNA for human cell surface antigen Fas can mediate apoptosis. Cell, *66:* 233–243, 1991.
26. Nagata, S. Apoptosis by death factor. Cell, *88:* 355–365, 1997.
27. Watanabe-Fukunaga, R., Brannan, C. I., Itoh, N., Yonehara, S., Copeland, N. G., Jenkins, N. A., and Nagata, S. The cDNA structure, expression, and chromosomal assignment of the mouse Fas antigen. J. Immunol., *148:* 1274–1279, 1992.
28. Suda, T., Okazaki, T., Naito, Y., Yokota, N., Arai, S., Ozaki, K., Nakao, K., and Nagata, S. Expression of the fasL in cells of T cell lineage. J. Immunol., *154:* 3806–3813, 1995.
29. Suda, T., Takahashi, T., Golstein, P., and Nagata, S. Molecular cloning and expression of the Fas ligand, a novel member of the tumor necrosis factor family. Cell, *75:* 1169–1178, 1993.
30. Hanhe, M., Remo, T., Schroeter, M., Imiler, M., French, L., Bornand, T., MacDonald, H. R., and Schopp, J. Activated B cells express functional fas ligand. Eur. J. Immunol., *26:* 721–724, 1996.
31. Bisehen, C. M., Schilling, J. D., Lynch, D. H., Krammer, P. H., and Leibson, P. J. Fc-induced expression of fas ligand on activated NK cells facilitates cell-mediated cytotoxicity and subsequent autocrine NK cell apoptosis. J. Immunol., *156:* 2693–2699, 1996.
32. Wu, M. X., Ao, Z., Hegen, J., Morimoto, C., and Schlossman, S. F. Requirement of Fas (CD95), CD45, and CD11a/CD18 in monocyte-dependent apoptosis of human T cells. J. Immunol., *157:* 707–713, 1996.
33. Hug, H. Fas-mediated apoptosis in tumor formation and defense. Biol. Chem., *378:* 1405–1412, 1997.
34. Walker, P. R., Saas, P., and Dietrich, P-Y. Role of fas ligand (CD95L) in immune escape: the tumor cell strikes back. J. Immunol., *158:* 4521–4524, 1997.
35. Gruss, C., Tohma, Y., Barnas, C., Tamiere, P., Hainaut, P., and Ohgaki, H. Up-regulation of Fas (APO-1/CD95) ligand and down-regulation of Fas expression in human esophageal cancer. Cancer Res., *58:* 2057–2062, 1998.
36. O'Connell, J., Bennett, M. W., O'Sullivan, G. C., Roche, D., Kelly, J., Collins, J. K., and Shanahan, F. FasL expression in primary colon adenocarcinomas: evidence that the Fas counterattack is a prevalent mechanism of immune evasion in human colon cancer. J. Pathol., *186:* 240–246, 1998.
37. Bennett, M. W., O'Connell, J., O'Sullivan, G. C., Brady, C., Roche, D., Collins, J. K., and Shanahan, F. The Fas counterattack *in vivo*: apoptotic depletion of tumor-infiltrating lymphocytes associated with fasL expression by human esophageal carcinoma. J. Immunol., *160:* 5669–5675, 1998.
38. Hanhe, M., Rimoldi, D., Schroter, M., Romero, P., Schreier, M., French, L. E., Schneider, P., Bornand, T., Fontana, A., Lienard, D., Cerottini, J-C., and Tschopp, J. Melanoma cell expression of Fas(APO-1/CD95) ligand: implications for tumor immune escape. Science (Washington DC), *274:* 1363–1366, 1996.
39. Nagata, S. Fas ligand and immune evasion. Nat. Med., *2:* 1306–1307, 1996.
40. Strand, S., and Galle, P. R. Immune evasion by tumours: involvement of the CD95(APO-1/Fas) system and its clinical implications. Mol. Med. Today, *4:* 63–68, 1998.
41. Sata, M., and Walsh, K. TNFα regulation of Fas ligand expression on the vasculature endothelium modulates leukocyte extravasation. Nat. Med, *4:* 415–420, 1998.
42. Walsh, K., and Sata, M. Negative regulation of inflammation by fas ligand expression on the vascular endothelium. Trends Cardiovasc. Med., *9:* 34–41, 1999.
43. Hellerqvist, C. G., Wang, E., Wamil, B. D., Price, J. O., Yan, H-P., Carter, C. E., Wang, Y-F., DeVore, R. F., Johnson, D. H., and Lloyd, R. S. Evidence of induced apoptosis in cancer patients treated with CM101. Proc. Am. Soc. Clin. Oncol., *16:* 546, 1997.
44. Lin, Y., and Benchimol, S. Cytokines inhibit p53-mediated apoptosis but not p53-mediated G_1 arrest. Mol. Cell. Biol., *15:* 6045–6054, 1995.
45. Hasnaharvi, T., Pitkanen, K., Taubari, , and Laiho, M. p53 transactivation and protein accumulation are independently regulated by UV light in different phases of the cell cycle. Mol. Cell. Biol., *17:* 3074–3080, 1997.
46. Darfler, M. M., and Kaniszkiewicz, J. W. *In situ* localization of apoptosis using terminal deoxynucleotidyl transferase. Focus. *17:* 81–83. 1995.
47. Kalechman, Y., Sredni, B., Albeck, M., and Sredni, B. Up-regulation by ammonium trichloro(dioxoethylene-0,0') tellurate (AS101) of Fas/APO-1 expression on B16 melanoma cells: implications for the antitumor effects of AS101. J. Immunol., *161:* 3536–3542, 1998.
48. Wamil, B. D., Yakes, F. M., Thurman, G. B., Juliao, S., Venkov, C., Page, D. L., and Hellerqvist, C. G. CM101: evidence of an anti-pathoangiogenic mechanism of action. Proc. Am. Assoc. Cancer Res., *39:* 97, 1998.
49. Quinn, T. E., Thurman, G. B., Sundell, A. K., Zhang, M., and Hellerqvist, C. G. CM101, a polysaccharide antitumor agent, does not inhibit wound healing in murine models. J. Cancer Res. Clin. Oncol., *121:* 253–256, 1995.
50. Fukumura, D., Salchi, H. A., Witwer, B., Tuma, R. F., Melder, R. J., and Jain, R. K. Tumor necrosis factor α-induced leukocyte adhesion in normal and tumor vessels: effect of tumor type, transplantation site, and host strain. Cancer Res., *55:* 4824–4829, 1995.
51. Devore, R. F., Hellerqvist, C. G., Wakefield, G. B., Wamil, B. D., Thurman, G. B., Minton, P. A., Sundell, H. W., Yan, H-P., Carter, C. E., Wang, Y-F., York, G. E., Zhang, M-H., and Johnson, D. H. Phase I study of the antineovascularization drug CM101. Clin. Cancer Res., *3:* 365–372, 1997.
52. Wamil, B. D., Thurman, G. B., Sundell, H. W., DeVore, R. F., Wakefield, G., Johnson, D. H., Wang, Y-F., and Hellerqvist, C. G. Soluble E-selectin in cancer patients as a marker of the therapeutic efficacy of CM101, a tumor-inhibiting anti-neovascularization agent, evaluated in Phase I clinical trial. J. Cancer Res. Clin. Oncol., *123:* 173–179, 1997.
53. Ropponen, K. M., Eskelinen, M. J., Lipponen, P. K., Alhava, E., and Kosma, V. M. Prognostic value of tumour-infiltrating lymphocytes (TILs) in colorectal cancer. J. Pathol., *182:* 318–324, 1997.
54. Bouvet, M., Ellis, L. M., Nishizaki, M., Fujiwara, T., Liu, W., Bucana, C. D., Fang, B., Lee, J. J., and Roth, J. A. Adenovirus-mediated wild-type *p53* gene transfer down-regulates vascular endothelial growth factor expression and inhibits angiogenesis in human colon cancer. Cancer Res., *58:* 2285–2292, 1998.

T cell induced tumor ablation in naïve mice

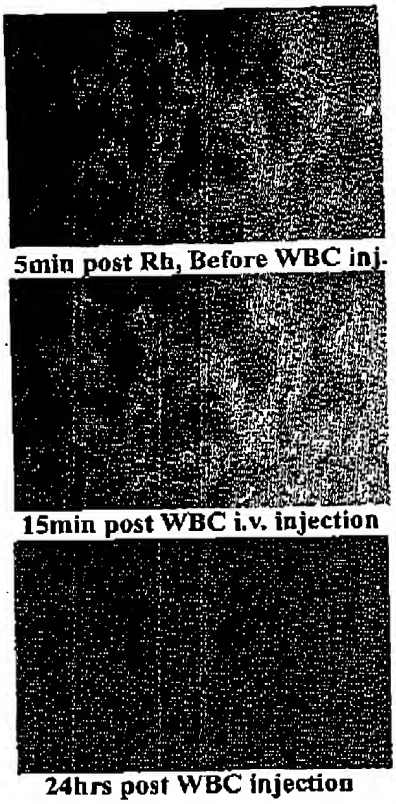

T cells from mice immunized with HP59-derived peptides and resistant to repeat i.v. infusions with B16 Melanoma cells were i.v. infused in naïve mice carrying melanoma tumors in cutaneous windows. Rhodamine G was injected 5 min prior to infusion of the donor T cells. Extravasation of florescent T cells into Tumor interstitial space was evident 15min post T cell infusion. Infusion of Rhodamine 24 hours post T cell infusion demonstratesd that the tumor and its vasculature ablated.

EXHIBIT
G

ELSEVIER

Seminars in Cell & Developmental Biology 16 (2005) 554–563

seminars in CELL & DEVELOPMENTAL BIOLOGY

www.elsevier.com/locate/semcdb

Review

Hypoxia-induced dedifferentiation of tumor cells – A mechanism behind heterogeneity and aggressiveness of solid tumors

Håkan Axelson [a], Erik Fredlund [a], Marie Ovenberger [a], Göran Landberg [b], Sven Påhlman [a,*]

[a] Division of Molecular Medicine, Department of Laboratory Medicine, Lund University, University Hospital MAS, Entrance 78, SE-20502 Malmö, Sweden

[b] Division of Pathology, Department of Laboratory Medicine, Lund University, University Hospital MAS, Malmö, Sweden

Available online 26 April 2005

Abstract

Histopathological examination of solid tumors frequently reveals pronounced tumor cell heterogeneity with regards to cell organization, cell morphology, cell size, nuclei morphology, etc. Analyses of gene expression patterns by immunohistochemistry or in situ hybridization techniques further strengthen the actual presence of phenotypic heterogeneity, often demonstrating substantial diversity within a given tumor. The molecular mechanisms underlying the phenotypic heterogeneity are very complex with genetic, epigenetic and environmental components. Hypoxia, shortage in oxygen, greatly influences cellular phenotypes by altering the expression of specific genes, and is an important contributor to intra- and inter-tumor cell diversity as revealed by the pronounced but non-uniform expression of hypoxia driven genes in solid tumors (reviewed in [Semenza GL. Targeting HIF-1 for cancer therapy. Nat Rev Cancer 2003;3:721–32; Harris AL. Hypoxia – a key regulatory factor in tumour growth. Nat Rev Cancer 2002;2:38–47.]). The oxygen pressure in solid tumors is generally lower than in the surrounding non-malignant tissues, and tumors exhibiting extensive hypoxia have been shown to be more aggressive than corresponding tumors that are better oxygenized [Vaupel P. Oxygen transport in tumors: characteristics and clinical implications. Adv Exp Med Biol 1996;388:341–51; Vaupel P, Thews O, Hoeckel M. Treatment resistance of solid tumors: role of hypoxia and anemia. Med Oncol 2001;18:243–59.]. We recently observed that hypoxic neuroblastoma cells and breast cancer cells loose their differentiated gene expression patterns and develop stem cell-like phenotypes [Jögi A, Øra I, Nilsson H, Lindeheim A, Makino Y, Poellinger L, et al. Hypoxia alters gene expression in human neuroblastoma cells toward an immature and neural crest-like phenotype. Proc Natl Acad Sci USA 2002;99:7021–6; Helczynska K, Kronblad A, Jögi A, Nilsson E, Beckman S, Landberg G, et al. Hypoxia promotes a dedifferentiated phenotype in ductal breast carcinoma in situ. Cancer Res 2003;63:1441–4.]. As low stage of differentiation in neuroblastoma and in breast cancer is linked to poor prognosis, hypoxia-induced dedifferentiation will not only contribute to tumor heterogeneity but could also be one mechanism behind increased aggressiveness of hypoxic tumors. The effect(s) of hypoxia on tumor cell differentiation status is the focus of this review.

Keywords: Hypoxia; Differentiation; Neuroblastoma; Sympathetic nervous system; Breast carcinoma; HIF-1α; HIF-2α

Contents

* Corresponding author. Tel.: +46 40337403; fax: +46 40337322.
E-mail address: sven.pahlman@molmed.mas.lu.se (S. Påhlman).

1084-9521/$ – see front matter © 2005 Elsevier Ltd. All rights reserved.
doi:10.1016/j.semcdb.2005.03.007

1. Intra-tumoral phenotypic heterogeneity

It is generally believed that tumor development occurs in a stepwise manner, with a progressive accumulation of genetic and epigenetic changes. The driving force in this process is the selection of cells with a growth and/or survival advantage, leading to successive clonal expansion of tumor cell populations (Fig. 1). It is the accumulated, combined effects of these changes that lead to a full tumorigenic conversion. In some tumors, such as colorectal cancer, detailed molecular characterization of genetic events leading to the different stages of tumor development has allowed for a rather elaborate model outlining major sequential events from early adenoma into invasive carcinoma [7]. In most other tumor forms only few crucial genetic changes have been defined due to their consistent appearance, while the full picture of associated genetic or epigenetic changes remains more unclear. In most tumors and also in the case of colorectal cancer, there is a considerable variation in the prevalence of the genetic changes. In addition there seems to be a considerable intra-tumoral genetic variation within a given tumor. In advanced colorectal tumors for example, intra-tumoral heterogeneity regarding somatic mutations was detected for several genes including central players, such as *p53* and *K-ras*, and multiple genetically defined clones were detected in the same tumor [8]. The mechanisms behind intra-tumoral genetic diversity are not clear, but they certainly play important roles during tumor growth, in particular when the tumor is challenged with different cytostatic agents. Furthermore, we are just beginning to understand the interplay between tumor cells and surrounding normal cells. Accumulating data indicate that albeit tumor, and not non-transformed, cells harbor genetic modifications, the phenotypes of the surrounding normal cells are profoundly changed [9], demonstrating the potential importance of non-genetic events determining in vivo tumor growth.

Hypoxia represents an important condition that promotes both to intra-tumor cell heterogeneity and development of stromal and vascular support of solid tumors. Hypoxic regions develop in poorly vascularized areas of the growing tumor and thus only affect a subset of tumor cells. In hypoxic cells the phenotype is dramatically changed and several lines of evidence indicate that these changes significantly contribute to clonal selection during tumor growth (Fig. 1 and reviewed in [1]). Although these phenotypic changes primarily have a non-genetic cause, as will be further discussed in this review, hypoxia has been shown to cause genetic instability presumably by affecting the expression of genes involved in DNA repair mechanisms [10,11], but also as a consequence of increased reactive oxygen species (ROS) production [12]. Thus, hypoxia will affect tumor cells both genetically and epigenetically and contribute to tumor heterogeneity and aggressive growth patterns.

2. Cellular adaptation to hypoxia

As discussed in more detail by others in this issue, cells can adapt to low oxygen levels by changing their gene expression patterns through a transcriptional response pathway mediated by the hypoxia inducible factor (HIF)-1 and the related transcription factors HIF-2 and HIF-3. The α-subunits of these heterodimeric factors become stabilized and activated under hypoxic conditions, and form complexes with the constitutively expressed transcription factor ARNT/HIF-1β [1,2,13]. At normoxia, the HIFα subunits are hydroxylated at specific proline residues by one or several of four known oxygen-dependent prolyl hydroxylases, PHD 1–4, which leads to HIF interaction with the von Hippel-Lindau/E3 ligase-ubiquitination complex and degradation of the ubiquinated HIFs via the proteosomal pathway [13]. The transactivation activities of HIFs are also regulated by hypoxia, as an asparagine residue becomes hydroxylated by an oxygen sensitive asparagyl hydroxylase, leading to a reduction of the HIF transcriptional activity [14,15]. Thus, the oxygen dependent regulation of HIF activity is complex and occurs at several levels, and as will be exemplified below, appears to differ between HIF-1α and HIF-2α and between different cell types.

3. Hypoxia promotes an immature stem cell-like phenotype in neuroblastoma cells

3.1. Neuroblastoma derivation and development of the sympathetic nervous system

Neuroblastoma is a tumor of the early childhood. It has been recognized and extensively studied much due to the

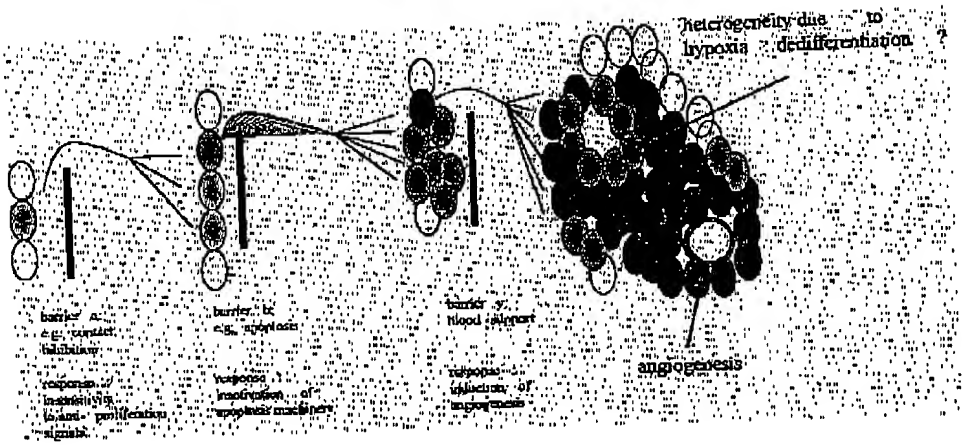

Fig. 1. Schematic illustration of putative sequential steps leading to solid tumor growth and hypoxia.

high frequency of spontaneous neuroblastoma cell maturation converting the tumor into a benign form, ganglioneuroma [16]. Primary tumor localization and a detailed characterization of marker gene expression of developing sympathetic nervous system (SNS) cell types in comparison to the expression of these genes in neuroblastoma tumors, reveal that neuroblastomas are derived from SNS precursor cells [17,18]. Thus, neuroblastomas can phenotypically be viewed as immortalized SNS neuroblasts, and the detailed knowledge of patterns of SNS marker gene expression allow us to monitor changes in neuroblastoma differentiation status, which is important for the discussion of the effects of hypoxia on the neuroblastoma cell phenotype. The SNS originates from the neural crest and the three major SNS cell lineages, the ganglionic/neuronal, the chromaffin and the small intensely fluorescent (SIF) lineages are derived from a common precursor, the sympathoadrenal precursor cells [19,20]. Ganglion cells constitute the ganglia proper, i.e. the SNS chain and trunkus ganglia where also the SIF cells localize, either solitary or as nests of cells. Ganglion cells/neuroblasts are also present in the developing adrenal medullary gland and form that organ together with the adrenal chromaffin cells, which is the major adrenal cell type. Extra-adrenal chromaffin cells build up the paraganglia, which are pre-natal chromaffin structures that involute or become reduced in size after birth. During this period, paraganglia are the major source of catecholamines, and in humans, their catecholamine-producing role is taken over by the chromaffin cells of the adrenal gland 2–3 years after birth [21]. Noradrenalin and adrenalin, the two major catecholeamines produced by the SNS, are involved in the regulation of the blood pressure, which in turn is indirectly regulated by the oxygen sensing carotid bodies. Tyrosine hydroxylase (TH) is the rate-limiting enzyme in the catecholamine synthesis, and in catecholamine producing cells such as those of SNS derivation, *TH* transcription is induced by hypoxia. In our studies, we have therefore used TH as a marker of developing human SNS cells, and in neuroblastoma cells increased expression of *TH* has also served as one marker of hypoxia.

3.2. *The hypoxic neuroblastoma phenotype*

A small subset of neuroblastomas forms frequent lobular structures with central zones of necrosis. In such neuroblastomas, tumor cells with a neuroblastic phenotype convert progressively into cells with paraganglionic/SIF cell features in hypoxic regions [22,23]. We have hypothesized that this process could be facilitated or driven by hypoxia [24]. This hypothesis was nourished by the discovery of HIF-2α and its involvement in murine sympathetic development, and its restrictive expression in developing SNS ganglia during embryonal days E10.5–E12.5 and in paraganglia during E14.5 and E16.5 [25]. We have confirmed the selective *HIF-2α* expression in the developing murine SNS, and recently we showed that HIF-2α is also selectively expressed in human fetal paraganglia [5,26] at week 8.5, a stage that developmentally corresponds to the mouse E14.5–16.5 stage [27].

In an attempt to test the hypothesis that hypoxia drives the neuronal to neuroendocrine lineage shift seen in the subset of neuroblastomas described above, we exposed a panel of human neuroblastoma cell lines to hypoxic conditions (1% oxygen) [5] and monitored the expression of sympathetic chromaffin differentiation marker genes such as *chromogranin A* and *B* (*ChrA/B*), *IGF-2* and *TH* [17,22]. Although both *IGF-2* and *TH* expression increased in hypoxic neuroblastoma cells, suggesting a chromaffin phenotype [5,28], the expression of the key chromaffin marker genes *ChrA/B* were downregulated together with a number of ganglionic/neuronal markers such as *NPY*, *GAP-43* and *SCG-10*. [5,29]. Importantly, also the SNS lineage specifying genes *HASH-1* and *dHAND* together with *MYCN* were downregulated at 1% oxygen, which taken together could suggest that hypoxia push neuroblastoma cells towards a more immature phenotype. In line with such an interpretation, hypoxia induced the expression of known neural crest-associated genes such as *Id2*, *Notch-1*, *Hes-1* and *c-kit*. Based on these data, we proposed that hypoxia in neuroblastoma cells induces dedifferentiation rather than paraganglionic/SIF differentiation, leading to the development of a

stem cell-like phenotype [5], while the induction of *IGF-2* and *TH*, known hypoxia-induced genes, is part of a general cellular response to hypoxia of these SNS derived cells.

In follow-up studies employing micro-array technique to analyze the expression of approximately 17,000 genes and ESTs in SK-N-BE(2)c human neuroblastoma cells, we could confirm that hypoxia induces a general response seen in most cells, i.e. induction of genes involved in the acute adaptation phase, e.g. promotion of glucose transport and glycolysis, and in long-term adaptive responses, e.g. induced catecholamine production and factors promoting angiogenesis [29]. We further found that several neuronal/neuroendocrine marker genes were down-regulated, including genes encoding the neurofilament proteins, which in this context is an important observation, as neurofilament expression is clinically used to histopathologically identify tumors of neuroendocrine derivation. The down-regulation of neurofilament genes was confirmed also at the protein level in hypoxic neuroblastoma cells, further demonstrating that hypoxic neuroblastoma cells do not develop neuroendocrine characteristics. In an extended micro-array study described in more detail below, we have compared the gene expression patterns of seven human neuroblastoma cell lines grown at 21 and 1% oxygen, respectively (Fredlund E., to be published). Again, a general hypoxic response (Table 1) and a hypoxia-induced loss of a neuronal phenotype could be confirmed in all seven cell lines. In particular, the well-established neuronal lineage marker gene, *β-III tubulin* was downregulated, while the neuronal stem cell marker *vimentin*, was up-regulated. Recently, it was reported that the nerve growth factor receptor TrkA exists in a truncated, NGF-independent, constitutively activated form in neural stem cells and in some neuroblastomas [30]. Treatment of neuroblastoma cells with the hypoxia mimic cobalt chloride induced the expression of the truncated, stem cell-associated form of TrkA, supporting our findings that hypoxia pushes neuroblastoma cells to a stem cell-like phenotype, although these authors never directly tested the effect of hypoxia [30]. Thus, the change in expression of a large set of recognized marker genes for neural precursor cells and neuroblasts/ganglion cells, respectively, shows that hypoxic cultured neuroblastoma cells become immature, and that these cells acquire an expression pattern resembling the phenotype of neural crest-derived neuronal precursor cells.

Table 1
Neuroblastoma cells show a consistent hypoxia response

Gene name	HUGO	Entrez gene
Cyclin G2	CCNG2	901
DEC1	BHLHB2	8553
Enolase 2/neuron-specific enolase	ENO2	2026
Glucose transporter 1	SLC2A1	6513
Glucose transporter 3	SLC2A3	6515
Hexokinase 2	HK2	3099
Insulin-like growth factor 2	IGF2	3481
N-myc downstream regulated gene 1	NDRG1	10397
Stanniocalcin 1	STC1	6781
Tyrosine hydroxylase	TH	7054
Vascular endothelial growth factor	VEGF	7422

The genes listed have previously been shown to be responsive to low oxygen pressure and are consistently upregulated two-fold or more in at least six out of seven neuroblastoma cell lines, as measured by a Wilcoxon signed rank test. Neuroblastoma cell lines SK-N-BE(2)c, KCN-69n, LA-N-5, SH-SY5Y, IMR-32, SK-N-RA, and SK-N-F1 were subjected to growth at 21 or 1% O_2 for 72 h. Labelled RNA was hybridised to spotted 70 mer microarrays representing approximately 27,000 genes and ESTs.

3.3. The effect of low glucose on hypoxia-induced dedifferentiation of neuroblastoma cells

Clearly, the spontaneous neuroendocrine differentiation occurring in the subset of neuroblastomas growing in lobular structures, was not recapitulated when studying the effect of hypoxia using established neuroblastoma cell lines. One reasonable explanation for this discrepancy could be that these cell lines are derived from highly aggressive neuroblastomas, often with *MYCN* amplification, while tumors growing in lobular structures might be of another derivation. Another explanation could be that the in vivo situation is more complex than just shortage in oxygen, as tumor hypoxia is also associated with hypoglycemia, acidosis and impaired supply of nutrients and clearance of waste products. Neuroblastoma cells are malignantly transformed neuroblasts, and neuroblasts as well as ganglion cells use glucose as their primary energy source, which led us to investigate the impact of different glucose levels on the hypoxia-induced dedifferentiation of neuroblastoma cells. High or low glucose by itself had little or no effect on the differentiation status of the tested neuroblastoma cell lines at normoxic conditions, and the HIF-protein levels were not affected, that is, HIF-1α was not detectable and the low basal HIF-2α protein levels seen in neuroblastomas both in vivo and in vitro were unchanged [26]. Furthermore, hypoxic (1% oxygen) growth conditions in combination with high (4.5 g/L) or medium (1.0 g/L) glucose concentrations did not substantially affect the expression of differentiation marker genes. However, the dedifferentiated phenotype of cells grown at hypoxia was slightly potentiated in hypoxic cultures without glucose in the medium [26]. Extrapolated into an in vivo situation, these data might suggest that tumor cells experiencing sustained hypoxia and hypoglycemia develop immature phenotypes, where hypoxia-related events are major contributors. Whether hypoglycemia affects other aspects of aggressive neuroblastoma cell behavior in general or at hypoxic conditions in particular, have not been studied and need further attention. However, we can rule out that growth of neuroblastoma cells at low glucose changes the dedifferentiation response induced by hypoxia alone into a lineage shift and development of a neuroendocrine phenotype.

3.4. Hypoxia contributes to tumor heterogeneity

When comparing HIF proteins and the expression of hypoxia driven genes at the cellular level in tumor sections, it is apparent that there is not always a perfect match between

HIF-1α/HIF-2α positivity and expression of established hypoxia driven genes such as *CAIX* or *Glut-1* in cervix carcinomas [31] and in breast cancer [32], and *TH* and *IGF-2* in neuroblastoma [26]. Thus, it seems that the response to hypoxia for poorly understood reasons is not uniform among tumor cells, within a given tumor but also between different tumors. Clearly, with regard to expression of specific genes under defined culture conditions, neuroblastoma cells respond slightly different to low oxygen, as exemplified by data obtained in our micro array analyses of cell lines grown at either 21 or 1% oxygen (Fredlund E., to be published). Overall, growth at 1% oxygen elicits a general hypoxic response in all seven tested neuroblastoma cell lines by activating the transcription of genes involved in the long- and short-term adaptation to low oxygen as exemplified by the induced expression of *VEGF*, *TH*, and the glycolytic gene *hexokinase 2* in Fig. 2. However, analysis of the expression levels of several hypoxia-induced genes, of which some have been shown to be bona fide HIF-1α targets, reveals that many of these genes are upregulated in only five or six of the seven cell lines, e.g. *GLUT1*, *GLUT3* and *ENO2*, coding for glucose transporters and the glycolytic enzyme neuron specific enolase/enolase-γ, respectively (Fig. 2). In the given examples, none of the cell lines is consistently insensitive to hypoxia. *GLUT1* for example, is not upregulated in SK-N-RA cells, while *GLUT3* is upregulated in SK-N-RA and five other cell lines but not in LA-N-5 cells. The examples of incongruent responses to hypoxia are plentiful and seem to be the rule rather than exceptions as suggested by data presented in Fig. 3. Only four out of approximately 27,000 genes and ESTs analyzed by 70-mer oligo nucleotide microarray were consistently altered two-fold or more in all seven neuroblastoma cell lines analyzed (Fredlund E., to be published). On the other hand, the generality in the hypoxic response is demonstrated by a robust induction of a substantial number of genes in most of the cell lines, 47 genes in six, and 150 genes in five of the seven analyzed cell lines (Fig. 3). Furthermore, the global impact on gene expression in response to hypoxia is illustrated by our finding that mRNA levels of more than 7000 different genes change two-fold or more in at least one cell line (Fig. 3). The fact that several genes proven to be HIF targets do not become activated in unison at 1% oxygen was unexpected and has no obvious explanation, as all neuroblastoma cell lines we have tested so far have the capacity to stabilize HIF-1α during growth at 1% oxygen [5,26], and unpublished data. Similar observations have been made also in other tumor systems (reviewed in [1]) suggesting that HIF activation is only one facet of the hypoxic response, and that other transcription factors or co-factors become activated in the hypoxic cell and cooperate with HIFs, leading to an additional level of regulation of the hypoxic phenotype. Numerous transcription factors are known to be affected by hypoxia

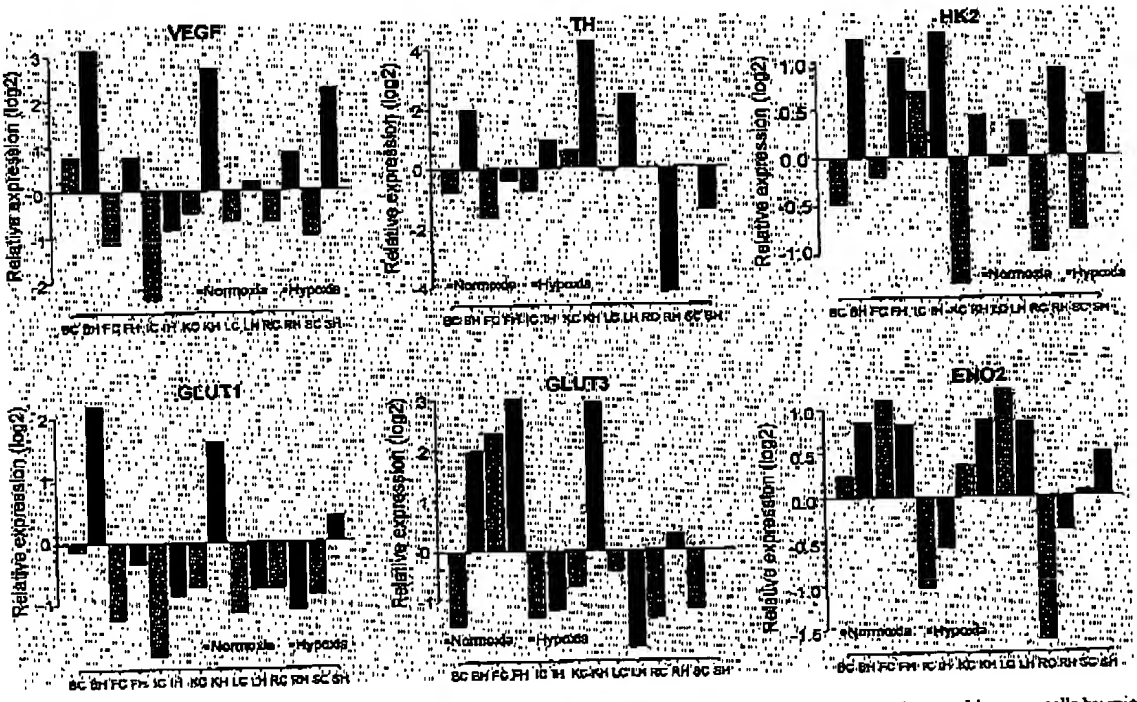

Fig. 2. Comparison of *VEGF*, *TH*, *Hexokinase 2*, *GLUT1*, *GLUT3* and *ENO2* expression levels in hypoxic and normoxic neuroblastoma cells by microarray analysis (see Table 1). Seven neuroblastoma cell lines were analyzed after growth for 72 h at either 21 or 1% oxygen. Abbreviations: the following normoxic (C) and hypoxic (H) cell lines were analyzed SK-N-BE(2)c (BC, BH), SK-N-F1 (FC, FH), IMR-32 (IC, IH), KCN-69n (KC, KH), LA-N-5 (LC, LH), SK-N-RA (RC, RH), and SH-SY5Y (SC, SH).

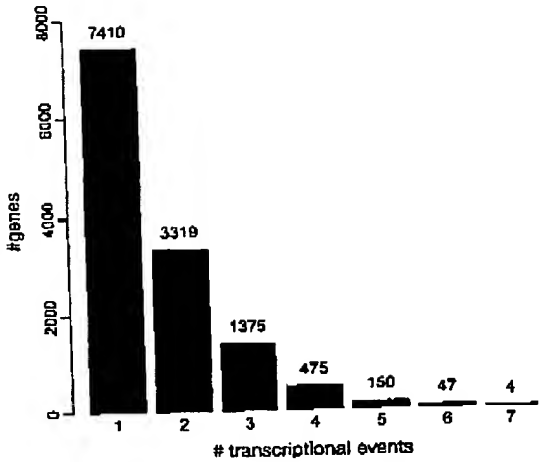

Fig. 3. Microarray analysis of hypoxia-induced genes in seven different neuroblastoma cell lines (SK-N-BE(2)c, KCN-69n, LA-N-5, SH-SY5Y, IMR-32, SK-N-RA, and SK-N-F1) grown at 1% O_2 for 72 h. The numbers of genes with a two-fold or more induction/reduction of mRNA levels in all seven (four genes), six out of seven (47 genes), five out of seven (150 genes) etc. cell lines, are given.

by HIF-dependent or independent mechanisms, such as c-Jun/AP-1, Ets, NF-kB, Id1, Id2 [33–36]. Many of these genes and their encoded activities are altered in tumor cells, and their putative interference upstream or downstream of HIF transcriptional events could provide molecular explanations for the non-conformal behavior of HIF target genes in specific tumor cell lines. As will be discussed below, there are emerging evidences for a diverse role of HIF-1α and HIF-2α, in part determined by their different regulation, which also could contribute to the unexpected heterogeneity in the hypoxic regulation of specific genes.

The vascularization and oxygenation status of solid tumors vary probably over time, as formation of new and collapse of sub-functional blood vessels appear to be dynamic processes and inherent properties of a growing tumor. Thus, tumor cells will frequently experience fluctuations in oxygen pressure, and phenotypic heterogeneity involving tumor hypoxia can most likely also be attributed to the kinetics by which cells from different tumors or between different regions within a tumor restore their normoxic phenotype upon reoxygenation. Some experimental support for this presumption was recently obtained when the kinetics by which cultured neuroblastoma cells restore their normoxic phenotypes was studied [37]. Comparison of the hypoxic and reoxygenated expression profiles of two cell lines revealed an overall stability for 24 h of the hypoxic characteristics when cells were brought from 1% to either 5 or 21% oxygen, where 5% oxygen was chosen to mimic a more physiological oxygen level. However, a closer analysis of the expression levels of the marker genes revealed that one cell line had a more stable hypoxic expression pattern at acutely restored normoxia than the other tested cell line, suggesting cell (line) specific differences in downregulation of the hypoxia-specific transcription machinery [37].

4. Hypoxia-induced dedifferentiation of neuroblastoma cells – molecular mechanisms

4.1. Hypoxia regulates lineage specifying basic helix-loop-helix (bHLH) transcription factors

The sequential molecular steps involved on the conversion of migrating neural crest cells to sympathetic precursors and finally to non-migrating sympathetic neuroblasts, or SNS chromaffin precursor cells, are far from known. However, gene elimination and overexpression approaches have identified several genes important to these processes, including those coding for the bHLH transcription factors HASH-1, dHAND and MYCN. Our initial observations that these genes were downregulated in hypoxic neuroblastoma cells supported the conclusion that hypoxic cells became dedifferentiated and gave the first hints as to the mechanisms involved. HASH-1 and dHAND, respectively, form functional heterodimeric complexes with E-proteins, which also are bHLH proteins, but ubiquitously expressed [38]. In neuroblastoma, E2-2 appears to be the preferential partner to HASH-1 and dHAND [39], and interestingly, *E2-2* expression is downregulated together with *HASH-1* and *dHAND* during hypoxic growth of these cells [5], presumably contributing to a decreased transcription of genes associated with the neuronal phenotype. bHLH transcription factors are also negatively regulated by interfering HLH factors lacking the basic, DNA binding domain. In the presence of ID proteins, E-proteins are sequestered from their lineage specific bHLH partners by binding to ID via the HLH domains with inhibition of tissue specific transcription as a result. The expression of two of these factors, *ID1* and *ID2*, become rapidly induced in hypoxic neuroblastoma cells [5,35], changes that in combination with the downregulation of *E2-2*, *HASH-1* and *dHAND* expression will reduce transcription of neuronal genes, and thus contribute to the development of a dedifferentiated phenotype. The induction of ID2 is particularly interesting as ID2 is required for proper chicken neural crest development [40] and in search for direct roles of HIF activation in the hypoxia-induced dedifferentiation and development of a stem cell-like phenotype, we tested if *ID2* expression was directly regulated by HIF-1α. The promoter of human ID2 contains several putative HREs, and by gel shift and chromosome immunoprecipitation assays it was shown that at least two of the eight identified putative HREs bind HIF-1α and are required for hypoxia-induced *ID2* transcription [35], results that provide a link between HIF activation and dedifferentiation of hypoxic neuroblastoma cells.

4.2. Notch-pathway regulation in hypoxic cells

Notch signaling is another important pathway that might contribute to a dedifferentiated hypoxic phenotype. In many,

but not all cell types, active Notch signaling is associated with immature, proliferating cells. The Notch pathway is initiated by juxtacrine signaling in which one of the five Notch ligands (Jagged-1, Jagged-2, Delta-1, Delta-3 and Delta-4) stimulate four Notch receptors (Notch1- to Notch-4) on neighbouring cells [41]. Upon ligand-binding, the Notch receptors are activated by a series of proteolytic cleavages leading to the release of the intra-cellular receptor domains, which translocate to the nucleus and activate transcription of a distinct set of transcriptional repressors out of which the Hes (Hes-1 and Hes-2) and Hes-related (Hesr-1 and Hesr-2, also known as HRT, CHF or Hey) gene families seem to be the most important (reviewed in [42]). In many cell types expression of these repressors leads to down regulation of differentiation-promoting factors of the bHLH type. In the sympathetic nervous system HASH-1 represents one such target gene. In our global expression analyses of hypoxic neuroblastoma cells we have noticed elevated expression of both ligands and receptors of the Notch signaling cascade, and consequently elevated expression of the principal transcriptional mediators of this cascade, Hes-1 and Hey-1 [43]. Though formally not proven, we suggest that increased Notch signaling contribute to the dedifferentiated phenotype. These changes would act in concert with induction of ID1 and ID2 and decreased expression of E-proteins to inhibit the action of components of the bHLH network, such as HASH-1 and dHAND [43]. If Notch activation is induced as a response to hypoxia also in tumor forms other than neuroblastoma, this pathway might represent an important pathway of tumor cell adaptation to hypoxia. Importantly, there are several potent inhibitors of Notch signaling available, which might be employed to block Notch-induction and thus allow for further studies on the contribution of this cascade to the hypoxic phenotype.

4.3. Differential regulation of HIF-1α and HIF-2α in neuroblastoma

Immunohistochemical analysis of neuroblastoma specimens reveals that HIF-2α is detectable in most tumors, while HIF-1α protein is primarily restricted to cells surrounding necrotic areas [26]. Also neuroblastoma cells grown at normoxia have detectable HIF-2α protein, showing that HIF-2α in contrast to HIF-1α to a certain extent can escape prolylhydroxylase-induced degradation at normoxia. An important difference in the regulation of these two proteins is the hypoxia-induced expression of *HIF-2α*, while *HIF-1α* mRNA levels are virtually unaffected by low oxygen [29]. Another difference is that neuroblastoma cells grown at 5% oxygen (a more physiological oxygen level) stabilize HIF-2α but not HIF-1α and that known hypoxia-induced genes like *TH* and *ID2* are slightly upregulated at 5% oxygen [26,37]. These findings suggest that HIF-2α could be transcriptionally active at 5% oxygen and that the phenotype of neuroblastoma cells grown at this "normoxic" condition to a certain extent is determined by HIF-2α. However, no exclusive HIF-2α target gene has been identified, while numerous genes appear to be activated by HIF-2α as well as by HIF-1α. A future emphasis is therefore to systematically screen for genes uniquely or predominantly targeted by HIF-2α and not by HIF-1α, as some of them might be important for proper development of the SNS or in the genesis of neuroblastoma, although it may turn out that such genes do not exist [44].

5. Hypoxia promotes an immature phenotype in breast carcinoma in situ

In neuroblastoma, there is a well-established association between low stage of differentiation and poor clinical outcome, suggesting that dedifferentiation of neuroblastoma cells caused by hypoxia could be one mechanisms behind the progression of a tumor from being treatment responsive to become refractive. Having disclosed that neuroblastoma cells lose differentiation characteristics during hypoxic growth, the obvious question was whether hypoxia had similar effects on other tumor forms. We choose to investigate the effects of hypoxia on mammary carcinoma cells with focus on ductal breast carcinoma in situ (DCIS) for three main reasons; the well-defined in situ lesions with central necrosis (comedo cancer) have regions of hypoxia surrounding the necrotic zones, there are histopathological criteria used in the clinic to assess differentiation stage and thus aggressiveness in breast carcinoma, and finally, numerous well-characterized cell lines derived from mammary carcinomas are available. In DCIS lesions HIF-1α protein is detected in cells surrounding the central necrosis [6], and in these lesions HIF-1α protein can serve as a criterion for defining hypoxic cell layers. In contrast to well-oxygenated tumor cells adjacent to the basal membrane in DCIS lesions, HIF positive cells lose their capacity to form pseudo-ducts, and the nuclear to cytoplasm ratio increases with growing distances from the basal membrane. Importantly, these two differentiation criteria are associated with unfavorable outcome of invasive breast carcinomas. Thus, based on established histopathological criteria we could conclude that hypoxic (HIF-1α positive) cells are less well differentiated compared to non-hypoxic tumor cells [6]. In addition, in estrogen receptor α (ERα) positive tumors, the ERα expression is downregulated, further supporting the conclusion that hypoxia promotes dedifferentiation of breast ductal carcinoma cells.

Gene expression patterns associated with breast ductal epithelial differentiation has not been extensively investigated, but in search for such markers, cytokeratin 19 turned out as one being used as a marker for breast ductal epithelial progenitor cells [45]. Interestingly, in DCIS lesions, cytokeratin 19 expression was upregulated in hypoxic, HIF-1α positive, regions, in accordance with a hypoxia-driven loss of differentiation characteristics. ERα and cytokeratin 19 was also down- and upregulated, respectively, in breast cancer cell lines exposed to hypoxia, lending further support to the notion that these changes are direct consequences of hypoxia

and not of hypoxia-associated alterations occurring in tissues, like hypoglycemia or acidosis [6,46].

6. Poor tissue oxygenation – a tumor-promoting condition?

Data presented so far have focused on a dedifferentiating effect on tumor cells of low oxygen, a consequence of hypoxia that is in keeping with the documented more aggressive phenotype of hypoxic tumors [3,4]. The generality of the dedifferentiating effect of hypoxia on tumor cells remains however to be investigated since so far only two tumor forms, neuroblastoma and breast cancer have been studies in any detail. However, hypoxic LnCap prostate carcinoma cells loose their *PSA* and *androgen receptor* expression during hypoxic growth [47], two genes that are expressed in more differentiated prostate carcinoma cells, indicating that also hypoxic prostate carcinoma cells loose characteristics associated with a differentiated phenotype. Given these effects of hypoxia on tumor cells, one might ask whether hypoxia by itself is promoting tumor development. In the case of neuroblastoma, a positive correlation between congenital heart disease and incidence of neuroblastoma, but not non-neuronal brain tumors, has been demonstrated [48], clearly suggesting a link between impaired tissue oxygenation and tumor development. In line with such data, an increased risk of acquiring carotid body paragangliomas is seen in individuals living above 2000 m above the sea level, and the tumor frequency increases with altitude [49]. Interestingly, the hereditary form of paraganglioma affecting the SDHD gene is virtually absent in this population, while it is comparatively common in populations living at the sea level, showing that life at conditions of low atmospheric oxygen selects against a hereditary predisposition for paraganglioma (reviewed in [50]). Low oxygen tensions can negatively affect normal development as hypoxia impairs adipocyte differentiation [51] and the cell fusion and differentiation process of developing cytotrophoblasts [52]. Finally, the von Hippel Lindau syndrome tumors, lacking functional VHL protein and thus the oxygen-dependent HIF degradation mechanism, indirectly exemplify a tumor promoting effect of hypoxia and stabilization of HIFs [53].

Although the examples linking hypoxia and HIF-activation to tumor development and/or tumor aggressiveness are many, the picture is far from clear. Our own observation that some neuroblastomas spontaneously differentiate into a neuroendocrine phenotype in areas adjacent to necrotic zones, show that hypoxia under some circumstances can have a differentiating, cell lineage re-directing effect on neuroblastoma cells [22,23]. Furthermore, neural crest stem cells cannot differentiate in vitro into a sympathoadrenal lineage at normoxia, but do so at 5% oxygen [54]. Whether the effect of low oxygen is dependent on HIF activity has not been investigated, but the observation that HIF-2α is stabilized and appears to be transcriptionally active at 5% oxygen in neuroblastoma cells, could suggest that HIFs indeed are required for in vitro and in vivo differentiation of sympathetic neuronal precursor cells, which would be in accordance with the HIF-2a knock-out phenotype reported by Tian et al. [25]. Finally, in cervical squamous cell carcinoma cells hypoxia induces the epithelial cell differentiation marker involucrin [55], further suggesting cell type specific effects of hypoxia on cell differentiation status.

7. Concluding remarks

With the disclosure of the negative effects of hypoxia on tumor growth and behavior, and HIFs as the main molecular triggers of these effects, HIF-1α has been identified and is explored as a molecular target for treatment of aggressive tumors (reviewed in [1]). As the hypoxic phenotype is principally restricted to tumors, genes selectively expressed due to poor oxygenation can be considered to be tumor-specific. Thus, one obvious advantage of targeting the HIF-1α protein is its tumor specific expression pattern. With the identification of hypoxia-induced genes and mapping of their tissue-specific expression patterns, the number of putative target genes for selective tumor forms will most likely increase, where genes encoding cell surface proteins will be particularly interesting. In the future one might be able to take advantage of, and even create tumor hypoxia by combining angiogenesis inhibitors with drugs or antibodies directed against hypoxia-induced target proteins. In this scenario, angiogenesis inhibitors will create acute tumor hypoxia leading to increased expression of the protein(s) to be specifically targeted, an approach that obviously needs to be tested in in vivo treatment models.

Acknowledgements

This work was supported by grants from the Swedish Cancer Society, Children's Cancer Foundation of Sweden, HKH Kronprinsessan Lovisas förening för barnasjukvård, Hans von Kantzows stiftelse, Ollie och Elof Ericssons stiftelse and the research funds of Malmö University Hospital. H.A. and E.F. are supported by grants from the Children's Cancer Foundation of Sweden and the KK-foundation, respectively.

References

[1] Semenza GL. Targeting HIF-1 for cancer therapy. Nat Rev Cancer 2003;3:721–32.
[2] Harris AL. Hypoxia – a key regulatory factor in tumour growth. Nat Rev Cancer 2002;2:38–47.
[3] Vaupel P. Oxygen transport in tumors: characteristics and clinical implications. Adv Exp Med Biol 1996;388:341–51.
[4] Vaupel P, Thews O, Hoeckel M. Treatment resistance of solid tumors: role of hypoxia and anemia. Med Oncol 2001;18:243–59.
[5] Jögi A, Øra I, Nilsson H, Lindeheim A, Makino Y, Poellinger L, et al. Hypoxia alters gene expression in human neuroblastoma cells

toward an immature and neural crest-like phenotype. Proc Natl Acad Sci USA 2002;99:7021–6.
[6] Helczynska K, Kronblad A, Jögi A, Nilsson E, Beckman S, Landberg G, et al. Hypoxia promotes a dedifferentiated phenotype in ductal breast carcinoma in situ. Cancer Res 2003;63:1441–4.
[7] Vogelstein B, Kinzler KW. The multistep nature of cancer. Trends Genet 1993;9:138–41.
[8] Losi L, Baisse B, Bouzourene H, Benhattar J. Evolution of intratumoral genetic heterogeneity during colorectal cancer progression. Carcinogenesis, in press.
[9] Allinen M, Beroukhim R, Cai L, Brennan C, Lahti-Domenici J, Huang H, et al. Molecular characterization of the tumor microenvironment in breast cancer. Cancer Cell 2004;6:17–32.
[10] Reynolds TY, Rockwell S, Glazer PM. Genetic instability induced by the tumor microenvironment. Cancer Res 1996;56:5754–7.
[11] Unruh A, Ressel A, Mohamed HG, Johnson RS, Nadrowitz R, Richter E, et al. The hypoxia-inducible factor-1 alpha is a negative factor for tumor therapy. Oncogene 2003;22:3213–20.
[12] Chandel NS, McClintock DS, Feliciano CE, Wood TM, Melendez JA, Rodriguez AM, et al. Reactive oxygen species generated at mitochondrial complex III stabilize hypoxia-inducible factor-1alpha during hypoxia: a mechanism of O_2 sensing. J Biol Chem 2000;275:25130–8.
[13] Masson N, Ratcliffe PJ. HIF prolyl and asparaginyl hydroxylases in the biological response to intracellular O(2) levels. J Cell Sci 2003;116:3041–9.
[14] Lando D, Peet DJ, Gorman JJ, Whelan DA, Whitelaw ML, Bruick RK. FIH-1 is an asparaginyl hydroxylase enzyme that regulates the transcriptional activity of hypoxia-inducible factor. Genes Dev 2002;16:1466–71.
[15] Mahon PC, Hirota K, Semenza GL. FIH-1: a novel protein that interacts with HIF-1alpha and VHL to mediate repression of HIF-1 transcriptional activity. Genes Dev 2001;15:2675–86.
[16] Cushing H, Wohlbach B. The transformation of a malignant paravertebral sympathicoblastoma into benign ganglioneuroma. Am J Pathology 1927;3:203–15.
[17] Hoehner JC, Gestblom C, Hedborg F, Sandstedt B, Olsen L, Påhlman S. A developmental model of neuroblastoma: differentiating stroma-poor tumors' progress along an extra-adrenal chromaffin lineage. Lab Invest 1996;75:659–75.
[18] Påhlman S, Hedborg F. Development of the neural crest and sympathetic nervous system. In: Brodeur GM, Sawada T, Tsuchida Y, Voute PA, editors. Neuroblastoma. Amsterdam: Elsevier; 2000. p. 9–19.
[19] Carnahan JF, Patterson PH. Isolation of the progenitor cells of the sympathoadrenal lineage from embryonic sympathetic ganglia with the SA monoclonal antibodies. J Neurosci 1991;11:3520–30.
[20] Verdi JM, Anderson DJ. Neurotrophins regulate sequential changes in neurotrophin receptor expression by sympathetic neuroblasts. Neuron 1994;13:1359–72.
[21] Coupland R. The development and fate of catecolamine secreting endocrine cells. Amsterdam: Elsevier/North-Holland Biomedical Press; 1980.
[22] Hedborg F, Ohlsson R, Sandstedt B, Grimelius L, Hoehner JC, Påhlman S. IGF2 expression is a marker for paraganglionic/SIF cell differentiation in neuroblastoma. Am J Pathol 1995;146:833–47.
[23] Gestblom C, Hoehner JC, Hedborg F, Sandstedt B, Påhlman S. In vivo spontaneous neuronal to neuroendocrine lineage conversion in a subset of neuroblastomas. Am J Pathol 1997;150:107–17.
[24] Hoehner JC, Gestblom C, Olsen L, Påhlman S. Spatial association of apoptosis-related gene expression and cellular death in clinical neuroblastoma. Br J Cancer 1997;75:1185–94.
[25] Tian H, Hammer RE, Matsumoto AM, Russell DW, McKnight SL. The hypoxia-responsive transcription factor EPAS1 is essential for catecholamine homeostasis and protection against heart failure during embryonic development. Genes Dev 1998;12:3320–4.
[26] Nilsson H, Jögi A, Beckman S, Harris AL, Poellinger L, Påhlman S. HIF-2alpha expression in human fetal paraganglia and neuroblastoma: relation to sympathetic differentiation, glucose deficiency, and hypoxia. Exp Cell Res 2005;303:447–56.
[27] Strachan T, Lindsey S, Wilson D. Molecular genetics of early human development. Oxford: BIOS Scientific Publishers Ltd.; 1997.
[28] Hedborg F, Ullerås E, Grimelius L, Wassberg E, Maxwell PH, Hero B, et al. Evidence for hypoxia-induced neuronal-to-chromaffin metaplasia in neuroblastoma. FASEB J 2003;17:598–609.
[29] Jögi A, Vallon-Christersson J, Holmquist L, Axelson H, Borg A, Påhlman S. Human neuroblastoma cells exposed to hypoxia: induction of genes associated with growth, survival, and aggressive behavior. Exp Cell Res 2004;295:469–87.
[30] Tacconelli A, Farina AR, Cappabianca L, Desantis G, Tessitore A, Vetuschi A, et al. TrkA alternative splicing: a regulated tumor-promoting switch in human neuroblastoma. Cancer Cell 2004;6:347–60.
[31] Airley RE, Loncaster J, Raleigh JA, Harris AL, Davidson SE, Hunter RD, et al. GLUT-1 and CAIX as intrinsic markers of hypoxia in carcinoma of the cervix: relationship to pimonidazole binding. Int J Cancer 2003;104:85–91.
[32] Vleugel MM, Greijer AE, Shvarts A, van der Groep P, van Berkel M, Aarbodem Y, et al. Differential prognostic impact of hypoxia induced and diffuse HIF-1alpha expression in invasive breast cancer. J Clin Pathol 2005;58:172–7.
[33] Figueroa YG, Chan AK, Ibrahim R, Tang Y, Burow ME, Alam J, et al. NF-kappaB plays a key role in hypoxia-inducible factor-1-regulated erythropoietin gene expression. Exp Hematol 2002;30:1419–27.
[34] Salnikow K, Kluz T, Costa M, Piquemal D, Demidenko ZN, Xie K, et al. The regulation of hypoxic genes by calcium involves c-Jun/AP-1, which cooperates with hypoxia-inducible factor 1 in response to hypoxia. Mol Cell Biol 2002;22:1734–41.
[35] Lõfstedt T, Jögi A, Sigvardsson M, Gradin K, Poellinger L, Påhlman S, et al. Induction of ID2 expression by hypoxia-inducible factor-1: a role in dedifferentiation of hypoxic neuroblastoma cells. J Biol Chem 2004;279:39223–31.
[36] Oikawa M, Abe M, Kurosawa H, Hida W, Shirato K, Sato Y. Hypoxia induces transcription factor ETS-1 via the activity of hypoxia-inducible factor-1. Biochem Biophys Res Commun 2001;289:39–43.
[37] Holmquist L, Jögi A, Påhlman S. Phenotypic persitence after reoxygenation of hypoxic neuroblastoma cells. Int J Cancer, in press.
[38] Massari ME, Murre C. Helix-loop-helix proteins: regulators of transcription in eucaryotic organisms. Mol Cell Biol 2000;20:429–40.
[39] Persson P, Jögi A, Grynfeld A, Påhlman S, Axelson H. HASH-1 and E2-2 are expressed in human neuroblastoma cells and form a functional complex. Biochem Biophys Res Commun 2000;274:22–31.
[40] Martinsen BJ, Bronner-Fraser M. Neural crest specification regulated by the helix-loop-helix repressor Id2. Science 1998;281:988–91.
[41] Hansson EM, Lendahl U, Chapman G. Notch signaling in development and disease. Semin Cancer Biol 2004;14:320–8.
[42] Iso T, Kedes L, Hamamori Y. HES and HERP families: multiple effectors of the Notch signaling pathway. J Cell Physiol 2003;194:237–55.
[43] Påhlman S, Stockhausen MT, Fredlund E, Axelson H. Notch signaling in neuroblastoma. Semin Cancer Biol 2004;14:365–73.
[44] Park SK, Dadak AM, Haase VH, Fontana L, Giaccia AJ, Johnson RS. Hypoxia-induced gene expression occurs solely through the action of hypoxia-inducible factor 1alpha (HIF-1alpha): role of cytoplasmic trapping of HIF-2alpha. Mol Cell Biol 2003;23:4959–71.
[45] Gudjonsson T, Villadsen R, Nielsen HL, Ronnov-Jessen L, Bissell MJ, Petersen OW. Isolation, immortalization, and characterization of a human breast epithelial cell line with stem cell properties. Genes Dev 2002;16:693–706.

[46] Kronblad Å, Helczynska K, Nielsen NH, Emdin S, Påhlman S, Landberg G. Regional cyclin D1 overexpression or hypoxia correlate inversely with heterogeneous oestrogen receptor-alpha expression in human breast cancer. In Vivo 2003;17:311–8.
[47] Ghafar MA, Anastasiadis AG, Chen MW, Burchardt M, Olsson LE, Xie H, et al. Acute hypoxia increases the aggressive characteristics and survival properties of prostate cancer cells. Prostate 2003;54:58–67.
[48] de la Monte SM, Hutchins GM, Moore GW. Peripheral neuroblastic tumors and congenital heart disease. Possible role of hypoxic states in tumor induction. Am J Pediatr Hematol Oncol 1985;7:109–16.
[49] Rodriguez-Cuevas S, Lopez-Garza J, Labastida-Almendaro S. Carotid body tumors in inhabitants of altitudes higher than 2000 meters above sea level. Head Neck 1998;20:374–8.
[50] Baysal BE. On the association of succinate dehydrogenase mutations with hereditary paraganglioma. Trends Endocrinol Metab 2003;14:453–9.
[51] Yun Z, Maecker HL, Johnson RS, Giaccia AJ. Inhibition of PPAR gamma 2 gene expression by the HIF-1-regulated gene DEC1/Stra13: a mechanism for regulation of adipogenesis by hypoxia. Dev Cell 2002;2:331–41.
[52] Alsat E, Wyplosz P, Malassine A, Guibourdenche J, Porquet D, Nessmann C, et al. Hypoxia impairs cell fusion and differentiation process in human cytotrophoblast, in vitro. J Cell Physiol 1996;168:346–53.
[53] Kaelin Jr WG. The von Hippel-Lindau tumor suppressor gene and kidney cancer. Clin Cancer Res 2004;10:6290S–5S.
[54] Morrison SJ, Csete M, Groves AK, Melega W, Wold B, Anderson DJ. Culture in reduced levels of oxygen promotes clonogenic sympathoadrenal differentiation by isolated neural crest stem cells. J Neurosci 2000;20:7370–6.
[55] Azuma Y, Chou SC, Lininger RA, Murphy BJ, Varia MA, Raleigh JA. Hypoxia and differentiation in squamous cell carcinomas of the uterine cervix: pimonidazole and involucrin. Clin Cancer Res 2003;9:4944–52.

RAKESH K. JAIN, PhD
E. L. Steele Laboratory
Department of Radiation Oncology
Massachusetts General Hospital
and Harvard Medical School
Boston, Massachusetts

Antiangiogenic Therapy for Cancer: Current and Emerging Concepts

ABSTRACT

Angiogenesis is an essential step in the growth and spread of solid tumors—the cause of more than 85% of cancer mortality. Inhibiting angiogenesis would therefore seem to be a reasonable approach to prevent or treat cancer. However, tumor angiogenesis differs from normal angiogenesis in that the resulting vessels are tortuous, irregularly shaped, and hyperpermeable. These abnormalities result in irregular blood flow and high interstitial fluid pressure within the tumor, which can impair the delivery of oxygen (a known radiation sensitizer) and drugs to the tumor. Emerging evidence suggests that antiangiogenic therapy can prune some tumor vessels and normalize the structure and function of the rest, thereby improving drug delivery and normalizing the tumor microenvironment. This normalization effect may underlie the therapeutic benefit of combined antiangiogenic and cytotoxic therapies. This paper reviews current and emerging concepts of the mechanism of action of antiangiogenic therapies and discusses the implications of these mechanisms for their optimal clinical use.

We have known for nearly a century that tumors induce growth of new blood vessels.[1,2] In 1971, Folkman proposed that blocking angiogenesis should be able to arrest tumor growth.[3] A few years later, Gullino demonstrated that cells in precancerous tissue acquire angiogenic capacity on their way to becoming cancerous, and thus proposed that inhibition of angiogenesis be used to prevent cancer.[4] In the past 3 decades our understanding of angiogenesis in general, and tumor angiogenesis in particular, has grown exponentially, culminating in the approval of the first antiangiogenic agent, bevacizumab (Avastin), for the treatment of advanced colorectal cancer and spawning more than 60 clinical trials using a variety of antiangiogenic agents.[5,6]

The widely accepted mechanism of action of antiangiogenic therapy is that these agents prevent the growth and metastasis of tumors by inhibiting the formation of new vessels. While this notion holds true, data from randomized clinical trials show that when used as monotherapy, currently available antiangiogenic agents produce modest objective responses and do not yield long-term survival benefit in patients with solid tumors.[7-9] However, when given in combination with chemotherapy, bevacizumab, an antibody directed against vascular endothelial growth factor (VEGF), produced unprecedented increases in survival (5 months) in patients with metastatic colorectal cancer.[10] These data support the earlier predictions of Teicher, who postulated that combined administration of antiangiogenic therapy and cytotoxic (chemotherapy and radiation) therapy would yield maximum benefit because such combinations would destroy both compartments in tumors: the cancer cells and the endothelial cells.[11]

However, this theory seems paradoxical. If antiangiogenic agents destroy the tumor vasculature, the delivery of chemotherapeutic agents and oxygen to the tumor would be compromised, resulting in less cytotoxicity and radiation resistance. The emerging concept of vascular normalization provides researchers with a potential resolution to this paradox: this hypothesis posits that judicious

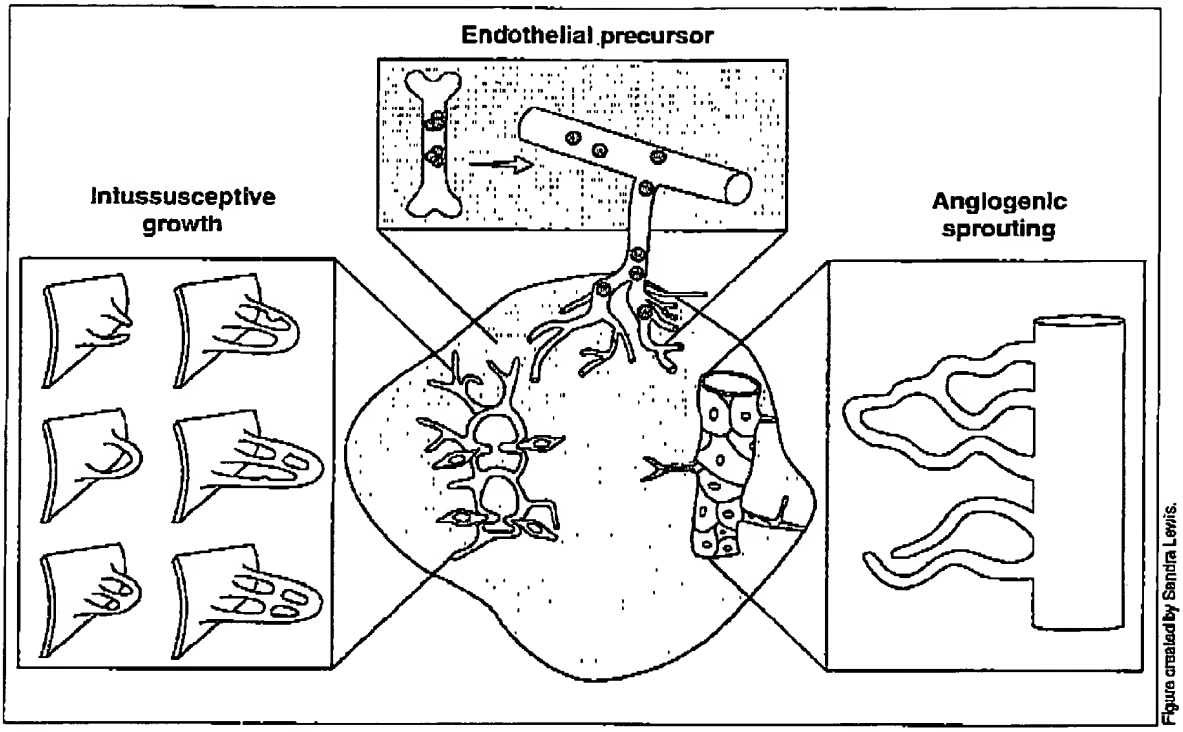

Figure 1: Four Cellular Mechanisms of Vascularization in Tumors—(1) Intussusception: tumor vessels enlarge and an interstitial tissue column grows in the enlarged lumen, expanding the network; (2) vasculogenesis: endothelial precursor cells mobilized from the bone marrow or peripheral blood contribute to the growth of the endothelial lining of tumor vessels; (3) sprouting (angiogenesis): the existing vascular network expands by forming sprouts or bridges; and (4) co-option (not shown): tumor cells grow around existing vessels to form perivascular cuffs. Adapted, with permission from Nature Publishing Group, from Carmeliet and Jain.[1]

application of antiangiogenic agents can improve the function of tumor vasculature and thus improve the delivery of oxygen and drugs to tumor cells.[12,13] Here I review this emerging counterintuitive concept and the currently well-accepted view that antiangiogenic therapy inhibits neovascularization, as well as the importance of optimizing the dose and sequencing of these therapies.

Role of Angiogenesis in Tumor Progression

In adults, normally occurring neovascularization is largely limited to female reproductive organs and healing wounds. Otherwise, adult neovascularization occurs as a result of a pathologic situation, such as cancer. Although tumors can initially co-opt normal blood vessels to support growth, a new blood supply is required for the tumor to grow beyond 1 to 3 mm. This concept has been firmly established by many supported studies and is well illustrated by a study that found numerous small thyroid gland tumors in individuals who died of other causes.[14] Prior to the development of tumor vasculature, tumors are dormant.[15] For angiogenesis to occur, the effect of proangiogenic factors must outweigh the effect of the antiangiogenic factors. When the balance tips towards proangiogenesis, the tumor undergoes what has been described as the angiogenic switch, which fosters the development of new vessels and allows tumor progression to ensue.[16] Further, once angiogenesis is prompted, tumors become invasive locally and systemically.

Evidence for the critical and pathologic role that angiogenesis plays in cancer progression comes from studies demonstrating that microvessel density within the tumor—the number of blood vessels in a defined area—is not only prognostic in some tumor types, but also correlates with the development of metastases.[17]

Mechanisms of Angiogenesis

At least four cellular mechanisms can result in the vascularization of tumors: co-option, intussusception, sprouting (angiogenesis), and vascu-

Table 1

Morphological and Functional Characteristics of the Vasculature in Normal Tissue, an Untreated Tumor, a Tumor During Early Stages of Treatment With an Antiangiogenic Drug (Normalized), and a Tumor Treated With High Doses of an Antiangiogenic Drug Over a Long Period (Regressing)

	Vessel Type				
Properties	Normal	Tumor (Untreated)	Tumor (Normalized)	Tumor (Regressing)	Reference
Global organization	Normal	Abnormal	Normalized	Fragmented	44
Pericyte	Normal	Absent or detached	Closer to normal	Missing	46,49,51,53
Basement membrane	Normal	Absent or too thick	Closer to normal, some ghost	Ghost	46,49,51
Vessel diameter	Normal distribution	Dilated	Closer to normal	Closer to or less than normal	49,51,52,58
Vascular density	Normal, homogeneous distribution	Abnormal, heterogeneous distribution	Closer to normal	Extremely low	46,47,49-53
Permeability to large molecules	Normal	High	Intermediate	Variable	47,49,51-53,58
MVP and IFP	MVP > IFP	MVP ~ IFP	MVP > IFP	Low IFP	48,49,53
(P)lasma and (I)nterstitial oncotic pressure*	P > I	P ~ I	P > I	Not known	49
pO_2	Normal	Hypoxia	Reduced hypoxia	Hypoxia	11,43,48,51
Drug penetration	Uniform	Heterogeneous	More homogeneous	Inadequate	11,43,49,50,53

*Osmotic pressure exerted by plasma proteins.

IFP = interstitial fluid pressure; MVP = microvascular pressure.

Updated, with permission, from Jain RK: Normalization of tumor vasculature: An emerging concept in antiangiogenic therapy. *Science* 307:58-62, 2005. Copyright 2005 AAAS.

logenesis (Figure 1). Tumor cells can co-opt and grow around existing vessels to form perivascular cuffs. However, these cuffs cannot grow beyond the diffusion limit of critical nutrients, and may actually cause the collapse of the vessels due to the compressive forces generated by tumor cell growth (referred to as solid stress). Alternatively, an existing vessel may enlarge in response to the growth factors released by tumors, and an interstitial tissue column may grow in the enlarged lumen and partition the lumen to form an expanded vascular network. This mode of intussusceptive microvascular growth has been observed during tumor growth, wound healing, and gene therapy.[18-21]

Angiogenesis is perhaps the most widely studied mechanism of vessel

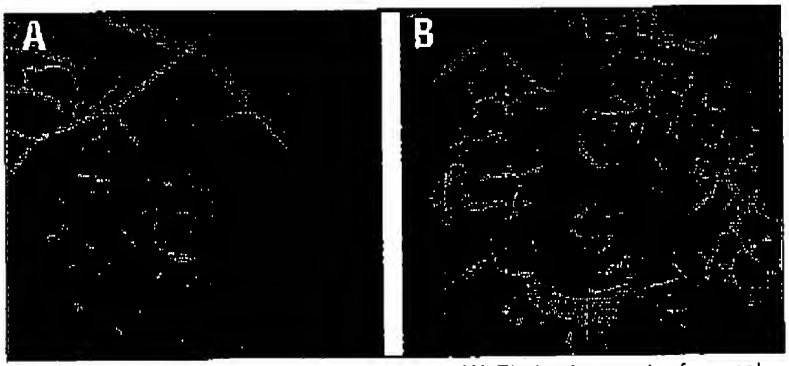

Figure 2: Normal and Tumor Vasculature—(A) Photomicrograph of normal vasculature in mouse brain. The vasculature is organized, appropriately connected, and optimally shaped to provide nutrients to all parenchymal cells. (B) Photomicrograph of mouse glioblastoma vasculature. This vasculature is disorganized, poorly connected, and tortuous, resulting in regions of hypoxia. (Courtesy of R. Tong, Steele Laboratory.)

Table 2

Molecules and Pathways in Neovascularization and Vessel Maturation

Signaling Pathways Ligand/Receptor (Cell Type)	Putative Roles
VEGF/VEGFR-1, -2 (EC)	Upregulates proteases for matrix organization Generates provisional matrix by increasing permeability Upregulates PDGF-β to recruit mural cells to stabilize vessels Suppresses apoptosis to stabilize vessels Induces EC specialization (such as VVOs and fenestration)
VEGF-154/VEGFR-2, NRP-1 (EC)	Promotes arterial growth
VEGF-C/VEGFR-3, NRP-2	Guides lymphatic development
EG-VEGF/PKR-1, -2 (EC)	Induces EC specialization in endocrine organs (such as fenestration)
Notch pathway (EC, mural cell)	Determines fate of the common progenitor cell Establishes vessel fate (artery versus vein, upstream of ephrin signaling)
Ephrin B2/EphB4 (EC)	Determines arterial and venous EC specialization Guides vessel branching
PDGF-B/PDGFR-β (EC, mural cell)	Promotes proliferation, migration, and recruitment of mural cells
S1P1/EDG1 (EC, mural cell)	Promotes recruitment of mural cells
Ang1/Tie2 (EC)	Stabilizes vessels by facilitating interaction (EC-mural cell and EC-matrix) Suppresses apoptosis of ECs Induces hierarchical arrangement of vascular branching in the absence of mural cells
Ang2/Tie2 (EC)	Induces apoptosis of ECs in the absence of VEGF Determines lymphatic patterning
Ang1/Tie2 (EC)	Coordinates vascular polarity
TGF-β1/TGF-βRII (EC, mural cell)	Promotes the production of ECM and proteases Promotes differentiation of fibroblast to myofibroblast to mural cell (through serum response factor)
TGF-β1/ALK1 (EC)	Regulates EC proliferation and migration (activation phase)
TGF-β1/ALK5 (EC)	Regulates vessel maturation (resolution phase)
TGF-β1/ALK1 and endoglin (EC)	Promotes arterio-venous specialization
Syk/SLP76 pathway	Separates lymphatic from blood vessels
BDNF/TrkB (EC, hematopoietic myeloid precursor cells)	EC survival[59] Promotes angiogenesis directly (via EC) and indirectly via hematopoietic cell recruitment[60]
Semaphorin 4D/Plexin-D1 (EC)	Vascular patterning[61,62]
ING4/NF-κB pathway	Inhibits angiogenesis[63]
Slit2/Robo1 pathway (EC)	EC migration and tube formation[64]

(Table continued)

formation. During angiogenesis, the existing vessels become leaky in response to growth factors released by normal cells or cancer cells; the basement membrane and the interstitial matrix dissolve; pericytes dissociate from the vessel; endothelial cells migrate and proliferate to form an array or sprout; a lumen is formed in the sprout—a process referred to as canalization; branches and loops are formed by confluence and anastomoses of sprouts to permit blood flow; and finally, these immature vessels are invested in basement membrane and pericytes. During normal physiologic angiogenesis, these vessels differentiate into mature arterioles, capillaries, and venules, whereas in tumors they may remain immature.[12,22-24]

Finally, vasculogenesis occurs during embryonic development when a primitive vascular plexus is formed from endothelial precursor cells (also known as angioblasts). Circulating endothelial precursor cells mobilized from the bone marrow or peripheral blood also can contribute to postnatal vasculogenesis in tumors and other tissues.[25,26] However, recent data have questioned the importance and role of these cells in tumor angiogen-

Financial Disclosure: Dr. Jain is a consultant to AstraZeneca.

Table 2 (continued)

Molecules Governing Cell-Cell Interactions

Molecules (Cell Type)	Putative Roles
VE-cadherin (EC)	Forms EC-EC junctions
N-cadherin (EC, mural cell)	Facilitates EC junctions–mural cell communication
Connexins (EC, mural cell)	Facilitate EC junctions–EC junctions and EC junctions–mural cell communications
Occludins, claudins, zona occludins (ZO1, ZO2, ZO3) (EC)	Form tight junctions in brain and retinal capillaries
CD148 (EC)	Regulates EC–mural cell interaction

Molecules Governing Cell-Matrix Interactions

Molecules (Cell Type)	Putative Roles
Integrins $\alpha_5\beta_1$, $\alpha_1\beta_1$, $\alpha_2\beta_1$, $\alpha_v\beta_3$, $\alpha_v\beta_5$	Suppress EC apoptosis[a] Modulate EC migration and proliferation[65]
UNC5B	Negative regulator of vascular guidance[66]
Matrix metalloproteinases	Control degradation of basement membrane and extracellular matrix and cause release of other angiogenic factors[24]
Proteases (EC, mural cell)	Provide cues for vascular patterning by releasing growth factors Cleave matrix molecules (such as collagen XVIII to endostatin), plasma proteins (such as plasminogen to angiostatin), and protease molecules (such as MMP2 to PEX); cleaved products cause EC apoptosis
Protease inhibitors	Stabilize vessels by preventing dissolution of matrix
Thrombospondin-1, -2	Inhibits EC migration, growth, adhesion, survival[31]

[a]Genetic approach does not support this role for $\alpha_1\beta_1$ and $\alpha_v\beta_5$.

EC = endothelial cells; ECM = extracellular matrix; MMP2 = matrix metalloproteinase 2; PDGF = platelet-derived growth factor; VEGF = vascular endothelial growth factor; VVO = vesiculo-vacuolar organelle.

Adapted and updated, with permission from Nature Publishing Group, from Jain.[24] Updated information is referenced accordingly.

esis.[27] One of the current challenges in tumor treatment is to discern the relative contribution of each of the four mechanisms of neoangiogenesis to the formation of tumors to optimize antiangiogenic treatment of cancer.[28]

Structure and Function of Tumor Vessels

Despite the critical role of blood vessels in tumor growth and metastasis, the structure and function of tumor vasculature is abnormal (Table 1, Figure 2). The organized structure of the vascular network is lost. The system lacks defined arterioles, venules, and capillaries, and connections among vessels are sometimes incomplete. The vessels themselves are irregularly shaped with areas of dilation and constriction. Endothelial cell arrangement is abnormal with the cells separated by wide gaps at one location or stacked on one another nearby. Endothelial cells can lose their reactivity to common endothelial markers.[29] Similarly, the patterns and functions of mural cells are also abnormal. Tumor-associated pericytes demonstrate abnormal protein expression and morphology. Significantly, abnormal pericytes have a loose association with endothelial cells, contributing to the high vascular permeability. The differences between normal and abnormal vasculature are summarized in Table 1.

These structural abnormalities result in uneven tumor perfusion and high tumoral interstitial fluid pressure (IFP).[13,30,31] High tumoral IFP is caused in part by tumor vessel hyperpermeability. In normal tissues, the vessel is able to maintain a gradient of fluid pressure from inside the vessel to the outside. In tumors, this gradient disappears and the pressure outside the blood vessels (IFP) tends to become equal to that inside, ie, microvascular pressure (MVP). Similarly, in normal tissues, the colloid osmotic pressure (osmotic pressure exerted by large proteins) inside blood vessels (P) is much higher compared to that outside (I). In tumors, these two become approximately equal due to vessel leakiness. The loss of these pressure gradients between the vessels and the tumor impedes the delivery of large molecular weight therapeutics to the tumor. Uneven tumor perfusion impedes the delivery of all blood-borne molecules, including oxygen and nutrients as well as chemotherapeutics.

Tumor vessel hyperpermeability also contributes to sluggish blood flow in tumors, which results in regions of hypoxia and acidosis. Hypoxia contributes to resistance to some drugs and radiotherapy by decreasing the

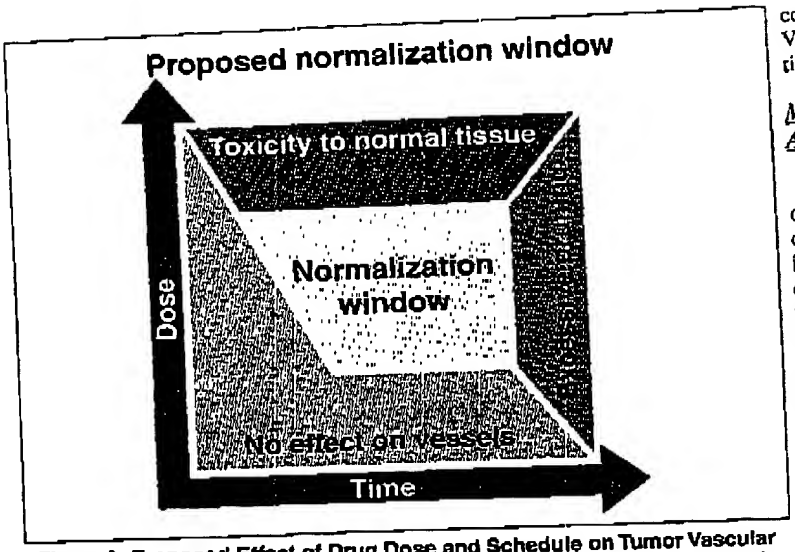

Figure 3: Proposed Effect of Drug Dose and Schedule on Tumor Vascular Normalization—The efficacy of cancer therapies that combine antiangiogenic and cytotoxic drugs depends on the dose and delivery schedule of each drug. The vascular normalization model posits that a well-designed strategy should passively prune away immature, dysfunctional vessels and actively fortify those remaining, while incurring minimal damage to normal tissue vasculature. During this normalization window, cancer cells may be more vulnerable to traditional cytotoxic therapies and to novel targeted therapies. The degree of normalization will be spatially and temporally dependent in a tumor. Vascular normalization will occur only in regions of the tumor where the imbalance of pro- and antiangiogenic molecules has been corrected. Reproduced, with permission, from Jain RK: Normalization of tumor vasculature: An emerging concept in antiangiogenic therapy. *Science* 307:58-62, 2005. Copyright 2005 AAAS.

availability of reactive oxygen species. In addition, it can induce genetic instability and upregulate angiogenesis and metastasis genes.[32,33] Furthermore, both hypoxia and acidosis can impede the cytotoxic effects of immune cells infiltrating the tumor. Thus pathologic tumor vasculature results in conditions that protect the tumor from cytotoxic therapy and from host immune cells.

Role of VEGF in Tumor Angiogenesis

Numerous pro- and antiangiogenic molecules orchestrate the different steps of vessel formation. These molecules can be grouped into three categories: (1) ligands and receptors, (2) molecules that govern cell to cell interactions, and (3) molecules governing cell to matrix interactions (Table 2). The imbalance of these molecules is thought to promote the pathologic angiogenesis characteristic of tumors.

Of the known angiogenic factors, VEGF is the most prominent and critical.[1,2,18] VEGF promotes the survival and proliferation of endothelial cells, increases the display of adhesion molecules, and dramatically increases vascular permeability. VEGF expression is elevated in most human tumors and is upregulated by a variety of mechanisms, including hypoxia,[33] oncogenes,[5] and hormonal activity.[34] The expression of VEGF correlates with both the extent of angiogenesis and prognosis in many tumor types.[18,35] As a result of its central role in tumor angiogenesis, VEGF has become a prime therapeutic target for antiangiogenic therapy.

Mechanisms of Antiangiogenic Therapies

The widely accepted mechanism of antiangiogenic therapies is based on the hypothesis that tumor growth is dependent on angiogenesis.[3] Specifically, these therapies are thought to choke the blood supply of tumors, depriving cancer cells of nutrients and subsequently resulting in an indirect cell kill. Indeed, anti-VEGF treatments have proven to be effective in a large number of preclinical studies.[5,6] To date, anti-VEGF treatments—when given as monotherapy—have unfortunately produced only modest responses in patients with solid tumors and have not yet provided significant survival benefit to patients.[9]

There are many possible reasons for this failure. For example, as tumors progress, their vessels may become dependent on factors other than VEGF.[36] Thus, blocking VEGF alone may not be enough to induce persistent vessel regression. However, increasing the dose or duration of anti-VEGF treatment might also cause damage to normal tissues (eg, kidney,[37] lung,[38] thyroid,[39] and developing bone[40]) and may even result in death due to thromboembolic events in certain subpopulations of patients.[41] As a result, antiangiogenic agents have been combined with cytotoxic therapies (eg, chemotherapy or radiation therapy). Indeed, in a landmark phase III trial, bevacizumab combined with chemotherapy has led to an impressive and significant increase in survival in patients with advanced colorectal carcinomas.[10] At the same time, a phase III trial combining bevacizumab and chemotherapy has not shown a significant survival advantage in breast cancer patients.[42] although it did show a significant increase in response rates. These positive and negative survival results with combination antiangiogenic and chemotherapy mimic preclinical findings of augmentation vs antagonism of the efficacy of cytotoxic therapies by antiangiogenic agents.

Address all correspondence to:
Rakesh K. Jain, PhD
Department of Radiation Oncology
Massachusetts General Hospital
100 Blossom St
Boston, MA 02114
e-mail: jain@steele.mgh.harvard.edu

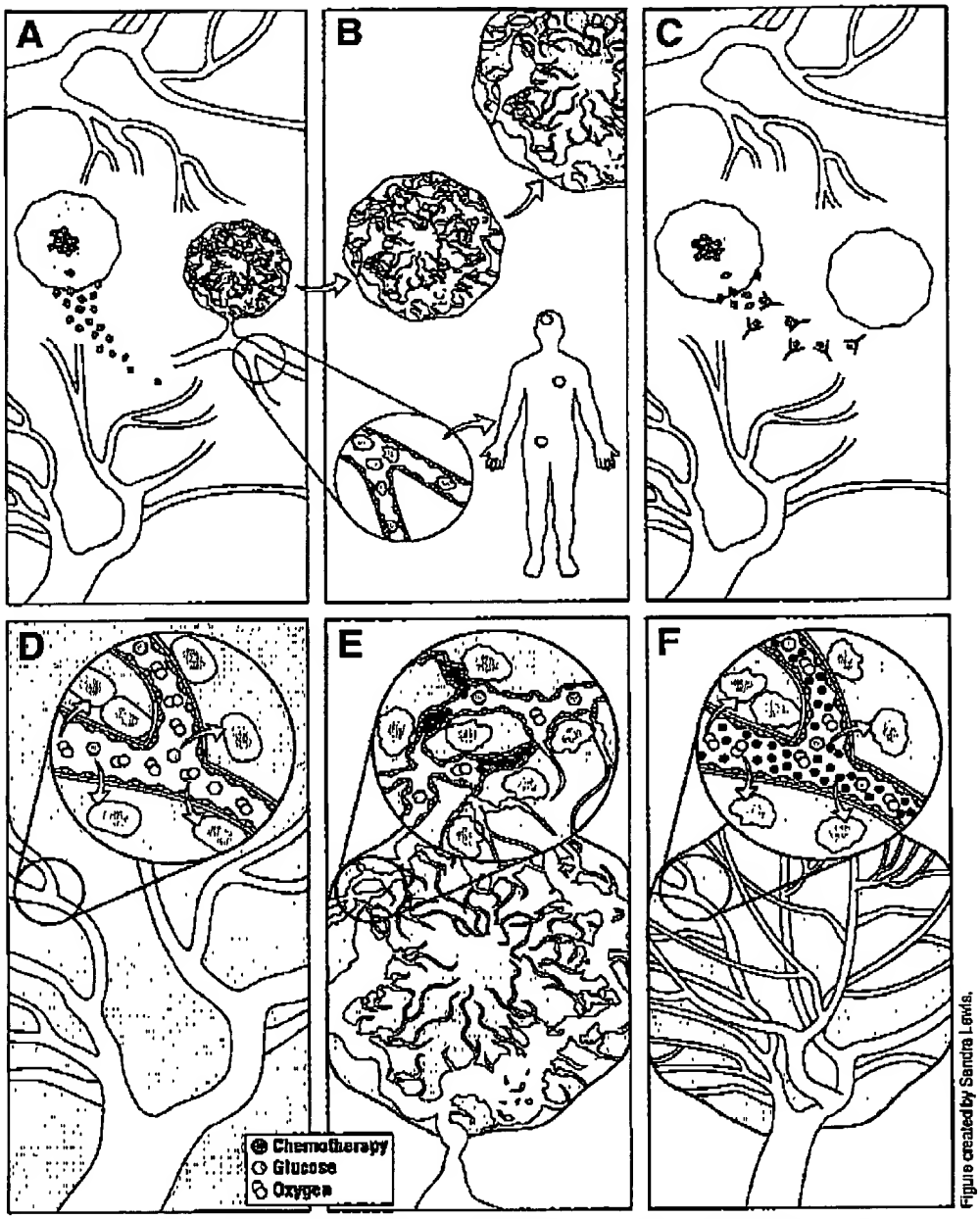

Figure 4: Dual Mechanism of Action of Antiangiogenic Therapy—(A) Angiogenic factors released by the tumor promote tumor vascularization. (B) This results in tumor growth (top) and provides a means for metastasis by providing access to the systemic vasculature (bottom). (C) Blockade of these factors would be expected to prevent these actions, keeping avascular tumors dormant and inhibiting metastatic potential. (D) Normal vasculature is optimally structured to facilitate the delivery of oxygen and nutrients to the surrounding tissues. (E) Tumor vasculature is abnormally structured resulting in uneven perfusion and blood flow, promoting hypoxia and acidosis, and impeding the delivery of chemotherapy to the tumor. (F) Antiangiogenic agents can normalize the tumor vasculature, relieving hypoxia, and facilitating chemotherapy delivery.

To reconcile these contrasting effects of antiangiogenic therapy, in 2001 I proposed another mechanism of antiangiogenic therapy—normalization of pathologic tumor vasculature by antiangiogenic therapy[12]—and have recently summarized compelling evidence in support of this new concept.[13] This theory proposes that normalization occurs because antiangiogenic agents transiently restore the balance of pro- and antiangiogenic factors. By normalizing the structure and function of the tumor vasculature, chemotherapeutic agents and oxygen can be more effectively delivered to the tumor, resulting in improved chemotherapy delivery and radiotherapy sensitivity. While this mechanism is a relatively new concept, it appears to explain the pronounced clinical benefit observed with blockade of VEGF in conjunction with standard chemotherapy.[10]

Of interest, there is now increasing evidence in the literature for vascular normalization as a result of VEGF blockade, both in preclinical[11,43-52] and clinical studies.[53] A clinical study in patients with rectal cancer showed that bevacizumab decreased tumor microvascular density, vascular volume, and IFP.[53] The lack of a concurrent decrease in the uptake of radioactive FDG in these tumors suggested that the normalized vessels were more efficient at delivering these agents to the tumor parenchyma when treated. The reductions in tumor vascular density and permeability were consistent with another study in patients with colorectal cancer treated with an inhibitor of the VEGF receptor tyrosine kinase 2.[54] Unfortunately, in the latter study, there were no measurements of IFP or vessel wall structure to draw any conclusions about vessel normalization.

It is important to note that following antiangiogenic drug delivery, a specific time window exists during which vascular normalization occurs. In a murine study that evaluated an antibody to VEGF receptor 2, this normalization window lasted for about 6 days and was characterized by increased tumor oxygenation and vessel pericyte coverage.[51] Consistent with the concept of a normalization window, a recent study showed a transient increase in tumor oxygenation and radiation response of a murine fibrosarcoma when animals were treated with thalidomide (Thalomid), an agent that blocks VEGF and bFGF signaling.[43] Thus, future research must focus on identifying the optimal timing of administration of antiangiogenic agents with chemotherapy or radiation to maximize the benefits that may be attained during this crucial time period (Figure 3).

Finally, emerging data show that some cancer cells harbor the receptors for growth factors modulating angiogenesis, and thus may be a direct target of some antiangiogenic agents. For example, some cancer cells express VEGF receptors,[55-57] and ligation of these receptors induces tumor cell proliferation.[57] Blockade of these receptors inhibits VEGF-induced proliferation, providing a mechanism by which some antiangiogenic agents could have direct inhibitory effects on tumor cells.

In summary, current data support two key mechanisms of antiangiogenic therapy: (1) inhibition of new vessel formation inside the tumor, and (2) pruning nascent vessels and normalizing the remaining tumor vasculature (Figure 4). Clinical data to date suggest that the latter mechanism may be a key driver of the clinical benefit of combined antiangiogenic and cytotoxic therapies.

Future Directions in Antiangiogenic Therapy

Angiogenesis is a complex process involving an increasing number of molecular players (Table 2). In addition, there is a likelihood of redundancy in the system and various factors may be critical at different times during vascular development. Because of its critical role in tumor angiogenesis, current therapy has focused largely on blockade of VEGF. Future angiogenic therapy may target VEGF in addition to other angiogenic factors. For example, it has recently been found that the anti-HER2 antibody trastuzumab (Herceptin) blocks multiple angiogenic pathways[58]; combination bevacizumab and trastuzumab therapy is currently in clinical trials. As these combination antiangiogenic therapies are developed, it will be important to balance the benefit of complete angiogenic blockade with any safety concerns that may arise from a potentially too-effective blockade (eg, impaired wound healing, adverse effects in kidneys, thyroid, lung, brain, and heart). Judicious administration of antiangiogenic agents may provide a viable strategy in which multiple pathways are targeted but the blockade does not induce toxic effects.

The optimal dosing of antiangiogenic therapy is another key issue for further research. Preclinical data suggest that the concept of using the maximum tolerated dose may not apply in this setting. In some studies the blockade of VEGF activity resulted in adverse effects on normal vessels in multiple organs.[37-40] In addition, some early dose-escalating clinical studies of VEGF blockade suggest that increasing the dose increases toxic effects, which may be directly related to antiangiogenic activity.[7,8] However, large-scale trials must be completed before any conclusions can be drawn.

Finally, as clinical development of antiangiogenic agents continues, it may be necessary to reconsider standard metrics of clinical response. Early data suggest that these agents are primarily cytostatic. Thus a greater emphasis on patient survival relative to objective response may be a more appropriate way to evaluate the efficacy of these therapies. In addition, measurement of surrogate markers for functional blockade of angiogenic factors (eg, tumor IFP, blood flow, permeability, vascular density, pericyte coverage, circulating endothelial cells) is critical to optimize the dose and schedule of antiangiogenic agents and cytotoxic therapies.

Conclusions

Neovascularization is an important physiologic process that enables the growth and metastasis of malignant tumors. This process is tightly regulated, and a number of proangiogenic factors are required for angiogenesis

to occur. Both pro- and antiangiogenic factors represent important potential therapeutic targets in cancer therapy. Of these factors, VEGF is the most potent and predominant. Emerging clinical data show that anti-VEGF therapy inhibits tumor growth and metastasis by inhibiting angiogenesis and by normalizing tumor vasculature. This latter effect is an intriguing area of study that may lead to the optimization of combination antiangiogenic and cytotoxic therapy.

Acknowledgments: The author would like to thank his laboratory members and clinical collaborators, especially Dan Duda and Ricky Tong, for their helpful comments on this article. This article is based on two recent reviews by the author in *Nature Medicine* (2003) and *Science* (2005). The author's work for the past 25 years has been supported by the National Cancer Institute.

References

1. Carmeliet P, Jain RK: Angiogenesis in cancer and other diseases. *Nature* 407:249-257, 2000.

2. Ferrara N, Hillan KJ, Gerber HP, et al: Discovery and development of bevacizumab, an anti-VEGF antibody for treating cancer. *Nat Rev Drug Discov* 3:391-400, 2004.

3. Folkman J: Tumor angiogenesis: Therapeutic implications. *N Engl J Med* 285:1182-1186, 1971.

4. Gullino PM: Angiogenesis and oncogenesis. *J Natl Cancer Inst* 61:639-643, 1978.

5. Kerbel R, Folkman J: Clinical translation of angiogenesis inhibitors. *Nat Rev Cancer* 2:727-739, 2002.

6. Hicklin DJ, Ellis LM: Role of the vascular endothelial growth factor pathway in tumor growth and angiogenesis. *J Clin Oncol* 23:1011-1027, 2005.

7. Cobleigh MA, Langmuir VK, Sledge GW, et al: A phase I/II dose-escalation trial of bevacizumab in previously treated metastatic breast cancer. *Semin Oncol* 30(5 suppl 16):117-124, 2003.

8. Yang JC, Haworth L, Sherry RM, et al: A randomized trial of bevacizumab, an anti-vascular endothelial growth factor antibody, for metastatic renal cancer. *N Engl J Med* 349:427-434, 2003.

9. Mayer RJ: Two steps forward in the treatment of colorectal cancer. *N Engl J Med* 350:2406-2408, 2004.

10. Hurwitz H, Fehrenbacher L, Novotny W, et al: Bevacizumab plus irinotecan, fluorouracil, and leucovorin for metastatic colorectal cancer. *N Engl J Med* 350:2335-2342, 2004.

11. Teicher BA: A systems approach to cancer therapy (antioncogenics + standard cytotoxics → mechanism(s) of interaction). *Cancer Metastasis Rev* 15:247-272, 1996.

12. Jain RK: Normalizing tumor vasculature with antiangiogenic therapy: A new paradigm for combination therapy. *Nat Med* 7:987-989, 2001.

13. Jain RK: Normalization of tumor vasculature: An emerging concept in antiangiogenic therapy. *Science* 307:58-62, 2005.

14. Harach HR, Franssila KO, Wasenius VM: Occult papillary carcinoma of the thyroid. A "normal" finding in Finland. A systematic autopsy study. *Cancer* 56:531-538, 1985.

15. Folkman J, Kalluri R: Cancer without disease. *Nature* 427:787, 2004.

16. Hanahan D, Folkman J: Patterns and emerging mechanisms of the angiogenic switch during tumorigenesis. *Cell* 86:353-364, 1996.

17. Hasan J, Byers R, Jayson GC: Intra-tumoural microvessel density in human solid tumours. *Br J Cancer* 86:1566-1577, 2002.

18. Dvorak HF: Vascular permeability factor/vascular endothelial growth factor: A critical cytokine in tumor angiogenesis and a potential target for diagnosis and therapy. *J Clin Oncol* 20:4368-4380, 2002.

19. Patan S, Munn LL, Jain RK: Intussusceptive microvascular growth in a human colon adenocarcinoma xenograft: A novel mechanism of tumor angiogenesis. *Microvasc Res* 51:260-272, 1996.

20. Patan S, Munn LL, Tanda S, et al: Vascular morphogenesis and remodeling in a model of tissue repair: Blood vessel formation and growth in the ovarian pedicle after ovariectomy. *Circ Res* 89:723-731, 2001.

21. Patan S, Tanda S, Roberge S, et al: Vascular morphogenesis and remodeling in a human tumor xenograft: Blood vessel formation and growth after ovariectomy and tumor implantation. *Circ Res* 89:732-739, 2001.

22. Carmeliet P: Mechanisms of angiogenesis and arteriogenesis. *Nat Med* 6:389-395, 2000.

23. Jain RK, Schlenger K, Hockel M, et al: Quantitative angiogenesis assays: Progress and problems. *Nat Med* 3:1203-1208, 1997.

24. Jain RK: Molecular regulation of vessel maturation. *Nat Med* 9:685-693, 2003.

25. Isner JM: Myocardial gene therapy. *Nature* 115:234-239, 2002.

26. Rafii S, Lyden D, Benezra R, et al: Vascular and haematopoietic stem cells: Novel targets for anti-angiogenesis therapy? *Nat Rev Cancer* 2:826-835, 2002.

27. Jain RK, Duda DG: Role of bone marrow-derived cells in tumor angiogenesis and treatment. *Cancer Cell* 3:515-516, 2003.

28. Stoll BR, Migliorini C, Kadambi A, et al: A mathematical model of the contribution of endothelial progenitor cells to angiogenesis in tumors: Implications for antiangiogenic therapy. *Blood* 102:2555-2561, 2003.

29. Di Tomaso E, Capen D, Haskell A, et al: Mosaic tumor vessels: Cellular basis and ultrastructure of focal regions lacking endothelial cell markers. *Cancer Res* (in press).

30. Jain RK: Barriers to drug delivery in solid tumors. *Sci Am* 271:58-65, 1994.

31. Jain RK: Vascular and interstitial biology of tumors, in Abeloff M, Armitage J, Kastan M, et al (eds): *Clinical Oncology*, 3rd ed, chap 9, p 153. Philadelphia, Elsevier, 2004.

32. Bottaro DP, Liotta LA: Cancer: Out of air is not out of action. *Nature* 423:593-595, 2003.

33. Semenza GL: Targeting HIF-1 for cancer therapy. *Nat Rev Cancer* 3:721-732, 2003.

34. Jain RK, Safabakhsh N, Sckell A, et al: Endothelial cell death, angiogenesis, and microvascular function after castration in an androgen-dependent tumor: Role of vascular endothelial growth factor. *Proc Natl Acad Sci USA* 95:10820-10825, 1998.

35. Ferrara N, Gerber HP, LeCouter J: The biology of VEGF and its receptors. *Nat Med* 9:669-676, 2003.

36. Rolf M, LeJeune S, Scott PA, et al: Expression of the angiogenic factors vascular endothelial cell growth factor, acidic and basic fibroblast growth factor, tumor growth factor beta-1, platelet-derived endothelial cell growth factor, placenta growth factor, and pleiotrophin in human primary breast cancer and its relation to angiogenesis. *Cancer Res* 57:963-969, 1997.

37. Sugimoto H, Hamano Y, Charytan D, et al: Neutralization of circulating vascular endothelial growth factor (VEGF) by anti-VEGF antibodies and soluble VEGF receptor 1 (sFlt-1) induces proteinuria. *J Biol Chem* 278:12605-12608, 2003.

38. Kasahara Y, Tuder RM, Taraseviciene-Stewart L, et al: Inhibition of VEGF receptors causes lung cell apoptosis and emphysema. *J Clin Invest* 106:1311-1319, 2000.

39. Baffert F, Thurston G, Rochon-Duck M, et al: Age-related changes in vascular endothelial growth factor dependency and angiopoietin-1-induced plasticity of adult blood vessels. *Circ Res* 94:984-992, 2004.

40. Zelzer E, Mamluk R, Ferrara N, et al: VEGFA is necessary for chondrocyte survival during bone development. *Development* 131:2161-2171, 2004.

41. Ratner M: Genentech discloses safety concerns over Avastin. *Nat Biotechnol* 22:1198, 2004.

42. Miller KD, Chap LI, Holmes FA, et al: Randomized phase III trial of capecitabine compared with bevacizumab plus capecitabine in patients with previously treated metastatic breast cancer. *J Clin Oncol* 23:792-799, 2005.

43. Ansiaux R, Baudelet C, Jordan BF, et al: Thalidomide radiosensitizes tumors through early changes in the tumor microenvironment. *Clin Cancer Res* 11:743-750, 2005.

44. Cazit Y, Baish JW, Safabakhsh N, et al: Fractal characteristics of tumor vascular architecture during tumor growth and regression. *Microcirculation* 4:395-402, 1997.

45. Hobbs SK, Monsky WL, Yuan F, et al: Regulation of transport pathways in tumor vessels: Role of tumor type and microenvironment. *Proc Natl Acad Sci USA*, 95:4607-4612, 1998.

46. Inai T, Mancuso M, Hashizume H, et al: Inhibition of vascular endothelial growth factor (VEGF) signaling in cancer causes loss of endothelial fenestrations, regression of tumor vessels, and appearance of basement membrane ghosts. *Am J Pathol* 165:35-52, 2004.

47. Kadambi A, Mouta Carreira C, Yun CO, et al: Vascular endothelial growth factor (VEGF)-C differentially affects tumor vascular function and leukocyte recruitment: Role of VEGF-receptor 2 and host VEGF-A. *Cancer Res* 61:2404-2408, 2001.

48. Lee CG, Heijn M, di Tomaso E, et al:

Anti-vascular endothelial growth factor treatment augments tumor radiation response under normoxic or hypoxic conditions. *Cancer Res* 60:5565-5570, 2000.

49. Tong RT, Boucher Y, Kozin SV, et al: Vascular normalization by vascular endothelial growth factor receptor 2 blockade induces a pressure gradient across the vasculature and improves drug penetration in tumors. *Cancer Res* 64:3731-3736, 2004.

50. Wildiers H, Guetens G, De Boeck G, et al: Effect of antivascular endothelial growth factor treatment on the intratumoral uptake of CPT-11. *Br J Can* 88:1979-1986, 2003.

51. Winkler F, Kozin SV, Tong RT, et al: Kinetics of vascular normalization by VEGFR2 blockade governs brain tumor response to radiation: Role of oxygenation, angiopoietin-1, and matrix metalloproteinases. *Cancer Cell* 6:553-563, 2004.

52. Yuan F, Chen Y, Dellian M, et al: Time-dependent vascular regression and permeability changes in established human tumor xenografts induced by an anti-vascular endothelial growth factor/vascular permeability factor antibody. *Proc Natl Acad Sci USA* 93:14765-14770, 1996.

53. Willett CG, Boucher Y, di Tomaso E, et al: Direct evidence that the VEGF-specific antibody bevacizumab has antivascular effects in human rectal cancer. *Nat Med* 10:145-147, 2004.

54. Morgan B, Thomas AL, Drevs J, et al: Dynamic contrast-enhanced magnetic resonance imaging as a biomarker for the pharmacological response of PTK787/ZK 222584, an inhibitor of the vascular endothelial growth factor receptor tyrosine kinases, in patients with advanced colorectal cancer and liver metastases: Results from two phase I studies. *J Clin Oncol* 21:3955-3964, 2003.

55. Soker S, Takashima S, Miao HQ, et al: Neuropilin-1 is expressed by endothelial and tumor cells as an isoform-specific receptor for vascular endothelial growth factor. *Cell* 92:735-745, 1998.

56. Bachelder RE, Crago A, Chung J, et al: Vascular endothelial growth factor is an autocrine survival factor for neuropilin-expressing breast carcinoma cells. *Cancer Res* 61:5736-40, 2001.

57. Li M, Yang H, Chai H, et al: Pancreatic carcinoma cells express neuropilins and vascular endothelial growth factor, but not vascular endothelial growth factor receptors. *Cancer* 101:2341-2350, 2004.

58. Izumi Y, Xu L, di Tomaso E, et al: Tumour biology: Herceptin acts as an anti-angiogenic cocktail. *Nature* 416:279-280, 2002.

59. Donovan MJ, Lin MI, Wiegn P, et al: Brain derived neurotrophic factor is an endothelial cell survival factor required for intramyocardial vessel stabilization. *Development* 127:4531-4540, 2000.

60. Duda DG, Jain RK: Pleiotropy of tissue-specific growth factors: From neurons to vessels via the bone marrow. *J Clin Invest* 115:596-598, 2005.

61. Conrotto P, Valdembri D, Corso S, et al: Sema4D induces angiogenesis through Met recruitment by Plexin B1. *Blood* 2005. E-published ahead of print.

62. Torres-Vazquez J, Gitler AD, Fraser SD, et al: Semaphorin-plexin signaling guides patterning of the developing vasculature. *Dev Cell* 7:117-123, 2004.

63. Garkavtsev I, Kozin SV, Chernova O, et al: The candidate tumour suppressor protein ING4 regulates brain tumour growth and angiogenesis. *Nature* 428:328-332, 2004.

64. Wang B, Xiao Y, Ding BB, et al: Induction of tumor angiogenesis by Slit-Robo signaling and inhibition of cancer growth by blocking Robo activity. *Cancer Cell* 4:19-29, 2003.

65. Holden SN, Morrow M, O'Bryant C, et al: Correlative biological assays used to guide dose escalation in a phase I study of the antiangiogenic αVβ3 and αVβ5 integrin antagonist EMD 121974 (EMD) (abstract 110). *Proc Am Soc Clin Oncol* 21:28a, 2002.

66. Lu X, Le Noble F, Yuan L, et al: The netrin receptor UNC5B mediates guidance events controlling morphogenesis of the vascular system. *Nature* 432:179-186, 2004.

y7n-▒ьы_□ohttp://gateway.ut.ovid.com/gw1/ovidweb.cgi?S=IDNJHKIDOAPGLK00D&Graphic=00007529-200008180-00019%7cFF3%7cT%
7cjpgт□□□□WXY□тq□□□rstu_□□WebResourceTextEncodingNameUUTF-8O□□□Л

Volume 289(5482),6=18 August 2000,6=pp 1197-1202

Genes Expressed in Human Tumor Endothelium

[Research: Reports]

Croix, Brad St.[1]; Rago, Carlo[1,2]; Velculescu, Victor[1]; Traverso, Giovanni[1]; Romans, Katharine E.[3]; Montgomery, Elizabeth[3]; Lal, Anita[4]; Riggins, Gregory J.[4]; Lengauer, Christoph[1]; Vogelstein, Bert[1,2]; Kinzler, Kenneth W.[1*]

[1]Johns Hopkins Oncology Center, [2]Howard Hughes Medical Institute, [3]Department of Pathology, Johns Hopkins University School of Medicine, Baltimore, MD 21231, USA. [4]Department of Pathology, Duke University Medical Center, Durham, NC 27710, USA.

*To whom correspondence should be addressed. E-mail: kinzlke@jhmi.edu

15 May 2000; accepted 28 June 2000

Abstract

To gain a molecular understanding of

Links

Abstract

Complete Reference

Library Holdings

Outline

- Abstract
- References and Notes

Graphics

- Fig. 1
- Table 1
- Fig. 2
- Table 2
- Fig. 3

EXHIBIT I

tumor angiogenesis, we compared gene expression patterns of endothelial cells derived from blood vessels of normal and malignant colorectal tissues. Of over 170 transcripts predominantly expressed in the endothelium, 79 were differentially expressed, including 46 that were specifically elevated in tumor-associated endothelium. Several of these genes encode extracellular matrix proteins, but most are of unknown function. Most of these tumor endothelial markers were expressed in a wide range of tumor types, as well as in normal vessels associated with wound healing and corpus luteum formation. These studies demonstrate that tumor and normal endothelium are distinct at the molecular level, a finding that may have significant implications for the development of anti-angiogenic therapies.

Tumors require a blood supply for expansive growth (1-3), an observation that has stimulated a profusion of research on tumor angiogenesis. However, several basic questions about tumor vessels remain unanswered. For example, is endothelium that lines blood vessels in tumors qualitatively different from endothelium in vessels of normal tissue? What is the relation of tumor angiogenesis to angiogenesis associated with wound healing or other physiological processes? The answers to these questions critically impact the potential for new therapeutic approaches to inhibit angiogenesis in a tumor-specific manner.

To determine if tumor-specific endothelial markers exist, we compared gene expression profiles in endothelium derived from normal and tumor tissue. Human colorectal cancer was chosen for these studies because it has a high incidence, tends to grow slowly, and is often resistant to chemotherapeutic drugs. Importantly, the progressive growth of this tumor type appears to be angiogenesis-dependent (4).

Global analysis of gene expression in tumor and normal endothelium is difficult because (i) the endothelium is enmeshed in a complex tissue consisting of vessel wall components, stromal cells, and epithelial cells, and (ii) only a small fraction of the cells within these tissues are endothelial. Thus, we needed to develop methods for isolating highly purified endothelial cells (ECs) and for evaluating gene expression profiles from relatively few

cells.

To overcome the first obstacle, we attempted to purify ECs from dispersed human colorectal tissue using CD31, an endothelial marker commonly used for this purpose (5-8). This resulted in a substantial enrichment of ECs but also in contamination of the preparations by hematopoietic cells, most likely due to expression of CD31 by macrophages (9). We therefore purified ECs from human tissues using P1H12, a recently described marker for ECs (10). Unlike CD31, CD34, and VE-cadherin, P1H12 specifically localized to ECs of all vessels including microvessels of normal and cancerous colorectal tissue (Fig. 1A). Our purification protocol also optimized the detachment of ECs from neighboring cells, leaving cell surface proteins intact, and included positive and negative affinity purifications using a mixture of antibodies (Fig. 1B). The ECs purified from normal colorectal mucosa and colorectal cancers were essentially free of epithelial and hematopoietic cells as judged by reverse transcription-polymerase chain reaction (RT-PCR) (Fig. 1C) and subsequent gene expression analysis (see below).

---

[x] Graphic

[Help with image viewing] [Email Jumpstart To Image]

Fig. 1. Purification of ECs from human normal and malignant tissue. (**A**) Vessels (red) of frozen sections were stained by immunofluorescence with anti-P1H12 (Chemicon, Temecula, California) and detected with a biotinylated goat anti-mouse IgG secondary antibody followed by rhodamine-linked strepavidin. The vessels stained are from within the lamina propria of normal colonic mucosa. E-cadherin-positive epithelial cells (green) at the edge of the crypt were simultaneously visualized with a rabbit polyclonal antibody (Santa Cruz Biotechnology, Santa Cruz, California), followed by a goat anti-rabbit IgG secondary antibody labeled with Alexa (Molecular Probes, Eugene, Oregon). Bar, 50 6╢M. (**B**) For isolation of pure EC populations from collagenase-dispersed tissues, the epithelial and hematopoietic cell fractions were sequentially removed by negative selection with magnetic beads. The remaining cells were stained with P1H12, and ECs were isolated by positive selection with

magnetic beads (39). (**C**) RT-PCR analysis used to assess the purity of the EC preparations. Semiquantitative PCR analysis was performed on cDNA generated directly from colorectal cancer tissue (Unfractionated Tumor) or from purified ECs isolated from normal colonic mucosa (Normal Endothelial Fraction) or colorectal cancer (Tumor Endothelial Fraction). Expression of the epithelial-specific transcript cytokeratin 20 (CK20) was limited to the unfractionated tumor. Two endothelial-specific transcripts, vWF and VE-cadherin (VE-Cad), showed robust amplification only in the endothelial fractions, whereas transcripts corresponding to the ubiquitous housekeeping enzyme glyceraldehyde phosphate dehydrogenase (GAPDH) were amplified in all samples. No signal was detected in the no-template (N.T.) control. cDNA templates were diluted 1:10, 1:100, 1:1000, 1:4000, and 1:40,000, as indicated by the declining wedge. (**D**) The relative expression level of select genes was determined by measurement of the tag abundance from several SAGE libraries combined into four groups. The first was composed of ~193,000 tags from the two in vivo-derived EC preparations (Endothelial Cell Fraction), whereas the second contained a single library of ~57,000 tags containing macrophages and other leukocytes derived from the negative selection (Hematopoietic Fraction). The third group contained ~401,000 tags from cultured HUVEC and HMVEC (Endothelial Cells in Culture), and the fourth consisted of ~748,000 tags from six colon cancer cell lines in culture (Epithelial Cells). After normalization, the library with the highest tag number for each marker was given a value of 100%, and the corresponding relative expression levels of the remaining three libraries were plotted on the ordinate. A high level of CD31 is apparent on hematopoietic cells, the likely cause of the impurity of the initial endothelial selection, compared with the selectivity of P1H12.

To evaluate gene expression, we used a modification of the serial analysis of gene expression (SAGE) technique (11). SAGE associates individual mRNA transcripts with 14-base pair (bp) tags derived from a specific position near their 3' termini (12). The abundance of each tag provides a quantitative measure of the transcript level present within the mRNA population studied. SAGE is not dependent on preexisting databases

of expressed genes and therefore provides an unbiased view of gene expression profiles. This feature is particularly important in the analysis of cells that constitute only a small fraction of the tissue under study, as transcripts from these cells are unlikely to be well represented in extant expressed sequence tag (EST) databases.

We generated a SAGE library of ~96,000 tags from the purified ECs of a colorectal cancer and a similar library from the ECs of normal colonic mucosa from the same patient. These ~193,000 tags corresponded to over 32,500 unique transcripts (13). The expression pattern of hematopoietic, epithelial, and endothelial markers confirmed the purity of the preparations (Fig. 1D).

We next identified pan endothelial markers (PEMs), that is, transcripts that were expressed at substantially higher levels in both normal and tumor-associated endothelium compared with other tissues. Tags expressed at similar levels in both tumor and normal ECs were compared with ~1.8 million tags from a variety of cell lines derived from tumors of nonendothelial origin. This simple comparison identified 93 transcripts that were expressed at levels at least 20-fold higher in ECs in vivo compared with nonendothelial cells in culture (14). Among the most abundant transcripts, there were 15 tags corresponding to characterized genes, 12 of which had been previously shown to be preferentially expressed in endothelium (10, 15-26), and the other 3 genes not previously associated with endothelium (Table 1). These data also revealed many novel PEMs, which became increasingly prevalent as tag expression levels decreased (Table 1). We validated the expression of selected PEMs in vivo using a highly sensitive nonradioactive in situ hybridization method that allowed the detection of relatively rare transcripts from frozen sections of human tissues (27). Expression of PEM3 and PEM6 was limited to vascular ECs in both normal and neoplastic tissues (Fig. 2, A and B). For other PEMs, their endothelial origin was confirmed by SAGE analysis of ~401,000 transcripts derived from primary cultures of human umbilical vein endothelial cells (HUVEC) and human dermal microvascular endothelial cells (HMVEC) (Table 1). These data also suggest that ECs maintained in culture do not completely recapitulate expression patterns observed in vivo. For example,

Hevin and several other PEMs were expressed at high levels in both tumor and normal ECs in vivo, but few or no transcripts were detected in cultured HUVEC or HMVEC (Table 1). The source of the Hevin transcripts was confirmed to be endothelium by in situ hybridization in normal and malignant colorectal tissue (Fig. 2C).

Graphic

[Help with image viewing] [Email Jumpstart To Image]

Table 1. SAGE analysis reveals previously characterized and novel pan endothelial markers. The most abundant characterized or novel tags derived by summing the tags from normal EC (N-ECs) and tumor EC (T-ECs) SAGE libraries are listed in descending order. For comparison, the corresponding number of SAGE tags found in HUVEC and HMVEC endothelial cell cultures, and several nonendothelial cell lines (14), are shown. Tag numbers for each group were normalized to 100,000 transcripts. A description of the gene product corresponding to each tag is given, followed by alternative names in parentheses. Some uncharacterized genes have predicted full-length coding sequence. The sequence CATG precedes all tags, and the 15th base (11th shown) was determined as described (38).

Graphic

[Help with image viewing] [Email Jumpstart To Image]

Fig. 2. Expression of PEMs is limited to ECs. (**A** to **C**) The endothelial origin of PEMs identified by SAGE was confirmed by a highly sensitive in situ hybridization assay (27). Localization of novel PEMs to the ECs (red stain) was demonstrated by examining two representative PEMs, PEM3 (A) and PEM6 (B), in lung cancer and colon cancer, respectively. Hevin expression was readily detected in the ECs of a colon tumor (C) despite its low level of expression in cultured ECs. Bars, 50 6╣M.

We next identified transcripts that were differentially expressed in endothelium derived from normal or neoplastic tissues. This comparison

revealed 33 tags that were elevated at least 10-fold in normal endothelium and 46 tags that were elevated 10-fold or more in tumor endothelium (28). Because transcripts expressed at higher levels in tumor endothelium are most likely to be useful for diagnostic and therapeutic purposes, our subsequent studies focused on this class. Of the top 25 tags most differentially expressed, 12 tags corresponded to 11 previously identified genes, 1 containing alternative polyadenylation sites (Table 2). Of these 11 genes, 6 were previously recognized as markers of angiogenic vessels (16, 22, 29-33), and at least 7 encode proteins involved in extracellular matrix formation or remodeling. These matrix-related processes are likely to be critical to the growth of new vessels. The remaining 14 tags corresponded to uncharacterized genes, most of which have been deposited as ESTs (Table 2).

Graphic

[Help with image viewing] [Email Jumpstart To Image]

Table 2. SAGE tags elevated in tumor endothelium. The top 25 tags with the highest tumor EC (T-ECs) to normal EC (N-ECs) tag ratios are listed in descending order. To calculate tag ratios, we assigned a value of 0.5 in cases where zero tags were observed. The SAGE libraries are the same as those listed in Table 1. Tag numbers for each group were normalized to 100,000 transcripts. A description of the gene product corresponding to each tag is given, followed by alternative names in parentheses. TEM9 was uncharacterized at the outset of these studies but was recently characterized as a lectin present on ECs in culture and on microvascular vessels of human placenta in vivo (41).

To validate the expression patterns of these genes, we focused on nine tumor endothelial markers (TEM1 through TEM9) for which EST sequences but no other information was available (Table 2). RT-PCR analysis was used to evaluate the expression of the corresponding transcripts in purified ECs derived from normal and tumor tissues of two patients different from the original one used to construct the SAGE libraries. As expected on the basis of the SAGE data, von Willebrand Factor (vWF) and PEM6 were expressed at similar levels in normal and tumor ECs from both patients. These controls

were not detected in purified tumor epithelial cells (Fig. 3A). In contrast, all nine TEMs chosen for this analysis were prominently expressed only in tumor ECs, but were absent or barely detectable in normal ECs (Fig. 3A). These RT-PCR assays were sensitive indicators of expression, and the absence of detectable transcripts in the normal endothelium, combined with their presence in tumor endothelial RNAs even when diluted 100-fold, provides important confirmation of their differential expression. These results also show that these transcripts were not simply expressed differentially in the ECs of the original patient, but were characteristic of colorectal cancer endothelium in general.

Graphic

[Help with image viewing] [Email Jumpstart To Image]

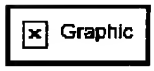

Fig. 3. Expression of TEMs. (**A**) RT-PCR analysis confirmed the tumor-specific expression of novel TEMs. Semiquantitative PCR analysis was performed on cDNA generated from purified tumor epithelial cells as a negative control (Control) or from purified ECs isolated from normal colonic mucosa (Normal ECs) or colorectal cancer (Tumor ECs) from two different patients. Two endothelial-specific markers, vWF and PEM6, showed robust amplification only in the endothelial fractions, whereas GAPDH was observed in all samples. TEM1, TEM7, and TEM9 were specifically expressed in tumor ECs. The cDNA template was diluted 1:10, 1:100, 1:1000, and 1:10,000, as indicated by the declining wedge. (**B** to **J**) The endothelial origin of TEMs identified by SAGE was confirmed by in situ hybridization, as in Fig 2. Expression of TEM1 (B) and TEM7 (C) was highly specific to the ECs in colorectal cancers; sections were imaged in the absence of a counterstain to show the lack of detectable expression in the nonendothelial cells of the tumor. TEM7 was also expressed in ECs from a metastastic liver lesion (D) arising from a primary colorectal cancer, and primary tumors derived from lung (E), breast (F), pancreatic (G), and brain cancer (H), as well as in a sarcoma (I). TEM7 expression was also localized to vessels during normal angiogenesis of human corpus luteum (J). Bars, 50 6╣M.

To exclude the possibility that the differentially expressed transcripts

were derived from contaminating nonendothelial cells, we performed in situ hybridization on normal and neoplastic colon tissue. In every case where transcripts could be detected (TEM 1, 3, 4, 5, 7, 8, and 9), they were specifically localized to ECs (34) (Fig. 3, B and C). Although caution must be used when interpreting negative in situ hybridization results, none of the TEMs were expressed in vascular ECs associated with normal colorectal tissue even though vWF and Hevin were clearly expressed (34).

To determine whether TEMs were specifically expressed in the endothelium from primary colorectal cancers, or whether they were characteristic of tumor endothelium in general, we studied the expression of a representative TEM (TEM7) in a liver metastasis from a colorectal cancer, a primary sarcoma, and in primary cancers of the lung, pancreas, breast, and brain. As shown in Fig. 3, the TEM7 transcript was expressed specifically in the endothelium of each of these cancers, whether metastatic (Fig. 3D) or primary (Fig. 3, E to I). Analysis of the other six TEMs (TEM 1, 3, 4, 5, 8, and 9) revealed a similar pattern in lung tumors, brain tumors, and metastatic lesions of the liver (34).

Finally, we investigated whether these transcripts were expressed in angiogenic states other than that associated with tumorigenesis. As assessed by in situ hybridizations, these transcripts were generally expressed both in the corpus luteum and in the granulation tissue of healing wounds (34) (Fig. 3J). One possible exception is TEM8, which we failed to detect in corpus luteum. In all tissues examined, expression of the genes was either absent or confined to the EC compartment.

The studies described above provide a definitive molecular characterization of ECs in an unbiased and general manner. They lead to several important conclusions that have direct bearing on long-standing hypotheses about angiogenesis. First, normal and tumor endothelium are highly related, sharing many endothelial cell-specific markers. Second, the endothelium derived from tumors is qualitatively different from that derived from normal tissues of the same type and is also different from primary endothelial cultures. We identified 46 transcripts that were expressed at substantially higher levels (>10-fold) in tumor endothelium than in normal

endothelium, and 33 transcripts that were expressed at substantially lower levels in tumor than in normal endothelium. Most of these genes were either not expressed or were expressed at relatively low levels in ECs maintained in culture. Third, these genes are characteristically expressed in tumors derived from several different tissue types, demonstrating that tumor endothelium, in general, is different from the endothelium in surrounding normal tissue. Fourth, most of the genes expressed differentially in tumor endothelium are also expressed during angiogenesis of corpus luteum formation and wound healing. This is consistent with the idea that tumors may recruit vasculature by means of the same signals elaborated during other physiological or pathological processes. Indeed, the notion that tumors represent "unhealed wounds" is one of the oldest ideas in cancer biology (35). However, the fact that TEM8 expression was not detectable in developing corpus luteum suggests that there may be discrete differences between tumor angiogenesis and normal angiogenesis.

Finally, it is perhaps not surprising that so many of the endothelial-specific transcripts identified in this study, whether expressed only in neovasculature or in endothelium in general, have not been previously characterized, and some are not even represented in EST databases. ECs represent only a minor fraction of the total cell population within normal or tumor tissues, and only those EC transcripts expressed at the highest levels would be expected to be represented in libraries constructed from unfractionated tissues. The genes described in the current study should therefore provide a valuable resource for basic and clinical studies of human angiogenesis in the future.

References and Notes

1. J. Folkman, *N. Engl. J. Med.* **285,** 1182 (1971). [Context Link]

2. J. Folkman, in *Cancer Medicine,* J. Holland *et al.,* Eds. (Williams & Wilkins, Baltimore, 1997), pp. 181-204. [Context Link]

3. R. S. Kerbel, *Carcinogenesis* **21,** 505 (2000). [Context Link]

4. For example, see www.sagenet.org/angio/vwf.htm . [Context Link]

5. Q. G. Dong *et al., Arterioscler. Thromb. Vasc. Biol.* **17,** 1599 (1997). [Context Link]

6. P. W. Hewett and J. C. Murray, *In Vitro Cell. Dev. Biol. Anim.* **32,** 462 (1996). **Bibliographic Links**| **Library Holdings**| [Context Link]

7. M. A. Hull, P. W. Hewett, J. L. Brough, C. J. Hawkey, *Gastroenterology* **111,** 1230 (1996). [Context Link]

8. G. Haraldsen *et al., Gut* **37,** 225 (1995). **Bibliographic Links**| **Library Holdings**| [Context Link]

9. The original EC isolation protocol was the same as that described in Fig. 1B except that dispersed cells were stained with antibody to CD31 (anti-CD31) instead of anti-P1H12, and magnetic beads against CD64 and CD14 were not included in the negative selection. Analysis of 120,000 SAGE tags from these two EC preparations revealed high levels of more than 15 selected markers predominantly expressed on macrophages. [Context Link]

10. A. Solovey *et al., N. Engl. J. Med.* **337,** 1584 (1997). [Context Link]

11. Several modifications to the original SAGE protocol have reduced the amount of starting material required (36, 37). A detailed version of our modified "MicroSAGE" protocol is available at www.sagenet.org/sage_protocol.htm . [Context Link]

12. V. E. Velculescu, L. Zhang, B. Vogelstein, K. W. Kinzler, *Science* **270,** 484 (1995). [Context Link]

13. We analyzed 96,694 and 96,588 SAGE tags from normal and tumor-derived ECs, respectively, of which 50,298 tags were unique. We derived a conservative estimate of 32,703 unique transcripts by considering only those tags observed more than once in the current data set or in the 134,000 transcripts previously identified in human transcriptomes (38). [Context Link]

14. To identify pan endothelial-specific transcripts, we normalized the number of tags analyzed in each group to 100,000 and limited our analysis to transcripts that were expressed at levels at least 20-fold higher in ECs than in nonendothelial cell lines in culture and present at fewer than five copies per 100,000 transcripts in nonendothelial cell lines and the hematopoietic fraction (~57,000 tags) (39). Nonendothelial cell lines consisted of 1.8 $\mu \approx 10^6$ tags derived from a total of 14 different cancer cell lines including colon, breast, lung, and pancreatic cancers, as well as one nontransformed keratinocyte cell line, two kidney epithelial cell lines, and normal monocytes. A complete list of PEMs is available at www.sagenet.org/angio/table1.htm . [Context Link]

15. M. Tucci *et al., J. Endocrinol.* **157,** 13 (1998). [Context Link]

16. T. Oono *et al., J. Invest. Dermatol.* **100,** 329 (1993). **Bibliographic Links| Library Holdings|** [Context Link]

17. E. Jendraschak and E. H. Sage, *Semin. Cancer Biol.* **7,** 139 (1996). [Context Link]

18. N. Bardin *et al., Tissue Antigens* **48,** 531 (1996). [Context Link]

19. D. M. Bradham, A. Igarashi, R. L. Potter, G. R. Grotendorst, *J. Cell Biol.* **114,** 1285 (1991). [Context Link]

20. K. Akaogi *et al., Proc. Natl. Acad. Sci. U.S.A.* **93,** 8384 (1996). [Context Link]

21. Y. Muragaki *et al., Proc. Natl. Acad. Sci. U.S.A.* **92,** 8763 (1995). **Bibliographic Links| Library Holdings|** [Context Link]

22. M. L. Iruela-Arispe, C. A. Diglio, E. H. Sage, *Arterioscler. Thromb.* **11,** 805 (1991). [Context Link]

23. J. P. Girard and T. A. Springer, *Immunity* **2,** 113 (1995). **Bibliographic Links| Library Holdings|** [Context Link]

24. E. A. Jaffe *et al., J. Immunol.* **143,** 3961 (1989). **Bibliographic Links| Library Holdings|** [Context Link]

25. J. P. Girard *et al., Am. J. Pathol.* **155,** 2043 (1999). [Context Link]

26. H. Ohtani and N. Sasano, *J. Electron Microsc.* **36,** 204 (1987). **Bibliographic Links| Library Holdings|** [Context Link]

27. For nonradioactive in situ hybridization, digoxigenin (DIG)-labeled antisense RNA probes were generated by PCR amplification of 500- to 600-bp products and incorporation of a T7 promoter into the antisense primer. In vitro transcription was performed with DIG RNA labeling reagents and T7 RNA polymerase (Roche, Indianapolis, IN). Frozen tissue sections were fixed with 4% paraformaldehyde, permeabilized with pepsin, and incubated with RNA probe (200 ng/ml) overnight at 556‖C. For signal amplification, a horseradish peroxidase (HRP) rabbit anti-DIG antibody (DAKO, Carpinteria, CA) was used to catalyze the deposition of Biotin-Tyramide (GenPoint kit, DAKO). Further amplification was achieved by adding HRP rabbit anti-biotin (DAKO), biotin-tyramide, and then alkaline-phosphatase (AP) rabbit anti-biotin (DAKO). Signal was detected with the AP substrate Fast Red TR/Napthol AS-MX (Sigma, St. Louis, MO), and cells were counterstained with hematoxylin unless otherwise indicated. A detailed protocol including the list of primers used to generate the probes can be obtained from the authors upon request. [Context Link]

28. Differentially expressed endothelial-specific transcripts were defined as those

expressed at levels at least fivefold higher in ECs in vivo than in nonendothelial cell lines in culture (14) and present at no more than five copies per 100,000 transcripts in nonendothelial cell lines and the hematopoietic cell fraction (39). Transcripts showing statistically different levels of expression ($P < 0.05$) were then identified by Monte Carlo analysis (40). Transcripts preferentially expressed in normal endothelium were then defined as those expressed at levels at least 10-fold higher in normal endothelium than in tumor endothelium. Conversely, tumor endothelial transcripts were present at levels at least 10-fold higher in tumor versus normal endothelium. See www.sagenet.org/angio/table2.htm and www.sagenet.org/angio/table3.htm for a complete list of differentially expressed genes. [Context Link]

29. M. Iurlaro *et al., Eur. J. Clin. Invest.* **29,** 793 (1999). **Ovid Full Text| Bibliographic Links| Library Holdings|** [Context Link]

30. W. S. Lee *et al., Circ. Res.* **82,** 845 (1998). **Bibliographic Links| Library Holdings|** [Context Link]

31. J. Niquet and A. Represa, *Brain. Res. Dev. Brain Res.* **95,** 227 (1996). **Bibliographic Links| Library Holdings|** [Context Link]

32. L. Fouser, L. Iruela-Arispe, P. Bornstein, E. H. Sage, *J. Biol. Chem.* **266,** 18345 (1991). **Bibliographic Links| Library Holdings|** [Context Link]

33. M. L. Iruela-Arispe, P. Hasselaar, H. Sage, *Lab Invest.* **64,** 174 (1991). [Context Link]

34. See www.sagenet.org/angio/table4.htm . [Context Link]

35. H. F. Dvorak, *N. Engl. J. Med.* **315,** 1650 (1986). [Context Link]

36. N. A. Datson, J. van der Perk-de Jong, M. P. van den Berg, E. R. de Kloet, E. Vreugdenhil, *Nucleic Acids Res.* **27,** 1300 (1999). **Bibliographic Links| Library Holdings|** [Context Link]

37. B. Virlon *et al., Proc. Natl. Acad. Sci. U.S.A.* **96,** 15286 (1999). [Context Link]

38. V. E. Velculescu *et al., Nature Genet.* **23,** 387 (1999). [Context Link]

39. Human colon tissues were obtained <30 min after surgical removal. Normal tissue was taken from regions >10 cm away from bulk tumor tissue that had clearly defined margins. For normal tissue, sheets of epithelial cells were removed with a glass slide after treatment with 5 mM dithiothreitol, then 10 mM EDTA, leaving an intact lamina propria for subsequent processing. After a 2-hour incubation in collagenase at 37°C, cells were filtered sequentially through 400-, 100-, 50-, and 25-μm mesh and centrifuged through a 30% preformed Percoll

gradient to sediment red blood cells. Epithelial cells (Epithelial Fraction), which were found to nonspecifically bind magnetic beads, were removed with Dynabeads coupled to BerEP4 (Dynal, Lake Success, NY). Subsequently, macrophages and other leukocytes (Hematopoietic Fraction) were removed with a mixture of beads coupled to anti-CD45, anti-CD14, and anti-CD64 (Dynal). The remaining cells were stained with P1H12 antibody, purified with anti-mouse immunoglobulin G (IgG)-coupled magnetic beads, and lysed in mRNA lysis buffer. A detailed protocol can be obtained from www.sagenet.org/angio/protocol.htm . [Context Link]

40. L. Zhang *et al., Science* **276,** 1268 (1997). [Context Link]

41. H. Sheikh, H. Yarwood, A. Ashworth, C. M. Isacke, *J. Cell Sci.* **113,** 1021 (2000). **Bibliographic Links| Library Holdings|** [Context Link]

42. We thank L. Meszier (Johns Hopkins Oncology Cell Imaging Facility) for expert help with the microscopic imaging and S. Kem and R. Hruban for pancreatic cancer samples. Supported by NIH grants CA57345, CA62924, and CGAP S98-146A. B.S.C. is a research Fellow of the National Cancer Institute of Canada supported with funds provided from the Terry Fox Run. K.W.K. received research funding from Genzyme Molecular Oncology (Genzyme). Under a licensing agreement between the Johns Hopkins University and Genzyme, the SAGE technology was licensed to Genzyme for commercial purposes, and V.V., B.V., and K.W.K. are entitled to a share of royalty received by the university from sales of the licensed technology. The SAGE technology is freely available to academia for research purposes. V.V., B.V., and K.W.K. are consultants to Genzyme. The university and researchers (V.V., B.V., and K.W.K.) own Genzyme stock, which is subject to certain restrictions under university policy. The terms of these arrangements are being managed by the university in accordance with its conflict of interest policies.

Accession Number: 00007529-200008180-00019

_□*http://gateway.ut.ovid.com/gw1/ovidweb.cgiYtext/html□ □1NWm□▌╔
□ Ю4ЮеЮпЮwДЛФ╤ФЫГ□Г К|Лул╧Л6Я:Р@Р├Р□ЖЧВ ВыВБЭV□с□╔□╝
□□□□□>□□~□□┤□ В□□□□□Z□□с□□я□□
□□_□□h□□в□□n□□╝□□╤□□$□□s□□┤□□╧□#-□'х□'╥
□'ю□,6□0R□0▪□0²□5□□9?□9}
□9├□=ь□В#□Bb□Bk□Fч□JК□К*□К3□Оё□Р3□Ps□Р|□ТК□Uщ□V□□V
□Z▒□[╬□[ь□\□□`m□`6□`ч□а□□е□□┬F□┬╥□┬ц□┬л□■э□╔я□╔с□╔
|□╘|□©≥□ю □ю□□д$□ш □э
□э□□Ю&□□Z□□л□□у□□ч□□Э□□□□0Т□1!□□v□1+

Angiogenesis 4: 61–70, 2001.

CM101 stimulates cutaneous wound healing through an anti-angiogenic mechanism*

Lillian B. Nanney[1,2], Barbara D. Wamil[4], Jeffrey Whitsitt[3,7], Nancy L. Cardwell[1], Jeffrey M. Davidson[3,7], He-Ping Yan[6] & Carl G. Hellerqvist[4,5]

[1]*Department of Plastic Surgery.* [2]*Department of Cell Biology.* [3]*Department of Pathology.* [4]*Department of Biochemistry.* [5]*Department of Medicine.* [6]*Department of Biology.* [7]*Department of Veterans' Affairs, Vanderbilt School of Medicine, Nashville, Tennessee, USA*

Received 31 October 2000; Accepted in revised form 15 March 2001

Key words: angiogenesis, CM101, endothelium, laser doppler perfusion, wound healing

Abstract

CM101, an anti-pathoangiogenic polysaccharide derived from group B streptococcus, has been shown to inhibit inflammatory angiogenesis and accelerate wound healing in a mouse model and minimize scarring/gliosis following spinal cord injury. To evaluate the *in vivo* effects of CM101 on cutaneous wound healing in the pig, intravenously delivered CM101 or placebo vehicle was given 1 h after cutaneous wounding and again at 72 h after injury. Tissues from partial-thickness and full-thickness excisions were collected at days 4 and 7 after wounding and evaluated for a variety of standard healing parameters. Both types of CM101-treated wounds showed significantly less evidence of inflammatory angiogenesis when assessed by macroscopic photography of the wound surface, qualitative histological observations, laser doppler perfusion imaging, and quantitative morphometric analysis of microvessel area from endothelium selectively immunostained for factor VIII. Resurfacing was accelerated in partial-thickness and full-thickness excisions that received two doses of CM101 as compared to the placebo-treated excisional wounds. Neodermal thickness was increased in CM101-treated wounds at day 4 and was slightly reduced in comparison with placebo by day 7. New collagen accumulation appeared to be unaffected by the CM101 treatment. Immunohistochemical staining using a polyclonal antisera directed against the anti-pathoangiogenic CM101 target protein HP59 on day 7 indicated a strong immunoreactivity on the microvessels present in the control wounds but not in wounds of the CM101-treated animals. In summary, the immunolocalization HP59 in the microvessels of the cutaneous wound bed in control but not in CM101 treated wounds suggests that CM101 inhibits the pathologic inflammatory angiogenesis accompanying the normal granulation processes. The net biological effect of inhibited inflammatory pathoangiogenesis is a diminished, suggested and purely physiologic, microvascular bed which translates into an enhanced rate of epithelial resurfacing and therefore an overall accelerated rate of wound repair.

Abbreviations: bFGF – basic fibroblast growth factor; C3 – C3 complement factor; GBS – group B streptococcus; PDGF – platelet derived growth factor; TGFβ – transforming growth factor-β; TNFα – tumor necrosis factor α

Introduction

Under normal physiological conditions, noticeable angiogenesis in adults is largely restricted to cyclical phenomena occurring in female reproductive tissues and to angiogenesis in the early phases of wound healing [1, 2]. Ischemia-driven inflammatory angiogenesis occurs during the initial acute inflammatory phase of wound repair [3]. Rapid vascular sprouting through the fibrin clot leads to infiltration of inflammatory cells and formation of granulation tissue. The subsequent re-epithelialization and remodeling process and removal of necrotic tissue involves additional blood vessel formation during non-inflammatory conditions [4]. This phase of growth of new microvessels is tightly controlled by the interplay of growth regulatory proteins that act either to stimulate or to inhibit blood vessel growth [5]. Normally, their balance is tipped towards inhibition and consequently microvessel growth is restrained. This is thought to be the prevailing condition of the endothelial cells under normal circumstances and is referred to as angiogenic homeostasis [6]. Under pathological conditions, however, local inhibitory controls are unable to

Correspondence to: Lillian B. Nanney, S-2221 MCN Plastic Surgery Research Laboratory, Vanderbilt School of Medicine, Nashville, TN 37232, USA. Tel: +1-615-322-7265; Fax: +1-615-343-2050; E-mail: lillian.nanney@mcmail.vanderbilt.edu

*This work was presented on 5 June 2000 in Toronto, Canada, at the Wound Healing Society.

restrain the increased activity of angiogenic promoters upregulated by hypoxia inducible factor (HIF) [7]. Such changes in the relative balance of inducers and inhibitors may activate the 'angiogenic switch' [8]. Angiogenesis in chronic ulcers, inflammatory diseases and tumors, may originate in sprouting, in intussusception and by incorporation of endothelial precursor cells [9].

The angiogenesis that occurs during the repair of connective tissues via the formation of new microvessels has long been considered essential for all forms of cutaneous wound repair [1, 10]. Since the integrity of the nascent endothelium within the wound bed also governs leukocyte trafficking, any angiogenic perturbations are expected to have a profound impact on the inflammatory responses that modulate wound repair [11, 12].

Subsequent to wounding, the tissues undergo a degree of hypoxia which triggers secretion of VEGF [13] and induces the inflammatory angiogenesis [7]. Numerous studies have associated increased vascular density during wound healing with accelerated wound repair [14]. To date, studies have shown that traditional cytokines such as transforming growth factor-β (TGFβ), tumor necrosis factor-α (TNFα), basic fibroblast growth factor (bFGF), platelet derived growth factor (PDGF), VEGF increase the angiogenic response when they are topically applied [15–19]. Conversely, delays or reductions in microvessel ingrowth due to impaired blood circulation have long been correlated with negative wound healing outcomes in the diabetic and aging population [20–26].

The present study differentiates between physiological and pathologic angiogenesis [9, 27] in the wound healing process. CM101 is derived from group B streptococcus (GBS) which is linked to the respiratory distress syndrome in neonates known as early onset disease [28, 29]. CM101 binds to a unique membrane glycoprotein HP59 which is expressed only in the neonatal vasculature and later in life in pathologic vasculature associated with pathologic angiogenesis [30]. Complement (C3) is activated by the alternative pathway and binds immediately to CM101 when it is bound to the endothelial target protein HP59 [31]. CM101 can be detected 5 min post-i.v. infusion in the tumor endothelium. Monocyte infiltration occurs at 5 min post-infusion and leads to endothelial apoptosis within minutes [31].

The CM101 target protein HP59 has been shown by immunohistochemistry on the endothelial cells of the pathologic vasculature in human and murine tumor [30], human neonatal and hemangioma lung vasculature (C. Fu et al., unpublished); and pathologic vasculature in rheumatoid arthritis and atherosclerotic lesions (BD Wamil et al., unpublished). In human adults, HP59 protein is selectively expressed in the tumor vasculature. The binding of CM101 to these receptors induces an inflammatory reaction targeted to the vasculature of the tumor [32]. This cascade of events leads to tumor shrinkage and to rapid wound healing of classic Kaposi sarcoma lesions [33]. CM101 was also shown not to inhibit wound healing in a mouse sponge model suggesting its selectivity for pathologic angiogenesis [34].

CM101 was demonstrated to be an anti-pathoangiogenic agent [31], which also inhibits the hypoxia-induced vascular sprouting associated with vascularization of glioma spheroids [35] and with inflammatory angiogenesis in wounds [36]. The inhibition of formation of inflammatory angiogenic sprouts led to a remarkably rapid wound closure (24 h) and full tensile strength was achieved within 7 days in a mouse model [36]. We postulate that when mature endothelial cells de-differentiate, in order to sprout [9], they express the HP59 protein and become targeted by the polysaccharide CM101 and eliminated by leukocytes [31, 37].

In this report, we present data suggesting that intravenous administration of CM101 accelerates wound re-epithelialization and healing. The collective data support that normal wound healing involves both physiologic and inflammatory pathologic angiogenesis and that inhibition of the latter accelerates the wound healing process.

Materials and methods

Porcine wound model

The porcine model was utilized since its cutaneous vasculature and thermoregulatory properties more closely resemble human skin as compared to furry rodent models. All procedures were carried out in accordance with the guidelines specified by the Institutional Animal Care Committee at Vanderbilt University and were similar to our previously described procedures [15, 16, 38–40]. Adolescent Yorkshire pigs weighing approximately 80 lbs were induced with an intramuscular injection of ketamine (0.22 mg/kg) and xylazine (0.22 mg/kg). Pigs were maintained under general anesthesia on an inhaled mixture of halothane and oxygen. Skin over the dorsal surface of the animals was shaved, cleansed with soap and prepped with betadine antiseptic. A Padgett dermatome (Kansas City, Missouri) was used to create 2–6 full-thickness wounds (extending into the superficial layer of cutaneous fascia) and 2–6 partial-thickness wounds (approximately 1250 μ in depth) along the paravertebral region of each animal. The four experimental animals had 2, 2, 5, and 6 wounds for a total of 15 wounds of each kind. Both control pigs had five wounds of each kind. After hemostasis was achieved, wounds were covered with a semi-permeable, adhesive, polyurethane dressing (Op-Site, Smith and Nephew, Largo, Florida) to prevent contamination and minimize dehydration of the wound bed. Subcutaneous injections of Buprenex analgesic were administered every 8 h for the first 48 h after injury. On alternating days, pigs were lightly anesthetized to cleanse the wounds with saline moistened gauze, and wounds were re-covered with occlusive bandage. Photographic documentation of the surface of each wound was performed on days 4 and 7.

Half of the wounds were excised on day 4 after injury and the remaining wounds were removed at the conclusion of the experiment on day 7.

Treatment regime for CM101

After the initial wounding procedure was completed, hemostasis achieved and the bandaging completed on day 0, pigs were randomly assigned into groups. The experiment group ($n=4$) was given an intravenous bolus of 7.5 μg CM101/kg and a control group ($n=2$) received a similar volume of the placebo vehicle. This dosage was selected based on previous studies with CM101 in cancer patients [33]. Pigs were returned to their cages and closely observed for signs of fever or hyperthermia during the first 4 h following introduction of CM101. At 72 h after injury, pigs were lightly sedated and were given a second intravenous bolus of either CM101 or placebo vehicle.

CM101 preparation

CM101 was purified from autoclaved culture media of GBS fermentations [41]. The culture supernatant after centrifugation was concentrated by recovering the retentate from a 10 K polysulfone cassette (Millipore, Bedford, Massachusetts). The concentrate was made 70% in alcohol and the precipitate was subjected to phenol/water extraction. CM101 was recovered from the water phase following DEAE-sephadex and sepharose column chromatography. Final purification was achieved by Lentil Lectin chromatography. CM101 was sterile filtered into vials, lyophilized and subjected to sterility, pyrogen, and efficacy tests for use in the clinic. A sample from this lot was used in this study. CM101 was dissolved in PBS for i.v. injection at 7.5 μg/kg in 1 ml.

Photographic analysis/laser Doppler perfusion imaging

On days 4 and 7, the animals were lightly anesthetized. Following the cleansing procedure, wounds were photographed with a DC260 zoom camera (Kodak Digital Science). Images were downloaded into Adobe Photoshop Software where composite photographs were formatted. Laser Doppler perfusion imaging (LDPI) was used for real time assessments of blood flow in each wound bed on days 3 and 7. The Lisca PIM II device (North Brunswick, New Jersey) with a high-resolution head was placed at a standard distance from each wound site in anesthetized animals while under standard room illumination. The scan area included the entire wound site and margins. When the scanning procedure was terminated, a color-coded image representing the microvascular blood flow distribution appeared on the computer screen. Low perfusion was displayed in dark blue and the highest perfusion areas were displayed in red. Pseudo color images were transferred to the NIH Image 1.62 software, and perfusion was calculated as a mean voltage signal for a standardized area.

Preparation of monoclonal antibodies to HP59-derived peptides

Balb/c mice were initially injected with 100 μg of a synthetic peptide based on the hydrophobic HP59 sequence from a.a. 50-63 (GenBank AF 244 578) conjugated with keyhole limpet hemocyonin (KLH) (Sigma Genosys, Inc., Texas) in complete Freund's Adjuvant followed after 2 weeks with 100 μg of HP59 peptide in incomplete Freund's Adjuvant (Sigma). Four weeks after the initial injection, the mice were boosted with 100 μg of peptide alone. The boost was repeated twice at 1 week intervals. Antibody titers were determined by ELISA. Three days prior to cell fusion, 50 μg of HP59 peptide was injected intravenously into the mice as a final boost. Spleen cells from mice immunized with HP59 peptides were fused with X63-Ag-8653 murine mycloma cells as described by Fu and Carter [42]. Fused cells are plated into 96 well-culture plates (Costar Corporation, Cambridge, Massachusetts), and subsequently screened for IgG recognizing synthetic HP59 peptides. Positive cultures were then expanded, subcloned and screened for hybridomas producing mAbs for immunohistochemistry on frozen or fixed tissue sections. The mAbs were affinity purified by HP59 peptide affinity chromatography [42].

Histological preparation and immunohistological staining procedures

All excisional wounds submitted for histopathology included normal skin margins at both edges. Partial-thickness wounds also contained underlying non-wounded dermis. The wounds, 15 experimental and 10 control wounds of each kind, were divided into five pieces. Three random slices running from normal margin to normal margin were collected from each piece. These samples were fixed in 4% paraformaldehyde for 48 h and embedded in paraffin. Representative sections (6 μm) were stained with Gomori's Trichrome for morphometric analysis of the percentage of resurfacing and the depth of the granulation tissue [15, 39, 40, 43]. For immunohistochemical staining, sections were deparaffinized through xylenes and rehydrated through a graded alcohol series to PBS. Endogenous peroxidase activity was quenched by treating with 3% hydrogen peroxide in aqueous methanol for 20 min at 25 °C followed by PBS rinses.

Immunohistochemical analysis for vWF and HP59

To detect the presence of the receptor for CM101 (HP59) in the neovasculature within porcine wounds, sections of partial-thickness and full-thickness wounds at post-injury day 4 were reacted with a monoclonal antisera to CM101 receptor. Sections were deparaffinated by immersing slides in xylene at RT twice for 5 min. The

slides were then transferred to fresh absolute alcohol and rehydrated through a graded alcohol series, ending with PBS. The sections were digested with proteinase K (Dako Corp, Carpintera, California) for 5 min and rinsed with PBS. Tissue sections were then treated with 0.1 M sodium borate buffer for 20 min and washed with PBS. The sections were blocked with a Biotin blocking system (Dako) washed with PBS and blocked for 40 min with PBS containing 5% BSA and 5% normal goat serum. Ten μg/ml of affinity purified monoclonal anti-HP59 antibody in PBS was added to each section and incubated in a humidified chamber for 1 h at RT. The slides were washed three times with PBS containing 0.1% triton X-100 (T-PBS) and incubated with biotinylated goat anti-mouse Fc IgG (Dako) using the same conditions as described for the primary antibody. The slides were then washed three times with T-PBS. Streptavidin fluorescein isothiocyanate (FITC) conjugate (Gibco BRL) was added to the sections and incubated for 40 min in a humidified chamber. The slides were washed again with T-PBS and rabbit anti-human Van Willibrand factor fgG (Dako) diluted 1:2000, was added to the sections and incubated for 1 h. The slides were washed with T-PBS, and incubated for 1 h with biotinylated goat anti-rabbit IgG (Jackson Immuno-Research). After washing with T-PBS a Streptavidin Cy3 conjugate (Molecular Probe) was added to the sections and incubated for 40 min at RT. The slides were washed with T-PBS, dehydrated and mounted with cover slips.

To selectively highlight all endothelial cells within wounded areas for the purpose of automated morphometric analysis, sections from 7 day wounds were immunostained for factor VIII antigen (von Willebrand factor) at a dilution of 1/900 followed by incubation for 30 in the reagents supplied in an Envision+ kit (Dako) [16, 39]. Sites of immunoreactivity were visualized with brown DAB chromogen (BioGenix, San Ramon, California). Slides were lightly counterstained with Mayer's hematoxylin, dehydrated and coverslipped.

Morphometric analysis techniques

Image ProPlus software (Media Cybernetics, Silver Springs, Maryland) was used to analyze tissue sections viewed on the stage of a Vanox light microscope interfaced via a Progressive Research Digital Camera (Konatron Electronik, Germany). Three random sections from each wound of both types (15 of each experimental; 10 of each for control) were used to collect measurements. These data were obtained by an observer blinded to the experimental protocol. In brief, the percentage of wound resurfacing was determined by measuring the sum of the new epidermal islands and migrating margins within the wound section and dividing this by the total distance from the right to the left wound margin [15, 16]. The depth of the granulation tissue was defined as the distance, in microns from the bottom of the migrating epidermis to the interface of the granulation tissue with the normal, non-wounded epidermis in the partial-thickness wounds.

The granulation tissue in partial-thickness wounds is visually obvious on Trichrome-stained sections [39, 40]. Dermal depth was not assessed near the wound edge, nor was it taken immediately adjacent to hair follicles. Since factor VIII immunostaining selectively highlights only the endothelial components of the skin, this circumstance facilitates the computerized identification of the microvascular bed. The color scale on the Image-Pro software was adjusted to recognize the brown stained area representing microvessels whether they were in cross-section, longitudinal or tangential sections [16]. Within each wound, ($n=15$ experimental or 10 control for each kind) measurements of 20 random fields of 230,000 μ^2 were performed. All fields were sampled from the upper region of the granulation tissue on day 7 wounds.

Results

Assessment of revascularization within wound beds

Visible differences between treatment groups

Macroscopic differences in the color and healing characteristics of the wounds were readily apparent between the animals receiving CM101 vs. those receiving the placebo vehicle. To the unaided human eye, wounds from animals receiving two intravenous CM101 treatments appeared less red (Figure 1). This finding is indicative of at least three possibilities: (a) diminished neovascularization (b) a decline in microvessel number that marks a more mature wound or (c) an increased deposition of extracellular matrix molecules such as

Figure 1. Photographs of the surface of partial-thickness and full-thickness wounds at day 7 after injury. (A) Non-treated partial thickness, (B) non-treated full thickness, (C) partial-thickness CM101 treatment, (D) full-thickness CM101 treatment. Note that the non-treatment full-thickness wound is redder as compared to the CM101-treated full-thickness excision. The full-thickness CM101-treated wound appears opaque and fully resurfaced.

Figure 2. (a) LDPI indicates that areas of highest blood flow in red followed by yellow, medium levels are depicted in green and areas of lowest flow in blue to purple. On both days 3 and 7, blood flow is highest in the placebo-treated wounds as compared to the CM101-treated wounds. This finding was consistent whether wounds were partial thickness or full thickness. (b) Mathematical expression of the colorimetric laser Doppler perfusion index for the same day 3 and 7 wounds. In all examples, less blood flow was present in the CM101-treated wounds as compared to the placebo-treated wounds.

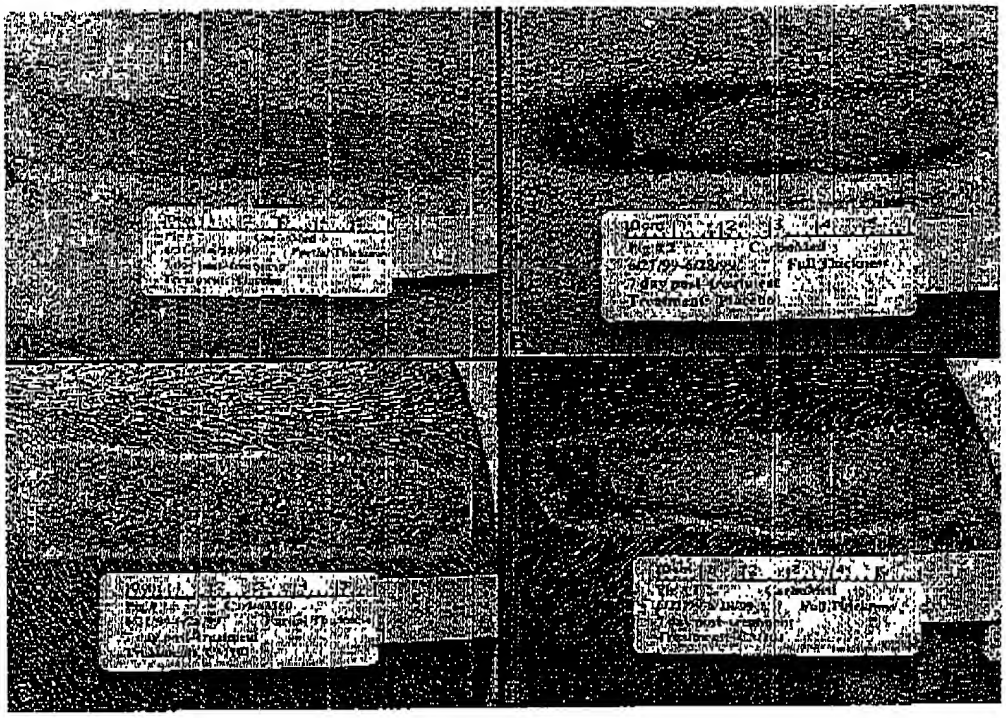

Figure 1

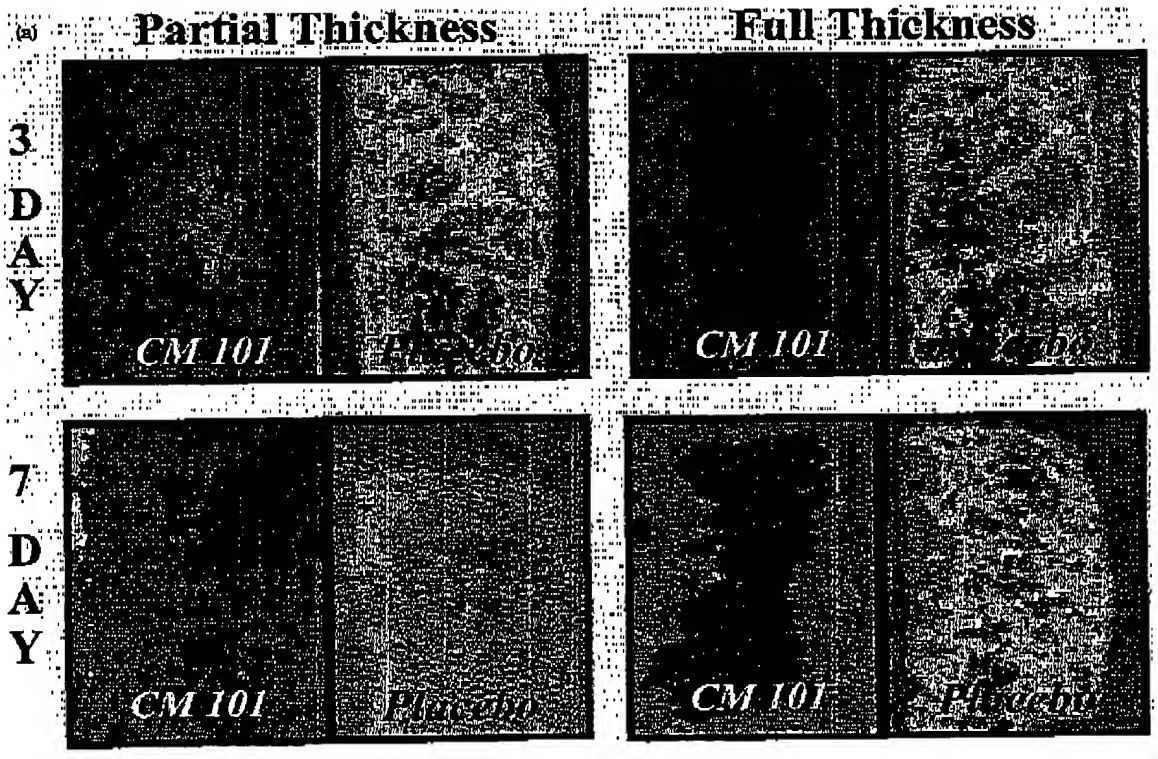

Figure 2

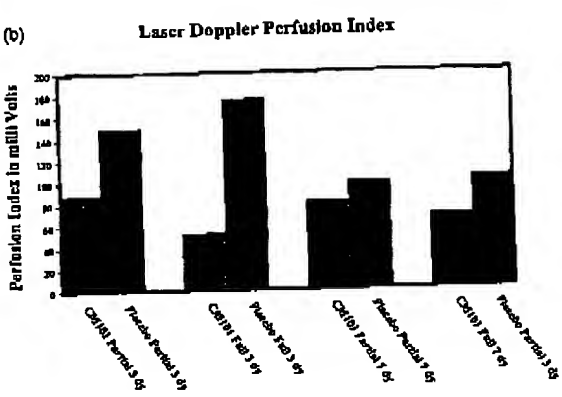

Figure 2. Continued.

collagens. In addition to an apparent difference in vascularity, the chief surface characteristics of wounds from CM101-treated animals were increased opacity and dullness, a circumstance that is normally observed as wounds become resurfaced with new epithelium (Figure 1). These findings were consistently observed in partial thickness as well as full-thickness wounds.

Dynamic blood flow differences as assessed by the laser Doppler perfusion index

Steady state *in vivo* assessments of blood flow within wounds were obtained on days 3 and 7 using laser Doppler perfusion imaging (Figures 2a, b). Figure 2a is a pseudocolored representation of differential blood flow scanned with a wound on day 3 and its companion data is numerically displayed in the Figure 2b graph. These dynamic data show that in partial-thickness wounds on day 3, blood flow is greatly reduced in the CM101-treated wound group ($P = 0.001$). The magnitude of the difference was more prominent in the full-thickness wounds, where the blood flow in the CM101-treated wounds was threefold less than the non-treated control wound bed. By 7 days after injury, the partial-thickness wounds on pigs treated with CM101 were still showing diminished blood flow as compared to the non-treatment group ($P = 0.05$). It is noteworthy that the blood flow in non-involved skin between the partial-thickness wounds remained at a steady state level between days 3 and 7 after wounding of CM101-treated animals. Flow imaging of full-thickness wounds on day 7 revealed that wounds in animals treated with CM101 continued to have a diminished blood flow compared the wounds in the control animals ($P = 0.05$).

Histology vascular density

Histological differences between the CM101-treated and placebo-treated wounds were most pronounced on day 7 post-injury. These differences were apparent in both the Trichrome stained sections (data not shown) and the sections selectively immunostained with the endothelial marker (factor VIII) (Figure 3). Wound beds from placebo-treated animals showed an influx of fibroblasts, macrophages and numerous dilated microvessels (Figure 3). By contrast, in the CM101 treated animals, the vascular density and influx of inflammatory cells were visibly diminished (Figure 3).

Computerized morphometric analyses of factor VIII immunostained tissue ($n = 20$ fields $\times$ 15 wounds) were used to quantitate the histological observations. The differences in vascular density between the wounds on experimental animals and the wounds on control ($n = 20$ fields $\times$ 10 wounds) in both the partial-thickness wounds ($P < 0.05$) and full-thickness wounds ($P < 0.001$) were significant (Figure 4). The most dramatic impact of CM101 treatment on vascular density was evident in the full-thickness injuries. Full-thickness wounds on animals treated with CM101 had 1/3 the vascular density compared to wounds of untreated animals. The magnitude of the difference in CM101 treated wounds was greater in the full-thickness injuries than in the partial-thickness injuries. This was not unexpected since the neovasculature comprises a larger volume within the granulation tissue that develops within a full-thickness wound as compared to a partial-thickness wound.

Qualitative assessment of vasculature

CM101 binds HP59 receptors that are expressed in de-differentiated pathologic endothelial cells. To illustrate the spatial localization of physiologic and pathologic vasculature, double immunofluorescent staining for HP59 and VWF was performed (Figure 5). Endothelial cells within the wound beds were identified with factor VIII immunostaining (red:rhodamine distribution). Sites where co-localization of factor VIII and the HP59 receptors were present are visible as yellow within the wound bed (Figure 5). Thus immunohistochemical analysis demonstrated that the microvascular bed in wounds from CM101-treated animals is devoid of HP59 positive pathologic angiogenesis. By contrast, endothelial cells expressing HP59 receptors comprised the majority of the endothelial network within the wound beds of the placebo-treated pigs.

Qualitative evaluation of granulation tissue

Histologic differences between the CM101-treated and placebo-treated wounds were most pronounced on day 7 post-injury. An important parameter for assessment of the extent of healing is the production of granulation tissue or neodermis. Quantitative dermal depth evaluations were conducted on Gomori stained Trichrome sections on days 4 and 7 after the excisional injury. Measurements collected from these wounds showed notable differences between the experimental and control groups (Figure 6). On day 4, both the partial- and

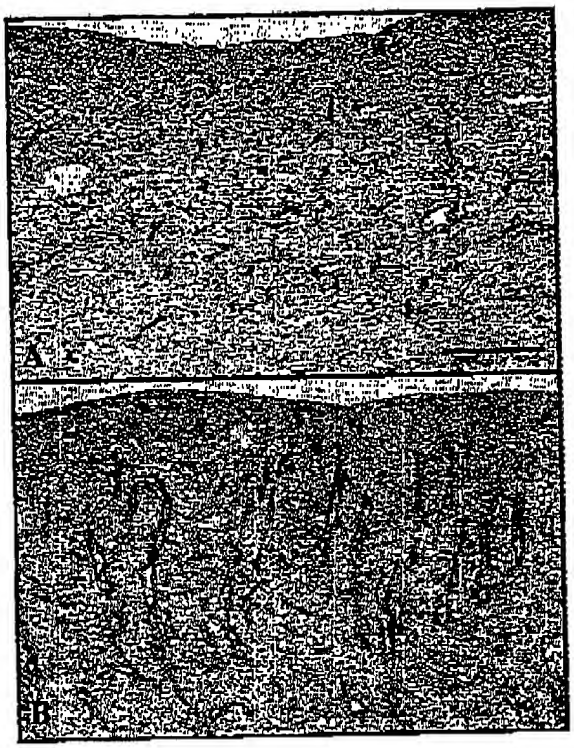

Figure 3. Immunohistochemical staining for factor VIII within full thickness porcine wounds on day 7. Panel A shows the granulation tissue with the center of a wound from a pig treated with two dosages of CM101. Microvessels are sparse, very small in diameter and the granulation tissue has an organized horizontal organization. Panel B shows the central wound bed from a placebo treated pig. Microvessels comprise a large percentage of the material in this granulation tissue but the organizational character of the granulation tissue appears more irregularly arranged and heavily populated than in the CM101 treated wound. Size bar = 100 μ.

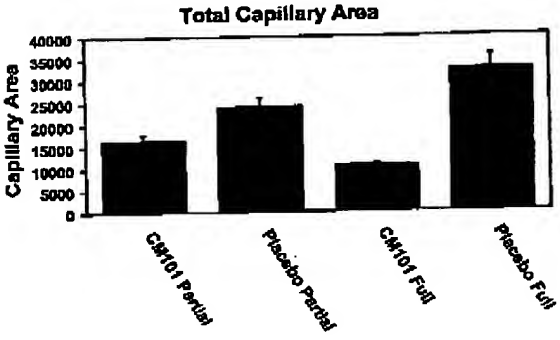

Figure 4. Quantitative assessment of microvascular density within porcine wounds at day 7. Total areas occupied by microvessels within standard high magnification fields (230,000 μ^2) were colorimetrically assessed from factor VIII immunostained sections. Values represent the mean ± SEM of 20 fields from each of the 15 experimental and 10 control wounds within the upper region on the granulation tissue. Statistical significance was achieved for partial thickness wounds ($P = 0.05$) and for full-thickness wounds ($P = 0.001$) by a student's *t*-test.

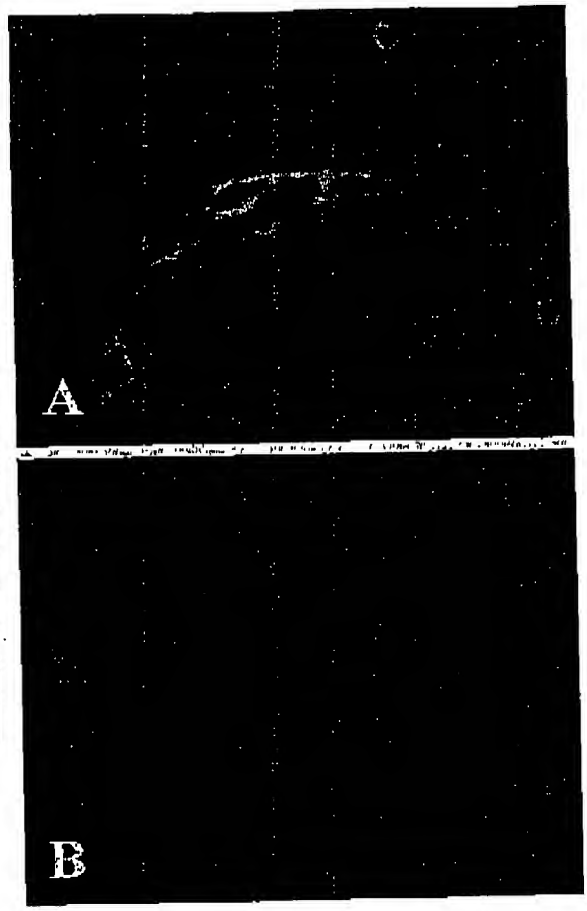

Figure 5. Sites of the CM101 receptor (HP59) on microvascular endothelium are shown by double immunostaining (yellow). The location of the endothelium is shown in red. HP59 receptor co-localizes with endothelial cells (yellow) in most of the endothelial cells (Panel A) in control wounds on day 4. No co-localization was detected on any of the microvessels from a wound removed from a pig receiving two doses of CM101 and fewer were present within the wound bed. magnification = 100×.

full-thickness CM101-treated wounds had significantly thicker granulation tissue ($P = 0.05$ and 0.001, respectively) than the non-treated wounds. By day 7 after wounding, there was no significant difference in the thickness of the granulation tissue between the control and CM101-treated groups for the partial-thickness wounds. The full-thickness wounds treated with CM101 showed a significant decrease in the thickness of the neodermis ($P = 0.001$).

Quantitative evaluation of re-epithelialization

An additional parameter for evaluating the success of wound healing treatments is surface closure. The effects of re-epithelialization after 7 days of healing is shown

macroscopically in Figure 1. The surface of the full-thickness CM101-treated wound appears to be covered with a rather thick epidermis that renders the surface rather opaque. The quantitative assessment of resurfacing is expressed in Figure 7. Among the wound groups at the early time point (day 4) after injury, differences in the extent of resurfacing were negligible and no significant differences were observed. However, by 7 days after injury, a dramatic effect was observed in the CM101-treated groups. Resurfacing was nearly complete in the partial-thickness wounds of the CM101-treated pig while the comparable wounds from the control pig were 55% resurfaced on the average ($P = 0.001$). Although the full-thickness wounds lagged behind in their rate of resurfacing as compared to the more shallow partial-thickness excisions, the CM101-treated full-thickness wounds by day 7 showed more extensive resurfacing than the full-thickness control wounds ($P = 0.05$).

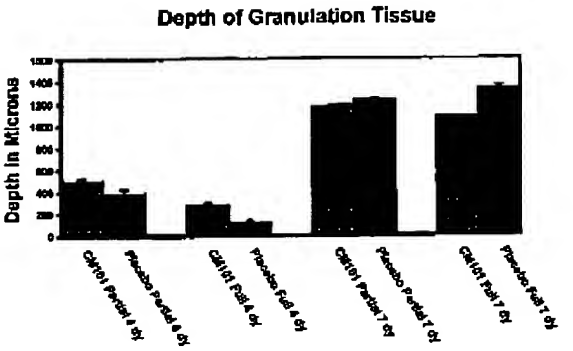

Figure 6. Quantitative assessment of the depth of granulation tissue in the porcine wounds on days 4 and 7. The mean depth of the granulation tissue or neodermal region was determined as described in the Materials and Methods. Values are expressed as the mean ± SEM. Statistical significance was as follows: 4 day partial thickness ($P = 0.05$). 4 day full thickness ($P = 0.001$), 7 day full thickness ($P = 0.001$). Computerized measurements were collected from Trichrome stained sections.

Discussion

The field of angiogenesis in wound repair is currently receiving intense attention. For the past 15 years, increased angiogenesis has been associated with accelerated repair [14]. Only a few rare papers have suggested that moderate impairment of angiogenesis alone did not necessarily retard normal wound healing. In one study, $\alpha(v)$ integrin was blocked but the reduction in angiogenesis did not prove detrimental to numerous wound parameters [44]. In another, CM101 was shown to inhibit scarring in the spinal cord following trauma [45].

To date, work with wound healing models has shown that impaired wound repair is associated most often with delayed or impaired angiogenesis. In an aged mouse model, a positive correlation was demonstrated between the age of the mice and delayed angiogenesis [24]. Similarly, eNOS-deficient mice showed a significant delay in microvessel ingrowth suggesting that a lack of endothelial derived nitric oxide synthetase was associated with delayed angiogenesis as well as wound closure and strength [25]. In addition, Davidson and Broadley [18] using neutralizing anti-bFGF antibody showed impaired healing. Decreased VEGF correlated with declining levels of angiogenesis and poorer healing outcomes in db/db/mice [26].

The present study provides strong evidence that administration of the bacterial toxin CM101 has a profound impact on the angiogenic process that normally occurs following cutaneous injury. Our data suggest that inhibition of the hypoxia induced inflammatory angiogenesis which occurs during normal wound repair can accelerate the physiologic process. By inhibiting the inflammatory process, activated leukocyte infiltration is reduced leading to less secondary tissue damage. The systemic delivery of CM101 produces a positive biological outcome. Dynamic blood flow measurements, morphometric analysis of vascular density within the wound bed, and double immunofluorescent immunostaining all support the supposition that CM101 selectively targets and thwarts the development of only a portion of the microvascular network within healing wounds. While considerably fewer microvessels are detected within the CM101-treated wound, the granulation tissue appears, upon histological examination, otherwise normal in its histological features on days 4 and 7 after injury.

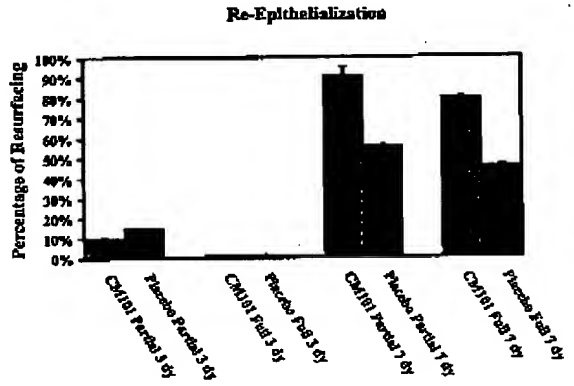

Figure 7. Quantitative assessment of re-epithelialization in porcine wounds measured at 4 and 7 days after injury. At 4 days after injury, no significant differences were observed among the different treatment groups. As expected negligible resurfacing was present after 4 days in the full thickness injuries. At 7 days after injury both the partial- and full-thickness CM101 treatment wounds were significantly more resurfaced than their corresponding non-treated wounds. The full-thickness CM101-treated wounds were almost twice as resurfaced as non-treated wounds.

Earlier studies have shown that the target protein for CM101, HP59 is expressed in pathologic inflammatory angiogenesis that is associated with granulation tissue and also with tumor development [30]. The HP59 receptor is not, however, present on the surface of normal adult endothelial cells and does not affect physiological vasculature. CM101 binds to the membrane glycoprotein, HP59 in tumor neovasculature which activates complement and the targeted endothelial cells are eliminated by leukocytes within minutes [31] and CM101 is eliminated in the urine [28]. We postulate that under the hypoxic conditions, inflammatory angiogenesis is initiated and endothelial cells become committed to sprouting and express HP59. These cells are immediately targeted by CM101 and the sprout would be eliminated by leukocytes [35, 36]. The subsequent reduction in the microvessel network produced a desirable biological outcome, accelerated wound healing in the mouse [36] and a reduction in tumor size in both tumor-bearing mice and humans [32, 33, 46]. The expression of the HP59 receptor on endothelial cells within the similar hypoxic environments that exists within both tumors and wounds is not surprising since many years ago Dvorak proposed that tumors are really wounds that fail to heal [47]. In our clinical application of CM101, a patient with classic Kaposi sarcoma experienced not only tumor ablation but it was noted that within 3 weeks there were no scars left behind [33].

In this study, we examined the effect of CM101 on re-epithelialization in full- and partial-thickness wounds in the pig model. The result obtained when CM101, was infused 1 h post-injury, show that CM101 inhibited formation of blood vessels expressing its target HP59 in the wounds, whereas vessels containing the pathoangiogenic marker HP59 were abundant in the placebo-treated animals.

The present findings would suggest that the angiogenic processes of wound repair involve both physiologic and pathologic angiogenesis and that inhibition of the latter could prove beneficial for wound repair in a clinical application.

Acknowledgements

We appreciate the expert technical assistance of Nancy Cardwell, Joseph Watson, Jesse Britton, Amy Nunnelly. We thank Pamela L. Chunn for preparing the manuscript. This work was supported by GM 40439 (LBN), AG06528 (JMD), the Office of Naval Research (JMD), and the Department of Veterans Affairs (JMD). A portion of this research was supported by CarboMed, Inc, in which BDW, H-PY, and CGH have a financial interest.

References

1. Singer MW. Role of leukocytes and endothelial cells in the development of angiogenesis in inflammation and wound healing. Arch Pathol Lab Med 2001; 125: 67–71.
2. Arnold F, West DC. Angiogenesis in wound healing. Pharmacol Ther 1991; 52: 407–22.
3. Shweiki D, Itin A, Soffer D, Keshet E. Vascular endothelial growth factor induced by hypoxia may mediate hypoxia-initiated angiogenesis. Nature 1992; 359(6398): 843–45.
4. Battegay J. Angiogenesis: Mechanistic insights, neovascular diseases, and therapeutic approaches. J Mol Med 1996; 73: 333–46.
5. Folkman J. Angiogenesis and angiogenic inhibition: An overview. In Goldberg ED, Rosen EM (eds): Regulation of Angiogenesis. Basel: Birkhauser Verlag 1997; 1–8.
6. Casey R, Li WW. Factors controlling ocular angiogenesis. Amer J Ophtalmol 1997; 124: 521–29.
7. Forsythe JA, Jiang BH, Iyer NV et al. Activation of vascular endothelial growth factor gene transcription by Hypoxia-Inducible Factor 1. Mol Cell Biol 1996, 16: 4604–13.
8. Bussolino F, Mantovani A, Persico G. Molecular mechanisms of blood vessel formation. Trends Biochem Sci 1997; 22: 251–56.
9. Carmeliet P, Jain RK. Angiogenesis in cancer and other diseases. Nature 2000; 407: 249–57.
10. Kovacs EJ, DiPietro LA. Fibrogenic cytokines and connective tissue production. FASEB J 1994; 8: 854–61.
11. Detmar M, Crown LF, Schon MP et al. Increased microvascular density and enhanced leukocyte rolling and adhesion in the skin of VEGF transgenic mice. J Invest Dermatol 1998; 111: 1–6.
12. Arbiser JL. Angiogenesis and the skin: A primer. J Am Acad Dermatol 1996; 34: 486–97.
13. Brown LF, Yeo KT, Berse B et al. Expression of vascular permeability factor (vascular endothelial growth factor) by epidermal keratinocytes during wound healing. J Exp Med 1992; 176: 1375–79.
14. Kyriakides TR, Tam JW, Bornstein P. Accelerated wound healing in mice with a disruption of the thrombospondin 2 gene. J Invest Dermatol 1999; 113: 782–87.
15. Quaglino D, Nanney LB, Kennedy R, Davidson JM. Transforming growth factor-beta stimulates wound healing and modulates extracellular matrix gene expression in pig skin. I. Excisional wound model. Lab Invest 1990; 63: 307–19.
16. Roesel JF, Nanney LB. Assessment of differential cytokine effects on angiogenesis using an *in vivo* model of cutaneous wound repair. J Surg Res 1995; 58: 449–59.
17. Nissen NN, Polverini PJ, Gamelli RL, DiPietro LA. Basic fibroblast growth factor mediates angiogenic activity in early surgical wounds. Surgery 1996; 119: 457–65.
18. Davidson JM, Broadley KN. Manipulation of the wound-healing process with basic fibroblast growth factor. Ann NY Acad Sci 1991; 638: 306–15.
19. Pierce GF, Tarpley JE, Yanagihara D et al. Platelet-derived growth factor (BB homidimer), transforming growth factor-beta 1, and basic fibroblast growth factor in dermal wound healing. Neovessel and matrix formation and cessation of repair. Am J Pathol 1992; 140: 1375–88.
20. Rivard A, Fabre JE, Silver M et al. Age-dependent impairment of angiogenesis. Circulation 1999; 99: 111–20.
21. Ortega S, Ittman M, Tsang SH et al. Neuronal defects and delayed wound healing in mice lacking fibroblast growth factor 2. Proc Natl Acad Sci USA 1998; 95: 5672–77.
22. Reed MJ, Corsa A, Pendergrass W et al. Neovascularization in aged mice: delayed angiogenesis is coincident with decreased levels of transforming growth factor beta-1 and type I collagen. Am J Pathol 1998; 152: 113–23.
23. Rivard A, Silver M, Chen D et al. Rescue of diabetes-related impairment of angiogenesis by intramuscular gene therapy with adeno-VEGF. Am J Pathol 1999; 154: 355–63.
24. Swift ME, Kleinman HK, DiPietro LA. Impaired wound repair and delayed angiogenesis in aged mice. Lab Invest 1999; 79: 1479–87.
25. Lee PC, Salyapongse AN, Bragdon GA et al. Impaired wound healing and angiogenesis in iNOS-deficient mice. Am J Physiol 1999; 277: H1600–08.

26. Frank S, Hubner G, Breier G et al. Regulation of vascular endothelial growth factor expression in cultured keratinocytes. Implications for normal and impaired wound healing. J Biol Chem 1995; 270: 12607–13.
27. Polverini PJ. The pathophysiology of angiogenesis. Rev Oral Biol Med 1995; 6(3): 230–47.
28. Sundell HW, Yan H-P, Wamil BD et al. Isolation and identification of a group b β-hemolytic streptococcal toxin from septic infants. J Pediatr 2000; 137: 338–44.
29. Hellerqvist CG, Rojas J, Green RS et al. Studies on Group B β-hemolytic streptococcus. I. Isolation and partial characterization of an extracellular toxin. Pediatr Res 1981; 15: 892–98.
30. Fu C, Ceratanu ND, Bardhan S et al. Identification and characterization of HP59: A unique pathoangiogenic marker targeted by CM101. AACR Annual Meeting (2000).
31. Yan H-P, Carter CE, Wang E et al. Functional studies on the anti-pathoangiogenic properties of CM101. Angiogenesis 1998; 2: 219–33.
32. Wamil BD, Thurman GB, Sundell HW et al. Soluble e-selectin in cancer patients as a marker of the therapeutic efficacy of CM101, a tumor-inhibiting anti-neovascularization agent, evaluated in phase I clinical trial. J Cancer Res Clin Oncol 1997; 123: 173–79.
33. DeVore RF, Hellerqvist CG, Wakefield GB et al. Phase I study of the antineovascularization drug CM101. Clinical Can Res 1997; 3: 365–72.
34. Quinn TE, Thurman GB, Sundell A-K et al. CM101, a polysaccharide anti-tumor agent, does not inhibit wound healing in murine models. J Can Res Clin Oncol 1995; 121: 253–56.
35. Abramovitch R, Frenkiel D, Meir G et al. Mapping neovascularization and anti-neovascularization therapy: Correlation between NMR and light microscopy. Proceedings of the 5th Conference of the International Society of Magnetic Resonance in Medicine (ISMRM) 1997, 490 pp.
36. Hellerqvist CG, Neeman M, Wamil BD, Abramovitch R. Facilitation of wound healing with CM101/GBS toxin. 1999; U.S. 5,858,991; see web site: http://www.uspto.gov/.
37. Vetvicka V, Thornton BP, Ross GD. Soluble beta-glucan polysaccharide binding to the lectin site of neutrophil or natural killer cell complement receptor type 3 (CD11b/CD18) generates a primed state of the receptor capable of mediating cytotoxicity of iC3b-opsonized target cells. J Clin Invest 1996; 98: 50–61.
38. Schaffer CJ, Reinisch L, Polis SL et al. Comparisons of wound healing among excisional, laser-created, and standard thermal burns in porcine wounds of equal depth. Wound Repair Regen 1997; 5: 52–61.
39. Nanney LB. Epidermal and dermal effects of epidermal growth factor during porcine wound repair. J Invest Dermatol 1990; 94: 624–29.
40. Nanney LB, Paulsen S, Davidson M et al. Boosting of EGF receptorsa by gene gun stimulates epidermal growth *in vivo*. Wound Repair Regen 2000; 8: 117–27.
41. Hellerqvist CG, Thurman GB, Page DL et al. Anti-tumor effects of GBS toxin: A polysaccharide exotoxin from group B b-hemolytic streptococcus. Can Res Clin Oncol 1993; 120: 63–70.
42. Fu C, Carter CE. Detection of circulating antigen in human schistosomiasis japonica using monoclonal antibody. Am J Trop Med Hyg 1990; 42: 347–351.
43. Feng X, Clark RA, Galanakis D, Tonnesen MG. Fibrin and collagen differentially regulate human dermal microvascular endothelial cell integrins: Stabilization of alphav/beta3 mRNA by fibrin 1. J Invest Dermatol 1999; 113: 913–19.
44. Jung YC, Arumugam S, Gibran NS, Isik FF. Role of alpha(v) integrins and angiogenesis during wound repair. Wound Repair Regen 1999; 7: 375–80.
45. Wamil AW, Wamil BD, Hellerqvist CG. CM101-mediated recovery of walking ability in adult mice paralyzed by spinal cord injury. Proc Natl Acad Sci USA 1998; 95: 13188–93.
46. Thurman GB, Russell BA, York GE et al. Effects of GBS toxin on long-term survival of mice bearing transplanted Madison lung tumors. J Can Res Clin Oncol 1994; 120: 479–84.
47. Dvorak HF. Tumors: Wounds that do not heal. Similarities between tumor stroma generation and wound healing. N Engl J Med 1986; 315: 1650–59.